UNIVERSITY OF Southampton

University of Southampton Research Repository
ePrints Soton

Copyright © and Moral Rights for this thesis are retained by the author and/or other copyright owners. A copy can be downloaded for personal non-commercial research or study, without prior permission or charge. This thesis cannot be reproduced or quoted extensively from without first obtaining permission in writing from the copyright holder/s. The content must not be changed in any way or sold commercially in any format or medium without the formal permission of the copyright holders.

When referring to this work, full bibliographic details including the author, title, awarding institution and date of the thesis must be given e.g.

AUTHOR (year of submission) "Full thesis title", University of Southampton, name of the University School or Department, PhD Thesis, pagination

http://eprints.soton.ac.uk

University of Southampton

School of Medicine

Division of Clinical Neurosciences

A molecular-genetic study of Congenital Nystagmus

Mr Jay Self BM MRCOphth

PhD Thesis

March 2009

UNIVERSITY OF SOUTHAMPTON

ABSTRACT

FACULTY OF MEDICINE HEALTH AND LIFE SCIENCES

SCHOOL OF MEDICINE

Doctor of Philosophy

A MOLECULAR-GENETIC STUDY OF CONGENITAL NYSTAGMUS

By Mr James Edward Self BM MRCOphth

Nystagmus is a disorder of eye movement characterised by irregular, uncontrolled and repetitive eye movements. It can occur in a broad spectrum of clinical situations and diseases or it may occur in isolation and an inherited disorder. Surprisingly little is known about the underlying mechanisms of ocular-motor control. Similarly, the pathophysiological mechanisms underpinning nystagmus is also poorly understood. By studying pedigrees in whom nystagmus seems to be inherited as an isolated trait (Congenital Idiopathic Nystagmus), it may be possible to identify some of the genetic causes of this disorder and subsequently understand the pathophysiology.

This thesis describes a molecular genetic study of congenital nystagmus. A clinical phenotyping study is followed by linkage analysis and positional cloning. A novel nystagmus gene is investigated in a large cohort of Congenital Idiopathic Nystagmus (CIN) patients and X-inactivation studies are performed. Subsequently, cell culture and RT-PCR work is performed to study expression of this gene. Additionally a pedigree with an atypical congenital nystagmus disorder is investigated and a new mutation within a known cerebellar disease gene is identified.

This work contributed to the identification of the first gene for Congenital Idiopathic Nystagmus (CIN). The first detailed temporal expression study of the *FRMD7* nystagmus gene was also performed in this study which has directed further studies into the pathogenesis of CIN. Identification of a new mutation in the *CACNA1A* gene in a pedigree with nystagmus and subtle cerebellar signs has lead to the consideration of this gene in patients who present to hospital with isolated atypical nystagmus.

STATEMENT OF ORIGINALITY

During the course of this project it was necessary to enlist the help of a number of experts for specific experiments and techniques. I am very grateful to these colleagues and wish to thank them formally for their time and support. Specifically:

- Professor Andrew Collins and Dr Sarah Ennis who assisted with the bioinformatic analysis on a UNIX platform for the linkage work detailed in chapter 3.
- Dr Fatima Shawkat who completed some of the electrophysiological recordings including Electroretinograms and Visual Evoked Potentials detailed in Chapters 3 and 8.
- Dr Simon N Thomas kindly performed the genotyping necessary for the X inactivation studies detailed in chapter 7.
- Dr Hans Michael Haitchi kindly provided murine genetic samples and performed some sexing experiments on these samples as detailed in chapter 9.

All other work in these project was completed by me during the tenure of this PhD training program.

ACKNOWLEDGEMENTS

It is a pleasure for me to thank the many people who helped me throughout the course of this work.

Professor Andrew Lotery has provided the most enthusiastic and supportive guidance possible over the past 4 years. He has helped me at every stage of the journey from the initial intent to undergo a PhD to this final stage of submission. I have learned an enormous amount from him and for this I will always have the greatest admiration and gratitude.

I would also like to thank Professor Andy Collins, Professor David Mackey, Professor David Wilson and Professor Chris Harris for their supervision during this research. I would also like to thank the lab team, in particular Angela, Helen, Heather and Xiaoli for their help, advice and most of all, patience.

Finally, I would like to thank my wife Rachel for her support and encouragement over the last 4 years, and my son William for helping me relax after long days in the lab.

PUBLICATIONS ARISING FROM THIS WORK

The following is a list of publications arising from this body of work. These papers are presented at the end of this thesis:

Self J, Lotery A. **The molecular genetics of congenital idiopathic nystagmus**. Semin.Ophthalmol. 2006;21:87-90.

Self J, Lotery A. **A Review of the Molecular Genetics of Congenital Idiopathic Nystagmus (CIN)**. Ophthalmic Genet. 2007;28:187-91.

Self JE, Ennis S, Collins A, Shawkat F, Harris CM, Mackey DA et al. **Fine mapping of the X-linked recessive congenital idiopathic nystagmus locus at Xq24-q26.3**. Mol.Vis. 2006;12:1211-6.

Self JE, Shawkat F, Malpas CT, Thomas NS, Harris CM, Hodgkins PR et al**. Allelic Variation of the FRMD7 Gene in Congenital Idiopathic Nystagmus**. Arch.Ophthalmol. 2007;125:1255-63.

Self JE, Haitchi H, Chen X, Holgate S, Davies D, and Lotery AJ. ***FRMD7* expression in developing mouse brain**. Eye 2009.

Self J, Mercer C, Boon E, Murugavel M, Shawkat F, Hammans S, Hodgkins P, Griffiths H, and Lotery AJ. **Infantile nystagmus and late onset ataxia associated with a CACNA1A mutation in the intracellular loop between s4 and s5 of domain 3**. Eye 2009.

Contents

1 CHAPTER ONE – INTRODUCTION....13

1.1 The unique X chromosome....13
1.1.1 Introduction....13
1.1.2 X-inactivation....13
1.2 Eye movements....16
1.3 Nystagmus....18
1.3.1 Introduction....18
1.3.2 Early descriptions....18
1.3.3 Significance....19
1.3.4 Classification of Nystagmus....19
1.3.5 Pathophysiological mechanisms of nystagmus....32
1.3.6 Congenital Idiopathic Nystagmus....32

2 CHAPTER TWO - METHODS....40

2.1 Standard Laboratory techniques....40
2.1.1 DNA and RNA collection....40
2.1.2 DNA quantification and quality measurement....49
2.1.3 The Polymerase Chain Reaction....51
2.1.4 Large plate 2% Agarose gel preparation....54
2.1.5 Operation of CAS-1200™ precision liquid handling system robot....55
2.2 Genetic variations and molecular mutation detection systems....55
2.2.1 Mutations vs Polymorphisms....56
2.2.2 Polymorphisms....56
2.2.3 Mutations....57
2.2.4 Mutation detection methods....58
2.2.5 Designing primer oligonucleotides....65
2.3 Methods used for RNA work....66
2.3.1 Tissue storage prior to RNA extraction....66
2.3.2 RNA extraction and cDNA synthesis....67
2.3.3 Real-time quantitative polymerase chain reaction (RT qPCR) protocol....72
2.4 Cell culture methods and protocols....72
2.4.1 Standard growth media for SHSY5Y neuroblastoma derived cells....72
2.4.2 NB-B27 growth media for SHSY5Y neuroblastoma derived cells....73
2.4.3 Standard growth media for Y-79 Retinoblastoma derived cells....73
2.4.4 Haemocytometer method of cell counting....73
2.4.5 Cell freezing....74
2.4.6 Defrosting cells....74
2.4.7 Poly-L-Lysine coating culture wells....75
2.4.8 Immunohistochemistry....75

3 CHAPTER THREE - POSITIONAL CLONING OF A NYSTAGMUS GENE BY LINKAGE ANALYSIS....77

3.1 Introduction....77
3.2 Methods....77
3.2.1 Clinical methods....77
3.2.2 Laboratory methods....80
3.2.3 Bioinformatic methods....81
3.3 Results....82
3.3.1 Clinical Results....82
3.3.2 Linkage Analysis Results....85

3.4 Discussion....89
3.4.1 Clinical Phenotyping....89
3.4.2 Linkage Studies....90

4 CHAPTER FOUR – SCREENING PEDIGREE 1 FOR MUTATIONS IN THE CEREBELLAR DEGENERATION-RELATED PROTEIN 1 (CDR1) GENE 93

4.1 Introduction....93
4.2 Methods....93
4.3 Results....95
4.4 Discussion....95

5 CHAPTER FIVE – MUTATION SCREENING GENES FROM WITHIN THE IDENTIFIED NYSTAGMUS LINKAGE INTERVAL FOR PEDIGREE 1....98

5.1 Introduction....98
5.2 Methods....98
5.3 Results....100
5.3.1 Sequencing results....100
5.3.2 PstI Restriction Enzyme Digest Results....103
5.4 Discussion....104

6 CHAPTER SIX – ASSESSING THE GENETIC CONTRIBUTION OF THE FRMD7 GENE TO CONGENITAL IDIOPATHIC NYSTAGMUS....105

6.1 Introduction....105
6.2 Methods....105
6.3 Results....107
6.4 Discussion....109

7 CHAPTER SEVEN - ASSESSMENT OF THE ROLE OF X-INACTIVATION IN PEDIGREE 1....112

7.1 Introduction....112
7.2 Methods....112
7.3 Results....113
7.4 Discussion....114

8 CHAPTER EIGHT – CLINICAL AND GENETIC INVESTIGATION OF A FAMILY WITH AN ATYPICAL CONGENITAL NYSTAGMUS SYNDROME....118

8.1 Introduction....118
8.2 Methods....118
8.2.1 Clinical methods....118
8.2.2 Molecular genetic methods....120
8.3 Results....121
8.3.1 Clinical phenotyping results....121
8.3.2 Molecular genetic results....124
8.4 Discussion....128

9 CHAPTER NINE – SPATIAL AND TEMPORAL FRMD7 EXPRESSION PROFILING DURING MURINE DEVELOPMENT....135

9.1 Introduction....135

9.2 Methods.....136
9.2.1 Preparation of cDNA samples.....136
9.2.2 Quantitative real time PCR protocol.....136
9.2.3 Data analysis methods.....138
9.3 Results.....140
9.3.1 Assessment of assay validity.....140
9.3.2 Changes in FRMD7 gene expression during murine development.....151
9.4 Discussion.....155

10 CHAPTER TEN – A SURVEY OF FRMD7 EXPRESSION 159

10.1 Introduction.....159
10.2 Tissues used in this experiment.....160
10.3 Methods.....161
10.3.1 Differentiation and RNA extraction from SHSY5Y cells 161
10.3.2 Differentiation and RNA extraction from Y-79 cells 162
10.3.3 RNA extraction from human adult kidney tissues.....163
10.3.4 Imaging of cell lines during differentiation protocols.....163
10.3.5 Quantitative real time PCR protocol.....164
10.3.6 Data analysis methods.....165
10.4 Results.....165
10.4.1 Differentiation of SHSY5Y cells.....165
10.4.2 Immunohistochemistry results.....172
10.4.3 Differentiation of Y-79 cells.....174
10.4.4 Relative expression in SHSY5Y and Y-79 cells.....175
.....177
10.5 Discussion.....182

11 CHAPTER ELEVEN – FINAL DISCUSSION.....184

11.1 Thesis summary.....184
11.2 Future work.....185
11.2.1 Clinical and genetics studies.....185
11.2.2 Understanding the function of FRMD7 192
11.2.3 Summary of future work.....194

PUBLICATIONS ARISING FROM THIS WORK.....225

List of Figures

FIGURE 1 CLASSIFICATION OF EARLY ONSET NYSTAGMUS (EON) BY CASTEELS ET AL.....21

FIGURE 2 BASIC NYSTAGMUS WAVEFORMS. 22

FIGURE 3 A SUGGESTED CLASSIFICATION SYSTEM FOR FIXATION INSTABILITIES.....31

FIGURE 4 INSTRUCTIONS FOR USING THE ORAGENE DNA SALIVA KIT. .42

FIGURE 5 INSTRUCTIONS FOR USING THE DNA SPONGE COLLECTION KIT FOR CHILDREN.....45

FIGURE 6 INSTRUCTIONS FOR USING THE MOUTH-BRUSH DNA COLLECTION METHOD.....46

FIGURE 7 A HIGH QUALITY DNA SAMPLE MEASURED ON THE NANODROP® ND-1000 SPECTROPHOTOMETER.....50

FIGURE 8 A TYPICAL HIGH RESOLUTION (HRM) MELT CURVE. 62

FIGURE 9 A COMPARISON OF 2 METHODS OF RNA EXTRACTION AND CDNA SYNTHESIS. 68

FIGURE 10 PEDIGREE 1; A LARGE APPARENT X-LINKED CONGENITAL IDIOPATHIC NYSTAGMUS PEDIGREE.....78

FIGURE 11 SKALAR IRIS IR LIGHT EYE TRACKER EQUIPMENT USED FOR EYE MOVEMENT RECORDINGS.....79

FIGURE 12 EYE MOVEMENT RECORDINGS FROM A PEDIGREE WITH CIN (PEDIGREE 1). 84

FIGURE 13 MULTIPOINT LOD SCORE RESULTS.....87

FIGURE 14 HAPLOTYPE ANALYSIS FOR NYSTAGMUS PHENOTYPE TRANSMISSION IN PEDIGREE 1. 88

FIGURE 15 DIAGRAM OF THE X CHROMOSOME SHOWING THE Q24-Q26 LOCUS FOR X-LINKED CIN. 91

FIGURE 16 THE CEREBELLAR DEGENERATION-RELATED PROTEIN 1 (CDR1) GENE SEQUENCE. 94

FIGURE 17 A COMPARISON OF REFERENCE MRNA SEQUENCES FOR THE CDR1 GENE.....97

FIGURE 18 PRIORITISED GENES IDENTIFIED FROM WITHIN A NYSTAGMUS LOCUS.....99

FIGURE 19 A RESTRICTION ENZYME DIGEST ANALYSIS OF AN FRMD7 VARIATION.....103

FIGURE 20 X-LINKED CONGENITAL NYSTAGMUS PEDIGREES. 106

FIGURE 21 A SINGLE STRANDED CONFORMATION POLYMORPHISM (SSCP) GEL. 108

FIGURE 22 AN ILLUSTRATION OF THE MUTATIONS IDENTIFIED IN THE FRMD7 GENE. 111

FIGURE 23 A PEDIGREE DIAGRAM OF A FAMILY WITH ATYPICAL HEREDITARY NYSTAGMUS. 119

FIGURE 24 ELECTROPHEROGRAM RESULTS OF DIRECT SEQUENCING FOR THE CACNA1A GENE. 125

FIGURE 25 CO-SEGREGATION OF A VARIATION IN A NYSTAGMUS PEDIGREE. 126

FIGURE 26 VALIDATING A HIGH RESOLUTION MELT (HRM) ASSAY. 127

FIGURE 27 A HIGH RESOLUTION MELT (HRM) ASSAY OF A CACNA1A GENE VARIATION.....128

FIGURE 28 AN ILLUSTRATION OF THE LOCATIONS OF PATHOGENIC MUTATIONS IN THE CACNA1A GENE.....131

FIGURE 29 EVOLUTIONARY CONSERVATION OF THE CACNA1A GENE. 133

FIGURE 30 AN AMPLIFICATION PLOT FROM A REAL-TIME QUANTITATIVE PCR RUN. 140

FIGURE 31 A CALIBRATING AMPLIFICATION PLOT FROM A REAL-TIME QUANTITATIVE PCR RUN. 142

FIGURE 32 A MELT CURVE ANALYSIS SHOWING SPECIFIC PCR PRODUCT AMPLIFICATION.....143

FIGURE 33 A MELT CURVE ANALYSIS FROM A REAL-TIME QUANTITATIVE PCR RUN. 144

FIGURE 34 STANDARD CURVES FOR THE QPCR ASSAYS FOR 2 HOUSEKEEPING GENES. 146

FIGURE 35 A MELT CURVE ANALYSIS FOR THE FRMD7 QPCR ASSAY.. 147

FIGURE 36 A MELT CURVE ANALYSIS FOR THE FRMD7 CALIBRATION CURVE QPCR ASSAY. 148

FIGURE 37 A STANDARD CURVE FOR A QPCR ASSAY FOR THE FRMD7 GENE.....149

FIGURE 38 RELATIVE EXPRESSION PROFILES FOR THE FRMD7 GENE. 155

FIGURE 39 DIFFERENTIATION OF SHSY5Y CELLS. 167

FIGURE 40 MORPHOLOGY OF SHSY5Y CELLS AFTER 24 HOURS OF DIFFERENTIATION.....170

FIGURE 41 MORPHOLOGY OF SHSY5Y CELLS AFTER 10 DAYS OF DIFFERENTIATION.....171

FIGURE 42 IMMUNOSTAINING OF DIFFERENTIATED AND UNDIFFERENTIATED SHSY5Y CELLS. 173

FIGURE 43 DIFFERENTIATION OF Y79 CELLS. 174

FIGURE 44 STANDARD CURVES FOR THE HUMAN PROBE BASED QPCR ASSAYS. 177

FIGURE 45 RELATIVE EXPRESSION OF FRMD7 IN 3 TISSUES.....181

FIGURE 46 ANNOTATION OF THE FRMD7 GENE SEQUENCE.....187

List of tables

TABLE 1 ANTIBODIES USED IN THIS RESEARCH. 76

TABLE 2 INFRA RED LIMBAL NYSTAGMOLOGY IN AFFECTED MEMBERS OF A NYSTAGMUS PEDIGREE (PEDIGREE 1). 83

TABLE 3 TWO POINT LOD SCORE RESULTS FOR NYSTAGMUS PHENOTYPE IN PEDIGREE 1.....85

TABLE 4 TWO POINT LOD SCORE RESULTS FOR NYSTAGMUS PHENOTYPE IN PEDIGREE 1 86

TABLE 5 SEQUENCING PRIMERS FOR THE CEREBELLAR DEGENERATION-RELATED PROTEIN 1 (CDR1) GENE.....94

TABLE 6 CANDIDATE NYSTAGMUS GENES SCREENED FOR MUTATIONS. 101

TABLE 7 PCR PRIMERS USED FOR SEQUENCING THE FRMD7 GENE....102

TABLE 8 MUTATIONS IDENTIFIED IN THE FRMD7 GENE. 109

TABLE 9 HUMAR AND ZNF261 X-INACTIVATION ASSAYS FOR PEDIGREE 1. 114

TABLE 10 SUMMARY OF NYSTAGMUS WAVEFORMS IDENTIFIED IN THE VNCM PEDIGREE. 124

TABLE 11 RESULTS OF A REAL-TIME QUANTITATIVE PCR RUN.....141

TABLE 12 RESULTS OF A REAL-TIME QUANTITATIVE PCR ANALYSIS. .150

TABLE 13 AN EXAMPLE OF THE METHOD FOR ANALYSIS OF COMPARATIVE EXPRESSION LEVELS. 179

List of commonly used abbreviations

CIN	Congenital Idiopathic Nystagmus
EON	Early Onset Nystagmus
VEP	Visual Evoked Potential
ERG	Electroretinogram
OCA	Oculo-Cutaneus Albinism
VOR	Vestibulo Ocular Reflex
SNP	Single nucleotide polymorphism
SSCP	Single strand conformational polymorphism
HRM	High Resolution Melt
PCR	Polymerase Chain Reaction
ELB	Erythrocyte Lysing Buffer
NLB	Nuclear lysis buffer
TAE	Tris acetate buffer
FRMD7	FERM domain containing 7
LD	Linkage disequilibrium
PAN	Periodic Alternating Nystagmus
CACNA1A	Calcium channel, voltage-dependent, P/Q type, alpha 1A subunit
EA2	Episodic Ataxia Type 2
SCA6	Spinocerebellar Ataxia Type 6
FHM	Familial Hemiplegic Migraine
MLN	Manifest Latent Nystagmus
EOM	Extra Ocular Muscles
GAPDH	Glyceraldehyde-3-phosphate dehydrogenase
ACTB	Actin, beta
CAMP	Cyclyc AMP
FBS	Foetal Bovine Serum

1 CHAPTER ONE – Introduction

1.1 The unique X chromosome

1.1.1 Introduction

The X chromosome holds a unique place in the history of medical genetics. Identification of X-linked diseases is enhanced by the relative ease of recognizing this mode of inheritance. Furthermore, a disproportionately large number of disease conditions have been associated with the X chromosome because of the phenotypic consequence of a recessive mutation which is revealed directly in males. This occurs because all males are constitutionally hemizygous for any gene that has no active counterpart on the Y chromosome. Thus, although the X chromosome contains only 4% of all human genes, almost 10% of diseases with a mendelian pattern of inheritance have been assigned to the X chromosome (307 out of 3,199; information obtained from the OMIM2TM repository (Online Mendelian Inheritance in Man). These aspects of the medical genetics of the X chromosome have greatly stimulated progress in the positional cloning of many genes associated with human disease.

Identifying genes involved in rare conditions yields important biological insights. For example, discovery of mutations in the SH2D1A gene[1] (involved in X-linked lymphoproliferative disease (XLP, OMIM 308240)) led to identification of a new mediator of signal transduction between T and NK cells, and a novel family of proteins involved in the regulation of the immune response. Discovering the genes for these and other rare, monogenic disorders is of critical value in extending our understanding of fundamental new processes in human biology, and the annotated X chromosome will further facilitate this process[2].

1.1.2 X-inactivation

One of two X chromosomes is randomly inactivated in each cell early in female embryonic development[3], so that it becomes transcriptionally inactive and thereby

equalizes the dosage of X-linked genes between males and females. Each daughter cell then inactivates the same X chromosome as its parent such that cells are clonally expanded with a particular X chromosome inactivated. After this period, techniques able to distinguish between the two X chromosomes can be used to track the fate of the two different cellular populations. Initially, distinction was achieved using polymorphic enzyme variants[4], but, more recently, the fact that placental mammals methylate the inactive X chromosome and certain restriction enzymes selectively cut the unmethylated allele, has allowed more widespread application[5]. In particular, the human androgen receptor locus has been found to be useful due to its high degree of heterozygosity (about 90%) [6]. Interestingly, many tumours, including leukaemias, myelodysplasia, and myeloproliferative disorders, have been shown in this way to express only one X chromosome, implying derivation from a single cell[7-10].

The process of X-inactivation is complex and poorly understood. In humans the process involves methylation and modification of the chromatin structure of the inactivated X chromosome resulting in a condensed, hyper-chromatinized structure called the Barr body. This process occurs before the gastrula stage of embryonic development and probably at the late blastula stage when cells are differentiating from pluripotent and totipotent lineages[11]. The process is thought to be controlled by 2 important genes and their regulatory elements: the X inactive specific transcript gene (XIST) and its antisense partner, the X-inactivation-Specific Transcript-Antisense gene (TSIX)[12-15]. These genes are located within a region of the X chromosome called the X-inactivation centre (XIC/Xic). It is believed that the two X chromosomes within a cell physically interact (observed using fluorescence in situ hybridization (FISH)) at which time the XIC from each chromosome are in direct contact. Following this, the TSIX mRNA levels on the chromosome to be inactivated, rapidly plummet for unknown reasons. This reduction in TSIX causes alterations in the chromatin structure of the DNA at the XIC region resulting in a closed, hetero-chromatinized structure. Paradoxically, this causes the XIST gene in this region to increase expression and XIST mRNA then coats the X chromosome to be inactivated, rendering it inactive. TSIX also interacts with a molecule

that attaches methyl groups to the XIST promoter, which inactivates it. This possibly represents a secondary mechanism for ensuring the XIST gene is inactivated on the active X chromosome. The X-inactivation that ensues is believed to be random as to whether the maternal or paternal X is inactivated. X-inactivation ratios in tissues then follow a binomial distribution. This phenomenon has been used to explain the observation of manifesting female carriers of X-linked recessive diseases due to variable degrees of silencing the X chromosome harbouring the disease gene. However, some tissues have been shown to exhibit skewed X-inactivation such that its constituent cells tend to show inactivation of one or other X chromosomes to a greater degree than would be expected by chance. Again this phenomenon has been used to explain manifesting female carriers of X-linked recessive diseases where females have a phenotype which is equally as severe as affected males suggesting near total silencing of the 'normal' X chromosome. Mechanisms underlying skewed X-inactivation have been proposed and comprise both stochastic and non-stochastic processes. Firstly, a "selective advantage" of one X chromosome over the other is a well-described phenomenon in the extreme case where one X chromosome is known to carry a disease gene and appears to be selected against[16;17]. That this mechanism can operate in the absence of an obviously deleterious phenotype has also been shown in cats, where the X chromosome of the Geoffroy cat has a selective advantage over that of the domestic cat[18]. Secondly, because it is believed that stem cell division may stochastically result in zero, 1, or 2 daughter stem cells, certain stem cells may become overrepresented or correspondingly underrepresented by chance[19-21]. Thirdly, expansion of a clone derived from a single stem cell or stem cell precursor may occur with a proliferate advantage (cell selection)[21;22] and therefore by overrepresented. Fourthly, mutations or polymorphisms affecting the control of X-inactivation such as those occurring at the X-inactivation centre or the X inactive specific transcript gene may skew inactivation ratios [16;23]. All of these proposed mechanisms lead to a somewhat confusing picture.

To prove definitively that X-inactivation is responsible for an observed phenotype would be difficult and would require some knowledge of how a phenotype is

caused (including which cell population or tissue is responsible), whether the abnormal phenotype causes cell selection and what the tolerance to abnormal gene product levels are. Similarly, it would be necessary to show that the tissue sampled, is indeed responsible for the phenotype. This is because of the observation that although in normal females X-inactivation ratios are often similar between tissues[24], for certain X-linked conditions complete skewing may be restricted to specific cell lineages and different patterns of X-inactivation are seen in all other tissues[25]. Furthermore, approximately 15% of X-linked genes escape X-inactivation to some degree, and this proportion of genes differs dramatically between different regions of the X chromosome[26;27] reflecting the evolutionary history of the sex chromosomes. An additional 10% of X-linked genes show variable patterns of inactivation and are expressed to different extents from some inactive X chromosomes[27].

Therefore, the degree of X-linked gene expression heterogeneity among females is great and complex. Methods of assessing X-inactivation and its contribution to phenotype are therefore accompanied by an array of important caveats.

1.2 Eye movements

Eye movements have evolved to subserve the specific visual requirements of particular organisms. For example, afoveate animals such as the rabbit (who lack a fovea; an area of the retina with the best visual discriminatory function) need eye movements primarily to stabilize the eyes in space during head movement. To this end, two distinct mechanisms evolved to stabilize images on the retina during such head perturbations. The first comprises the Vestibulo-Ocular Reflexes (VOR), which depend on the ability of the labyrinthine mechanoreceptors to sense head accelerations. The second consists of visually mediated reflexes (Optokinetic and Smooth-pursuit tracking), which depend on the ability of the brain to determine the speed of image drift on the retina. Together, these reflexes stabilize the angle of gaze and eyes remain pointed at the object of regard whenever the head is moving[28].

With the development of the fovea it became necessary to change the line of sight independently of head movements. Eye movement subsystems evolved both to bring eccentric targets onto the fovea (foveation) and keep it there[28]. Saccades are fast foveating eye movements that bring the object of interest onto the fovea. This function was described elegantly as early as the late nineteenth century by the American Ophthalmologist William James who said;

"The peripheral retina is like a Sentinel and when an object of regard falls upon it, it shouts 'hark, who goes there' and calls the fovea to the spot."[29]

However, it is also necessary to hold even stationary objects on the fovea and for this purpose a gaze-holding system evolved which constantly holds the object of regard on the fovea and prevents the gaze from drifting off target.

With the evolution of frontal vision and binocularity came a requirement to place an object of interest on the fovea of both eyes simultaneously. Vergence movements are binocular movements which achieve this aim by moving the eyes simultaneously in opposite directions such as adduction of one eye and abduction of the other.

Therefore, it can be seen that for foveate primates such as humans, the ocular motor system consists of several subsystems that generate different types of eye movements in response to different stimuli[30].

1.3 Nystagmus

'Never write about nystagmus, it will lead you nowhere'. (Wilbrand 1921[31])

1.3.1 Introduction

Nystagmus is a disorder of eye movement which can be defined as "a repetitive, to-and-fro movement of the eyes that is initiated by slow phases"[30].

The word nystagmus is derived from a Greek word 'nustagmos' meaning nodding of the head or drowsiness. The word is thought to have evolved due to a comparison with slow downward drift and sudden upward jerk of the head during drowsiness[32].

In humans, there are three main control mechanisms for maintaining steady gaze; the fixation movements, the vestibulo-ocular reflex; and the gaze-holding system[30]. Failure of any of these control systems will bring about a disruption of steady fixation. Two types of abnormal fixation can result; nystagmus and saccadic intrusions/oscillations. The difference between them lies in the initial movement that takes the line of sight away from the object of regard. The initial anomalous movement in saccadic intrusions/oscillations is a fast saccadic movement. In the case of nystagmus, it is a slow drift or 'slow phase' away from the target[30] such that the corrective saccade (quick phase) is a normal compensatory movement. It has been suggested that that nystagmus results from an anomaly within the gaze-holding pathways or the tissues comprising the brainstem mechanism that generates the tonic innervation needed to maintain lateral gaze (neural integrator) [30;33;34].

1.3.2 Early descriptions

One of the first known descriptions of nystagmus is that found in case 99, picture 855 of the Ebers Papyri (c. 1500 BC)[35;36]. These are a collection of medical papyri comprising 250 pictures and 887 paragraphs depicting and describing medical scenes. It has been suggested that these may be copies of even earlier work by Imhotep the vizier,

physician, architect and high priest of Heliopolis in the 3rd dynasty of ancient Egypt. In either case, these probably represent the first recorded descriptions of nystagmoid eye movements and may date back to as early as c.2800 BC.

1.3.3 Significance

Many different forms of nystagmus exist and it occurs in a wide variety of pathological and non-pathological situations. For example it occurs as a normal finding on extreme eccentric gaze (end-point nystagmus) or when viewing passing objects from a moving train (opto-kinetic nystagmus). Conversely, very similar eye movements may herald the onset of significant neurological disease or represent the earliest neurological sign in an infant with a devastating visual or neurological condition[37]. Little is understood about which tissues malfunction to cause nystagmus or indeed which tissues communicate to allow eye movement control in healthy subjects[38]. Consequently, with such complexity and ambiguity surrounding the significance of its presence, physicians have attempted to understand nystagmus by classification since its earliest descriptions.

1.3.4 Classification of Nystagmus

Nystagmus forms part of a larger group of eye movement disorders called fixation instabilities. It differs from other fixation instabilities such as Saccadic intrusions and Saccadic oscillations as it is thought to arise primarily from an abnormality in the slow pursuit eye movement system or the system which holds eccentric gaze rather than being a disorder of the saccades[30].

Over 40 different named types of nystagmus are described and the nomenclature is exceptionally inconsistent, with some types being identified by an eponym (for example, Bruns' nystagmus), by behaviour (gaze-evoked nystagmus), by direction (downbeat nystagmus) or by age of onset (early onset nystagmus)[39]. It is likely that this has arisen due to a number of factors including a lack of knowledge of; its aetiology, its underlying anatomical basis, the significance of minute features of the

specific phenotype, the ever increasing number of clinical situations in which it forms a part and the fact that nystagmus is relatively common. Consequently, many complex classifications and descriptions have arisen all of which were designed for, and are therefore biased in favour of, a specific use.

1.3.4.1 Ophthalmologists classification of nystagmus in infancy

Nystagmus before six months of age can be defined as early onset nystagmus[37]. It may be divided into three categories: sensory defect nystagmus (SDN) in which there is a proven sensory impairment, congenital idiopathic nystagmus (CIN) also known as "motor nystagmus" in which no visual or neurological impairment can be found and neurological nystagmus (NN) which is associated with neurological disease[37]. The sensory type occurs as a result of aberrant visual stimulation and most commonly with recognisable genetic ocular diseases such as albinism, X-linked congenital stationary night blindness and Leber congenital amaurosis[37]. In the case of CIN, visual acuity may be decreased by the decreased foveation time but is usually well preserved. It is presumed that this form of nystagmus represents a primary defect in the parts of the brain responsible for ocular motor control although as yet its pathophysiological aetiology is unknown[37].

This classification system for nystagmus is often used in conjunction with other methods such as description by phenotype.

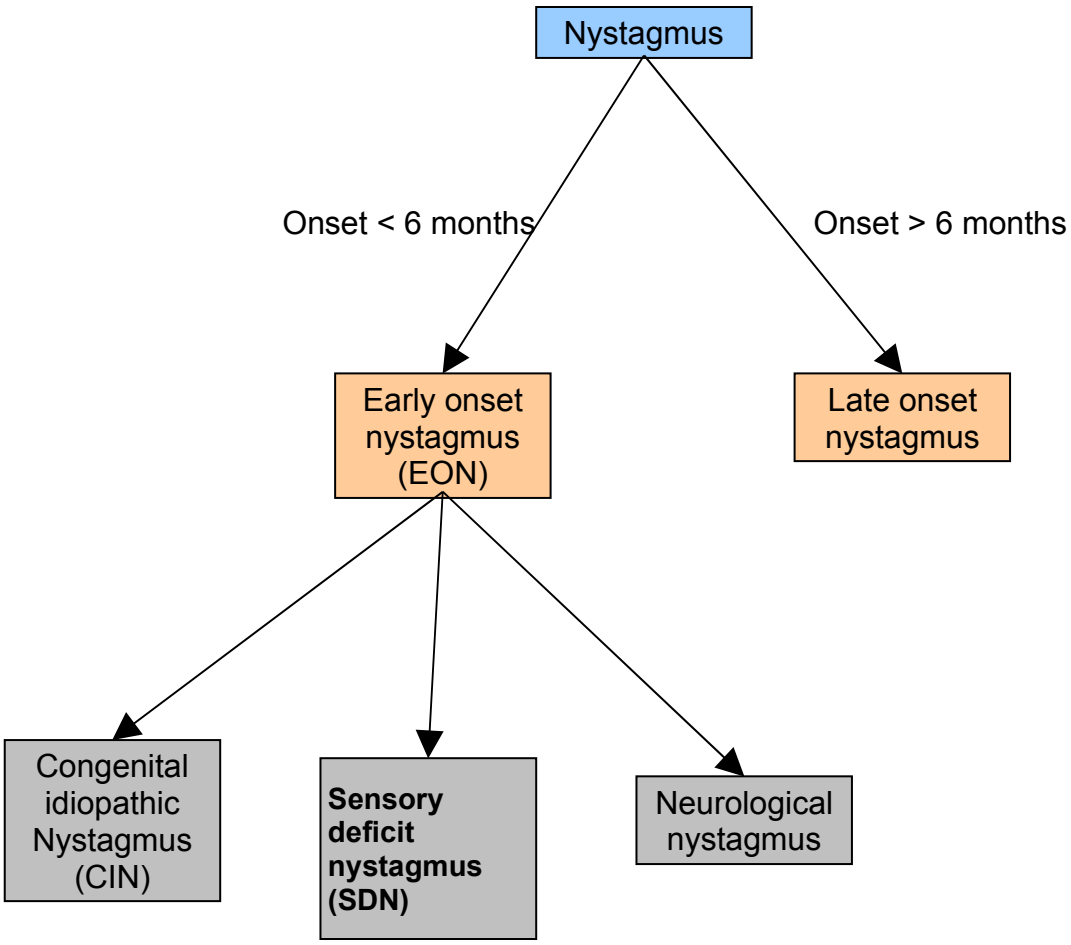

Figure 1 **Classification of Early Onset Nystagmus (EON) by Casteels *et al***

1.3.4.2 Classifying nystagmus by phenotype:

Classifying Nystagmus by its detailed clinical features is complex and few features are pathognomic of any particular underlying aetiology. However, some features can be indicative of specific aetiologies when used in conjunction with other clinical information.

1.3.4.2.1 Slow - phase characteristics

The broadest classification of nystagmus by phenotype is into either jerk or pendular waveform. Jerk nystagmus refers to an abnormal slow movement followed by

a corresponding fast movement in the opposite direction. Pendular nystagmus refers to a slow movement followed by a similar slow movement in the opposite direction. Jerk nystagmus can be further subdivided by the morphology of the slow phases into accelerating, linear or decelerating slow phase[37]

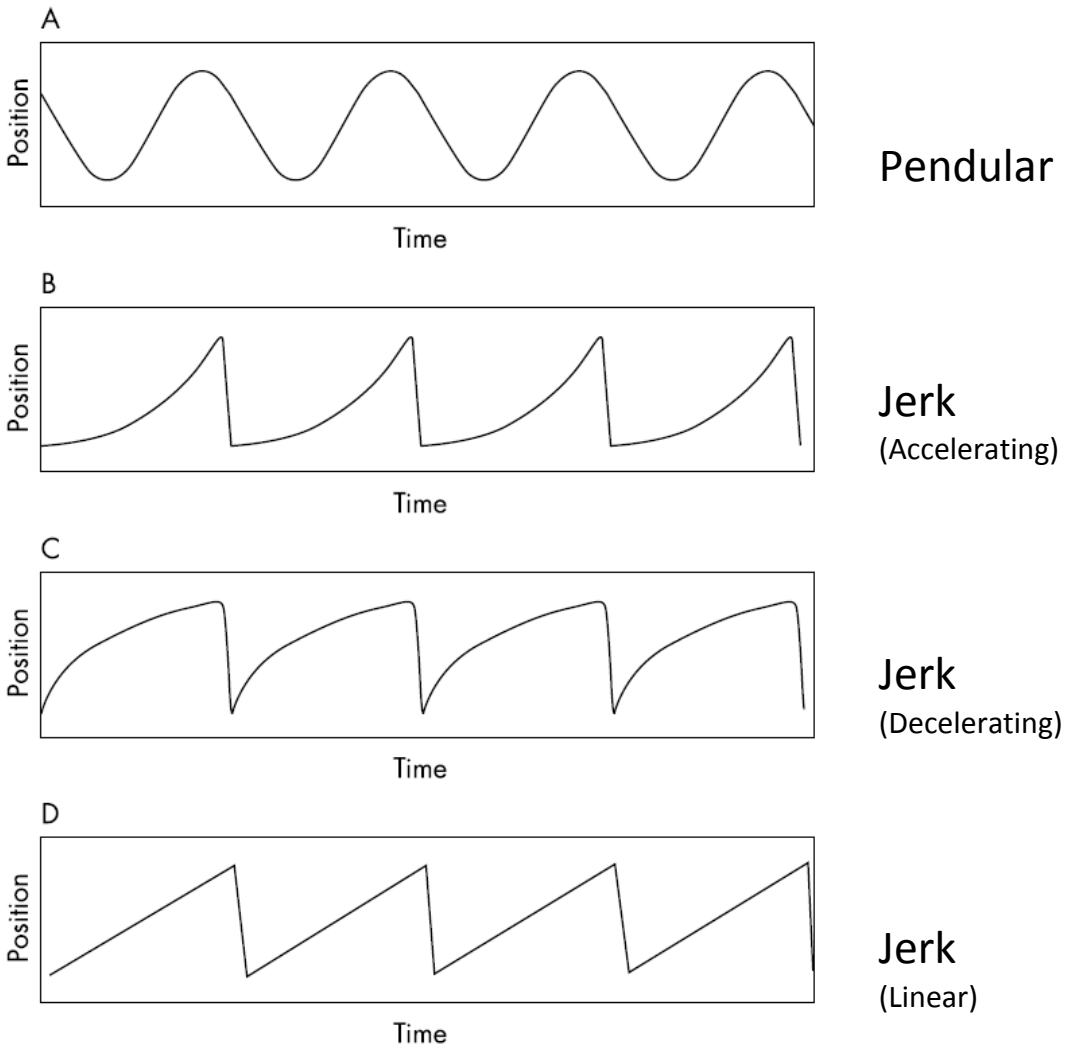

Figure 2 Basic Nystagmus waveforms.

* adapted from Abadi *et al* 2002.

A schematic illustration of nystagmus waveforms. (A) pendular nystagmus, (B) an accelerating velocity exponential slow phase jerk nystagmus (CIN), (C) a decelerating exponential slow phase jerk nystagmus (MLN), (D) a linear or constant velocity slow phase jerk nystagmus (MLN). In (A) a slow phase is followed by a slow phase while in (B)–(D) a slow phase is followed by a fast phase.

1.3.4.2.1.1 Accelerating slow phase

Typically, infants with CIN are thought to have waveforms with characteristic features including uni-planar jerk nystagmus with accelerating slow phases[37]. Indeed Jerk nystagmus with accelerating slow phases when horizontal, has been described as pathognomic for CIN[37] (although it has also been seen in the vertical plane in downbeat nystagmus associated with an Arnold-Chiari malformation). However, there is increasing evidence that jerk nystagmus with accelerating slow phases does not distinguish CIN from SDN[37]. Eye movement recordings have revealed at least 12 distinct waveforms associated with SDN and CIN[37] consisting of variants of pendular, jerk and mixed types, with no correlation between waveform and aetiology[37;40;41] and even affected monozygotic twins can have different waveforms[42;43]. Acquired accelerating slow phase jerk nystagmus, caused by a cerebellar lesion in an adult has also been described[44].

1.3.4.2.1.2 Linear and decelerating slow phase

Jerk nystagmus with a linear slow phases has been reported in CIN, SDN and NN[40;45]. Jerk nystagmus with decelerating slow phases is usually associated with latent nystagmus or NN but sometimes CIN or SDN[37]. It is most often seen when the neural integrator is defective and thereby allows the eyes to drift back towards the primary position[39]. Because this form of nystagmus, when acquired, occurs in lateral gaze positions that bring out the inadequacy of the integrator mechanism, such nystagmus is often known as gaze-evoked nystagmus. It is rarely the predominant waveform in CIN but may be seen in instances of damage to the cerebellum[37]; it also arises when gaze maintenance is affected by drugs, such as alcohol[46;47].

1.3.4.2.1.3 Pendular waveform

If nystagmus is always pendular, clinical context is crucial in determining whether such an oscillation is acquired or congenital, although eye movement recordings may be useful in many cases. For example a pendular congenital nystagmus often contains small saccades that arrest the eyes at one side of the oscillation[37] or becomes jerk nystagmus in extreme gaze[39]. However, in most cases and when eye movement recordings are not possible, pendular nystagmus with no quick phase is not diagnostically useful as it can be due to either CIN, SDN or NN[48].

1.3.4.2.1.4 Nystagmus direction

Nystagmus waveform can also be broadly classified by direction into horizontal, vertical, cyclorotational (torsional/circular) or a mixture of any of these types e.g oblique. Other patterns exist including 'Gaze evoked nystagmus' but are not included here.

1.3.4.2.1.5 Differences between CIN and SDN nystagmus direction

Although vertical, oblique and rotational congenital nystagmus have been reported, the great majority of CIN patients have a mainly horizontal nystagmus, albeit sometimes with a minor torsional component[37]. Patients with SDN however, are more likely to have complex and multidirectional nystagmus and more often have a torsional component[37]. One of the striking features of typical CIN is that this horizontal oscillation often remains horizontal, even in vertical or oblique directions of gaze[37].

1.3.4.2.1.6 Vertical nystagmus

Vertical nystagmus may be present as part of gaze evoked nystagmus in which the nystagmus direction varies with the position of gaze and does not remain vertical[30].

Up beating nystagmus has been reported in association with Wernicke's encephalopathy, multiple sclerosis, brainstem infarction and other lesions. It is thought to be caused by lesions of the medulla, the ventral tegmentum, the anterior vermis of the cerebellum, and the adjacent brachium conjunctivum and midbrain. It is also found in smokers as a side effect of nicotine, and as a side effect of other medications[49;50].

Down beating nystagmus is classically attributed to the Chiari malformation. Numerous large studies have been published, largely concluding that while the Chiari malformation may contribute as many as 1/3 of cases, cerebellar degenerations, demyelinating disease, drug toxicity, neoplasia, and "idiopathic" are other common causes[30].

Early onset vertical nystagmus is often associated with toxic causes[37], intracranial space-occupying lesions or demyelinating disorders[51], though it can sometimes be idiopathic[52] or associated with familial vestibulo-cerebellar disorders[53].

1.3.4.2.1.7 See-saw nystagmus

See-saw nystagmus (SSN) is a very characteristic eye movement comprising intorsion and elevation of one eye, with synchronous extorsion and depression of the other[54]. If the underlying waveform is pendular this is described as classical SSN but if it is jerk, in which case the slow phase corresponds to one half-cycle, this is described as hemi-seesaw nystagmus[54]. Acquired SSN most often occurs with parasellar or chiasmal mass lesions[55-57]. However, a seesaw component has been reported in association with a variety of disorders[58-60] some of which present as forms of congenital nystagmus[55;61;62].

Interestingly, SSN has also been reported with visual loss due to cone-rod dystrophy[63] and a patient who progressively lost vision due to retinitis pigmentosa[64].

One theory suggests that the two variants of seesaw nystagmus probably arise from either imbalance or miscalibration of vestibular responses that normally function to optimize gaze during head rotations in roll[30]. However, Dell'Osso *et al* recently found

sub-clinical SSN embedded in 46.67% of patients with apparent typical horizontal congenital nystagmus waveforms and hypothesized that in this case SSN is due to slight innervational (or force) imbalances of the vertical and oblique extraocular muscles[65]. Therefore, it seems likely that even SSN may results from differing aetiologies.

1.3.4.2.1.8 Periodic Alternating Nystagmus

Acquired periodic alternating nystagmus (PAN) is a spontaneous horizontal nystagmus, present in primary gaze, that reverses direction approximately every 2 minutes[30]. It has been reported in association with a number of conditions, many of which involve the cerebellum[66;67]. It may also occur in a congenital form[68]. In some CIN patients, the nystagmus periodically reverses direction, but this reversal seldom occurs in the regular manner seen in PAN[40;69].

1.3.4.2.1.9 Nystagmus amplitude

Amplitude measurements have little value in either diagnosis or classification of nystagmus[70] although one study suggests that in rod monochromacy, horizontal nystagmus in primary gaze often has pendular and jerk waveforms with much lower amplitude than patients with other SDN[71].

1.3.4.2.1.10 Null position

Another important diagnostic feature of CIN is the presence in the majority of patients of a null position of gaze[39]. This describes a particular position of the eyes within the orbit in which the nystagmus slow-phase velocity is at a minimum. Many patients with EON but few with acquired nystagmus develop the presence of a null position[39;70] so its presence can direct diagnosis and classification. Null positions are also important for management, as treatment options for congenital nystagmus without null positions are currently limited[72].

1.3.4.2.1.11 Visual effort

Congenital nystagmus is often said to intensify with visual effort or near viewing. Most patients can recall instances in which a visual task was necessary but not possible due to worsening of their nystagmus. However, most do not report this phenomenon during clinical examination and it is possible that a combination of psychological factors influence either the nystagmus intensity, or the patient's perception of it[39]. Interestingly, there has been little published research in this area although one study designed to quantify how increased visual demand affects the severity of CN concluded that there was no relationship between the two[73]. This may suggest that either the reported decreased visual function in times of high demand in CN patients is purely a subjective phenomenon or perhaps more likely, the visual tasks asked of CN patients in clinic do not accurately model 'real life tasks'[39]. However, in a different study 44% of CN patients demonstrated a decrease in nystagmus intensity during near fixation (1/3 metre) compared with distance fixation (6 metres)[70]. Results from such studies are therefore variable.

1.3.4.2.1.12 Oscillopsia

In healthy subjects, perceptual stability is maintained only as long as retinal image motion is less than approximately 4°/s[74;75]. In CN, despite slow phases that may exceed 100°/s, oscillopsia is rarely perceived[76]. Conversely, oscillopsia is a common complaint of subjects with acquired types of nystagmus despite the similarly moving retinal images[77].

On careful questioning, many CIN patients describe particular specific short episodes of oscillopsia. Some studies have found that greater than 40% of CIN cases have experienced episodes of oscillopsia and that many of these instances are associated with exacerbations of the nystagmus by fatigue, illness, stress or looking in their 'non-preferred' gaze direction[78].

The mechanism of oscillopsia suppression is not fully understood and explanations have included: reduced sensitivity to retinal image motion, adaptation to

retinal image motion, information sampled only when the eyes are moving relatively slowly during the foveation periods and the use of extraretinal information (efference copy) to cancel the effects of eye movements[79].

1.3.4.2.1.13 Manifest-Latent vs Congenital Nystagmus characteristics

Early onset nystagmus is often grouped into either congenital nystagmus (CN) type or manifest-latent nystagmus (MLN) type[39]. This classification is based on a group of clinical features including slow phase velocity and nystagmus direction under certain viewing conditions. The CN type is classically found in CIN whereas the MLN type is thought to be more commonly seen in SDN. MLN is also closely associated with the presence of strabismus and dissociated vertical divergence[80]. In either case the anomalous eye movements are typically conjugate, horizontal, and jerk. Differential diagnosis is made on the basis that the CN slow phases are typically of an increasing exponential velocity form, whereas in MLN the slow phase is decelerating or linear. Additionally, for monocular viewing, the fast phase of MLN always beats toward the viewing eye which is not the case for CN[80;81]. A third, but less common, type is pure latent nystagmus (LN)[81]. In this type, during binocular viewing conditions, the eyes are steady, but during monocular viewing, bilateral conjugate jerk nystagmus becomes manifest. As for MLN, the LN slow phase is either a decreasing or linear velocity, with the fast phase directed toward the viewing eye[81].

One large study of MLN concluded that MLN and LN should be grouped together as a continuum called Latent Manifest Latent Nystagmus (LMLN) and then subdivided into 4 types based on the ocular movements seen during binocular viewing: Type 1; ocular stability (formally LN), Type 2; square-wave jerks, Type 3; Torsional nystagmus and Type 4; typical MLN waveform. In this study 94.6% of subjects exhibited a single constant MLN subtype throughout all recording sessions [82].

However, the distinction between LMLN and CN is not always clear. For example CN in addition to MLN may show a directional change with occlusion. In CN, this has

been termed a 'latent shift' or a 'latent component'[83]. Furthermore, LMLN and CN may also coexist in a single patient[80].

1.3.4.3 Classification of nystagmus by clinical frequency

Practical clinical classifications are often based on clinical frequency in addition to other criteria such as nystagmus waveform and inheritance pattern. It has been suggested that classifying nystagmus by using a single criterion is unhelpful in the clinical setting as it puts the cart before the horse[84].

1.3.4.4 Summary of Nystagmus classification and nomenclature

As detailed above, common classification systems for nystagmus employ either one, or a combination of the following features:

- Detailed features of the abnormal eye movements
- Observed heritability
- Clinical scenario
- Assumed aetiology
- Clinical frequency

Consequently, classification systems often serve a specific function. For example, a Paediatric Ophthalmologist may use a classification and protocol in the clinical setting whose primary purpose is to identify those paediatric patients who have features suspicious of serious underlying disease (see Figure 1)[37] . Conversely, a clinical geneticist will use a system predominantly in order to describe the underlying mode of inheritance within a congenital nystagmus pedigree.

In 2001 the National Eye Institute sponsored a workshop by the Committee for the Classification of Eye Movement Abnormalities and Strabismus (CEMAS). The remit was to produce a new classification system for eye movement anomalies including nystagmus which was based on up-to-date clinical and scientific information and designed to be used as a resource for scientists, clinicians and educators[85]. However, as can be expected from an 'all encompassing' classification system its overview is neat but for specific uses it falls short for both clinical and research applications. For example the diagnosis of 'Infantile Nystagmus Syndrome' under the CEMAS classification would comprise a multitude of aetiologies and pathologies and if using this classification strictly, different members of the same nystagmus pedigree may have different 'diagnoses'. It seems likely that until the pathophysiological basis of eye movement disorders is fully understood, classification systems and nomenclature will necessarily vary between professionals with differing priorities.

In Figure 3, I suggest a classification system for fixation instabilities which is an amalgam of other systems and geared towards the interests of a clinical Ophthalmologist / Geneticist. This classification system has been used for the work presented in this thesis and in publications arising from it.

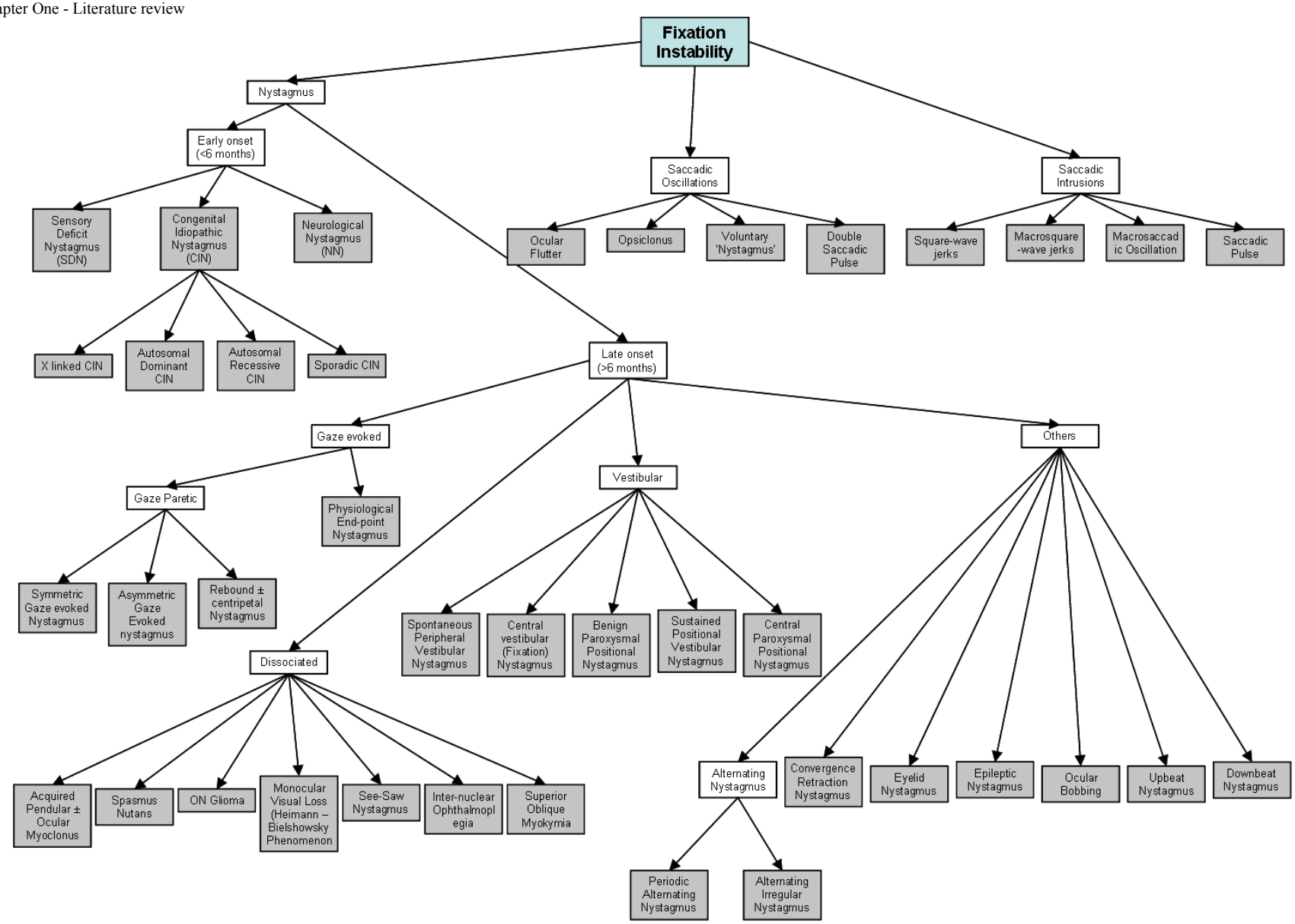

Figure 3 A suggested classification system for fixation instabilities

1.3.5 Pathophysiological mechanisms of nystagmus

The pathogenesis of CIN remains poorly understood, and whether it represents a primary defect in the visual sensory system, or the ocular motor system is unknown. Some insights have arisen from patients with specific neurological injury's[86-92] and have allowed some interpretation as to structures and possible pathways involved in ocular motor stability. Several proposed mechanisms underlying CIN have been suggested but are currently out of favour, these include: the presence of a leaky neural integrator[93], misdirection of the retinogeniculate or subcortical visual pathway[94], and albino-like abnormal chiasmatic decussation of the optic axons[95]. CIN is currently thought by many to represent a primary disorder of some part of the oculomotor pathways, in particular the gaze-holding pathway [93]. Another recent theory has suggested that CIN represents a developmental adaptive response by the gaze-holding pathway to an early sensory anomaly[96]. There is also some support for microscopically anomalous, incompletely developed, or dysmorphic extra-ocular muscle (EOM) ultrastructure in CIN. Findings have described abnormal proprioceptors, muscle fibres, sensory nerve endings and even vascular endothelial cells[97-100]. However, there is no strong evidence that these changes are primary rather than secondary to nystagmus.

It is hoped that identification of the responsible genes and characterisation of their expression should provide insights into the pathophysiology of this disorder and the normal functioning of the ocular motor system[101].

1.3.6 Congenital Idiopathic Nystagmus

CIN as described by Casteels et al[37] is defined as nystagmus occurring before the age of six months and with no identifiable underlying visual or neurological disorder.

1.3.6.1 Inheritance

Prevalence rates for CIN of 1:1000 to 1:1500 have been reported [102;103]. It is genetically heterogeneous as autosomal dominant (MIM 164100), autosomal recessive (MIM 257400) and X-linked (MIM 31700) patterns of inheritance have been reported. It has been suggested that X-linked inheritance with incomplete penetrance is the most common form[104]. It is important to note that the different inheritance patterns cannot be distinguished clinically by visual acuity or waveform characteristics.

1.3.6.1.1.1 Autosomal Dominant CIN

One form of autosomal dominant CIN has been mapped to an 18 cM region on chromosome 6p12. The causative gene was mapped to an 18 cM region between D6S271 and D6S455 by haplotype analysis[105]. However, other autosomal dominant CIN genes also exist, e.g. in a German family with autosomal dominant CIN, exclusion of the 6p12 locus and suggestive linkage to 7p11 has been demonstrated[106]. Interestingly, the 7p11 locus (or possibly a locus on chromosome 15) was has also been implicated when CIN was found to co-segregate with a balanced (7;15t(7;15)(p11.2;q11.2)) translocation in another family with autosomal dominant CIN[107]. Studies of patients with deletions of 18q have shown that within this group, individuals with nystagmus shared deletions between markers D18S812 (68.4 Mb) at 18q22.3 and D18S1141 (75.0 Mb) at 18q23. This suggests that the expression of at least one gene occurring at this site is also important for oculomotor control and the prevention of nystagmus[108]. In a paper by Oetting in 2000, all three presumed autosomal dominant CIN pedigrees showed negative linkage to the 6p12 locus with $Z=-3.82$, $\theta = 0.0$ [109]. In 2004, Hoffman et al. excluded the 6p12, 15q11 and 7p11 loci in a German pedigree[110].

Together these papers suggest at least three distinct loci for autosomal dominant CIN.

1.3.6.1.1.2 Autosomal recessive CIN

No loci have currently been identified for autosomal recessive CIN genes although pedigrees consistent with this mode of inheritance have been described[104].

1.3.6.1.1.3 X-linked CIN

In 1999, two X-linked CIN loci were reported, demonstrating that X-linked CIN is also genetically heterogeneous with a locus for X-linked irregularly dominant CIN reported by Kerrison et al. at Xq26-q27[104] in three families and a family with X-linked dominant CIN by Cabot et al. at Xp11.4 –p11.3[104]. These loci were shown to be distinct when the family reported by Cabot was subsequently excluded by linkage analysis from the Xq26-27 locus (MIM entry 310700). The critical gene interval for these two loci were 18.6 cM on Xp11.4 –p11.3 and 7 cM on Xq26-q27. Subsequently, the Xq26-q27 critical gene interval was narrowed to 5.4 cM in an additional Iowa family[104], and then reduced further by Kerrison et al to 5 cM[101]. In January 2005 an interval within this region was narrowed to 4.4 cM in 22 members of a Chinese family with X-linked CIN. Two genes within this region were screened for mutations (SLC9A6 and FGF13) but no mutations were detected[104]. In 2000 Oetting et al described 5 pedigrees with CIN, two with apparent X-linked inheritance and three with male–male transmission suggesting autosomal dominant inheritance[104]. One of the X-linked families demonstrated suggestive linkage to the Xp11.4 –p11.3 locus with Z=2.08, $\theta = 0.0$. The other X-linked family showed no linkage to either of the previously described loci. In October 2005 *Guo et al* described the first genetic locus for X-linked recessive CIN by linkage analysis of two Chinese pedigrees. These families (a total of 25 subjects) inherit CIN as an apparent X-linked recessive trait with full penetrance. No other ocular disease was identified and no affected females were observed in either family. However, VEP recordings and detailed eye movement recordings were not performed. The disease mapped to Xq23–q27, between markers *DXS8055* and *DXS1205* with a highest LOD score of 3.53 for the marker *DXS1047.* This interval includes the locus described by Kerrison et al for X-linked dominant CIN which raises the possibility that X-linked recessive CIN and X-linked dominant CIN may be caused by the same gene with different mutations as has been

observed in several other genes related to ocular diseases (for example *RP1*[104], *RHO* [111] and *LRP5*[112]). However, linkage to the same region does not rule out the possibility that the disease may result from mutations in different genes at the same gross chromosomal location.

In X-linked CIN pedigrees, penetrance among female obligate carriers has been variable. Values have ranged from 30 to 100%[101;113-115].Reasons for this may include skewed X-inactivation, interactions with other genes, and other non-genetic developmental influences on oculomotor development.

In summary, for X-linked CIN, two loci have been identified, at least one other locus is thought to exist and no genes have currently been identified.

1.3.6.1.1.4 Limitations of previous X-linked CIN linkage work

Several X-linked disorders have been associated with nystagmus, including Nettleship-Falls ocular albinism (Mendelian inheritance Man (MIM) # 300500), complete congenital stationary night blindness (MIM # 310500) and blue cone monochromatism (MIM # 303700). Therefore, as for any 'diagnosis of exclusion' it is important to exclude these other disorders by clinical examination[37;83;84;101], electroretinography (ERG)[37;37;101;101;116-118] and preferably visual evoked potentials (VEP)[37;119;120] before making a diagnosis of X-linked CIN. However, as has been previously noted[101], much of the previous linkage work on X-linked CIN has not included VEP[101;104;121-125] or even ERG[124] to exclude masquerading conditions. This is important because just one of the genetic intervals (Xq26-27) includes genes for; congenital stationary night blindness, retinitis pigmentosa, Norrie disease protein, cone dystrophy, exudative vitreoretinopathy, Aland island eye disease and X-linked optic atrophy. Therefore, nystagmus in pedigrees phenotyped without detailed electrophysiology may, in fact be allelic with one of these disorders [101]. Furthermore, even when exhaustive investigations have been completed it seems likely that the underlying causation may vary such that 'CIN' describes a group of patients with differing underlying pathophysiologys. Therefore, combining multiple

families with apparent CIN may include more than one genetic cause and disrupt linkage results.

Subtle eye movement abnormalities have been detected among relatives of CIN patients[126;127] and it is also known that nystagmus waveform and phenotype may vary significantly, not only within pedigrees but even between monozygotic twins with CIN[42;128]. Therefore, in order to avoid significant assignment errors in linkage projects of CIN it has been suggested that detailed eye movement recordings are performed on family members in order to identify subtle nystagmus which might otherwise go unseen[101]. However, much of the linkage work of CIN has not included anything more for phenotyping than a gross pen-torch examination[101;104;122;124;125]. Furthermore, Zhang et al (2005) published linkage results based on the assumption that nystagmus in their subject pedigree was a truly X-linked dominant trait with 100% penetrance. The results relied on data from 2 apparently unaffected females for whom it was presumed the disease gene had not been inherited. However, this would represent a very unusual inheritance pattern for X-linked CIN and it was done without detailed eye movement recordings. The results were then combined with Kerrison's (2001) linkage data[101] which clearly demonstrated at least 6 females who necessarily carried the gene but do not have nystagmus.

Linkage work in CIN has been varied in its use of statistical analysis. LOD scores[129] (log base 10 of the likelihood ratio under the hypotheses of linkage and non-linkage) are used as a statistical measure of how likely it is that a disease causing sequence change resides within a particular genetic interval. However, a number of factors including; the threshold value for proof of linkage, the method of calculation, and statistical packages used to create LOD scores have varied significantly between X-linked CIN linkage work[130].

Interestingly, there is a discrepancy between the marker order used in the original Kerrison (1999) paper[131] and the latest marker mapping data (UCSE website) possibly due to a contig inversion in the earlier data. This means that the original paper and the subsequent refinement papers will have used incorrect marker locations for

haplotype reconstruction. Therefore, it is possible that the boundaries of the Xq26 interval described by these papers exclude the true nystagmus causing mutation.

In September 2005, following a meeting organised by the Nystagmus Network (http://www.nystagmusnet.org/) I was invited to write a review of CIN genetics by the Journal 'Seminars in Ophthalmology'. This paper included all the current linkage work in CIN, the limitations of previous work and suggestions for the design of future studies. It was published in April 2006[132].

1.3.6.2 Congenital Idiopathic Nystagmus Treatments

An important feature of CIN is the presence in the majority of patients of a null position of gaze; a position in which the nystagmus is least intense and vision is greatest. Even very young children may adopt this to improve their vision. Many simple therapies are intended to shift this null position as close to the primary position as possible, not only to increase acuity but also because nulls in eccentric gaze may lead to the development of another feature of CIN; abnormal head posture. The elimination or amelioration of head postures is important not only for cosmetic reasons but also to eliminate the possibility of later orthopaedic problems arising from long-term abnormal contracture of the neck muscles[39]. The presence of a null is also important because it may lead to disparities between visual acuity measurements[39]. For this reason, gaze-dependent visual acuity tests, both with and without time restriction have been suggested as the most useful measure of visual function in patients with CN[133].

Simple treatment strategies for both head position and head tilts/turns include; positioning of children in the classroom or prism spectacles to accommodate for their null position[39]. Additionally, vision therapy to improve binocular vision may also play a role for some patients with MLN type nystagmus, as restoration of binocularity has been shown to convert MLN to LN in some cases[134].

Null position surgery was first described in 1960[135], and since then more than 20 surgical procedures have been advocated for nystagmus, most of which employ

repositioning of the null, large recessions of all four horizontal rectus muscles, tenotomy of these same muscles or combinations of several of these proceedures[39;136;137]. However, it has been proposed that with so many suggested techniques, the likelihood of multiple operations and the variability of outcome, it seems sensible to reserve surgery for specific patients with particularly troubling symptoms such as oscillopsia (very rare in CIN)[138]. Currently, the majority of patients with nystagmus do not have a surgical treatment except perhaps correction of secondary squints.

Although several types of acquired nystagmus have been found to respond to various medical treatments[139;139-142] reports of drug-related reductions in CIN are often variable and in some cases possibly reflect the effects of sedation rather than a specific improvement in the oscillation itself[39]. While a large number of drugs have been used with mixed success for specific forms of nystagmus (usually acquired types), many patients fail to respond or develop intolerable side effects such as sedation or ataxia[141-144]. However, in recent years some success has been made with Gabapentin (synthetic GABA with unclear action) [145], Memantine (NMDA glutamate receptor blocker)[145] and the potassium channel blocker 4-Aminopyridine[146]. These drugs have been shown to reduce nystagmus waveforms and increase foveation times with some corresponding effects on acuity. However, effects are limited and are seen in only some patients. Currently, no drugs are in routine use for CIN.

Contact lenses have been recommended over spectacles in congenital nystagmus for many years because they have been reported to reduce the nystagmus, in addition to providing refractive correction[147-152]. A possible mechanism for this is provision of tactile feedback to the ocular motor system[39]. A similar approach has been adopted with the use of auditory biofeedback[72;153;154] with limited experimental success. Other suggested treatment modalities have included acupuncture[155] and injection of botulinum toxin into the oculomotor muscles[156;157].

In January 2008, a case report was published in which a patient with CIN had detailed eye movement recordings at 2 separate appointments, one after taking 10mg of cannabis and one after having no cannabis for 3 weeks. This patients eye movement

recordings showed a significant reduction in nystagmus intensity and a corresponding increase in visual acuity after taking cannabis[158]. This is in accord with anecdotal reports from 2 of my CIN patients. This effect has yet to be evaluated in a clinical trial setting.

Currently, most patients with nystagmus and especially those with CIN have no specific treatment of any sort.

1.3.6.3 New CIN work published during the course of this project

Following publication of my linkage work on the Xq26-q27 interval (Chapter 3), in November 2006 Tarpey et al identified 22 nystagmus causing mutations in the FERM domain-containing 7 (*FRMD7*) gene which resides within this refined interval[159]. 16 X-linked families underwent linkage analysis and 15 of these pedigrees had causative *FRMD7* mutations. 42 simplex cases were screened for mutations in this gene and yielded 3 mutations (7%). Therefore, the overall contribution of *FRMD7* mutations to the cause of both X-linked and singleton cases remained relatively unexplored.

2 CHAPTER TWO - Methods

2.1 Standard Laboratory techniques

This section details the standard laboratory techniques used throughout this work.

2.1.1 DNA and RNA collection

DNA and RNA can be collected by a variety of techniques depending on a number of factors including; the source of DNA/RNA required, the age of the patient and the amount of DNA/RNA required. 4 methods were used for this project. These protocols require some pre-made reagents which are listed below:

Proteinase K

Received as powder (Sigma-Aldrich, Dorset, UK)
Disssolve in sterile dH_2O to 50mg/ml
Store at -20°C

Re-suspension buffer

0.438g NaCL
4.9 mls 0.5M EDTA, pH 8
Make up to 100 mls with sterile dH_2O

TE Buffer

1 ml 1M Tris HCL pH 8
200 µl 0.5 M EDTA pH 8
Make up to 100 mls with sterile dH_2O, then autoclave

10% SDS

10g SDS
Make up to 100 mls with sterile dH_2O

6M NaCL

35 g NaCL
Make up to 100 mls with sterile dH_2O

0.5% TBE buffer

500 mls 10% TBE buffer

Make up to 20 L with dH_2O

BPB loading buffer

9.5 mls Formamide
50 µL Tris
20 µL EDTA
215 µL Bromophenol Blue
215 µL Xylenecyanine

2.1.1.1 DNA collection using ORAGENE™ Vial format Saliva collection kits

2.1.1.1.1.1 Sample collection

ORAGENE Vial Format™ (DNA Genotek Inc. Ontario, Canada, www.dnagenotek.com) saliva sampling kits were used for DNA collection. Samples were collected by patients according to the manufacturer's protocol (see Figure 4). Samples were then either frozen immediately or sent by post before freezing.

Instructions for using the ORAGENE DNA saliva kit

The plastic tub has a small pot in it with a lid. The idea is to:

1. Not eat or drink for 30 minutes
2. Undo the white lid and produce saliva (not flem) into the pot.
3. It can be filled over 30 minutes or so, you need to see 2cm's worth of liquid spit.
4. Close the white lid again **firmly** and you will feel the seal at the bottom break.
5. **Invert the pot a few times**.
6. Please label with your name, date of birth and the date you made the sample.

You must read the information sheet and sign the consent form

Then post back to me in the envelope provided (with the consent form)! The samples can last a year at room temperature so there is no rush to send them off.

Thanks again for your help

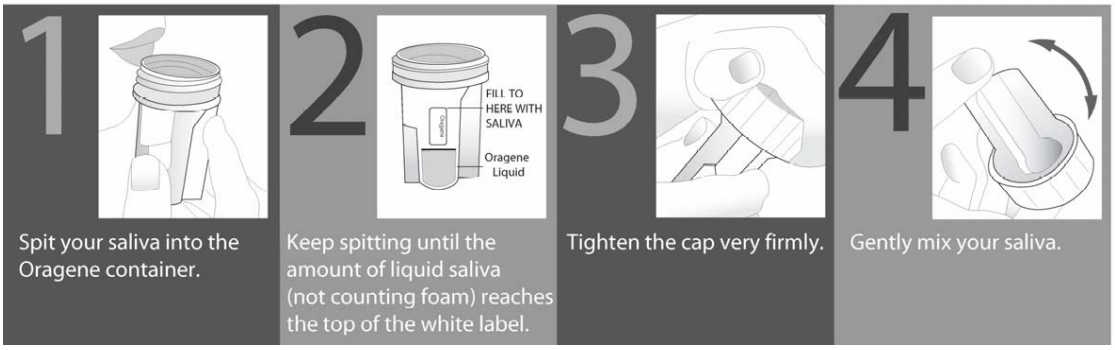

Dr. Jay Self Tel: (0)23 8079 4590 Email: Jes3@soton.ac.uk

Figure 4 Instructions for using the ORAGENE DNA saliva kit

2.1.1.1.1.2 DNA collection from sample

The samples were incubated at 50°C in a water incubator overnight. The sample was then transferred to a 15 mL centrifuge tube and the volume of sample noted. 1/25th of the sample volume of Oragene Purifier was added and mixed for a few seconds. The sample was then incubated on ice for 10 minutes. It was centrifuged at room temperature for 10 minutes at 2800 rpm. The clear supernatant was transferred with a pipette to a fresh 15 mL centrifuge tube and the pellet discarded. An equal volume of room temperature 95% ethanol was added to the supernatant and mixed by inversion. The sample was left to stand at room temperature for 10 minutes. The sample was then centrifuged at room temperature for 10 minutes at 2800 rpm. The supernatant was then poured away, as much of the alcohol was removed as possible and the tube left on the bench with the lid off for 30 minutes. Once dry, the DNA pellet was dissolved in 500 µL TE buffer, vortexed and left overnight to dissolve. The sample was then vortexed again and frozen when the pellet had dissolved.

2.1.1.2 DNA collection using ORAGENE™ Saliva Sponge format collection kits

2.1.1.2.1.1 Sample collection

ORAGENE Saliva Sponge format kits™ (DNA Genotek Inc. Ontario, Canada, www.dnagenotek.com) were used for DNA collection from children too young to produce sputum via the ORAGENE Vial method. Samples were collected by parents according to the manufacturer's protocol (see Figure 5). Samples were then either frozen immediately or sent by post before freezing.

Instructions for using the DNA sponge collection kit for children

Collecting Saliva

1. Place the saliva sponge into the child's mouth in the *cheek pouch* (the space between the gums and the inner cheek). Gently move the saliva sponge around the upper and lower cheek pouches on both sides of the mouth to soak up as much saliva as possible. There is no need to 'scrape' the inner cheek with saliva sponges – simply collect as much saliva as possible from the cheek pouches. The sponge will absorb more saliva if it is left in the child's mouth for a longer time (up to 60 seconds).

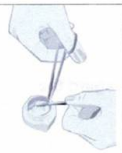

2. Once collected, cut the sponge into the blue base of the Oragene kit as follows. Place the sponge firmly against the bottom of the kit between the tooth and the kit wall (see picture below). This action will ensure that the sponge tip remains in the container during the cutting action. Using the scissors provided, cut the narrow part of the handle just above the sponge.

   Recycle/discard the plastic handle. If only one saliva sponge sample is to be collected, proceed to step 4.

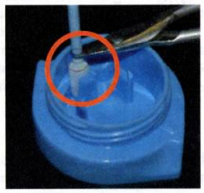

3. For the collection of up to 5 saliva sponge samples from the same child, repeat steps 1 and 2. Follow the sequence shown in the diagram below. A rest period of about 5 min between each collection of 2 sponges is helpful. To prevent the saliva samples from drying out, cap the vial (see step 4) within 15 min of the first collection. If you have not had a chance to collect all 5 sponges within 15 minutes, you may carefully re-open the kit. If you remove the cap be sure that the inside is facing upwards when putting it on any surface. Do not spill the contents.

   Follow these steps for collecting multiple sponges:

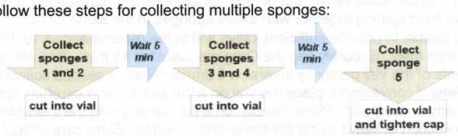

4. Carefully cap the kit and tighten it firmly. Once the Oragene liquid is released from the cap, it will preserve the DNA collected by the sponge(s).

5. Invert gently 5 times to mix the sample.
6. If the scissors are to be re-used, they should be rinsed with tap water and wiped dry between donors.

You must read the information sheet and sign the consent form

Then post back to me in the envelope provided (with the consent form)! The samples can last a year at room temperature so there is no rush to send them off.

Thanks again for your help

Dr. Jay Self Tel: (0)23 8079 4590 Email: Jes3@soton.ac.uk

Figure 5 Instructions for using the DNA sponge collection kit for children

2.1.1.2.1.2 DNA collection from sample

The sample pot was incubated at 50°C in a water incubator overnight. The free liquid was transferred to a 15 ml conical tube. The barrel of a 5 ml syringe (without plunger) was then put in the same 15 ml tube. The sponges were transferred to the barrel of the syringe using forceps. The 15 ml tube containing the syringe barrel with sponges was centrifuged for 10 minutes at 1000rpm at 20°C. The syringe barrel and dry sponges were then discarded. The final volume in the 15 ml tube was noted. 1/25th of the sample volume of ORAGENE Purifier was added and mixed for a few seconds. The sample was then incubated on ice for 10 minutes. It was then centrifuged at room temperature for 10 minutes at 2800 rpm. The clear supernatant was transferred with a pipette to a fresh 15 mL centrifuge tube and the pellet discarded. An equal volume of room temperature 95% ethanol was added to the supernatant and mixed by inversion. The sample was then left to stand at room temperature for 10 minutes and subsequently centrifuged at room temperature for 10 minutes at 2800 rpm. The supernatant was then discarded, as much of the alcohol removed as possible and the tube left on the bench with the lid off for 30 minutes. The DNA pellet was dissolved in 500 µL TE buffer, vortexed and left overnight to dissolve. The sample was then vortexed again and frozen when the pellet has dissolved.

2.1.1.3 DNA collection using mouth brushes

2.1.1.3.1.1 Sample collection

Plain sterile mouth brushes were used for DNA collection from children too young to produce sputum via the ORAGENE Vial method or the ORAGENE™ Saliva Sponge format. Samples were collected by parents according to a protocol in use in our department (see Figure 6). Samples were then either frozen immediately or sent by post before freezing.

Instructions for Mouth-brush DNA collection

In this pack contains 3 small sterile mouth brushes. The idea is to:

7. Collect the sample when you child has not eaten or drunk for 30 minutes.
8. Undo the black lid on one tube and gently rub the brush inside the left cheek for 10 seconds.
9. Re-sheath the tube and close the black lid again **firmly.**
10. Do the same with the right cheek and then a further time on the left cheek again with the further 2 brushes.
11. Please label with your child's name, date of birth and the date you made the sample.

You must read the information sheet and sign the consent form

Then post back to me in the envelope provided (with the consent form)! The samples can last a year at room temperature so there is no rush to send them off.

Thanks again for your help

Dr. Jay Self Tel: (0)23 8079 4590 Email: Jes3@soton.ac.uk

Figure 6 Instructions for using the Mouth-brush DNA collection method

2.1.1.3.1.2 DNA collection from sample

The first brush was snapped off at 1cm length and put into a 1.5 ml centrifuge tube. 500 µL of re-suspension buffer was added. This tube was vortexed vigorously for 10 seconds. The second brush was then snapped off into another 1.5 ml centrifuge tube and the process repeated. The cell suspensions were then combined in one of the 1.5 ml tubes and both the brushes were placed in the second tube. This tube (with the 2 brushes) was then vortexed again, then centrifuged for 10 seconds at 1000 rpm. Any more liberated cell suspension was combined with the bulk of the sample so that all the collection was now in one of the 1.5 ml centrifuge tubes. 3 µl of proteinase K and 10 µl of 10% SDS were added to the cell suspension. The sample was vortexed and incubated at 37°C overnight, or until clear. The sample was allowed to return to room temperature and 166 µl 6M NaCL was added and the sample vortexed. The sample was then centrifuged for 10 minutes at 9000 rpm. The supernatant was removed into a fresh 1.5 ml tube and 2x the volume of 100% ethanol was added. The sample was incubated at -20°C overnight. Subsequently, it was centrifuged at 9000 rpm for 10 minutes and the supernatant is carefully discarded using a pipette. 150 µl 70% ethanol was added and the sample was centrifuged for 10 minutes at 9000 rpm. The supernatant was carefully removed and discarded and the tube left on the lab bench for 30 minutes to dry the pellet. 50 µl of TE buffer was added and the sample gently vortexed. The sample was then left at room temperature and gently inverted occasionally for 12 hours before storing at -20°C.

2.1.1.4 DNA collection from blood

2.1.1.4.1.1 Sample collection

10 ml blood samples were collected from patients by standard techniques in 10 ml (K3E 15%) tubes. These were frozen within 12 hours of sampling.

2.1.1.4.1.2 DNA collection from sample

Blood samples were defrosted and mixed for at least 1 hr on a rotary mixer in a cold room. In a 50 ml conical tube: at least 30 ml of cold Erythrocyte Lysis Buffer (ELB) was added to 10 ml blood sample, mixed and placed on ice for 15 minutes, mixing gently on the shaker. It was then centrifuged at 1500rpm for 10 minutes at 4°C. The supernatant was then poured into Virkon. Another 30 ml of cold ELB was added, mixed and placed on ice for 15 minutes, mixing gently on a shaker. The sample was then centrifuged at 1500rpm for 10 minutes at 4°C. The supernatant was poured off and a final 30 ml of cold ELB was added, mixed and placed on ice for 15 minutes, mixing gently on the shaker. The tubes were then centrifuged at 1500rpm for 10 minutes at 4°C. The supernatant was poured off and then keeping the tube upright, the excess supernatant was removed by blotting the tube on tissue. 1 ml of Nuclear Lysis Buffer (NLB) was added to all tubes and then each pellet was poured into a fresh 15 ml conical tube. 250 µl 10% SDS was added and 150 µl 40mg/ml Protease to each of the tubes. The tubes were mixed and incubated at 37°C overnight in a shaker incubator.

The following day, 1 ml of saturated NaCl solution was added; the tubes were then shaken vigorously for 15 seconds, and centrifuged at 4000rpm for 20minutes at room temperature. As much as possible (3-4 ml) of the supernatant was removed and placed into fresh 15 ml tubes. If the last ml of supernatant was not clear, it was transferred it to a 1.5 ml eppendorf tube, labelled and spun in the micro-centrifuge at 14,000rpm for 5 minutes. This was poured into the corresponding 15 ml tube. Using a 5 ml pipette, exactly twice the volume of cold Absolute Ethanol was added and the tube gently inverted until the DNA precipitated out and formed a fluffy pellet. 1 ml of 70% Ethanol was added to labelled 1.5 ml centrifuge tubes. The sticky pellet was removed using a pipette tip on a 200 µl pipette and placed into the corresponding centrifuge tube. The tubes were pulse spun in micro-centrifuge, the ethanol poured off, the end of the tube blotted and the tube left open for 15 minutes on the bench to allow the DNA to

nearly dry. 500 µl of TE Buffer was then added and the DNA was allowed to dissolve overnight at room temperature and then transferred to the freezer.

2.1.2 DNA quantification and quality measurement

For most laboratory techniques requiring DNA, the quality and concentration of the sample is imperative to success of the experiment. DNA quantification during this work was initially acheived by the Picogreen method but in 2006 the method of choice became the Spectrophotometer method because of the additional benefit of assessing DNA purity.

2.1.2.1 Picogreen DNA quantification

DNA samples were defrosted if necessary and gently mixed. 50 µl of TE Buffer was added to each well of a flat bottom welled reaction plate with 2 µl of DNA sample or standards (we used 5 µl of undiluted Picogreen reagent for every 1 ml of water in the Picogreen mix). 50 µl of Picogreen mix was added to each well and incubated for 15 minutes in a dark room. Then the plate was scanned on a fluorescence imager and results are standardised according to serial dilutions of a DNA sample with a known concentration. This method is no longer in use in our laboratory and all samples have been reanalysed by spectrophotometer.

2.1.2.2 Spectrophotometer DNA quantification and quality assessment

The NanoDrop® ND-1000 Spectrophotometer (Wilmington, USA) was used according to the manufacturer's protocol and allowed an accurate and immediate measurement of DNA concentration and a simultaneous assessment of the DNA purity. Before starting the software module, the sample surfaces were cleaned with dH_2O to remove any dried sample that might be present. The Nanodrop program was opened and the appropriate module chosen (e.g., Nucleic acids - DNA). 1.5 µL of dH_2O was pipetted onto the sensor and the lever arm was brought down. The onscreen prompts

were then followed to complete calibration. The sensors were wiped and 1.5 µL of the corresponding blank (TE buffer or dH_2O depending on what the DNA sample is dissolved in) was pipetted onto the sensor. The level arm was brought down and the onscreen prompts are followed to complete a blank measurement. The sensor was wiped and 1.5µL of the DNA sample pipetted onto the sensor. The lever arm was brought down and the 'Measure' button selected. For DNA samples, the peak of the results curve should be at a wavelength of 260 nm, and as a quality measure, the 260/280 ratio should be between 1.8 and 2.0. If poor quality was seen (i.e. low 260/280 ratio) the sample was cleaned using the Qiagen purification Kit (Qiagen Ltd, UK) following the manufacturer's protocol, and then reanalysed.

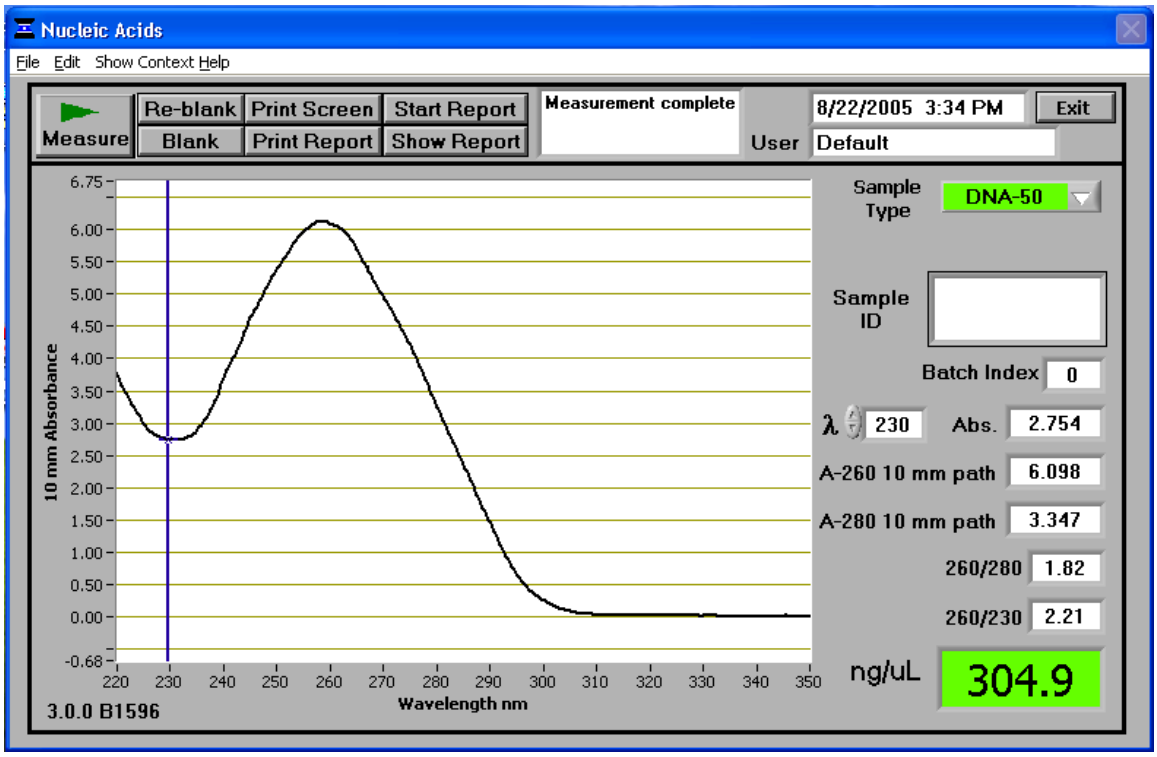

Figure 7 A high quality DNA sample measured on the NanoDrop® ND-1000 Spectrophotometer

To test multiple samples, the sensor was wiped in-between measurements with a clean tissue. Results were then exported as a CSV file into the CAS-1200™ robot (see section 2.1.2.2) for semi automated standard dilutions.

2.1.3 The Polymerase Chain Reaction

2.1.3.1 Introduction

The Polymerase chain reaction (PCR) is a technique which is used to amplify the number of copies of a defined target segment of DNA from a heterogeneous DNA source (genomic or cDNA population), in order to produce enough DNA to be adequately tested. Initially described in the 1980's[160] it has now become an indispensable technique in molecular genetics. The reaction requires the presence of a buffered solution containing DNA polymerase with the cofactor $MgCl_2$, the four deoxynucleotide building blocks of DNA precursors (the deoxynucleoside triphosphates dATP, dCTP, dGTP and dTTP), selected oligonucleotide primers and the DNA source. The PCR mixture proceeds through replication cycles consisting of three temperature states:

1. 30 seconds at 94-96 degrees C, during which the DNA is denatured into single strands.
2. 1 minute 50-65 degrees C, during which the primers hybridize or "anneal" (by way of hydrogen bonds) to their complementary sequences on either side of the target sequence.
3. One minute at 72 degrees C, during which the polymerase binds and extends a complementary DNA strand from each primer.

As amplification proceeds, the DNA sequence between the primers doubles after each cycle. Following thirty such cycles, a theoretical amplification factor of one billion is attained. A typical 35 cycle experiment theoretically produces a 2^{34} amplification of the original desired sequence (plus an insignificant 35 copies of products with variable 3' ends). In practice this means that one can start with nanogram amounts of DNA and following PCR have a sufficient quantity to visualise the desired product by a convenient means such as agarose gel electrophoresis.

Two important innovations were responsible for automating PCR. First, a heat-stable DNA polymerase was isolated from the bacterium *Thermus Aquaticus*, which inhabits hot springs. This enzyme, called the Taq polymerase, remains active despite repeated heating during many cycles of amplification. Secondly, DNA thermal cyclers

were invented that use a computer to control the repetitive temperature changes required for PCR. In this work the Tetrad® thermal cycler (GRI, Essex, UK) was used for PCR reactions.

Many variations of PCR techniques exist for specific applications. In this work the following PCR methods were used; a standard PCR technique, Long PCR, Nested primer PCR, High Resolution Melt application PCR and real-time quantitative PCR. The first 3 methods are described below and the latter 2 are detailed elsewhere.

2.1.3.2 Standard PCR protocol

A standard template of PCR amplification conditions (used for the majority of applications in this work for products <800 base pairs) are as follows:

10 µl PCR reaction mix:

Genomic DNA	1 µl of 10ng/ul
ddH_2O	7.6 µl
F primer	0.2 µl of 20 µM
R primer	0.2 µl of 20 µM
$MgCl_2$	0.4 µl
nTPs	0.4 µl of 20 µM
Taq polymerase	0.04 µl of 500 µ/ µL

Thermo-cycling conditions:

Denaturation	94°C (3 min)
Denaturation	**94°C (1 min)**

Annealing **52 – 62°C (depending on primers) (1 min)**

Extension **72°C (1 min)**

Steps 2-4 are repeated 30-35 times before step 5

Final extension 72°C (10 min)

For most applications the primers are optimised for the $MgCl_2$ concentration and annealing temperature. This is achieved by varying the $MgCl_2$ concentration from 1, 1.5 and 2 µM per reaction and running at a range of PCR annealing temperatures from -8°C to +8°C around the predicted Tm.

2.1.3.3 Long PCR

Small fragments of DNA can usually be amplified easily by a standard PCR protocol, however it becomes increasingly difficult to obtain efficient amplification as the desired product length increases. This target length limitation to PCR amplification of DNA has long been recognised[161] which has lead to the development of various 'Long PCR' protocols which allow the effective amplification of long DNA targets up to approximately 20 kb in length[162]. In this work PCR amplification of products >800 bp was achieved, when necessary, by a 'Long PCR' protocol previously described by our group[163]. In short, the method involves the use of an additional DNA polymerase which is extracted from *Pyrococcus woesii,* called Pwo polymerase. This polymerase has a lower error rate than Taq polymerase (approximately 1 in 10,000 bases) and is therefore called a 'high fidelity' DNA polymerase. This is achieved due to its 3'->5' exonuclease activity allowing it to proof read and correct mistakes in newly-synthesized DNA. When an incorrect base pair is recognized, the DNA polymerase reverses its direction by one base pair of DNA. The 3'->5' exonuclease activity of the enzyme allows the incorrect base pair to be excised. Following base excision, the polymerase can re-insert the correct base and replication can continue. This allows the production of long DNA

strands of high fidelity which are necessary for sequencing large DNA fragments. Pwo polymerase has a lower copy rate than Taq polymerase but has greater thermal stability with a half life of 2 hours at 100°C compared with 5 minutes for Taq. Therefore, the combination of both DNA polymerases combines the benefits of both which creates higher yields of product and allows amplification of longer templates than it is possible with single DNA polymerase[164;165].

For the long PCR protocol used in this work the 20 µl reaction comprised: 3 µl (6–7 ng/µl) of genomic DNA, 2 µl of 10xlong PCR buffer (140 mM ammonium acetate and 500 mM Tris-HCl, pH 8.9), 0.25 mM dNTPs, 0.4 pmol primers, 2 mM $MgCl_2$, 1.3 M betaine, 0.05 U/µl Gibco Taq DNA polymerase (Promega, Madison, WI, USA), 0.1 U/µl 1/250 *Pwo* (Roche Diagnostics, Lewes, UK), and water to 20 µl. Thermal cycling was on the Tetrad® thermal cycler (GRI, Essex, UK): 94°C for 2 min; 94°C for 20 s, 65°C for 30 s, 68°C for 3 min, repeated for 35 cycles; then 68°C for 20 min.

2.1.3.4 Nested Primer PCR

This method is a way of increasing the specificity of a PCR reaction especially when the region of interest includes highly repeated motifs. An initial PCR reaction (often Long PCR) provides a template for subsequent shorter PCR amplimers using different sets of primers designed to correspond to sequences which are located close, but internal to those used in the first reaction. PCR conditions are based on the standard Long PCR protocol for the initial reaction and the standard short PCR protocol for the second set of reactions.

2.1.4 Large plate 2% Agarose gel preparation

Agarose gels are used to asses the products of PCR by allowing an assessment of the approximate size, purity and quantity of the PCR product relative to a control. 10 g of Agarose was mixed with 500 µl of 0.5% TBE buffer in a 750 ml conical flask. This was

heated in the microwave oven for 3x 45 seconds bursts and mixed between bursts until the Agarose had dissolved. The gel was cooled to 65 °C in a water bath and 25 µl of ethidium bromide (10mg/ml, Sigma cat no. E1510) was added and mixed well. Combs are inserted into the slots on the gel tank along with the end plates and the gel is poured between the combs. The gel is allowed to set for 30 minutes before putting into the tank. The tank is filled with 1.5% TBE buffer and the combs removed. Samples are mixed with bromophenol blue (BPB) loading buffer at a ratio of 10:1 before loading 5.5 µl into each gel well. 3.5 µl of 100kb DNA ladder is loaded into the end lane as a marker. The gel is run for approximately 20minutes at 200mW for 250bp sample separation. Sections of the gel can be removed for imaging by cutting with a sharp spatula. Gel images are viewed and saved as TIFF (tagged image file format) files via a UV trans-illuminator attached to a PC. Unused sections of the gel can be kept submerged in the tank for up to 1 week.

2.1.5 Operation of CAS-1200™ precision liquid handling system robot

The CAS-1200™ precision liquid handling system robot (Corbett Life Science, Brisbane, Australia) was used for a variety of functions including simple dilutions and PCR plate setup but its main use was for setting up HRM runs on the ROTORGENE 6000 machine. For these functions all pipette speeds were set to 45 µl per second and tips were set to be used up to 5 times where possible. Blocks for holding reagents were kept in the fridge when not in use and either the 72 or 100 well rotor preparation blocks were used for all runs.

2.2 Genetic variations and molecular mutation detection systems

This section summarises the specific classes of genetic variation (polymorphisms and mutations) and mutation/polymorphism detection techniques utilised throughout this work.

2.2.1 Mutations vs Polymorphisms

'Mutation' refers to a heritable change in the DNA as opposed to polymorphisms which are allelic sequence variations (Mutation < 1% and Polymorphism > 1% frequency)[11]. However, many different definitions and distinctions between mutations and polymorphisms exist. The distinction has become complex and inconsistent such that the idea of mutations causing disease and polymorphisms being benign is seemingly over simplistic. Additionally, the idea that any change occurring in greater than 1% of the population must be a benign polymorphism is also over simplistic especially considering recent association studies which seeming link one, or a collection of common variants with a disease 'risk'[166] and rare polymorphisms occurring in less than 1% of people but with no apparent deleterious effect. Therefore, it is necessary to clarify the intended meaning of these words in any given document. Throughout this work the word 'mutation' is only used where a variation has been shown to be pathogenic with a reasonable level of supporting evidence including statistical or molecular data.

2.2.2 Polymorphisms

In any two unrelated individuals, 99.9% of the DNA sequence is similar and only 0.1% contains genetic variants that influence how people differ in their risk of disease. Many forms of genetic polymorphism exist in the human genome and we are only starting to unravel the complexities and mechanisms by which genetic information can vary between individuals. Traditionally, Single Nucleotide Polymorphisms (SNPs) which are sites in the genome where DNA sequences differ by a single base[11], have been thought to be responsible for the majority of differences between the DNA of individuals. However, recent full genome sequencing work has shown that non-SNP DNA variation accounts for 22% of all variation events in a single donor, however they involve 74% of all variant bases[167]. Therefore, significant variation besides the simple SNP exist

in the human genome. Below I describe the polymorphisms/variations which are important to this work.

2.2.2.1 Single Nucleotide Polymorphisms (SNPs)

Single Nucleotide Polymorphisms (SNPs) are responsible for approximately 78% of human DNA variation[167]. They represent possibly the simplest polymorphism class with only a single base change. For example, some people may have a chromosome with an A at a particular site where others have a chromosome with a G. As we have two copies of all chromosomes except for the sex chromosomes, for the above SNP a person could have the genotype AA, AG, or GG. Each form is called an allele and the set of alleles that a person has is called a genotype. A “Haplotype” refers to a set of associated SNP alleles in a region of the chromosome. Most chromosome regions have only a few common haplotypes (each with a frequency of at least 5%), which account for most of the variation in a population.

2.2.2.2 Short Tandem Repeat Polymorphisms (STRP or microsatellites)

Short Tandem Repeat Polymorphisms (STRP) represent a small run (usually less than 0.1kb) of tandem repeats of a very simple DNA sequence, usually 1-4 bp, for example (CA)n. They are a subclass of a larger group of polymorphism called Variable Number of Tandem Repeat polymorphisms (VNTR’s). They are common and often highly polymorphic making them useful as genetic markers particularly for linkage analysis[11].

2.2.3 Mutations

Mutations can take the form of a genome mutation such as a change in chromosome complement e.g. Down's syndrome (trisomy 21), a chromosomal mutation such as a translocation, or a gene mutation involving a number of bases. Gene

mutations include base pair substitutions, deletions or insertions. They may originate through the normal process of DNA replication or because of mutagens. If they occur in the germ line they could be passed on to offspring. A point mutation in a gene may not confirm it as the disease causing mutation. The mean heterozygosity of human genomic DNA has been estimated to be 0.0037. This means that 1:250 to 1:300 bases are different between allelic sequences[168]. This sequence variation is lower in conserved gene sequences, but in an average gene several neutral (non-pathogenic) variants are still likely to be found; without functional testing it may be impossible to differentiate a neutral from pathological variant. Mutation detection usually accomplishes one of two goals. Firstly, to detect or exclude known mutations (*specific mutation testing*) or secondly, to scan known genes or exons for *any* mutation (*mutation scanning*). There are several methods available for detecting mutations in candidate genes and a number have been employed in this project.

2.2.4 Mutation detection methods

Automated fluorescence sequencers are relatively standard laboratory equipment and direct dideoxy sequencing in the most reliable method of analysing genetic sequence. Although constantly improving, its use as a primary method of mutation scanning is limited by cost, relatively low throughput and requirement for output analysis. The other methods of mutation scanning serve mainly to reduce the sequencing load by scanning large fragments of sequence (amplicons) and identifying which amplicons contain sequence changes and therefore should be sequenced directly. These methods fall into three groups. The first is based on detecting aberrant migration of mutant molecules during electrophoresis through gel media. This includes hetero-duplex analysis, single-strand conformation polymorphism analysis (SSCP) and fluorescence-based short tandem repeat polymorphism (STRP) genotyping analysis using an Automated Capillary DNA Sequencer. The second is a relatively new technology called high resolution melt analysis (HRM) which is based on the relative differences between the melting characteristics of amplimers with small sequence differences. Both

these methods while simple do not reveal the position of the mutation and do not have 100% sensitivity[169]. The third group of methods relies on cleavage of RNA or DNA molecules prior to analysis and includes chemical and enzymatic mismatch cleavage for example the restriction enzyme digest method. All these methods have varying merits. For example some are quick (HRM), some are cheap (SSCP) and some provide special information in specific circumstances (STRP genotyping and restriction enzyme digests)[11]. The techniques used in this work are detailed in the following sections.

2.2.4.1 Single-Strand Confirmation Polymorphism Analysis (SSCP)

SSCP is probably the most widely used mutation screening method and is a technically simple method with moderate sensitivity. It is based on the principle that single stranded DNA folds up and develops a sequence dependent secondary structure (conformers) under non-denaturing conditions. The electrophoretic mobility of such DNA on non-denaturing gels therefore depends not only on its chain length but also on this secondary structure which is dictated by the DNA sequence. DNA differing by as little as a single base substitution can form different conformers and migrate differently on a non-denaturing polyacrylamide gel[170]. The precise pattern seen on a gel is very dependent on conditions used and variation being sought. Conditions need to be optimised for each amplimer being assessed. Wild type controls also need to be run on each gel. SSCP is most sensitive for detecting base substitutions for DNA fragments of 150 bp. SSCP in this work was optimised for maximum sensitivity by running for 3.5 hours using 6% polyacrylamide gels with added glycerol using standard protocols[171;172].

2.2.4.2 High resolution melt analysis (HRM)

HRM is a relatively new technique for detection of sequence variations. It works by characterizing nucleic acid samples based on their disassociation (melting) behavior. Samples can be discriminated according to their sequence, length, GC content or strand complementarity in this way with high sensitivity for single base changes. HRM requires the use of a dsDNA intercalation dye such as SYTO® 9 which intercalates between the complimentary DNA strands and fluoresces only when bound. Therefore, by performing conventional PCR followed by a slow ramp in temperature (melt) while simultaneously collecting florescence readings it is possible to accurately follow the liberation of dye (becoming non-fluorescent) as complimentary DNA strands dissociate on melting. This requires the use of a specialized real-time thermocycling machine capable of high-intensity optical data collection, high-speed data capture and precise temperature control. This was achieved in this work by the Rotor-Gene™ 6000 (Corbett Life Science, Brisbane, Australia).

A protocol for HRM was followed, as recommended by the manufacturer with the following reagents in a 10 µl reaction: 5 µl of sensimix dt (Catalogue Number:QT6T3-02, Quantace, Finchley, UK QT6T3-02), 0.15 µl of forward and reverse primer, 2.7 µl of ddH2O and 1 µl of Syto 9 (Catalogue Number:S34854, Invitrogen, Paisley, UK). It was found that in most cases, experimental conditions were identical. For the annealing temperature a touchdown method was used, where for 20 cycles the temperature dropped from 63°C to 59°C, where it remained for the last 20 cycles. The touchdown method involves starting at an annealing temperature 4°C above the predetermined temperature and followed by a 20 cycle touchdown phase in which the annealing temperature dropped by 0.5°C below the primer temperature. The PCR process also includes a normal cycle of denaturing (at 93°C for 20secs), then annealing (at 63°C for 15secs), and finally synthesis (at 72°C for 20secs). Also included are hold steps which were found to increase the sensitivity of the subsequent melt curves. Standard conditions were a follows:

Hold

Hold temperature: 95°C. Hold time: 10 minutes.

Cycling

Hold

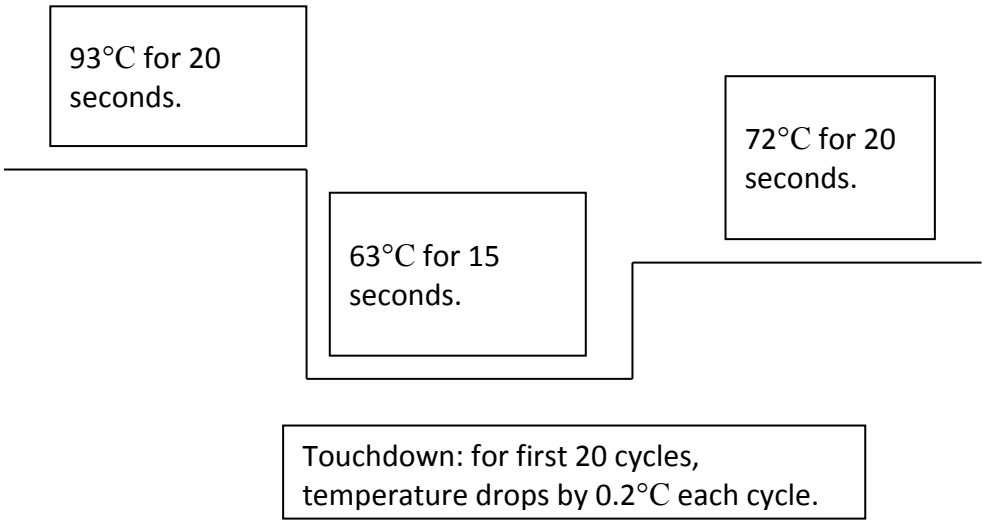

2

Hold temperature: 72°C. Hold time: 7 minutes.

Hold 3

Hold temperature: 95°C. Hold time: 5 seconds.

Hold 4

Hold temperature: 50C. Hold time: 5 minutes.

Following DNA amplification the melt curve was performed either immediately, or after storage of the amplification product.

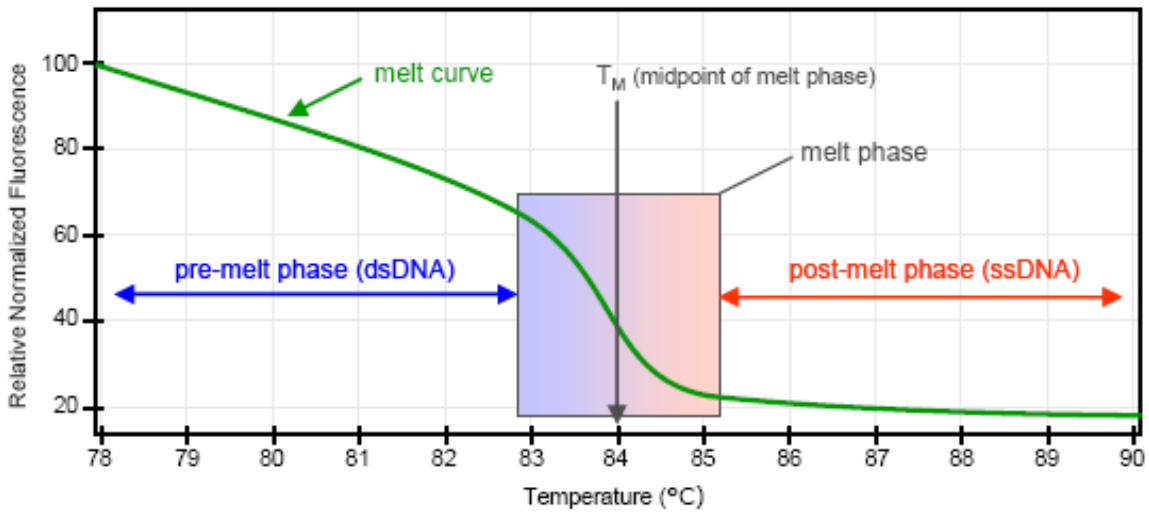

Figure 8 **A typical High resolution (HRM) melt curve.**

For all runs in this work a melt profile was run in which the temperature was incrementally increased by 0.5°C from 70-90°C and fluorescence readings were taken at each increment. Optimisation of all parts of this methodology was completed as part of this work including identification of the optimal DNA concentrations, tube formats, reagent formats and volumes, overall reaction volume, temperature conditions, thermocycling program, touch-down PCR, DNA quality requirements and results analysis.

2.2.4.3 Direct DNA sequencing

DNA sequencing is the determination of the precise sequence of nucleotides in a sample of DNA and is the 'Gold Standard' for point mutation detection. The most commonly used method for this is the "dideoxy method" which was developed by Fred Sanger winning him his second Nobel prize in 1980[11]. Automated capillary fluorescence sequencing is the most commonly used version of this technique in which a single stranded DNA template is labelled by incorporating fluorophore labelled dNTPs which then passes through a fine capillary filled with electrophoresis gel. As the samples pass through the capillary a monitor detects and records the fluorescence signal from all 4

fluorophores simultaneously[173]. For this project, Big Dye® Terminator v1.1.1 Cycle Sequencing Kit and the ABI Prism® 3100 (and later the 3130) Genetic Analyser were used. Samples to be sequenced were selected and a 50µl PCR reaction carried out for each. Samples were then run on a 2% Agarose Gel to ensure adequate product formation. Products appeared as distinct bands which were then sized by comparison with a 100bp PCR ladder run in an adjacent lane.

The products were then purified using the Qiagen purification Kit (Qiagen Ltd, UK) following the manufacturer's protocol. After purification, a 20µl sequencing reaction (using half strength Big Dye) was carried out on the Thermal Cycler according to protocol. This reaction contains 4µl Big Dye kit, 2µl 5X Buffer (Abgene), 3.2µl of 1µM primer, 3 – 10ng of the purified PCR product and 10.8µl sterile water. Both forward and reverse sequencing reactions were performed per sample fragment.

A Qiagen DyeEx 2.0 Spin Kit (Qiagen Ltd, UK) was used to remove excess big dye and precipitate the DNA from the sequencing reaction. The products from this were then re-suspended in HiDi Formamide and transferred to a 96-well optical plate approved for use in the ABI Prism® 3100/3130 Genetic Analyser. This was set to denature at 94°C for ten minutes and 4°C after that until it was ready to be loaded into the sequencer. The sequencer was loaded according to the recommended settings and left to run as long as necessary (45 minutes for 16 samples). Results were exported and sequences analysed by visual inspection of the sequence printout from sequence analysing software (BioEdit Version 7.0) and by sequence comparison using the BLAST algorithm from NCBI.

2.2.4.4 Restriction enzyme digests

Restriction enzymes are enzymes that digest DNA at specific DNA sequences. Many enzymes exist and libraries can be searched to identify an enzyme which will cut/not cut a given amplimer according to a known sequence variation. To digest DNA with a given restriction enzyme, DNA is combined with the enzyme in a buffer and is incubated at a specific temperature that is appropriate for optimal enzyme

performance. These conditions vary according to the DNA sample and the enzyme used. The ability of the enzyme to digest the DNA is assayed by gel electrophoresis. In this work, restriction enzymes were selected and purchased from Promega (Madison, WI, USA) and incubated with a PCR amplimer following standard PCR amplification. Incubation conditions and buffers varied according to the enzyme and manufacturer's protocols were followed. After incubation, products were identified on a 2% Agarose electrophoresis gel. A typical restriction enzyme digest protocol was for a 20 µl PstI enzyme digest which comprised; 16.3 µl of water, 2 µl of 10X buffer, 0.2 µl Acetylated BSA (10 µg/ul) and 1 µl of PCR amplimer. This mixture was combined and mixed before adding 0.5 µl of Pst1 enzyme (10 µ/ul) and incubating in a thermocycler for 1.5 hours at 37°C.

2.2.4.5 Short Tandem Repeat Polymorphism (STRP or Microsatellite) Genotyping

STRP genotyping was performed for subsequent linkage analysis. Primer pairs can be designed to amplify these markers and have a fluorescent tail allowing identification of product sizes on a capillary sequencer. By using a number of differing dyes and amplimers of significantly different sizes, four or more amplimers can be simultaneously run in one capillary to allow multiplexing and increased throughput. Optimised sets to cover particular chromosomal regions at particular density can be purchased for ease of use. In this work forty eight fluorescently labelled microsatellite markers from the ABI Prism Linkage Mapping Set v 2.5 – HD5 (Applied Biosystems, Foster City, USA, www.appliedbiosystems.com) were used for genotyping (panels 28, 83, 84, 85 and 86) with the polymerase chain reaction (PCR) according to manufacturer's instructions. These sets covered the X chromosome at a density of approximately one marker per 5cM and multiplexing was possible due to the 3 incorporated dyes VIC, 6-FAM and NED. Additional sets and individual primer pairs were subsequently designed (with 5-prime FAM labels) and run using identical conditions (Operon Biotechnologies GmbH, BioCampus Cologne, Nattermannallee 1, 50829 Cologne, Germany). Amplified

products were then analysed on an ABI Prism 3100 and later the 3130 Genetic Analyser (Applied Biosystems), and the Genotyper v 3.7 NT and later the GeneMapper® Software v4.0 software were used to identify and call alleles.

2.2.5 Designing primer oligonucleotides

Primers were custom made using "Primer 3" and “Exonprimer” software to balance the following considerations/principles:

1. If using genomic DNA, oligonucleotides should be greater than 20 bases (up to 24 bases) in length to ensure sequence specificity. It is extremely unlikely with this base length that a second sequence would exist which would be a perfect match to the target region. The primer design programs also Blast search human genome repositories for sequence similarity and exclude any primers with more than one matched product. Primer length is also proportional to annealing efficiency: in general, the longer the primer, the more inefficient the annealing. With fewer templates primed at each step, this can result in a significant decrease in amplified product.
2. Primers should not contain runs of a single base or a tandem repeat (Poly G or Poly C stretches). This avoids matching to known repetitive DNA sequences (which could produce non-specific products). The base composition of primers should ideally be between 45% and 55% GC. Poly A and Poly T stretches are also to be avoided as these will open up stretches of the primer-template complex lowering the efficiency of amplification. The ideal primer will have a near random mix of nucleotides, a 50% GC content and be ~20 bases long. This will put the T_m in the range of 56°C – 62°C.
3. To reduce primer-dimer formation there should be no base homology internally or at the 3' end of primers. The inclusion of a G or C residue at the 3' end (GC Clamp) helps to ensure correct binding at the 3' end due to the stronger hydrogen bonding of G/C residues.

4. The %GC content plus length of the primers should allow for the melting temperature (T_m) of the two primers to be equal. If primers are mismatched in terms of T_m, amplification will be less efficient or may not work at all since the primer with the higher T_m will mis-prime at lower temperatures and the primer with the lower T_m may not work at higher temperatures. The T_m is the temperature corresponding to the midpoint in the observed transition of double stranded to single stranded DNA. The PCR annealing stage is usually most efficient if set at a temperature corresponding to the T_m -5 °C of the chosen primers. The T_m (°C) may be calculated approximately by the equation: T_m (°C) = 2 $\times$ no. of (A + T) bases + 4 $\times$ no. of (G + C) bases.

Primers were ordered from either OPERON Biotechnologies (Cologne, Germany https://www.operon.com) or Applied Biosystems (Foster City, USA, www.appliedbiosystems.com). Most primer sets were ordered at the 10nmole scale and having undergone 'Salt-Free' purification.

2.3 Methods used for RNA work

This section details the techniques used for the extraction, storage, handling and quantification of RNA.

2.3.1 Tissue storage prior to RNA extraction

All cultured cells underwent RNA extraction directly after being removed from their supporting media with no prior storage of cells. Tissues and embryonic organs were placed in RNA*later*® (Catalog# AM7020; Ambion®, Applied Biosystems, Warrington, UK) according to the manufacturers guidelines. These samples were then stored at -20°C for 2 hours prior to indefinite storage at -80°C.

2.3.2 RNA extraction and cDNA synthesis

RNA extraction was performed by 2 methods. Initially the method used for cells was the SuperScript™ III CellsDirect cDNA Synthesis Kit (**Invitrogen**™ life technologies). This kit was used to directly synthesize the first-strand cDNA from our cells in one simple protocol combining RNA extraction and cDNA synthesis. However, due to the low abundance of the gene of interest, we sought to maximise the quality and yield of cDNA from each experiment. We found that the highest yields and greatest cDNA quality were produced by using an optimised method comprising RNA extraction by an adapted TRIZol method (Invitrogen, Paisley, UK), DNAse treatment by a method adapted from the DNA-free™ kit (AM1906, Ambion, UK) and a reverse transcription method adapted from the Primerdesign RT protocol (PrimerDesign Ltd, Southampton).

Control human kidney cDNA which had been extracted by commercial methods was purchased by PrimerDesign Ltd (Southampton). This was compared with cDNA extracted from the same quantity of SHSY5Y cells by either the CellsDirect cDNA Synthesis Kit (Invitrogen™ life technologies) method or the adapted method described above (see Figure 9). It can be seen that in both qPCR runs the control cDNA PCR amplifies after approximately 20 cycles. However, the 'cells direct' extracted cDNA amplifies after 27 cycles and the cDNA extracted by our adapted method, after only 16 cycles. This shows that the cDNA quality and abundance of GAPDH in the cDNA extracted by our adapted method is significantly higher.

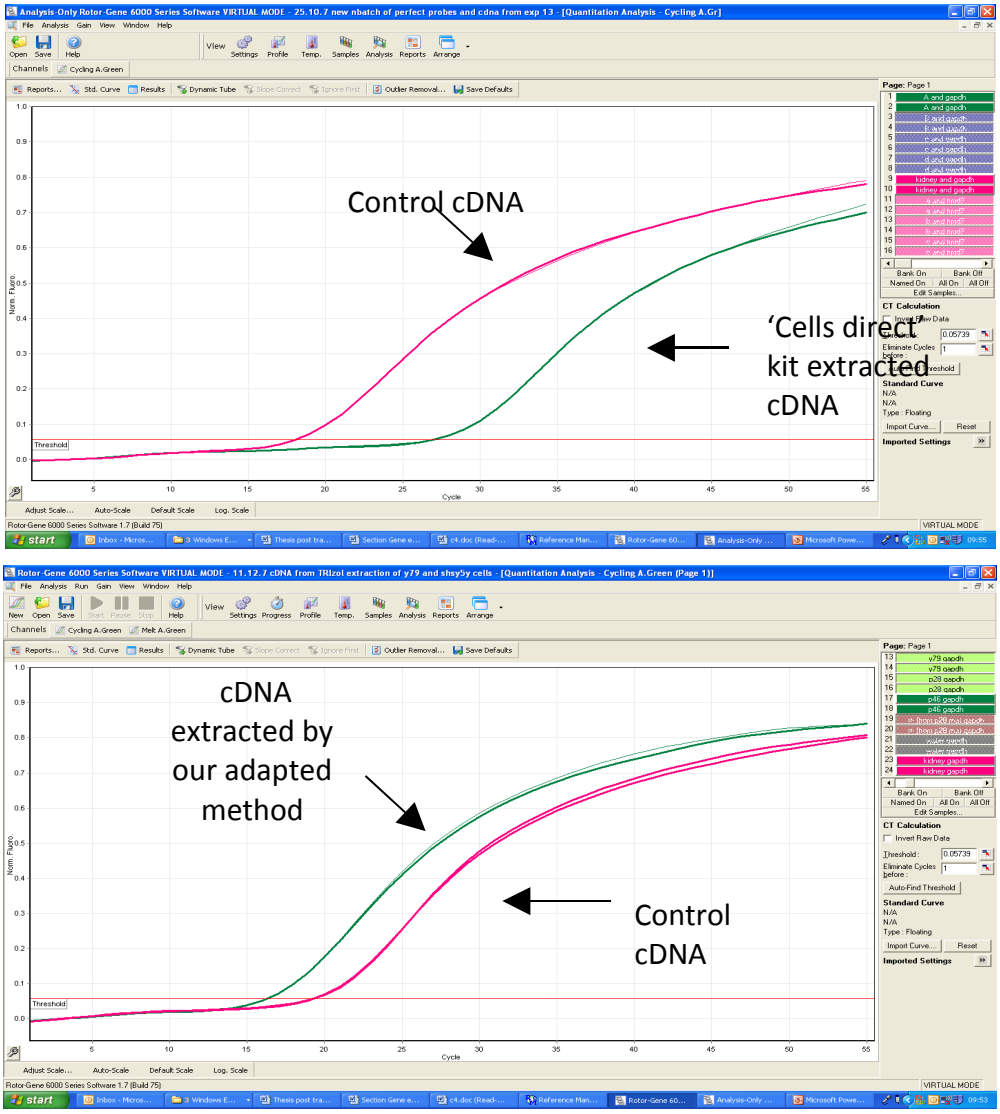

Figure 9 A comparison of 2 methods of RNA extraction and cDNA synthesis.

Quantitative real-time PCR results are shown for detection of the GADPH housekeeping gene in cDNA prepared from the human SHSY5Y cell line by the CellsDirect cDNA Synthesis Kit (Invitrogen™ life technologies), our adapted method and for control adult kidney cDNA purchased from PrimerDesign Ltd (Southampton). All further results presented in this project were obtained following RNA extraction and reverse transcription by our adapted method described below.

2.3.2.1 RNA extraction and reverse transcription by an optimised method

2.3.2.1.1 Cell lysis and RNA extraction adapted from the TRIzol method (Invitrogen, Paisley, UK)

Cell cultures were prepared for RNA extraction according to the TRIzol® (Invitrogen, Paisley, UK) standard protocol. Briefly, cell culture medium was removed and 1 ml of TRIzol reagent was added to the cells for each sample. This was mixed by pipetting and incubated at room temperature for 5 minutes. Samples were then incubated at -80°C until required.

For RNA extraction from tissues, samples were either placed in RNA*later*® (AM7020; Ambion®, Applied Biosystems, Warrington, UK) or directly homogenised (ribolysed) in TRIzol using Lysing Matrix D tubes (Qbiogene, UK) and 1 ml of TRIzol® on a Hybaid RiboLyser™ Cell Disrupter (Thermo Life Sciences, Hybaid UK). Such samples were homogenised in Lysing Matrix D impact-resistant 2.0 ml tubes containing 1.4 mm ceramic spheres (Qbiogene, UK) and 1 ml of TRIzol® ((Invitrogen, Paisley, UK) at speed settings 6.0 and for 40 seconds. Tubes were cooled on ice for 2 minutes and ribolysed for 2 to 4 times with the same settings to completely homogenise the pieces of tissue and then cooled down on ice for 2 minutes and incubated at room temperature for 5 minutes.

After homogenisation, tissue or cells samples were either processed immediately for RNA extraction or stored at -80°C. Further stages of RNA extraction and processing were performed in a specifically designated desktop RNA hood in the Gift of Sight research laboratory. The RNA work bench was cleaned with 'RNAseAWAY' (10328-011, Invitrogen, Paisley, UK) to prevent RNA degradation and DNA contamination of the samples before the start of each experiment. To prevent contamination from pipettes, aerosol resistant barrier tips were used for all experiments.

200µl of chloroform, minimum 99% (C2432-500 ml, Sigma, UK) per ml of TRIzol were added to tubes containing the fresh or defrosted samples in TRIzol. Samples were shaken vigorously by hand for 15 seconds and incubated at room temperature for 10 minutes. They were then centrifuged at 12,000rpm for 15 minutes at 4°C. After

centrifugation the mixture separated into a lower red, organic phenol-chloroform phase containing protein, an interphase containing DNA, and a colourless upper aqueous phase, containing RNA. The aqueous phase was carefully (to avoid carry over of genomic DNA from the interphase) transferred into fresh 1 ml centrifuge tubes. The organic phase and interphase were discarded. Prior to precipitation with isopropyl alcohol, 10ug of RNase-free glycogen (Cat. No 10814, Sigma-Aldrich, UK) was added to each sample as a carrier for the RNA. To precipitate RNA, 500µl of isopropyl alcohol (2-Propanol, for molecular biology, minimum 99%, I9516-500 ml, Sigma, UK) was added to each sample. The samples were then incubated overnight at -20°C to increase the precipitation of RNA. Samples were incubated at room temperature for 15 minutes and then vortexed for 10 seconds and centrifuged at 13,000rpm for 35 minutes at 4°C. The RNA precipitate, often invisible before centrifugation, formed a gel-like pellet on the side and bottom of the tube. The supernatant was removed by pouring off under visual control to prevent loss of the pellet. The RNA was washed in 75% ethanol by adding 1 ml of 75% ethanol to each sample and then centrifuging at 7,500rpm for 5 minutes at 4°C. The supernatant was poured off under visual control to prevent loss of the pellet and the samples were shortly pulse spun to collect all ethanol left on the walls of the tubes, after which it was carefully removed using a 200µl pipette tip. The pellet was air dried for 5 to 10 minutes (not completely to prevent decrease of its solubility) before it was dissolved in the DNase treatment mixture.

2.3.2.1.1.1 **DNase treatment** adapted from the **DNA-free™ kit (AM1906, Ambion, UK)**

To remove trace contamination by genomic DNA, samples were treated with DNA-free™ (AM1906, Ambion, UK) for DNase treatment and removal. The dry RNA pellet was dissolved in 20 µl of total DNase digestion reagents. This was made up by combining 17µl nuclease-free water, 2µl 10x DNase I buffer (100mM Tris-HCl pH 7.5, 25mM $MgCl_2$, 5mM $CaCl_2$) and 1µl of recombinant DNase I (2Units/µl). The samples were incubated in a water bath or warm air incubator at 37°C for 60 minutes after which

the DNase was inactivated by adding 5µl of the DNase Inactivation Reagent to the samples and incubating them for 2 minutes at room temperature and occasionally mixing them. The samples were spun at 12,000rpm for 2 minutes at 4°C and the RNA was kept on ice and used immediately for quantification and reverse transcription.

2.3.2.1.1.2 Quality check and quantitation of RNA

The method used to assess the quality and quantity of RNA was a spectrophotometric approach using a Nanodrop ND 1000 (Nanodrop Technologies, Wilmington, DE, USA) (see section 2.3.2.1.1.2). Briefly, 1.5µl of total undiluted RNA was placed into the machine on a pedestal that formed a sample column by surface tension (1mm path length) when the apparatus was closed. The absorbance at 260 and 280nm using a 10mm light path equivalent was measured and this was used to determine the RNA concentration and purity (pure RNA: A260/A280 ratio: 1.8 to 2.1).

2.3.2.1.1.3 Reverse transcription method adapted from the Primerdesign^{Ltd} RT protocol (PrimerDesign^{Ltd}, Southampton)

Following quantitation of RNA, a 10 µl reaction was prepared for each sample in a 200 µl thin-walled PCR tube with the following reagents from PrimerDesign Ltd. (Southampton): 100ng-1µg RNA (1 µg was preferred), 2µl Oligo dT primer/dNTP mix, 1µl hexamer primer, RNA/DNAase free water to make up to a final volume of 10µl. Each reaction was prepared on ice and then heated to 65°C for 5 minutes in a PCR thermocycler. Samples were then removed and placed immediately in an ice water bath. Each sample then had the following reagents added: 4 µl MMLV 5x buffer, 5.2 µl RNA/DNAase free water and 0.8 µl MMLV enzyme. Samples were then flicked to mix the contents and pulse centrifuged to collect the contents. They were incubated on a thermocycler to 37°C for 10 minutes and then 42°C for 50 minutes. Samples were then routinely diluted 1:10 with RNA/DNAase free water and stored at -20°C or 4°C prior to use.

2.3.3 Real-time quantitative polymerase chain reaction (RT qPCR) protocol

Real-time quantitative PCR has made quantifying mRNA transcripts a simpler automated process[174]. It is also considered to be a very sensitive technique for mRNA detection and quantitation[175] (Heid et al., 1996). It is particularly useful when compared to other commonly used techniques, such as Northern blot analysis, as it enabled researchers to quantify mRNA from small samples of RNA. It can also be an extremely sensitive technique for low copy number mRNAs and is possibly even capable of allowing quantification of RNA from single cells[176]. All methods of real-time quantitative PCR require measurement of the abundance of the PCR product during amplification. This can be achieved by a number of methodologies. Two different detection chemistries were employed in this project, namely the asymmetrical fluorescent cyanine dye SYBR green (PrimerDesign Ltd, Southampton) and a real time PCR probe called a PerfectProbe™ (PrimerDesign Ltd, Southampton). For both methods, sample reactions were prepared either by hand, or using the CAS-1200™ precision liquid handling system robot (Corbett Life Science, Brisbane, Australia). All experiments were run using the Rotor-Gene™ 6000 real time thermo-analyser (Corbett Life Science, Brisbane, Australia). Specific protocols are detailed in the relevant subsequent chapters.

2.4 Cell culture methods and protocols

The cell culture methods and protocols used in this work are varied. This section describes only the standard techniques used in multiple experiments. Details of the specific conditions and protocols for each experiment can be found in the relevant subsequent chapters.

2.4.1 Standard growth media for SHSY5Y neuroblastoma derived cells

This media comprised: 90 mls Minimum essential medium, Eagle (ATCC, Cat no. 30.2003), 90 mls nutrient mixture F-12 ham (Sigma, cat no. N6658), 20 mls foetal bovine serum (ATCC, Cat no. 30-20-21) and 1 ml of antibiotic/antimycotic solution (100x) (Sigma, Cat no. A5955). Media was made and used within 2 weeks. It was stored at 4°C in Plug seal cap 75 ml cell culture flask (Corning, Cat no.430720).

2.4.2 NB-B27 growth media for SHSY5Y neuroblastoma derived cells

This media comprised: 194 mls of Neurobasal-A medium (-L-Glutamine) (Gibco, Cat no.10888), 2 mls B-27 supplement (Gibco, 17504-044), 2 mls L-Glutamine (Sigma, Cat no.G7513) and 2 mls of antibiotic/antimycotic solution (100x) (Sigma, Cat no. A5955). Media was made and used within 2 weeks. It was stored at 4°C in Plug seal cap 75 ml cell culture flask (Corning, Cat no.430720).

2.4.3 Standard growth media for Y-79 Retinoblastoma derived cells

This media comprised: 90 mls RPMI with Glutamax (Invitrogen, Cat no. 72400-021), 10 mls foetal bovine serum (ATCC, Cat no. 30-20-21) and 0.5 ml of antibiotic/antimycotic solution (100x) (Sigma, Cat no. A5955). Media was made and used within 2 weeks. It was stored at 4°C in Plug seal cap 75 ml cell culture flask (Corning, Cat no.430720).

2.4.4 Haemocytometer method of cell counting

The Haemocytometer method was used for all cell counting in this work. Cell media was first discarded and 3 mls of 1x non-enzymatic cell dissociation solution (Sigma, Cat no. C5914) was added per 200 ml flask (1 ml was used for 75 mls flasks). Flasks were swirled and incubated at 37°C for 5 minutes. The flask was then swirled

again and tapped to remove any adherent cells. 5 mls of fresh media was added before centrifuging at 1000rpm for 5 minutes. Supernatant was then removed by pouring and 12 mls of fresh media added. This suspension was mixed by pipetting and a small amount was add to a 200 µl eppendorf tube with an equal volume of trypan blue (Trypan blue solution (0.4%) 100 mls (Sigma, Cat no.T8154)). This suspension was then mixed by pipetting. A clean haemocytometer chamber slide (Neubauer, Germany) was then cleaned again with 70% ETOH and a clean coverslip (Neubauer, Germany) was applied over the chamber. Cell suspension was then pipetted into each end of the chamber and the slide viewed on an inverted DM IRB microscope (Leica Microsystems UK Ltd, Milton Keynes, UK). All living cells located within the 4 large squares of the chamber were counted and the concentration of cells in the cell suspension calculated using the following formula:

Cells/ml = Total cell count per 4 large squares x 5000

2.4.5 Cell freezing

Cells were periodically frozen in aliquots at -80°C to maintain a stock of cells at low passage values. Cells were counted and 1 million cells were added to 1 ml of cell freezing buffer (Sigma Cat no.C6164) in a 2 ml centrifuge tube. Tubes were then frozen at -20°C for 2 hours and subsequently stored in the -80°C freezer for up to 6 months prior to use.

2.4.6 Defrosting cells

Cells were rapidly defrosted by swirling in a beaker of hand warm water. 10 mls of media was then added and this suspension and centrifuged at 1000rpm for 5 minutes. The supernatant was poured off and cells re-suspended in 10 mls of fresh media. This was incubated overnight at 37°C in 5% CO_2.

2.4.7 Poly-L-Lysine coating culture wells

6 well cell culture plates (Nunclon, Cat no.140685) or 24 well cell culture plates (Corning, Cat no.3524) were coated with Poly-L-Lysine to aid attachment for some experiments. 300 µl of Poly-L-Lysine 0.001% solution (Sigma, Cat no. P4707) was added to each well of a 24 well plate (600 µl for the 6 well plates) and incubated at room temperature for 5 minutes. Wells were then washed twice with the intended culture medium. 1 ml of culture medium was then added to each well and incubated at 37°C in 5% CO_2 until it reached 37°C. Medium was then removed and plates used immediately or stored at room temperature for up to 3 days prior to use.

2.4.8 Immunohistochemistry

Immunohistochemistry was performed on cell lines in this work using two primary antibodies (see Table 1). At the indicated times for each experiment, cells were rinsed free of medium with phosphate buffer solution (PBS) and immediately fixed in 4% paraformaldehyde (PFA) for a minimum of 30 minutes at 4°C. Fixed cells were then washed 3 times in PBS to remove the PFA. After rinsing, non-specific binding sites were blocked with 5% donkey blocking serum in 0.1%Triton-X in Tris-buffered saline (TBS) for 30 minutes at room temperature. Primary antibodies were then applied at the given concentration (see Table 1) in 1 ml of water containing 10 µl TBS with 0.1% Triton-X. These were then incubated at 4°C overnight. Cells were then rinsed once with PBS and incubated in PBS with 0.1% Triton-X containing: Cy3-conjugated anti-mouse diluted 1:250 and Cy2-conjugated anti-rabbit diluted 1:250 secondary antibodies for 2 hrs at room temperature. Cells were then washed once with PBS and counterstained with the nuclear stain 4',6-diamidino-2-phenylindole (DAPI;5 µg/mL) (Sigma) for 6 min. Finally, cells were washed twice in PBS to remove excess DAPI and were kept in 1 ml of water per well. For each experiment, negative controls (the addition of secondary in the absence of primary antibodies) were used to rule out any non-specific secondary

antibody binding. Imaging was performed using an inverted DM IRB microscope (Leica Microsystems UK Ltd, Milton Keynes, UK) with separate photographs taken at the specific wavelength required for each stain. The Volocity™ software package V4.2.1 (Improvision, Coventry, UK) was used to capture and combine images. For Cy2 absorbance is at 492nM and fluorescence is at 510nM, for Cy3 absorbance is at 550nM and fluorescence is at 590nM and for DAPI absorption is at 358 nM and emission when bound to DNA is at 461nM.

Primary antibody	**Working dilution**	**Company**
Mouse anti-GFAP	1:500	Sigma
Rabbit anti-TUJ1	1:500	Covance
Secondary antibodies	**Working dilution**	**Company**
Donkey Cy3 conjugated anti-mouse	1:250	Jackson ImmunoResearch
Donkey Cy2-conjugated anti-rabbit	1:250	Jackson ImmunoResearch

Table 1 Antibodies used in this research.

This table shows the different antibodies used with the working dilution as worked out from the dilution experiments and the company from which each antibody was purchased.

3 CHAPTER THREE - Positional cloning of a nystagmus gene by linkage analysis

3.1 Introduction

CIN is genetically heterogeneous and has been described as an autosomal dominant[177], autosomal recessive[104] and X-linked dominant [104] or recessive trait[178]. Although X-linked regions have been identified at Xp11.4 –p11.3 [178] and Xq26-q27 [104] no genes have been identified. These linkage studies have been criticised on a number of aspects including exclusion of alternative diagnoses, limited phenotyping, incorrect marker location information, combining families with different inheritance patterns and the variable measures of significant linkage (see 1.3.6.1.1.4 Limitations of previous X-linked CIN linkage work). Consequently, all of these issues were addressed in the design of the following linkage mapping work. A large 3 generation pedigree with apparent X-linked CIN was identified. This family underwent detailed phenotyping followed by X chromosome wide STRP genotyping and subsequent linkage analysis.

3.2 Methods

3.2.1 Clinical methods

The study had the approval of the local and regional ethics committee and conformed to the tenets of the Declaration of Helsinki. Twenty nine individuals (7 affected males, 2 affected females, 11 obligate female carriers and 9 unaffected members) in a single CIN pedigree (pedigree 1) underwent detailed clinical examination (see figure 10) including LogMAR visual acuity, refraction, colour vision testing with Ishihara plates, intra-ocular pressure (IOP) recording, anterior and posterior segment slitlamp examination including iris transillumination testing in a darkened room and orthoptic assessment.

Figure **10** Pedigree 1; a large apparent X-linked Congenital Idiopathic Nystagmus pedigree

Twenty four patients also had eye movement recordings using Skalar IRIS IR Light Eye Tracker equipment (Cambridge Research Systems Ltd. Rochester UK, www.crsltd.com) (see Figure 11).

Figure 11 Skalar IRIS IR Light Eye Tracker equipment used for eye movement recordings

Eye movement analysis comprised 24 recordings for each patient. Binocular and uniocular saccades were recorded to calibrate amplitude measurements at ±10° and ±20° from fixation in the horizontal plain using a 1° red square target moving at 500ms intervals. Binocular and uniocular optokinetic nystagmus (OKN) measurements were carried out to rightward and leftward drifting gratings measuring 0.2 cycles per degree at a velocity of 25° per second. Waveforms were analysed whilst viewing in 5 positions (primary, 10° right, 10° left, 20°right and 20°left of fixation) both binocularly and uniocularly using a 1° red square target.

Seven patients also had extensive clinical neurological examinations.

International Society for Clinical Electrophysiology of Vision (www.iscev.org) standardised electroretinograms (ERGs) and visual evoked potential (VEP) recordings were recorded in 2 affected males and 2 obligate female carriers. Monocular stimulation and a 3 channel trans-occipital electrode montage were employed for VEP recordings to optimise detection of neuronal misrouting suggestive of ocular albinism.

Informed consent was obtained from all subjects for genetic studies and genomic DNA was isolated from ORAGENE saliva sample kits (see section 2.1.1.2).

3.2.2 Laboratory methods

Forty eight fluorescently labelled microsatellite markers from the ABI Prism Linkage Mapping Set v 2.5 – HD5 (panels 28, 83, 84, 85 and 86) (Applied Biosystems, Foster City, USA, www.appliedbiosystems.com) and four further fluorescently labelled microsatellite markers (Operon Biotechnologies GmbH, BioCampus Cologne, Nattermannallee 1, 50829 Cologne, Germany) were used for genotyping with the polymerase chain reaction (PCR) according to manufacturer's instructions:

15 µl PCR reaction:

True Allele® PCR premix	9 µl
ddH_2O	3.8 µl
supplied labelled primer pair	1 µl
DNA template(50ng/ul)	1.2 µl

PCR conditions:

95°C for 12 min	x1
Melt at 94°C for 15 sec	x10
Anneal at 55°C for 15 sec	
Extend at 72°C for 30 sec	
Melt at 89°C for 15 sec	x20
Anneal at 55°C for 15 sec	
Extend at 72°C for 30 sec	
Extension at 72°C for 10 min	x1
Hold at 4°C Forever	

Samples were then multiplexed, pooled and diluted with ddH_2O to a concentration of 1/20 for 6-FAM and VIC labelled amplimers and 1/10 for NED labelled amplimers. 0.5 µl of these samples were then added to a 10 µl 18:1 mix of Hi-Di™

Formamide / Genescan™ -500 LIZ size standard. Samples were finally denatured at 95°C for 5 minutes immediately prior to analysis on an ABI Prism 3100 and later the 3130 Genetic Analyser (Applied Biosystems). The Genotyper® v 3.7 NT and later the GeneMapper® Software v4.0 were used to identify and call alleles. Manufacturer's recommendations for allele calling and binning were followed.

3.2.3 Bioinformatic methods

Bioinformatic methods for linkage analysis were completed with the assistance of the Southampton Bioinformatic group headed by Professor Andy Collins. Two-point and multipoint linkage analyses were performed using the VITESSE program [179]. The PEDCHECK program [180] was used to examine the pedigree for genotyping errors and mendelian inconsistencies. Both marker locations and inter-marker centimorgan distances (cM) were taken from the Rutgers combined linkage-physical map of the human genome[181] based on the NCBI build 35 (National Center for Biotechnology Information, U.S. National Library of Medicine, 8600 Rockville Pike, Bethesda, MD 20894 USA). Therefore, the marker position data quoted by ABI (based on an earlier map) was updated and refined. The inheritance pattern was assumed to be X-linked recessive and the disease gene frequency was taken at 0.001 with penetrance of 0.1 in female heterozygotes and 1 in female homozygotes and male hemizygotes. Other penetrance values between 0 and 0.25 for female heterozygotes were also tested but the results were consistent throughout.

3.3 Results

3.3.1 Clinical Results

Flash and pattern ERG and occipital pattern VEP recordings in 2 affected males and 2 obligate female carriers were normal thus excluding the most common masquerading eye conditions. Computerised Tomography brain scans were performed on 2 affected individuals at diagnosis with no abnormal findings. Ophthalmic examinations were also normal except for nystagmus in affected patients. The prevalence of squint was 4 of 9 (44%) affected subjects and 3 of 19 (15.8%) unaffected subjects. Refractive errors ranged from uni-ocular LogMAR acuities of 0.1 to 0.5 in affected subjects. Eye movement recording results are presented for all patients with positive findings in Table 2 and examples of nystagmus waveforms seen in this pedigree are presented in Figure 12. 18 unaffected subjects including 6 obligate female carriers had no abnormalities on any of the 24 recordings and so are not included. Also included are results for a female carrier with nystagmus possibly secondary to a cochlear implant (III:16) and a male subject (III:8) who has nystagmus but was excluded due to a history of congenital cataract. The results also exclude an affected subject (IV:15) for whom eye movement recordings were not collected.

	IV:15	IV:18	III:16	V:4	II:5	III:8	III:6	V:8	V:9	III:2	IV:2
Optokinetic nystagmus present? (OKN)	x	NP	Present*	NP	NP	NP	NP	NP	Low gain	Low gain†	NP
Direction in primary	x	P	R	P	R	P	P	R	R	R	R
Amplitude in primary	x	2.5°	0.25°	2.22°	1.7°	3.5°	2.5°	5.4°	0.31°	5.6°	4.2°
Frequency in primary (cycles per second)	x	2.66	1.10	3.92	3.33	3.00	4.44	3.60	1.47	1.40	4.50
Waveform in primary	x	P	D	P	A	P	P	A	Lin	D	A
Direction in L gaze	x	L	R	L	L	P	L	L	R	P	L
Amplitude in L gaze	x	2.6°	0.3°	2.8°	1.0°	3.2°	3.3°	2.2°	0.2°	2.8°	4.1°
Frequency in L gaze (cycles per second)	x	4.20	0.92	5.50	5.00	2.94	5.50	2.80	2.10	8.50	3.80
Waveform in L gaze	x	A	Lin	Lin	Lin	P	Lin	D	Lin	P	PC
Direction in r gaze	x	R	R	R	R	R	P	P	R	R	R
Amplitude in r gaze	x	2.9 °	0.3°	2.1°	2.1°	3.1°	1.6°	0.5°	0.2°	0.8°	5.3°
Frequency in r gaze (cycles per second)	x	4.16	1.20	3.00	2.25	3.06	5.00	3.33	1.12	3.56	3.42
Waveform in r gaze	x	PC	D	PC	Lin	PC	P	P	Lin	Lin	PC
Waveforms seen any direction	x	Lin,P,A PC	Lin,D,	D,PC,Lin, P, A	PC,A,Lin	A,PC,P	D,PS,Lin, A	Lin, D, PS,P, A	Lin	Lin, P, D,A	A,P, PC
Rebound seen Y/N	x	No	No	No	No	No	No	No	No	No	No
Changes in phenotype when viewing monocularly	x	MLN	No	MLN	No	No	No	No	No	MLN	MLN

Table 2 Infra red limbal nystagmology in affected members of a nystagmus pedigree (pedigree 1).

Abbreviations: **L**, left; **R**, right; **P**, pendular; **D**, decelerating slow phase; **Lin**, linear slow phase; **A**, accelerating slow phase; **PC**, pseudocycloid waveform; **MLN**, manifest-latent nystagmus; **NP**, not present (disrupted).

* OKN observed with monocular naso-temporal asymmetry

† Low gain OKN but only in the direction of the nystagmus

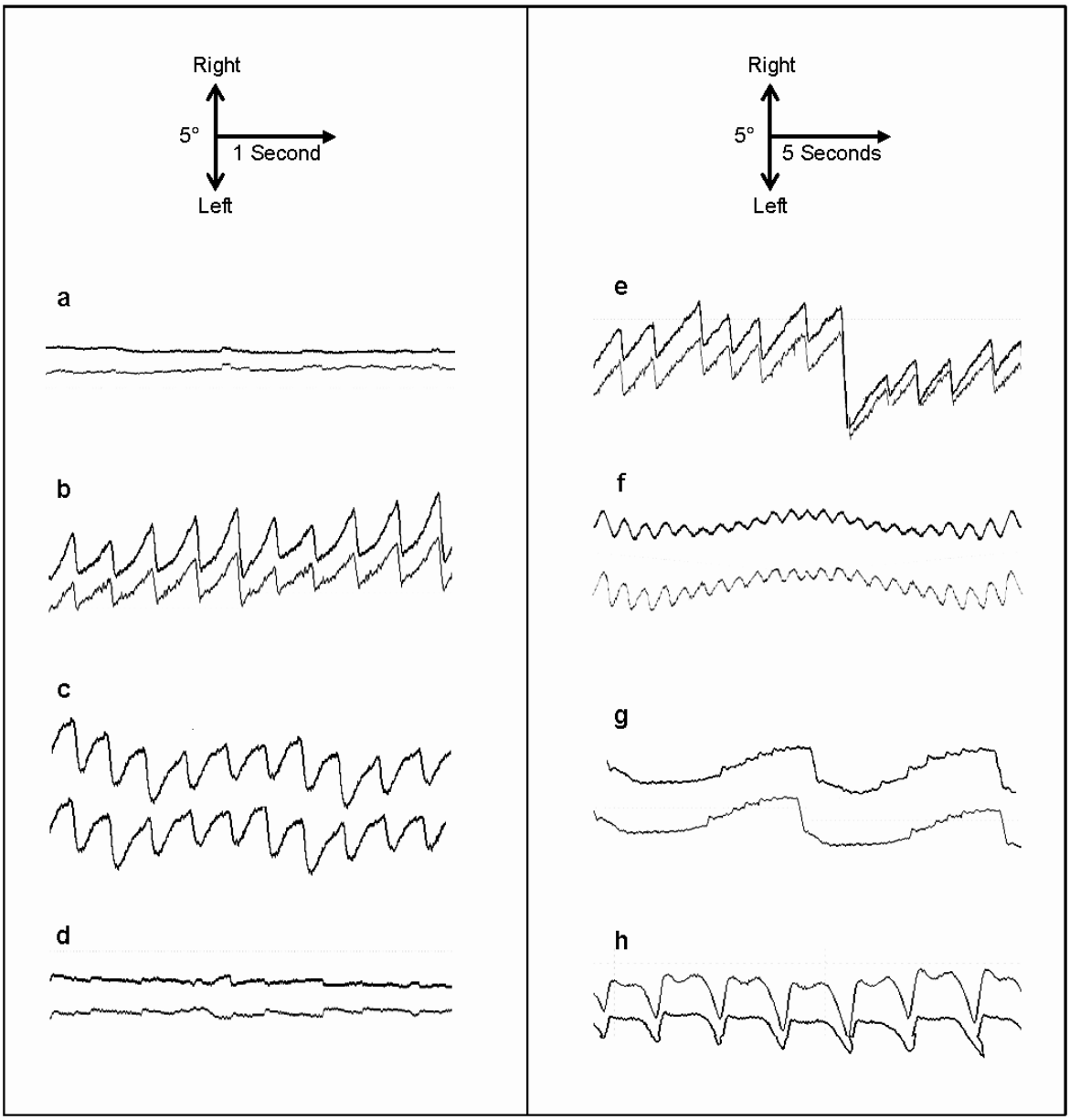

Figure 12 Eye movement recordings from a pedigree with CIN (pedigree 1).

Infrared eye movement recordings are shown. Each recording is binocular with the left eye trace on top of the right eye trace. The following examples are shown: normal recording from IV:17 with a normal finding of a square-wave jerk (a), accelerating slow phase nystagmus typical of CIN from IV:18 (b), decelerating slow phase nystagmus atypical for CIN from III:2 (c), subtle nystagmus waveforms missed by clinical examination from V:9 (d), normal OKN from IV:18 (e), disrupted (absent) OKN (on a pendular nystagmus background) typical of CIN from III:6 (f), low gain OKN unusual for CIN from V:9 (g), and pseudocycloid nystagmus (a combination of pendular and accelerating slow phase) common in CIN from V:9 (h).

Individual V:9 from pedigree 1 had been previously diagnosed as unaffected by an experienced ophthalmologist but was found to have subtle nystagmus only after examination with infra-red nystagmology. For subject III:16, a female carrier also known to have a cochlear implant, OKN was preserved, the nystagmus amplitude was very low and no accelerating slow phases were seen. Subject III:8 who has nystagmus but was excluded from linkage analysis due to a history of congenital cataract, has nystagmus waveforms that are very similar to the affected subjects including disrupted OKN and accelerating slow phases.

3.3.2 Linkage Analysis Results

The highest two-point LOD score (Z) of 3.0 at θ =0 was found for marker DXS1047 (see). Subsequently, 4 additional markers were added to increase resolution around the DXS1047 locus which resulted in a higher two-point LOD score (Z) of 4.24 at θ=0 for both markers DXS8044 and DXS994 (see Table 4).

Marker Order	LOD Score at θ = 0.0	0.1	0.2	0.3	0.4
DXS8055	-∞	1.64	1.57	1.17	0.59
DXS8064	-∞	0.00	0.00	0.00	0.00
DXS8067	-∞	1.08	1.02	0.79	0.45
DXS1001	-∞	2.08	1.76	1.25	0.61
DXS8009	1.19	1.01	0.81	0.58	0.31
DXS1047	3.00	2.54	2.03	1.45	0.79
DXS1062	-∞	0.66	0.85	0.73	0.44
DXS984	-∞	1.68	1.66	1.31	0.76
DXS1205	-∞	-0.61	-0.17	0.00	0.05

Table 3 Two point LOD score results for nystagmus phenotype in pedigree 1

Marker Order	LOD score at θ= 0.0	0.1	0.2	0.3	0.4	0.5

DXS8088	-∞	1.38	1.37	1.03	0.54	0.00
DXS8055	-∞	1.64	1.57	1.17	0.59	0.00
DXS8064	-0.00	-0.00	-0.00	-0.00	-0.00	0.00
DXS8067	-∞	1.08	1.02	0.79	0.45	0.00
DXS1001	-∞	2.08	1.76	1.25	0.61	0.00
DXS1212	-∞	1.08	1.02	0.79	0.45	0.00
DXS8009	1.19	1.01	0.81	0.58	0.31	0.00
DXS8044	4.24	3.55	2.77	1.91	0.94	0.00
DXS1047	3.00	2.54	2.03	1.45	0.79	0.00
DXS994	4.24	3.55	2.78	1.91	0.94	0.00
DXS8041	3.03	2.53	1.96	1.32	0.63	0.00
DXS1062	-∞	0.66	0.85	0.73	0.44	0.00
DXS984	-∞	1.68	1.66	1.31	0.76	0.00

Table 4 Two point LOD score results for nystagmus phenotype in pedigree 1

Multipoint analysis provided a maximum LOD score of 4.54 between markers DXS994 and a critical LOD-1 support interval of ≈8.0 cM between markers DXS1212 and DXS1062 (using the Rutgers combined linkage-physical map) (see Figure 13). The method of calculating critical interval in this work (LOD-1 method)[130] is a recognised method in which a threshold for the interval is drawn at a level of 1 LOD unit below the maximum multipoint calculated LOD score. This is a relatively conservative method.

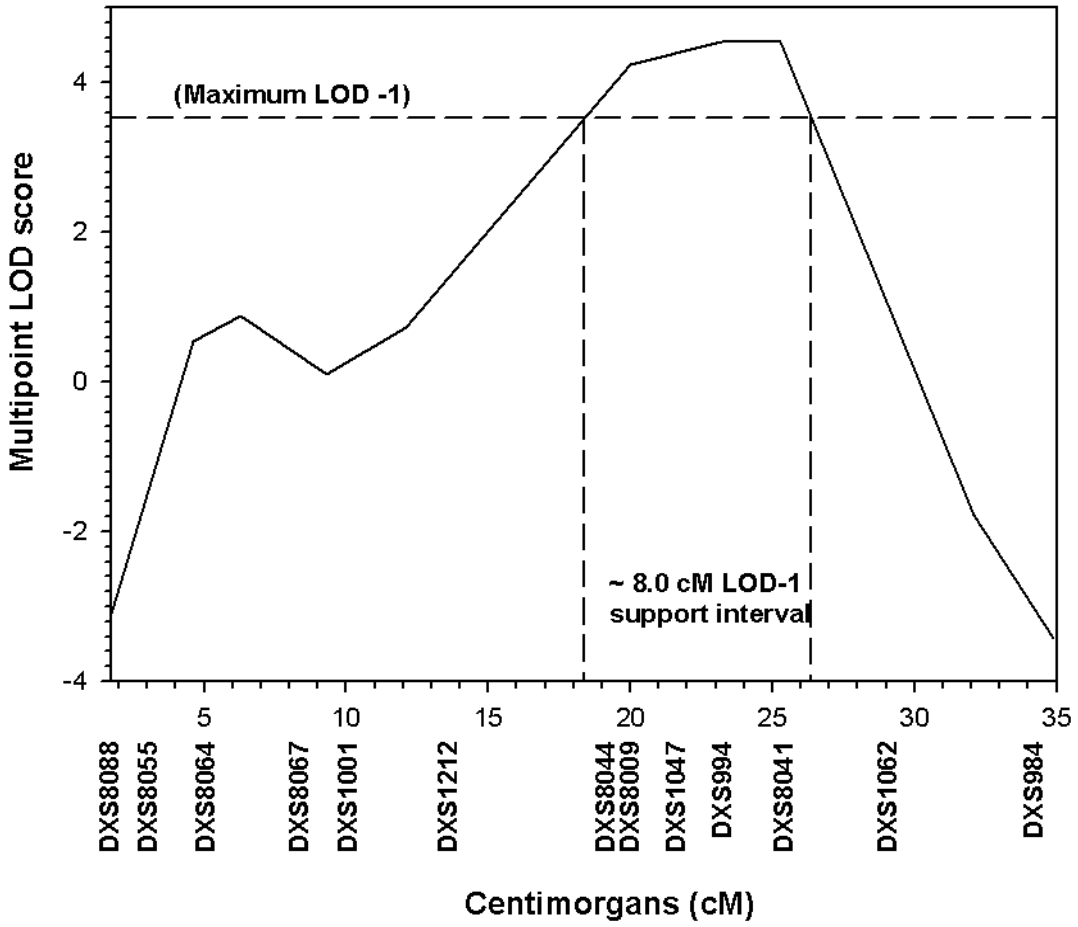

Figure 13 Multipoint LOD score results.

Results are presented with a LOD-1 support interval showing that the X-Linked recessive nystagmus locus has been narrowed to an 8.4 cM (approximately 14Mb) region between markers DXS1212 and DXS1062.

These results were confirmed by haplotype analysis (see Figure 14).

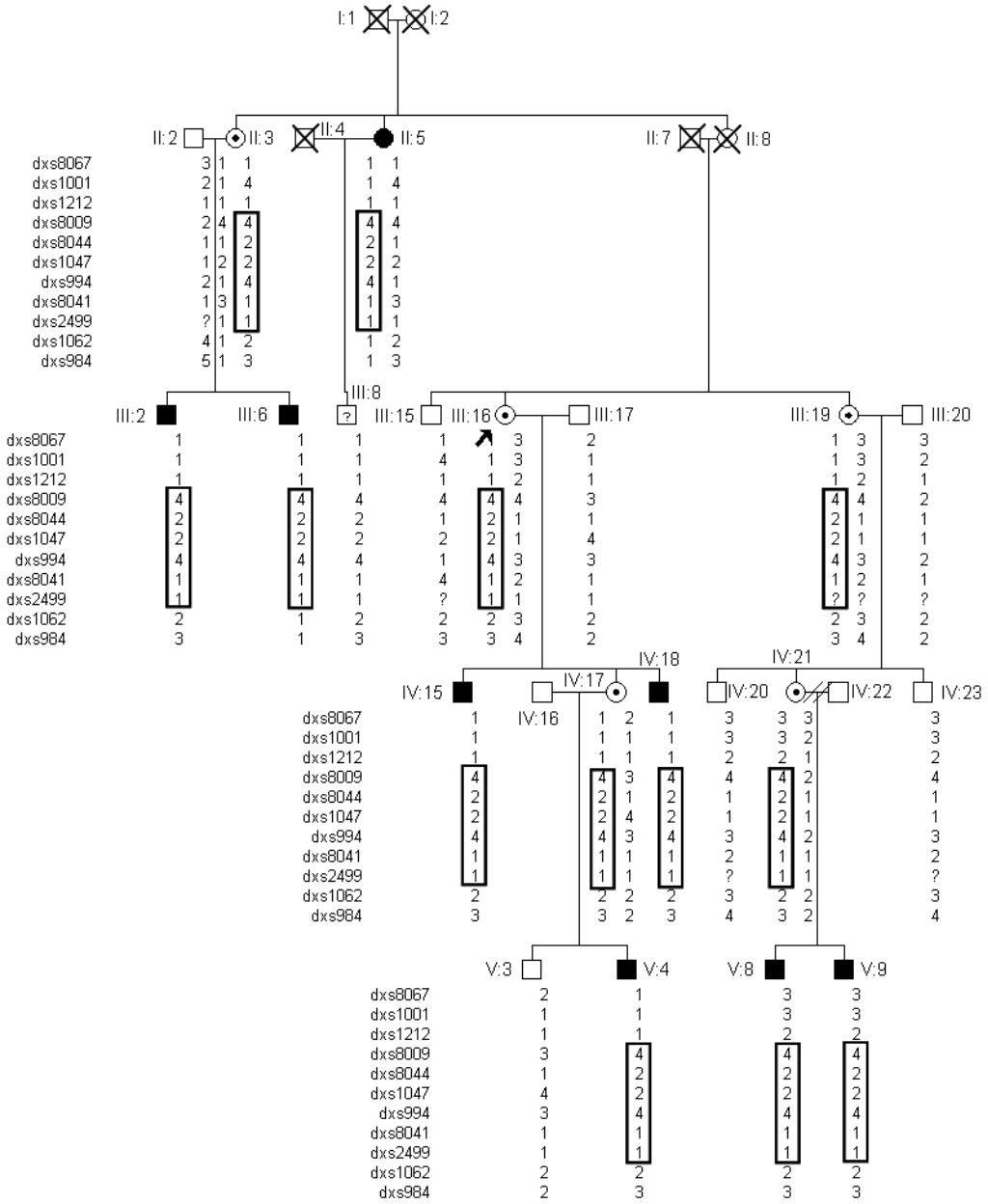

Figure 14 Haplotype analysis for nystagmus phenotype transmission in pedigree 1.

Markers are listed top to bottom centromere-DXS8067- DXS1001- DXS1212-DXS8009-DXS8044-DXS1047-DXS994-DXS8041-DXS2499-DXS1062-DXS984-telomere. The haplotype co-segregating with the nystagmus phenotype is boxed. A question mark indicates that the genotype is not determined and for clarity, identifiers from are used. Marker DXS2499 was uninformative in this pedigree.

It can be seen that centromeric and telomeric boundaries for the shared haplotype in this pedigree are defined by; a recombination between markers DXS1001 and DXS1212 for individual IV:21 and a recombination between markers DXS1062 and DXS2499 for individual III:6.

3.4 Discussion

3.4.1 Clinical Phenotyping

These results have shown that CIN patients in a single family have extremely variable nystagmus phenotypes. Classically the hallmarks of the CIN phenotype are accelerating slow phases, loss of OKN and no changes in phenotype on monocular viewing[37]. However, in pedigree 1, 7 out of 9 patients with CIN had 3 or more waveforms seen including prolonged periods of decelerating or linear slow phases which are more commonly seen in patients with nystagmus of neurological origin. Similarly, OKN was preserved to some degree in 2 patients which is considered to be rare in CIN. Interestingly, in subject III:16 (female carrier but also known to have a cochlear implant), OKN was preserved (rare in CIN), the nystagmus amplitude was very low and no accelerating slow phases were seen (also rare in CIN). These findings might suggest that her nystagmus is secondary to the cochlear implant and not CIN. Subject III:8 who has nystagmus but was excluded due to a history of congenital cataract, has nystagmus waveforms that are very similar to the affected subjects including disrupted OKN and accelerating slow phases. These findings would be more suggestive of CIN than Sensory Deficit Nystagmus (SDN)[37] due to congenital cataract. (This subject is subsequently found to be hemizygous for the causative mutation in this family).

The clinical phenotyping demonstrated that in some cases waveform characteristics were indicative of underlying aetiology in this family but conversely, many of the waveform characteristics seen in individuals of this pedigree would suggest

wholly different aetiologies. These results support the opinion that waveforms alone should be interpreted with caution when employed as a diagnostic tool in CIN. However, detailed eye movement recordings may be necessary to assign affection status in CIN pedigrees and the families of CIN singleton cases. An example is individual V:9 from pedigree 1 who had been previously diagnosed as unaffected by an experienced ophthalmologist but was found to have subtle nystagmus only after examination with infra-red oculography (and was subsequently found to be hemizygous for the causative mutation in this family). This has significant implications for diagnosis and genetic counselling for this individual and other currently undiagnosed individuals from CIN pedigrees.

3.4.2 Linkage Studies

The genetic intervals identified in previous linkage studies of X-linked CIN at the q27 locus are illustrated along side the results from this work in Figure 15.

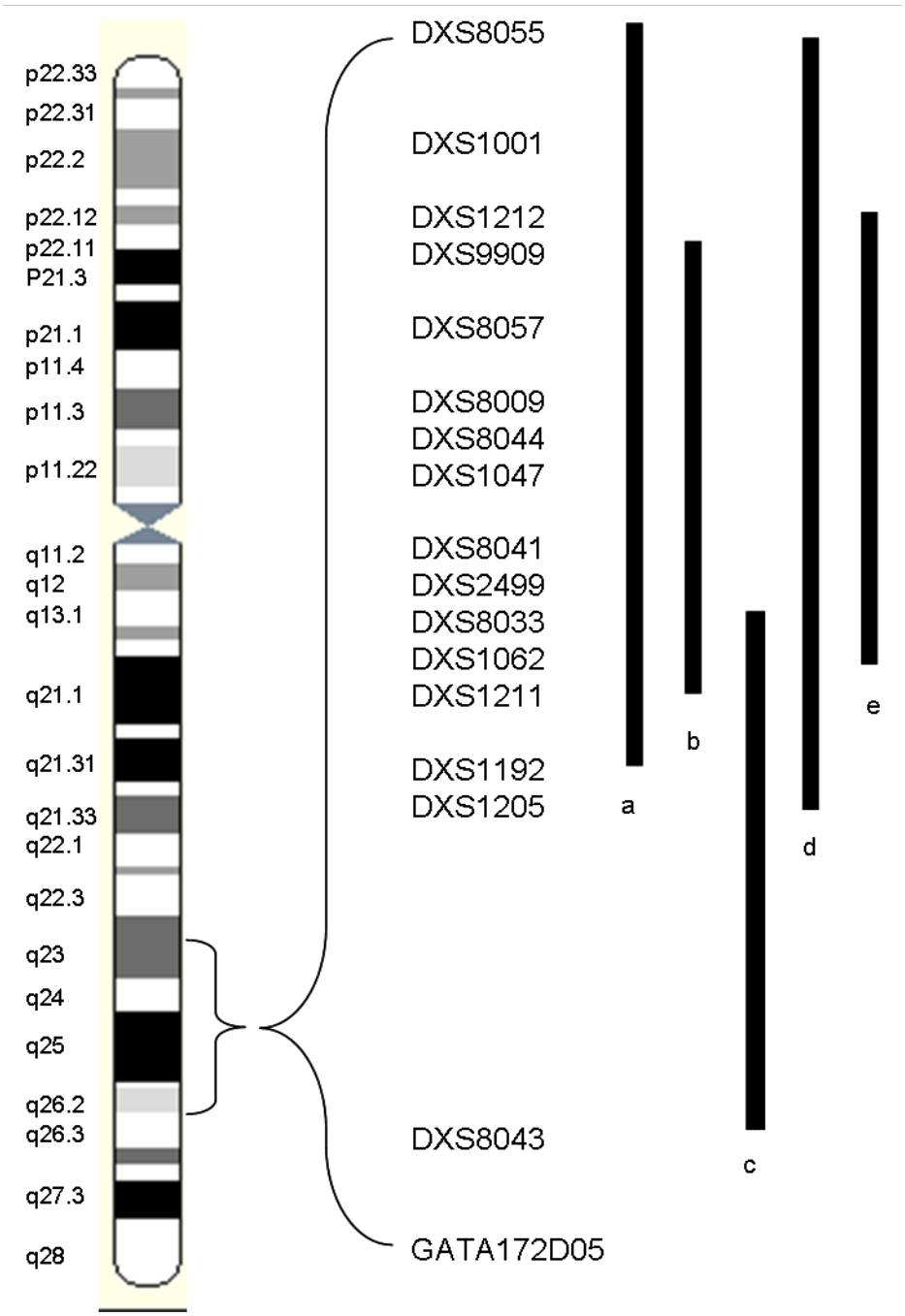

Figure 15 Diagram of the X chromosome showing the q24-q26 locus for X-linked CIN.

A, B and C represent the critical regions for X-linked dominant CIN reported by: (a) Kerrison et al. ***1999***, (b) Kerrison et al ***2001*** and (c) Zhang et al. ***2005***. D and E represent the critical regions for X-linked recessive CIN reported by: (d) Guo et al 2006 and (e) our work.

It can be seen from Figure 15 that the results from our linkage work significantly narrowed the only previous X-linked recessive CIN interval identified by Guo et al (≈37.9

cM to ≈8.0 cM). It was also completed using a single CIN pedigree which therefore reduced the risk of error due to locus heterogeneity. The identified interval still included a region of overlap (≈3.4cM interval between DXS8033 and DXS1062) with the interval for X-linked dominant CIN refined by Zhang to a 4.4 cM region between markers DXS8033 and DXS1211[125]. Therefore, these results did not rebuke the hypothesis that X-linked recessive CIN and X-linked dominant CIN may be caused by mutations in the same gene. However, comparison of overlapping linkage intervals from multiple studies should be interpreted with caution especially when studies employ different diagnostic criteria, different methods of phenotypic assignment, different methods of critical interval calculation and different families in a disease known to be heterogeneous. It is also important to note that previous linkage studies have employed various genetic maps to assign marker positions and cM distances. Many of these locations and even marker orders have changed over time due to updated mapping information.

In this work, the potential errors identified in previous linkage work by us and other groups were minimised. Exhaustive and high resolution methods of phenotyping to avoid errors of phenotypic assignation were employed and patients with any other possible cause for nystagmus were excluded. A single family was used for linkage analysis which reduced the risk of errors due to locus heterogeneity. Only the most up-to-date mapping information and statistical packages were used along with a conservative method of critical interval calculation. Previously published linkage data was not combined with our data as most of these studies had been criticised for the above reasons.

Therefore, this work represented the first study of an X-linked CIN pedigree to employ high resolution phenotyping and a single large pedigree for linkage analysis. We demonstrated that X-linked CIN families could have a small number of manifesting females and suggested that this may be due to X-linked recessive inheritance with X-inactivation. The interval for X-linked CIN was narrowed and the great variability in phenotype and necessity for accurate examination of all family members was confirmed. This work was published in October 2006[38].

4 CHAPTER FOUR – Screening pedigree 1 for mutations in the Cerebellar Degeneration-Related Protein 1 (CDR1) gene

4.1 Introduction

In May 2005 at the Association for Research in Vision and Ophthalmology (ARVO) conference in Fort Lauderdale USA, *Schorderet et al* presented the discovery of a sequence variation found in the Cerebellar Degeneration-Related Protein 1 (*CDR1*) gene in a family with CIN[182]. This gene is located on the X chromosome at position q27.1 and the sequence change reportedly segregated with the disease but no further information was provided at this time. The linkage work reported in chapter 3 was incomplete at this stage and so there was a possibility that a mutation in this gene was responsible for nystagmus in pedigree 1. Consequently, the *CDR1* gene was screened for mutations in this family while the linkage work was underway.

4.2 Methods

Two affected members of pedigree 1 (IV:15 and IV:18) were screened for sequence variations by direct sequencing on the ABI 3130 automated capillary sequencer as detailed in section 2.2.4.3. Primers were designed (as described in section 2.2.5) to include all coding sequence of the 1 exon *CDR1* gene and 30 bp of the 5-prime and 3-prime intronic sequence using reference mRNA sequence NM_004065.2. The Nested PCR technique (section 2.1.3.4) was used such that Long PCR (section 2.1.3.3) was initially performed to produce a 1.6 kb product which was then used as a template for 10 shorter amplimers which were amplified by conventional PCR methods (section 2.1.3.2). Problems were initially encountered with the shorter primer sequences due to multiple short sequence repeats in the *CDR1* gene (see Figure 16):

**ttgttggaagacatgaagatgctggaagacacagagatgctggaagacgtggagatgttggaagacgagcagatgctgga
agccctggagatgctggaagacctggagatataggaagacatggatttgttggaagacgtagcttagttggaagacatatatt
ttctggaagacgt**ggattttctggaagac**atggcttggttggaagacgt**ggattttctggaagac**gtacctttgttggaagacatac
ctttgttggaagacgtacctttgttggaagacgtacctttgttggaagacacaagtaggctggaagacattaatttgatggaaga
catggctttgttggaagacgtggatttgctggaagacacggatttcctggaagacctggatttttcggaagctatggatttgagg
gaagacaa**ggattttctggaagac**atggatagtctggaagacatggctttgttggaagacgtggacttgctggaagacacgga
tttcctggaagacccggatttttggaagctatagatttaagggaagacaa**ggattttctggaagac**atggatagtctggaagac
ctggaggccattggaagatgt**ggattttctggaagac**atggctttttggaagacgtagattttcaggaagacccaaattatccgg
aagacttggattgttgggaagacgt**ggattttctggaagac**tgggaggttactggaagacat**ggattttctggaagac**at**ggattttc
tggaagac**gtggatcttcaggaagacatatattggctggaagacctggatttttccggaagatgtggattgactggaagacct
ggatttggtggaagacgtagatttttctggaagacactgactgactggaagacctggatttctttctggaagacactgattgact
ggaagacctggatttctttctggaagacactgattgactggaagatctagattttctggaagaactagatttactggaagacttg
gatttggtggaagacacagatttttctggaagacatggattagctggaagatctgtatttgatggaagaccttgaaattattgga
agacatggatttcctggaagacgtggattttcctggaagatctggatttggtggaagaccagtaattgctggaagactggattt
gctggaagacttgatttactggaagacttggagcttcttggaagacatggattgtccggaagacatggattgtctggaagatgt
ggattttctggaagctcaggattatctgg**

Figure 16 The Cerebellar Degeneration-Related Protein 1 (CDR1) gene sequence.

The sequence of reference mRNA NM_004065 is shown with an example of a highly repeated motif shown in red.

Following these problems, new primers were designed which excluded any apparent repeat from the primer sequences. Primer sequences are detailed in Table 5. Sequencing results were analysed as detailed in section 2.2.4.3.

Long PCR primers		
	Forward primer	Reverse primer
Set 1	ggaagacctggagatataggaagac	caaatacagatcttccagctaatcc
Set 2	gttggaagacgtagcttagttgga	caagaagctccaagtcttccagta
Set 3	ggagatataggaagacatggatttgt	atttcaaggtcttccatcaaatacaga
Set 4	acctggagatataggaagacatgg	caaatacagatcttccagctaatcc

Short PCR Primers		
	Forward primer	Reverse primer
Set 1	ccaggtcttccagtcaatca	ggaagacatggctttgttgg
Set 2	acatcttccaatggcctcca	ggaagacgtggattttctgg
Set 3	tccacgtcttccaacaaagc	tgattgactggaagacctgga
Set 4	ctggaagacattaatttgatggaag	caatatatgtcttcctgaagatccac
Set 5	gattttcaggaagacccaaattatc	gtcttccctcaaatccatagcttc

Table 5 Sequencing primers for the Cerebellar Degeneration-Related Protein 1 (CDR1) gene.

4.3 Results

No sequence variations were identified for either affected member of pedigree 1.

4.4 Discussion

Mutations in the *CDR1* gene were excluded as the cause of nystagmus in pedigree 1. Interestingly, following completion of the linkage analysis for pedigree 1 (see section 3), it was noted that according to the latest Rutgers combined linkage-physical map (March 2006 build), the *CDR1* gene was located at position 139,693,500 which is just telomeric to the identified interval for pedigree 1 between markers DXS1212 (position 122,214,416) and DXS1062 (position 137,150,000). This suggested that even if additional, as yet un-identified, exons existed for *CDR1*, mutations in these exons were unlikely to be the cause of nystagmus in pedigree 1 as they would likely lie outside the linkage interval. Additionally, Kerrison et al in their 1999 linkage paper of this region screened the *CDR1* gene in one CIN pedigree that had linked to this region. No mutations were found, however the reference sequence used was not presented. In 2004 the NM_004065.1 reference sequence was updated to NM_004065.2 so it is likely that the sequence used by Kerrison et al in this paper was the NM_004065.1 version. By using the 'Blast 2 Sequences' algorithm of the online BLAST program via the National Centre for Biotechnology Information (NCBI) website (http://www.ncbi.nlm.nih.gov) it is possible to compare the two versions (NM_004065.1 and the updated NM_004065.2) of the *CDR1* reference mRNA. It can be seen that from bases 9-1165 of the older sequence (NM_004065.1) there are 3 small sequence changes between the two versions (see Figure 17). However, most significantly the latest sequence (NM_004065.2) includes an additional 141 base pairs at the 5-prime end. Furthermore, the primer sequences quoted in this paper for Long amplification of the initial 1.3-kb fragment were; forward 5'-GGAAGACCTGGAGATGTTGGAAGACGAGCAGA-3' and reverse 5'-

AATGTTTCAATGTCAGGAGTTCCGATGGCACC-3'. However, by using the 'Blast 2 Sequences' algorithm and the Vertebrate Genome Annotation (VEGA) database (http:// vega.sanger.ac.uk) (a central repository for high quality, frequently updated, genomic sequence) it can been seen that neither of these sequences exist in any orientation within the genomic sequence or 2000 bp flanking sequence of the *CDR1* gene. Therefore, it is possible that the reference genomic sequence also varies from the latest builds.

These inconsistencies illustrate the constantly updating nature of genetic sequence databases. Therefore, it is important to qualify all experiments using reference DNA sequences (most modern genetic techniques) with the possibility that the sequences used may be inaccurate or subsequently updated. Similarly, it is important to recognise these inconsistencies when comparing different studies using different resources and techniques. For the above reasons it is possible that a mutation in parts of the *CDR1* gene may have been missed by Kerrison's group in 1999. However, it is possible that a mutation could be missed in our family for the same reasons.

```
Score = 2192 bits (1140),  Expect = 0.0
 Identities = 1156/1159 (99%), Gaps = 2/1159 (0%)
 Strand=Plus/Plus

NM_004065.2  141   AGCTTAGTTGGAAGACATATATTTTCTGGAAGACGTGGATTTTCTGGAAGACATGGCTTG  200
NM_004065.1  9     ........................T...............................  68

NM_004065.2  201   GTTGGAAGACGTGGATTTTCTGGAAGACGTACCTTTGTTGGAAGACATACCTTTGTTGGA  260
NM_004065.1  69    ............................................................  128

NM_004065.2  261   AGACGTACCTTTGTTGGAAGACGTACCTTTGTTGGAAGACACAAGTAGGCTGGAAGACAT  320
NM_004065.1  129   ............................................................  188

NM_004065.2  321   TAATTTGATGGAAGACATGGCTTTGTTGGAAGACGTGGATTTGCTGGAAGACACGGATTT  380
NM_004065.1  189   ............................................................  248

NM_004065.2  381   CCTGGAAGACCTGGATTTTTCGGAAGCTATGGATTTGAGGGAAGACAAGGATTTTCTGGA  440
NM_004065.1  249   ............................................................  308

NM_004065.2  441   AGACATGGATAGTCTGGAAGACATGGCTTTGTTGGAAGACGTGGACTTGCTGGAAGACAC  500
NM_004065.1  309   ............................................................  368

NM_004065.2  501   GGATTTCCTGGAAGACCCGGATTTTTTGGAAGCTATAGATTTAAGGGAAGACAAGGATTT  560
NM_004065.1  369   ............................................................  428

NM_004065.2  561   TCTGGAAGACATGGATAGTCTGGAAGACCTGGAGGCCATTGGAAGATGTGGATTTTCTGG  620
NM_004065.1  429   ...............................-............................  487

NM_004065.2  621   AAGACATGGCTTTTTTGGAAGACGTAGATTTTCAGGAAGACCCAAATTATCCGGAAGACT  680
NM_004065.1  488   ............................................................  547

NM_004065.2  681   TGGATTGTTGGGAAGACGTGGATTTTCTGGAAGACTGGGAGGTTACTGGAAGACATGGAT  740
```

```
NM_004065.1  548   ......................................-.....................  606

NM_004065.2  741   TTTCTGGAAGACATGGATTTTCTGGAAGACGTGGATCTTCAGGAAGACATATATTGGCTG  800
NM_004065.1  607   ............................................................  666

NM_004065.2  801   GAAGACCTGGATTTTTTCCGGAAGATGTGGATTGACTGGAAGACCTGGATTTGGTGGAAG  860
NM_004065.1  667   ............................................................  726

NM_004065.2  861   ACGTAGATTTTTCTGGAAGACACTGACTGACTGGAAGACCTGGATTTCTTTCTGGAAGAC  920
NM_004065.1  727   ............................................................  786

NM_004065.2  921   ACTGATTGACTGGAAGACCTGGATTTCTTTCTGGAAGACACTGATTGACTGGAAGATCTA  980
NM_004065.1  787   ............................................................  846

NM_004065.2  981   GATTTTTCTGGAAGAACTAGATTTACTGGAAGACTTGGATTTGGTGGAAGACACAGATTT  1040
NM_004065.1  847   ............................................................  906

NM_004065.2  1041  TTCTGGAAGACATGGATTAGCTGGAAGATCTGTATTTGATGGAAGACCTTGAAATTATTG  1100
NM_004065.1  907   ............................................................  966

NM_004065.2  1101  GAAGACATGGATTTCCTGGAAGACGTGGATTTTCCTGGAAGATCTGGATTTGGTGGAAGA  1160
NM_004065.1  967   ............................................................  1026

NM_004065.2  1161  CCAGTAATTGCTGGAAGACTGGATTTGCTGGAAGACTTGATTTACTGGAAGACTTGGAGC  1220
NM_004065.1  1027  ............................................................  1086

NM_004065.2  1221  TTCTTGGAAGACATGGATTGTCCGGAAGACATGGATTGTCTGGAAGATGTGGATTTTCTG  1280
NM_004065.1  1087  ............................................................  1146

NM_004065.2  1281  GAAGCTCAGGATTATCTGG  1299
NM_004065.1  1147  ...................  1165
```

Figure 17 A comparison of reference mRNA sequences for the *CDR1* gene.

This figure shows the alignment of the NM_004065.1 and NM_004065.2 reference sequences for the CDR1 gene. Differences are highlighted in red.

5 CHAPTER FIVE – Mutation screening genes from within the identified nystagmus linkage interval for pedigree 1

5.1 Introduction

Following exclusion of the *CDR1* gene and the identification of a linkage interval for nystagmus in pedigree 1, it was necessary to identify and prioritise candidate genes from within the linked region. The coding sequence of these genes was subsequently screened for mutations by direct sequencing. During the course of this experiment another group (*Tarpey et al*) found mutations in the *FRMD7* gene (located within the identified interval for pedigree 1) in some families and sporadic cases of CIN. At this stage the *FRMD7* gene was immediately prioritised and screened in pedigree 1.

5.2 Methods

The UCSC Genome Browser (http://genome.ucsc.edu/index.html?org=Human), created by the Genome Bioinformatics Group of UC Santa Cruz and based on the March 2006 human reference sequence (NCBI Build 36.1) was used to identify all known protein coding genes and predicted genes from the region between the 2 markers DXS1212 and DXS1062. This region contained 70 known protein coding genes and 23 provisional RefSeq (NCBI) predicted genes (see Figure 18).

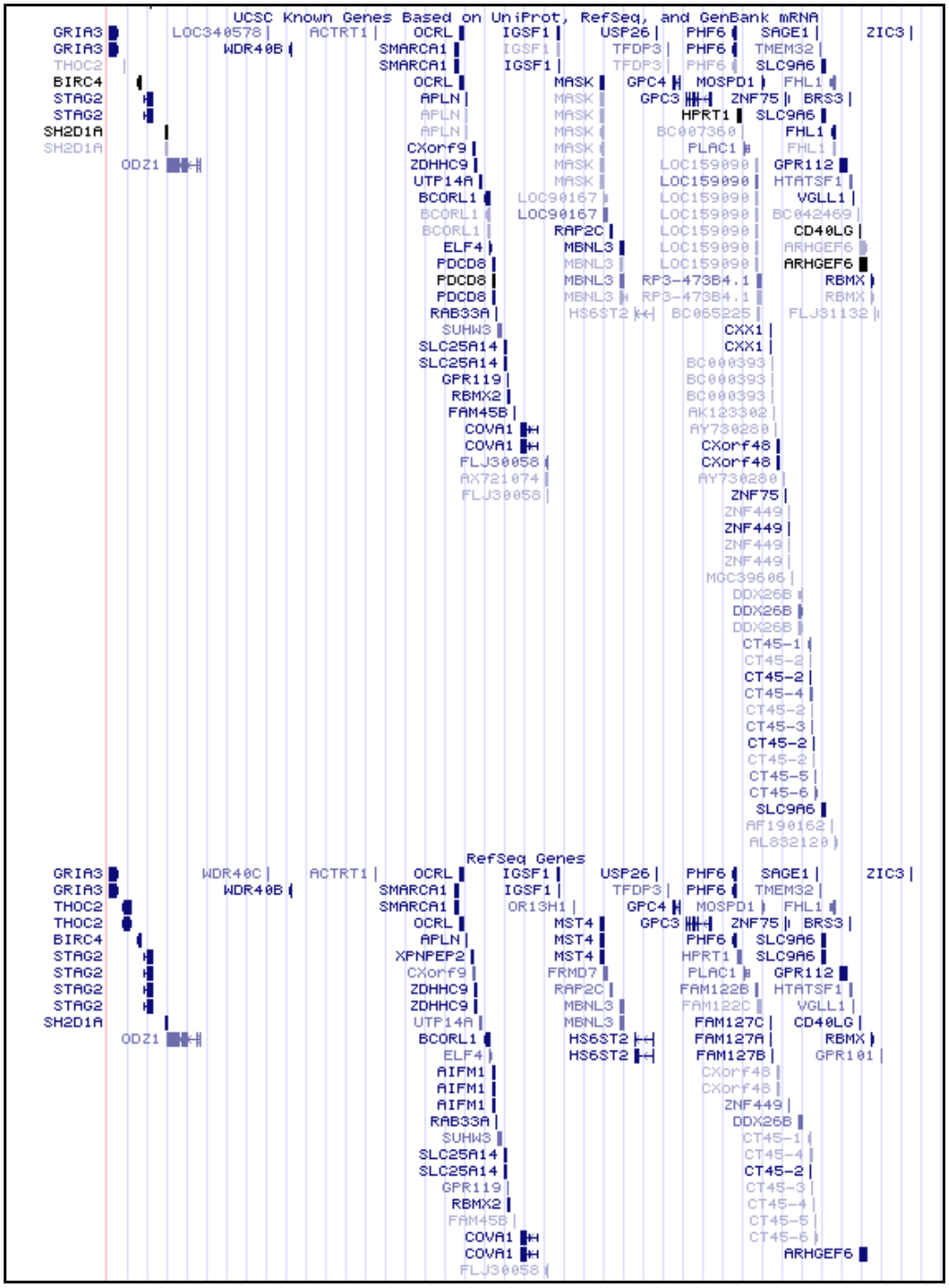

Figure 18 Prioritised genes identified from within a nystagmus locus.

Known protein coding and predicted genes from within the linkage interval identified for nystagmus phenotype in pedigree 1. (USCS genome browser)

The identified genes and predicted genes were then prioritised for mutation screening.

Initially, only protein coding genes were prioritised because of the likelihood that the causative mutation would lie in one of these genes. This has been the case for most recent gene discoveries and was described by Strachan and Read in 2003 as follows; 'as our knowledge of the human genome improves, it becomes increasingly likely that the cause of a disease under investigation will be mutation in a known gene'[11]. Following this, the process of prioritisation was achieved using a set of criteria including; expression pattern (UniGene, GEO Profiles and GEO Datasets, NCBI website), known or predicted function (GeneRIF and GeneOntology functions of the gene-centred information database, NCBI website), homology to relevant paralogous human genes (PSI- and PHIblast functions, NCBI website) and homology to relevant orthologous genes (PSI-, PHI- and RPS-blast functions, NCBI website). The online databases described offered an initial starting point for an extensive literature search for all genes which were subsequently priority ordered. Primers for PCR were designed to include all of the coding exons of each gene and 30 bp of intronic and UTR boundaries (as described by the NCBI and ENSEMBLE online annotation software systems). All amplimers were subsequently sequenced directly (see section 2.2.4.3) for one affected and one unaffected male from pedigree 1 (individuals V:4 and V:3 respectively). To assess segregation of a sequence variation in the pedigree, a restriction enzyme digest was designed using the PstI enzyme and the protocol was the same as that described in section 2.2.4.4. A digest was performed for all informative family members.

5.3 Results

5.3.1 Sequencing results

The results of candidate gene prioritisation are presented in Table 6. The top 9 prioritised genes (coloured red in Table 6) were screened with no mutations identified.

Priority	Gene	Number of Amplicons
1	MBNL3	18
2	ZIC3	20
3	FHL1	5

Priority	Gene	Number of Amplicons
35	RBMX2	-
36	FAM45B	-
37	COVA1	-

4	**OCRL**	**32**
5	**FGF13**	**7**
6	**SMARCA1**	**24**
7	**RP1-203C2.1**	**6**
8	**BCORL1**	**64**
9	**GPR119**	**5**
10	GRIA3	-
11	ODZ1	-
12	**RP6-213H19.2**	**29**
13	BRS3	-
14	GPC4	-
15	GPC3	-
16	THOC2	-
17	PDCD8	-
18	GLUD2	-
19	RP1-57A13.2	-
20	BIRC4	-
21	STAG2	-
22	SH2D1A	-
23	RP11-13E5.1	-
24	WDR40B	-
25	RP13-218H24.1	-
24	WDR40B	-
25	RP13-218H24.1	-
26	APLN	-
27	XPNPEP2	-
28	CXorf9	-
29	ZDHHC9	-
30	UTP14A	-
31	ELF4	-
32	RAB33A	-
33	SUHW3	-
34	SLC25A14	-

38	RP13-102H20.1	-
39	IGSF1	-
40	OR13H1	-
41	RP11-453F18__B.1	-
42	RP6-213H19.1	-
43	RAP2C	-
44	HS6ST2	-
45	USP26	-
46	TFDP3	-
47	PHF6	-
48	HPRT1	-
49	PLAC1	-
50	RP11-308B5.5	-
51	RP3-473B4.1	-
52	MOSPD1	-
53	CXX1	-
54	RP13-565O16.1	-
55	ZNF75	-
56	ZNF449	-
57	DDX26B	-
58	XX-FW88277B6.1	-
59	RP13-36C9.1	-
60	SAGE1	-
61	TMEM32	-
62	SLC9A6	-
63	GPR112	-
64	HTATSF1	-
65	VGLL1	-
66	CD40LG	-
67	ARHGEF6	-
68	RBMX	-
69	GPR101	-
70	F9	-

Table 6 Candidate nystagmus genes screened for mutations.

Sequencing was completed for genes marked red and the number of amplicons per gene is shown.

In October 2006, *Tarpey et al* published a series of families and sporadic CIN cases with a number of different causative mutations in the *FRMD7* gene. This gene was previously known as LOC90167 or RP6-213H19.2. At this stage screening had revealed no mutations in the top 9 prioritised genes and so the *FRMD7* gene (prioritised number 12 in Table 6) was screened in both subjects V:4 and V:3 using the primers listed in .

1f	AGGCCAGAACCAATCACTTC	**1R**	CAGTTTGTTTATCTAATATTTCCTGCC
2f	ACCTGGATTTTCCATCACAC	**2R**	AGAGCCAGACATAAACCAGATG

3f	TTCTGGCAGGAAATATTAGATAAAC	**3R**	GGAGGTGGTGGCATAGATCC
4f	TCATCTGGTTTATGTCTGGCTC	**4R**	GGGCCCAGTAGAAATGGTC
5f	TCTATGCCACCACCTCCTTC	**5R**	AGCGTCTAATGGCATTTAGTG
6f	ACTGGGCCCCACACAAATAG	**6R**	GCAAGGTGGGTATTTGTCATC
7f	TGAAGAGCCTGACCTTCACTC	**7R**	TTTTCTTGGTTACTACATATTCATTGG
8f	AGGCAACAGCTGGATCTTTC	**8R**	CAACACACCAACTGCTGAAG
9f	CGGTAACATGGAACTGGCTC	**9R**	CCAGCAGTTCTAATGGATCAAAG
10f	GCCATGGGTGACCTTATTTC	**10R**	AAAAGGTCCCAGAGCCAATC
11f	TGACTGAGAGCAGGACAAGG	**11R**	AAGAGCTTTCAGCAAGACCTG
12f	TTTGGGTCTTCCTCTTCTAGACC	**12R**	TTGGTATTATGCCTCCCCAG
13f	GGACTTGTCCTTTCCTCTGC	**13R**	AGCTCCTTCCAAACAAGCTG
14f	CACTTTGCTTGTGAGGCCAG	**14R**	CAACTGAGCTGGAGCATTCC
15f	AAAGAGGAACTGCTTTGGGAC	**15R**	CCTCCCCCAGCCCTAAC
16f	GCAGAATCAATTCATGGAAGC	**16R**	TTGGAGATTTCTATGTATCCTGG
17f	TGAAATGACCTTCATGTGAATACC	**17R**	TGATTTCAACAATAAACGAGGC
18f	GATTGAAATGGATTCTTTGTTGC	**18R**	TGCAAGGATACCTTGGAGTTC
19f	TTTGATTTGGGCTCTTCCG	**19R**	TTGGGATTTGAAGGTCTTTG
20f	AAACGATTTGCAGAAACAACC	**20R**	TGCACTGTCTTACAAGCCAAC
21f	TTGAGCCAAGATAACCACCC	**21R**	TGGAAATGTCATTCTTGAGGC
22f	AAGAGTCTGTCCCCAATTTTAGTG	**22R**	CCATTGCTAAGTTCCTCAAAGG
23f	TGTGCTTGGTTCTCTACCTGG	**23R**	TCATCTTGGATCTGGGAGAAG
24f	GAGCCAAATCCTTCTTTATTTG	**24R**	GGTCTGGTTTGGGGCTG
25f	CCAAACAGGAGACTGCCC	**25R**	GCTGCAAGCAGGCTCAG
26f	CTGACAGTGGGAATGCCTG	**26R**	TCTAATGGGCTGTTCACAAATG
27f	TACCCTTTATTCCGTGCTGC	**27R**	ACATACCTAGCTGCAAACTGC
28f	TGCTCAATGCCATGCTCTAC	**28R**	TTGTTGAAACCTTTCTCAAGCTC
29f	TGTGTGTGTGTACCTATAACTGTTGTG	**29R**	AGAATGGCCAGAAGCACTTG

Table 7 PCR primers used for sequencing the *FRMD7* gene.

Sequencing of the *FRMD7* gene revealed a single base insertion (A) after base 880 (reference cDNA sequence NM_194277) in affected subject V:4 but not unaffected subject V:3. The sequence change was designated '880insA, 293fs' using the reference cDNA sequence NM_194277 and the A of the first coding ATG at position 179 as a basis for numbering. This sequence change was evaluated using the SeqBuilder application of the LASERGENE 6 v6.1.3 build 143 sequence analysis software suite (DNASTAR, Inc. Madison, USA). The frameshift variation was predicted to cause a premature stop codon

at amino acid position 301 (reference protein sequence NP_919253) thereby truncating the *FRMD7* protein or leading to nonsense mediated decay of the mRNA.

5.3.2 PstI Restriction Enzyme Digest Results

The PstI enzyme was chosen to cut wildtype (5'..CTGCA^G..3') but not variant (5'..CTGCAAG..3') sequence in the PCR amplimer of exon 9. Therefore, the wildtype allele (cut) produced 2 fragments of 133-bp and 134-bp length and the variant allele (uncut) produced a single 267-bp fragment. Results are illustrated in Figure 19 along with a condensed pedigree to aid subject identification. The variant sequence co-segregated with all affected and carrier females but not unaffected patients. Notably, affected individual III:8 who was excluded from initial work because of a history of congenital cataract was also hemizygous for the 880insA, 293fs variation.

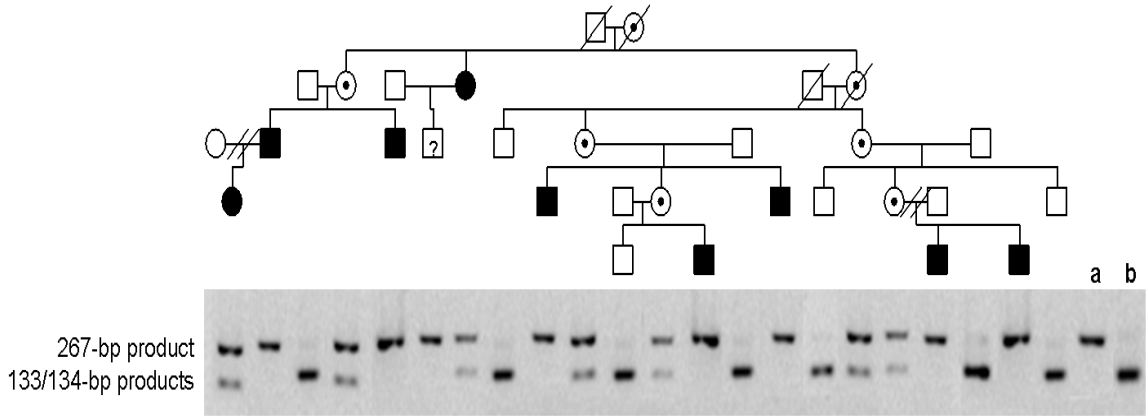

Figure 19 A Restriction Enzyme Digest analysis of an *FRMD7* variation

An abbreviated pedigree diagram and gel photograph of a restriction enzyme digest analysis are presented. The PstI enzyme was used to cut wildtype (5'..CTGCA^G..3') but not mutant (5'..CTGCAAG..3') sequence from the 880insA, 293fs variation in *FRMD7* in pedigree 1.The mutant (uncut) allele generates a 267-bp fragment, while the wild type allele (cut) produces fragments of 133-bp and 134-bp. Control lanes are included: (a) unaffected male III:17 with no PstI enzyme and (b) unaffected male III:17 with PstI enzyme.

5.4 Discussion

The 880insA, 293fs variation identified in pedigree 1 segregated with the disease and was predicted to cause a premature stop codon, thereby truncating the *FRMD7* protein or leading to nonsense mediated decay of the mRNA. The genetic cause of CIN in pedigree 1 had therefore been identified as this new mutation which had not been described in the *Tarpey et al* paper[159].

6 CHAPTER SIX – Assessing the genetic contribution of the *FRMD7* gene to Congenital Idiopathic Nystagmus

6.1 Introduction

The *FRMD7* gene had been identified as a 'nystagmus gene' however, its full contribution to the pathogenesis of CIN was not known. A large cohort of X-linked and sporadic CIN cases were screened for *FRMD7* mutations in order to identify how commonly mutations in this gene caused CIN and to identify new mutations which may provide insights into the significance of various domains within the *FRMD7* gene.

6.2 Methods

Following full Local and Regional Ethics Committee (LREC) approval, 28 simplex CIN cases and 9 additional apparent X-linked CIN pedigrees (see Figure 20) were identified. Patients were either recruited in the Southampton Eye Department or contacted us directly through a call for patients on the Nystagmus Net website (http://www.nystagmusnet.org). All patients had a diagnosis of CIN from an experienced Ophthalmologist and most had undergone full electro-diagnostic investigation with ERG/VEP studies. Where this had not occurred patients were questioned about family history, medical and ophthalmic history and degree of visual impairment before inclusion or exclusion. Patients were excluded if there was any history of other ophthalmic or medical conditions which may suggest an alternative diagnosis to CIN. Informed consent was obtained from all subjects for genetic studies and genomic DNA was isolated from either blood or ORAGENE saliva sample kits (see section 2.1.1).

Figure 20 X-linked congenital nystagmus pedigrees.

9 additional pedigrees screened for *FRMD7* mutations.

SSCP was performed (see section 2.2.4.1) following standard PCR amplification using the *FRMD7* primers in . Specifically, 6% polyacrylamide gels with glycerol were run for 3.5 hours at 25W per gel and at room temperature. 96 female controls (182 control X chromosomes) were screened along with the 37 probands. Direct sequencing (see section 2.2.4.3) was performed for samples with either 'shifts' or failed PCR seen on SSCP gels.

6.3 Results

13 shifts on SSCP gels were found in 9 amplimers in controls and affected probands in equal numbers and these were checked by sequencing and corresponded to known SNPs. In an affected male from X-linked pedigree 2 and an unrelated singleton female, a shift was seen in an amplimer containing exon 4 (see Figure 21).

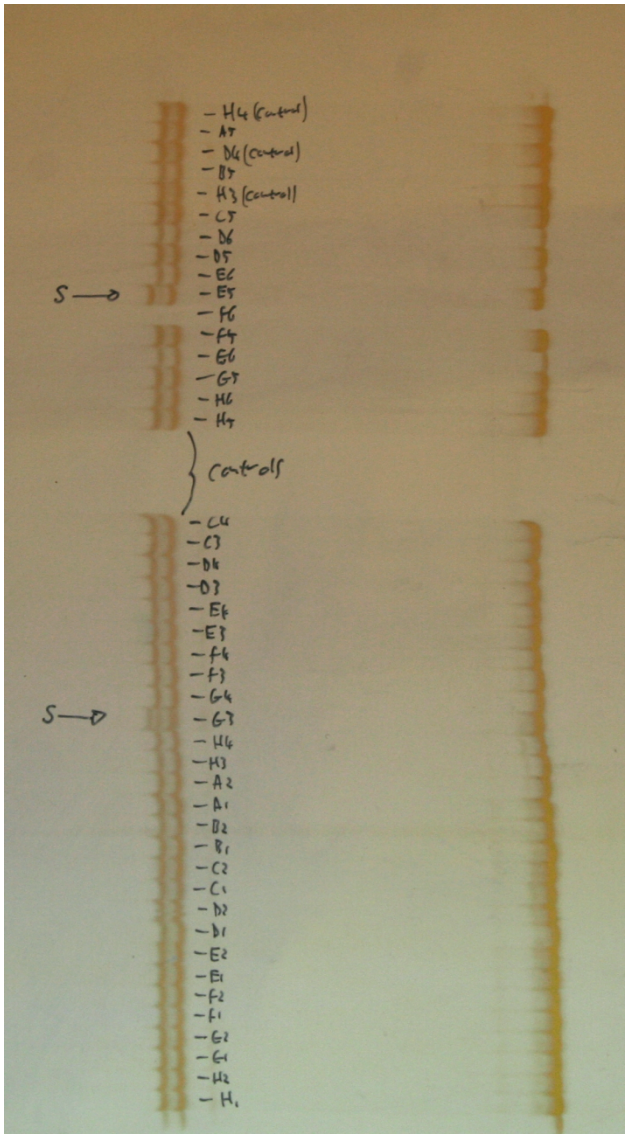

Figure 21 A Single Stranded Conformation Polymorphism (SSCP) gel.

This gel illustrates the two shifts found in single stranded DNA (S) from exon 4 of the *FRMD7* gene when screened in 37 affected nystagmus probands. 5 water controls (controls) and one failed PCR (F6) are also seen. The shifts and failed PCR were all subsequently screened for sequence changes by direct sequencing.

Sequencing subsequently identified a point mutation in the first intronic base after exon 4 in both subjects designated 'IVS4+1G→A'. This sequence change had been previously found in 2 subjects in the *Tarpey et al* paper. When assessed with the LASERGENE 6 v6.1.3 build 143 program this variation was predicted to cause a splice recognition site mutation leading to continued translation into intron 4-5 resulting in a

premature stop codon after 9 amino acids, thereby truncating the *FRMD7* protein or leading to nonsense mediated decay of the mRNA. The mutation was not seen in 182 control X chromosomes in this study or 300 male control individuals by *Tarpey et al*.

6.4 Discussion

The combined results of mutation screening the *FRMD7* gene in pedigree 1 and 37 probands are illustrated in .

Sample	Pedigree	Class	Mutation	Origin
XN3P	X-linked (pedigree 1)	Truncating	880insA, 293fs	English Caucasian
NRD2	Singleton	Truncating	IVS4+1G→A	English Caucasian
XNTW1	X-linked (pedigree 2)	Truncating	IVS4+1G→A	English Caucasian

Table 8 Mutations identified in the *FRMD7* gene.

The reference cDNA sequence NM_194277 is used as a basis for numbering the nucleotide of the mutation. All mutations are located relative to the A of the first coding ATG at position 179. The reference protein sequence NP_919253 is used as the basis for numbering the amino acid variation starting from the first methionine at position 1.

These results confirmed that *FRMD7* mutations are a cause of X-linked CIN and described a novel protein truncating mutation (880insA, 293fs). By screening all exons and splice sites of the *FRMD7* gene we identified mutations in 2/10 (20%) of apparent X-linked pedigrees. This percentage is significantly smaller than that found by Tarpey et al (2006) who identified mutations in 8 of 14 (57%) apparent X-linked pedigrees and 15 of 16 (94%) of proven X-linked pedigrees. This may be because SSCP was our initial method

of mutation screening as apposed to direct sequencing. In our experience, SSCP has a sensitivity of 89%: (95% confidence interval: 79%–96%) compared with direct DNA sequencing [183]. Therefore, our detection rate is likely to be lower than that found by *Tarpey et al* who used direct DNA sequencing. However, in addition, the cohort used by *Tarpey et al* had been previously used for linkage analysis to identify the causative gene inevitably leading to an ascertainment bias. We also identified *FRMD7* mutations in 1/28 (3.6%) singleton cases which is similar to 3/42 (7%) singleton cases found by *Tarpey et al*. Therefore, according to our results the majority (80% in this study) of unselected X-linked families and 96.4% singleton CIN cases do not have *FRMD7* mutations as a cause for nystagmus. This suggests the existence of other prevalent nystagmus genes on the X chromosome and possibly elsewhere. Alternatively, mutations in as yet uncharacterised parts of *FRMD7* such as additional exons, promoters, silencers or enhancers may also exist but would not be detected by the above work.

The *FRMD7* mutations found by Tarpey et al are clustered around the B41 and FERM-C domains[159] (see). The *FARP2* gene on chromosome 13 shares significant homology with a large portion of *FRMD7* including these domains. It is also known that *FARP2* alters neurite length and degree of sprouting in rat embryonic cortical neurones[184;185]. This has lead to the hypothesis that mutations in *FRMD7* may cause nystagmus by altering the neurite length and degree of branching of neurons as they develop in the midbrain, cerebellum and retina[159]. The mutation identified in our study is also located within these domains and thus our results support the hypothesis that mutations in this region of *FRMD7* are particularly important for nystagmus. *FARP2, FARP1* and other homologues may also be potential candidates for nystagmus genes.

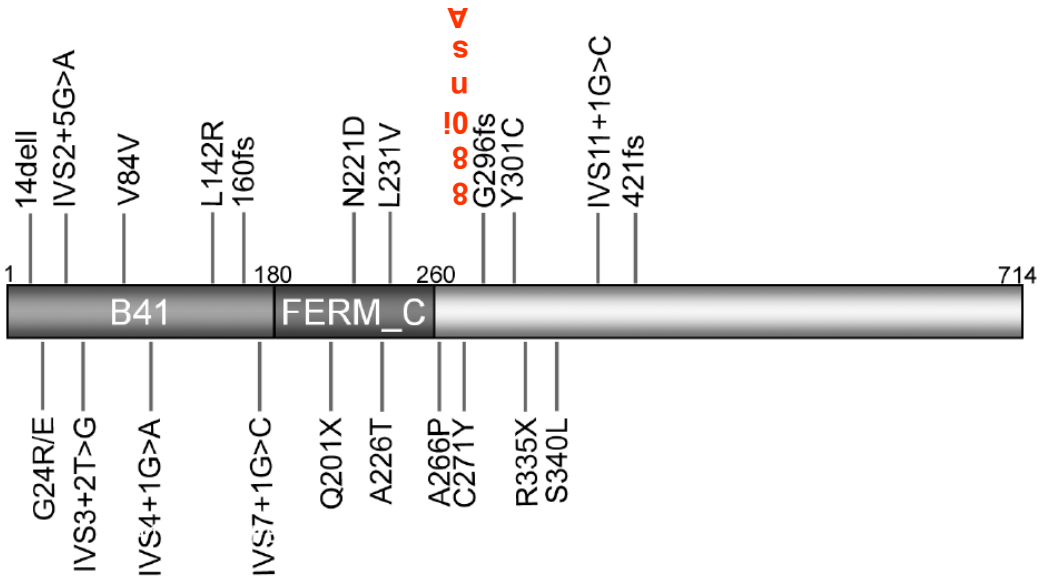

Figure 22 An illustration of the mutations identified in the *FRMD7* gene.

The novel mutation found in pedigree 1 is identified in RED print. (adapted from Tarpey et al 2006[159])

7 CHAPTER SEVEN - Assessment of the role of X-inactivation in pedigree 1

7.1 Introduction

In publications describing X-linked CIN pedigrees, penetrance among obligate female carriers has been variable ranging from 30 to 100%[38;104;125;178]. Possible mechanisms for this variability include skewed X-inactivation, genetic modifiers such as polymorphisms within interacting proteins and other non-genetic influences (such as environmental) on oculomotor development. These factors may also explain why X-linked dominant and recessive pedigrees, with nystagmus (or other ocular diseases), can show linkage to the same region [38;121;186]. In this study we investigate the hypothesis that skewing of X-inactivation is a major contributor to the variable penetrance seen in X-linked nystagmus pedigrees.

The laboratory work for this study was completed at the Wessex Regional Genetics Laboratory, Salisbury District Hospital, Salisbury, UK by Dr Simon N Thomas.

7.2 Methods

For X-inactivation analysis all informative female carriers and affected females were genotyped along with their informative relatives (usually their father) using 2 previously described methods involving the Human Androgen Receptor gene (HUMAR) [24] and the zinc finger, MYM-type 3 **(**ZNF261)[187] gene. Both assays comprised amplification of a short fragment of X chromosome (Xq13 in both assays) which was used to determine the activation status of each X chromosome (i.e. the maternal or paternal X chromosome). Each amplimer contains a polymorphic marker adjacent to the promoter of the gene (HUMAR or ZNF261) which is unmethylated on the active X chromosome and methylated on the inactive chromosome. Prior to amplification, both assays employed a methylation sensitive restriction enzyme which cuts at the promoter

site on the active (unmethylated) but not on the inactive (methylated) X chromosome. Therefore, by examining the size and peak heights of the amplification products and by tracking the inheritance of alleles from parents to offspring, we ascertained the percentage of cells in which the maternal or paternal X chromosome had been inactivated. To calculate the X-inactivation ratio, each sample was set up in duplicate: one digest and one mock digest without enzyme. Both were then PCR amplified and analysed on the ABI 3130 Genetic Analyser and the GeneMapper® Software v4.0 (see section 3.2.2). Manufacturer's recommendations were followed for allele calling and for heterozygotes, the ratio of the two peaks was compared between the undigested and digested samples. Male samples were used for haplotype reconstruction.

7.3 Results

The results of the X-inactivation assays are summarised in Table 9:

Sample	DNA	Sex	Status		HUMAR				ZNF			Degree of skewing
				Allele 1		Allele 2		Allele 1		Allele 2		
				Size	(% activity)	Size	(% activity)	Size	(% activity)	Size	(% activity)	
II : 3	Saliva	F	Carrier	233	(44) (failed)	241	(56) (failed)	264	(52) (53)	272	(48) (47)	**Random**
II : 5	Blood	F	Affected	233	(05) (04)	241	(95) (96)	264	(98) (98)	272	(02) (02)	**Very skewed**
III : 2	Saliva	M	Affected	233	-	-	-	264	-	-	-	**-**
III : 6	Saliva	M	Affected	233	-	-	-	272	-	-	-	**-**
III : 16	Saliva	F	Carrier	233	(n/i) (n/i)	-	-	256	(14) (15)	272	(86) (85)	**Skewed**
III : 17	Blood	M	Normal	233	-	-	-	268	-	-	-	**-**
III : 18	Blood	F	Normal	233	(n/i) (n/i)	-	-	256	(98) (98)	272	(02) (02)	**Very skewed**
III : 19	Blood	F	Carrier	233	(n/i) (n/i)	-	-	256	(88) (87)	272	(12) (13)	**Skewed**
IV : 1	Saliva	F	Carrier	241	(n/i) (n/i)	-	-	264	(73) (69)	270	(27) (31)	**Skewed**
IV : 2	Saliva	F	Affected	236	(27) (29)	241	(73) (71)	264	(n/i) (n/i)	-	-	**Skewed**
IV : 6	Saliva	F	Carrier	227	(39) (40)	233	(61) (60)	270	(42) (42)	272	(58) (58)	**Random**
IV : 7	Saliva	F	Carrier	230	(31) (27)	233	(69) (73)	262	(23) (27)	272	(77) (73)	**Skewed**
IV : 14	Blood	F	Normal	233	(73)	256	(27)	264	(18)	266	(82)	**Skewed**

					(71)		(29)		(18)		(82)	
IV : 15	Blood	M	Affected	233	-	-	-	272	-	-	-	**-**
IV : 17	Saliva	F	Carrier	233	(n/i) (n/i)	-	-	268	(51) (52)	272	(49) (48)	**Random**
IV : 17	Blood	F	Carrier	233	(n/i) (n/i)	-	-	268	(54) (57)	272	(46) (43)	**Random**
IV : 18	Blood	M	Affected	233	-	-	-	272	-	-	-	**-**
IV : 19	Blood	F	Normal	221	(20) (30)	233	(80) (70)	262	(44) (43)	270	(56) (57)	**Skewed**
IV : 21	Blood	F	Carrier	215	(94) (91)	233	(06) (09)	256	(04) (05)	274	(96) (95)	**Very skewed**
V : 2	Blood	F	Carrier	233	(63) (63)	256	(37) (37)	264	(21) (20)	272	(79) (80)	**Skewed**
V : 6	Saliva	F	Carrier	221	(53) (67)	233	(47) (33)	270	(55) (fail)	272	(45) (fail)	**Random**
V : 7	Saliva	F	Normal	221	(56) (56)	233	(44) (44)	256	(41) (33)	264	(59) (67)	**Random**

Table 9 Humar and ZNF261 X-inactivation assays for pedigree 1.

Random = average result of skewing between 50% and 70%; Skewed = average result of skewing between 70% and 90%; Very Skewed = average result of skewing greater than 90%.

Ten of the 16 females tested demonstrated at least moderate skewing, including both affected females, and three cases showed skewing of >95%. However, as illustrated it is not always possible to tell which X chromosome is inactivated. Mutation status of each X chromosome was known for one affected female and the X carrying the *FRMD7* mutation was active in 73% of cells. For informative unaffected carriers, the X chromosome carrying the *FRMD7* mutation was active in between 6 and 80 % of cells. Therefore, there was no clear-cut difference in the pattern of X-inactivation between affected and unaffected carriers of the mutations. Interestingly, for individual IV:17 assays were performed for both blood and saliva extracted DNA with identical results.

7.4 Discussion

We had previously proposed that the most likely explanation for the variable phenotype in carrier females in pedigree 1 was variability in the pattern of X-inactivation[38;132]. Skewed X-inactivation, (significant deviation away from the expected 50:50 contribution of each X chromosome) has been described in other ocular diseases[186;188] and may explain why other X-linked nystagmus pedigrees linked to the locus containing *FRMD7* have shown either dominant or recessive inheritance

patterns[38;104;159;178]. The vast majority of genes on the long arm of the X chromosome are subject to X-inactivation, including those immediately flanking *FRMD7*: *MST4*, *MBNL3* and *RAP2C* [27]. Since genes which are subject to, or escape from, X-inactivation tend to be clustered into domains, it is very likely that *FRMD7* is inactivated. Only a very small proportion of normal females show significant levels of skewed inactivation[189]. However, our results suggest an excess of skewing in pedigree 1 (10 of 16 females including 3 with >95% skewing). Interestingly, of the 10 females with skewing, 7 are under the age of 40 and for 3 of these patients the assays were performed on saliva samples. This suggests that the observed skewing in pedigree 1 is not due to age-related secondary skewing[24] or specific to blood.

In October 2007, Kaplan *et al* published the results of an X-inactivation study in a large Turkish pedigree with CIN caused by a novel non-truncating missense mutation in *FRMD7* (c.686C>G)[190]. Using the HUMAR assay they found that skewed X-inactivation was significantly increased in the CIN affected females when compared with the unaffected females in the pedigree (odds ratio was 26:1; 95% CI = 1.83 to 367.7). They also found that one female who was homozygous for the mutation, was not phenotypically different to the heterozygous manifesting females. These results added weight to our findings of skewed X-inactivation in an *FRMD7* mutant CIN pedigree. Furthermore, if a homozygous mutant female has a similar phenotype to a manifesting heterozygous female, this might also suggest that X-inactivation is occurring for the *FRMD7* gene.

By combining these data it seems likely that there are four possible explanations for the X-inactivation results in *FRMD7* mutant CIN pedigrees:

Firstly, the effect of X-inactivation on penetrance may be subtle, rather than all-or-nothing, as neither unaffected nor affected carrier females have complete skewing. It is possible that the proportion of cells in which the mutation-carrying X is active may be higher in the crucial tissues in the affected cases than in carrier females. Many X-linked disorders do not fit classical dominant or recessive modes of inheritance and female carriers display variable penetrance[191]. For example, mutations in the dystonia-deafness

peptide gene (DPP) cause incomplete penetrance in females with variable X-inactivation in blood from 50:50 to >95:5[192]. Thus mutations in X-linked genes can cause partial cell selection and incompletely skewed X-inactivation. This could explain variable clinical expression within the same family.

Secondly, the results obtained from lymphocytes and saliva samples may not necessarily reflect the patterns of X-inactivation in the tissue whose pathophysiology causes nystagmus (as yet unknown). In normal females X-inactivation ratios are normally similar between tissues[24]. However, for certain X-linked conditions complete skewing may be restricted to specific cell lineages and different patterns of X-inactivation are seen in all other tissues[25]. Selection against cells which have inactivated the normal X may be more pronounced in tissues where most *FRMD7* expression occurs, possibly parts of the developing brain and retina[159].

Thirdly, variable penetrance may be at least in part due to other genetic factors. The results of the X-inactivation studies give a clear overlap in the patterns of X-inactivation between unaffected and affected carrier females, and IV:18 who is negative for the *FRMD7* mutation is one of the females with severe skewing. It is possible that the higher frequency of skewed X-inactivation seen in this family may be unrelated to nystagmus as we know that skewed X-inactivation *per se* may run in families[23].

Finally, a major caveat of these results is that both assays used markers at the Xq13 locus. This is a considerable distance from the location of *FRMD7* at Xq26-27. This could be important as approximately 15% of X-linked genes escape X-inactivation to some degree, and this proportion of genes differs dramatically between different regions of the X chromosome[26;27]. Additionally, 10% of X-linked genes show variable patterns of inactivation and are expressed to different extents from some inactive X chromosomes[27]. Therefore, it is possible that the assays do not accurately represent X-inactivation occurring in the *FRMD7* gene. If it were possible to design an assay incorporating a polymorphic marker and methylation sensitive promoter at the *FRMD7* site, this would address these caveats.

Importantly, by showing that there is no definitive pattern of X-inactivation in carrier or manifesting females, this work has shown that determining the X-inactivation pattern in blood or saliva cannot be used to identify carrier status for nystagmus caused by *FRMD7* mutations using such assays. This is important from a diagnostic viewpoint as X-inactivation is used as a surrogate test for carrier status in other X-linked conditions[193;194].

8 CHAPTER EIGHT – Clinical and genetic investigation of a family with an atypical congenital nystagmus syndrome

8.1 Introduction

Nystagmus before six months of age can be defined as early onset nystagmus[37]. As detailed previously (see Chapter 1), it may be divided into three categories: sensory defect nystagmus (SDN) in which there is a proven sensory impairment, congenital idiopathic nystagmus (CIN) also known as "motor nystagmus" in which no visual or neurological impairment can be found and neurological nystagmus (NN) which is associated with neurological disease[37]. CIN is a diagnosis commonly made after full ophthalmic examination and ideally also after a normal ERG and VEP. Typically, CIN has a horizontal, uniplanar nystagmus waveform with accelerating slow phases[37] although other waveforms have been described in patients with CIN[37].

This chapter describes the clinical and genetic investigation of a family with apparent atypical CIN.

8.2 Methods

8.2.1 Clinical methods

The study had the approval of the local and regional ethics committee and conformed to the tenets of the Declaration of Helsinki. 8 individuals from a single pedigree (VNCM family, see Figure 23) underwent a full clinical history interview, detailed clinical examination including LogMAR visual acuity, intra-ocular pressure (IOP) recording, anterior and posterior segment slitlamp examination including iris trans-illumination testing in a darkened room and full orthoptic assessment. Clinical neurological examination was performed by a clinical geneticist and comprised cranial

nerve examination, cerebellar examination and both upper and lower limb examination for power, tone, sensation, vibration sense and coordination.

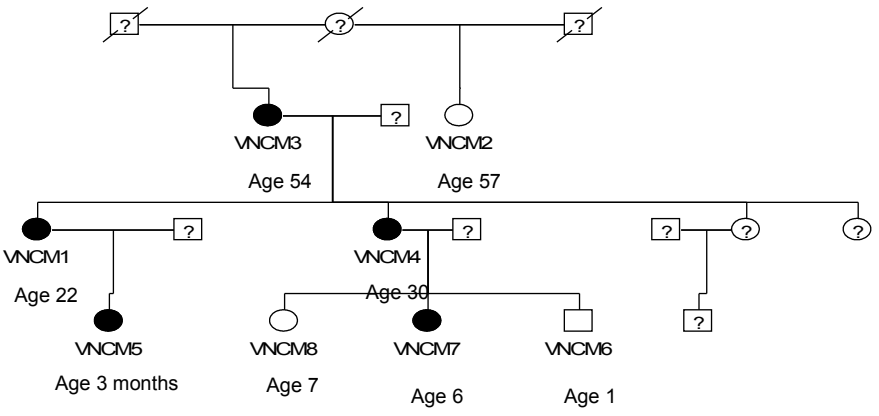

Figure 23 A pedigree diagram of a family with atypical hereditary nystagmus.

Subject ID codes and age at the time of examination are presented for all phenotyped family members of the VNCM pedigree. Black circles/squares are affected subjects; clear circles/squares are unaffected subjects.

All patients had detailed clinical eye movement examination by an orthoptist including: assessment in primary position and 9 positions of gaze, horizontal saccades, vertical saccades, smooth pursuit eye movements, cover/uncover test and accommodation testing. Subjects in whom nystagmus was found, also had eye movement recordings using a Skalar IRIS IR Light Eye Tracker equipment (Cambridge Research Systems Ltd. Rochester UK, www.crsltd.com) (see Figure 11) except for VNCM-5 who was a 3 month old baby and had clinical examination only. Measurements in all other subjects using a 1° red square target comprised; fixation waveform, fixation amplitude, fixation frequency, waveform in left gaze (20 degrees), waveform in right gaze (20 degrees), horizontal binocular OKN to rightward and leftward drifting gratings measuring 0.2 cycles per degree at a velocity of 25° per second, horizontal smooth pursuit, horizontal saccades using a 1° red square target moving at 500ms intervals,

waveform in vertical positions of gaze, vertical binocular OKN, vertical saccades using a 1° red square target moving at 500ms intervals and vertical smooth pursuit recordings.

Three patients also had extensive electrophysiological examinations. International Society for Clinical Electrophysiology of Vision (www.iscev.org) standardised electroretinograms (ERGs) and visual evoked potential (VEP) recordings were recorded in 3 females (VNCM-1, VNCM-3 and VNCM-5). Monocular stimulation and a 3 channel trans-occipital electrode montage were employed for VEP recordings to optimise detection of neuronal misrouting suggestive of ocular albinism.

Magnetic resonance brain scans had been performed and sagittal t1 and axial dual echo images were obtained in individuals VNCM-3 and VNCM-5.

Informed consent was obtained from all subjects for genetic studies and genomic DNA was isolated from ORAGENE saliva sample kits (see section 2.1.1.2).

8.2.2 Molecular genetic methods

Initially 2 samples from this pedigree (VNCM-1 and VNCM-2) were included in *FRMD7* gene screening by SSCP analysis as detailed in chapter 6.

Subsequently, exons 2-12 of the *FARP1* gene (VEGA transcript ID OTTHUMT00000045541) were also screened for mutations in the same 2 subjects by HRM analysis using optimised amplimers <200bp in length . These exons were targeted as they contain the domains which are homologous to the *FRMD7* gene as detailed previously (Chapter 6).

The *CACNA1A* gene (NM_000068.3) was subsequently screened in subject VNCM-1 by direct sequencing at the Leiden University Medical Centre (LUMC) postnatal DNA analysis service. This sequencing work was outsourced due to the significant financial saving when screening only one sample for a very large gene (48 exons). This gene was targeted following identification of certain similarities between the clinical features in this family and that of other patients with Episodic Ataxia 2 (EA2, MIM 108500)[195;196] and Spinocerebellar ataxia type 6 (SCA6, MIM 183086)[197;198], both of which are associated with genetic variations in this gene.

To assess co-segregation of an identified sequence variation in the pedigree, direct sequencing of this variation was performed in all 8 VNCM family members by standard methods.

This sequence variation was subsequently sought in 150 normal control subjects. An HRM assay was optimized to detect this variation within a 120bp fragment by standard methods using; AGCCCCTCATGCTCTCTGT sense primer and CGGCGAAGATGAACATGAATA antisense primer. This assay was run by standard methods (see section 2.2) using an annealing temperature of 60°C and a 10 µl reaction volume comprising: 1 µl genomic DNA, 5 µl of sensimix dt (Catalogue Number:QT6T3-02, Quantace, Finchley, UK QT6T3-02), 0.15 µl of each primer, 2.7 µl of water and 1 µl of Syto 9 (Catalogue Number:S34854, Invitrogen, Paisley, UK) on the Rotor-Gene™ 6000 (Corbett Life Science Ltd, Brisbane, Australia). The efficacy of the assay to discriminate the variation from wildtype was tested using the VNCM samples as controls. The positive control (VNCM-4), a negative control (VNCM-8) and two water controls were run in the same experiment. The 150 normal control DNA samples came from patients who had been evaluated and phenotyped for another study into Age Related Macular degeneration (ARMD) and did not have nystagmus or any other eye disease.

8.3 Results

8.3.1 Clinical phenotyping results

8.3.1.1 History and examination

VNCM-3 is a female who was 54 years old at the time of examination. On detailed questioning it was revealed that this subject had been found to have a subtle ataxia of unknown cause and had been discharged from care 10 years earlier. An MR brain in 1995 had shown a small cerebellar vermis, possibly an early sign of vermis atrophy. Onset of symptoms was at approximately 35 years and her symptoms had not

deteriorated greatly since then. A slightly fluctuating course with slurred speech and unsteady gait on bad days but without dramatic disabling episodes was described. She had occasional migrainous headaches but without any accompanying symptoms. Examination showed a broad based gate, no dysarthria, moderate finger-nose ataxia and mild shin-heal ataxia, no weakness, normal tendon reflexes, flexor plantar responses and no sensory loss. Interestingly, VNCM-3 had no response to oral acetazolamide treatment for 3 weeks and this was subsequently discontinued. This is notable as oral acetazolamide treatment can prevent or abort the episodic symptoms of EA2 and FHM[199;200].

MR brain scanning in subject VNCM-5 found no abnormalities and VEP and ERG recordings were normal for all the subjects recorded (VNCM-1,VNCM-3 and VNCM-5).

All the other family members had no clinical symptoms or signs of neurological disease. Other family members included; a 22 year old female VNCM-1, a 57 year old female VNCM-2, a 30 year old female VNCM-4, a 3 month old female VNCM-5, a 1 year old male VNCM-6, a 6 year old female VNCM-7 and an 7 year old female VNCM-8.

Interestingly, subsequent to our examination of this family, subject VNCM-4 (now age 31) has developed a mildly unsteady gait and minimal finger-nose ataxia with no other symptoms or signs. She still describes no episodic nature or migrainous symptoms.

8.3.1.2 Nystagmology

VNCM-2, 6 and 8 had no eye movement anomalies on clinical examination and therefore subsequent eye movement recordings were not performed. Subjects VNCM-1, 3, 4, 5 and 7 all had nystagmus. VNCM-5 had clinical nystagmology but not limbal infrared nystagmology because of her young age at the time of examination (3 months). She had conspicuous downbeat nystagmus in the primary position and in either lateral gaze or down gaze. She also had gaze-evoked nystagmus in either lateral gaze and horizontal eye movements on spinning were preserved with no evidence of a saccade

palsy. Eye movement findings for VNCM-5 and all other subjects with nystagmus are summarised in Table 10. All waveforms exhibited linear or decelerating slow phases, no accelerating slow phases were seen in any waveform.

Patient ID	**VNCM-1**	**VNCM-3**	**VNCM-4**	**VNCM-5***	**VNCM-7**
Clinical status	Nystagmus	Nystagmus	Nystagmus	Nystagmus	Nystagmus
Age at examination	22 years	54 years	30 years	3 months	6 years
Fixation waveform	downbeat nystagmus	downbeat nystagmus	left beating nystagmus	downbeat nystagmus	steady
Nystagmus amplitude/ frequency in primary	0.8 deg (2 beats/sec)	2.5 deg (3.5 beats/sec)	1 deg (2 beats/sec)	not recorded	na
Waveform in left gaze	left beating	left beating	left beating	left beating	left beating
Nystagmus amplitude/ frequency in left gaze	0.2 deg (2 beats/sec)	2 deg (4 beats/sec)	1 deg (4 beats/sec)	clinically moderate intensity	1 deg (2 beats/sec)
Waveform in right gaze	right beating	right beating	right beating	right beating	right beating
Nystagmus amplitude/ frequency in left gaze	5 deg (2.5 beats/sec)	3 deg (4 beats/sec)	3 deg (2.5 beats/sec)	clinically moderate intensity	2 deg (2 beats/sec)
Horizontal OKN	low gain in both directions	low gain in both directions	low gain in both directions	not recorded	low gain in both directions
Horizontal smooth pursuit	saccadic pursuit	mixed smooth and saccadic	mixed smooth and saccadic	not recorded	saccadic pursuit
Horizontal saccades	normal	dysmetric	dysmetric	not recorded	dysmetric, mainly hypermetric
Waveform in upgaze	steady	steady	upbeating	upbeating	upbeating
Nystagmus amplitude/ frequency in upgaze	na	na	2 deg (6 beats/sec)	clinically moderate intensity	2 deg (6 beats/sec)
Waveform in downgaze	downbeating	downbeating	downbeating	downbeating	downbeating
Nystagmus amplitude/ frequency in downgaze	2.5 deg (2.5 beats/sec)	2.5 deg (4 beats/sec)	1 deg (3 beats/sec)	clinically moderate intensity	2.5 deg (2.5 beats/sec)

Vertical OKN	low gain in both directions	low gain in upgaze, absent in downgaze	low gain in both directions	not recorded	not recorded
Vertical saccades	dysmetric	dysmetric	dysmetric	not recorded	dysmetric
Vertical smooth pursuit	saccadic pursuit	mixed smooth and saccadic	saccadic pursuit	not recorded	mixed smooth and saccadic
Rebound nystagmus	present	not seen	not seen	not recorded	not seen
Gaze paretic nystagmus	present	present	present	present	present

na = not applicable

*** = subject examined clinically only.**

Table 10 Summary of nystagmus waveforms identified in the VNCM pedigree.

All subjects (except for VNCM-5) had detailed nystagmology using the Skalar IRIS IR Light Eye Tracker equipment (Cambridge Research Systems Ltd. Rochester UK, **www.crsltd.com**)

8.3.2 Molecular genetic results

Screening of all known exons and splice sites of the *FRMD7* gene by SSCP analysis and of exons 2-12 of the *FARP1* gene by HRM analysis identified no mutations in either subject VNCM-1 or VNCM-2.

Direct sequencing of the *CACNA1A* gene for subject VNCM-1 identified a sequence variation; Chr19(NCBI 36):g.13233416T>G which corresponds to c.4110T>G p.Phe1370Leu in the NM_000068.3 transcript (see Figure 24). No other variations were identified in this gene.

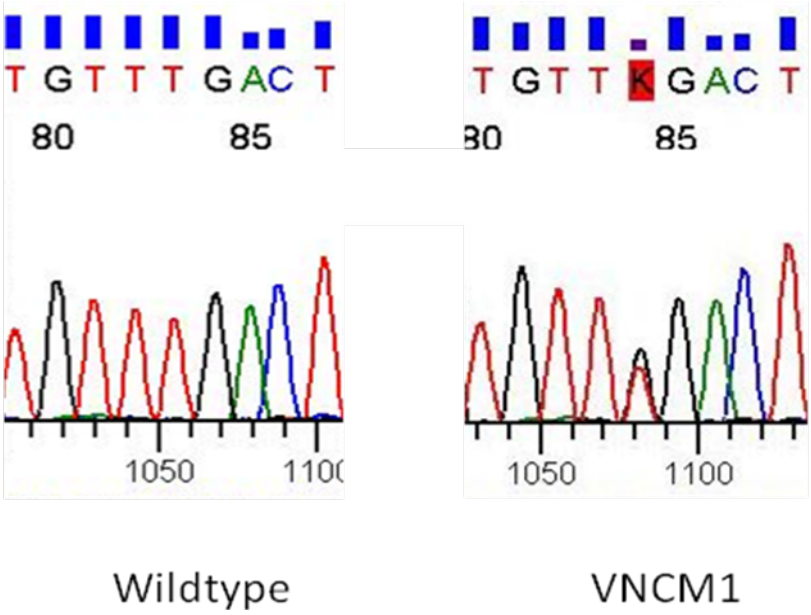

Figure 24 Electropherogram results of direct sequencing for the *CACNA1A* gene.

Direct sequencing of the *CACNA1A* gene in individual VNCM-1 reveals the Chr19(NCBI 36):g.13233416T>G mutation.

Direct sequencing of the c.4110T>G p.Phe1370Leu (NM_000068.3) variation in subjects VNCM-1:8 showed that the variation co-segregated with the disease phenotype. All affected subjects had the c.4110T>G p.Phe1370Leu (NM_000068.3) variation and all unaffected subjects the wildtype allele (see Figure 25).

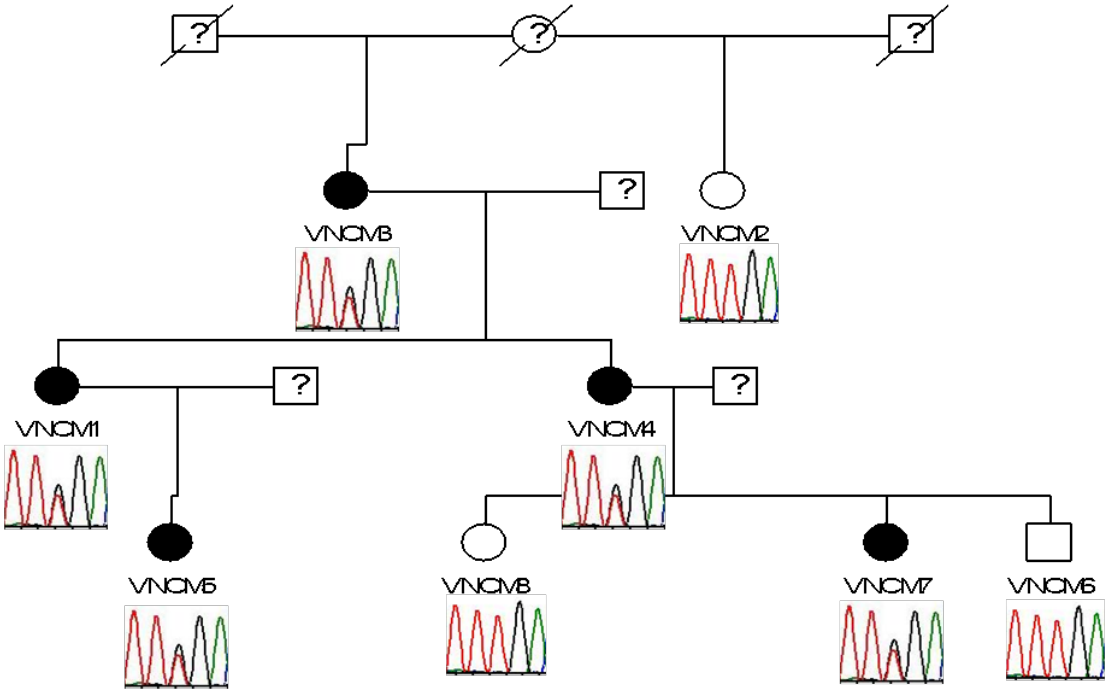

Figure 25 Co-segregation of a variation in a nystagmus pedigree.

Co-segregation of the c.4110T>G p.Phe1370Leu (NM_000068.3) variation in a pedigree with atypical hereditary nystagmus (VNCM family) is presented. Mutant sequence shows a heterozygote peak at position 3 of the electropherogram cut-outs and wildtype sequence shows a single red peak corresponding to a thymine base.

Co-segregation confirms that this sequence variation could be the causative mutation in this pedigree. Assuming that co-segregation of the disease phenotype with the variation would be expected to occur by chance in 50% of cases, a simple calculation could be applied to asses the likelihood of this apparent familial co-segregation occurring by chance. By multiplying the 1:2 probabilities for each of the 6 informative meioses (therefore excluding VNCM-2), it can be seen that the likelihood of this co-segregation occurring by chance is 1:64.

Another, similar way to asses the significance of this co-segregation is by using the LOD score[129]. For the purpose of this test we again excluded individual VNCM-2 whose contribution to the genetic information is negligible. Given all seven remaining meioses showed no evidence of recombination and our hypothesis that the c.4110T>G

p.Phe1370Leu variant may be causal, we assumed no recombination (θ = 0). Using standard methods[201] the LOD score for these data is calculated as 2.11. As the *CACNA1A* gene has already been identified for similar phenotypes by a number of groups, it is reasonable to impose a higher prior probability of linkage as has been described before[201]. Under such circumstances it has been asserted that the critical LOD score should be set to 2 rather than 3. Therefore, using these measures and corrections, a LOD score of 2.11 would be formally assessed as significant.

Prior to screening 150 control DNA samples for the variation, the efficacy of the HRM assay to discriminate the variation from wildtype was tested using the VNCM samples. VNCM-6 and VNCM 8 (wildtype) were compared with VNCM-4 and VNCM-7 (variation) and all were run in duplicate. Results showed that the variation could be readily discriminated (see Figure 26).

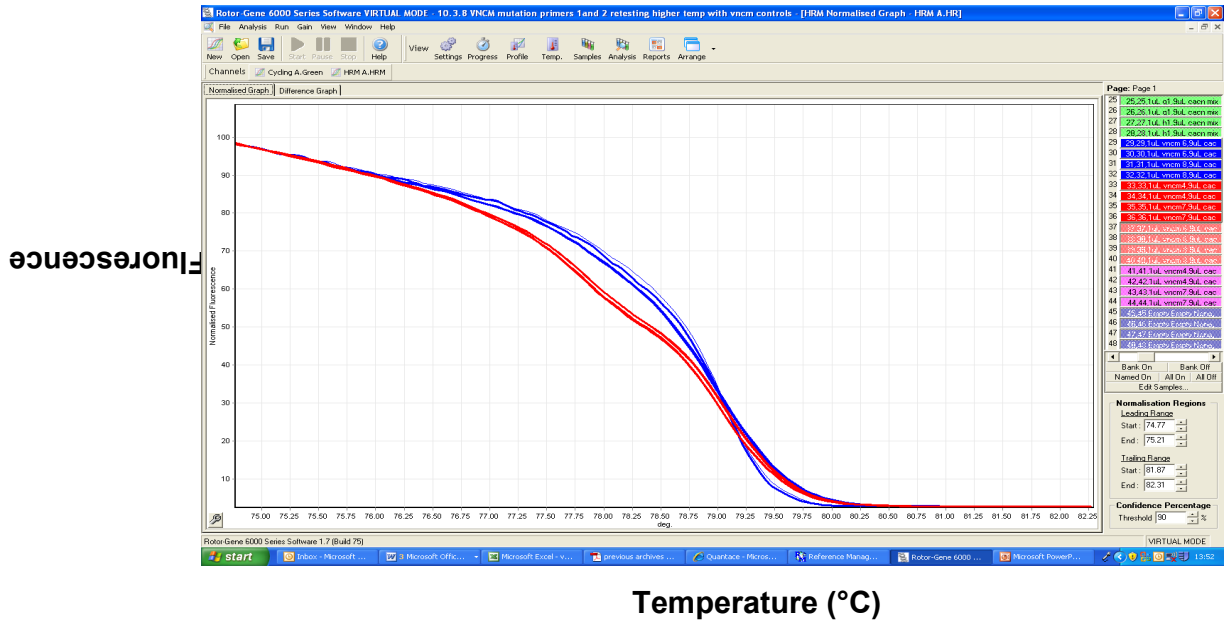

Figure 26 Validating a High resolution melt (HRM) assay.

A validation curve for the HRM assay is presented to highlight the melting differences between a wildtype amplimer and that with the *CACNA1A* C.4110T>G p.Phe1370Leu (NM_000068.3) variation. A screen shot from the Rotorgene 6000 real-time thermocycler demonstrates the discrimination between the melt profiles for the sequence variation (VNCM-4 and VNCM-7, RED) vs wildtype (VNCM-6 and VNCM-8, BLUE).

Subsequent screening for the C.4110T>G p.Phe1370Leu (NM_000068.3) variation using this assay in 150 unrelated control subjects (300 chromosomes) did not identify any heterozygous or homozygous individuals.

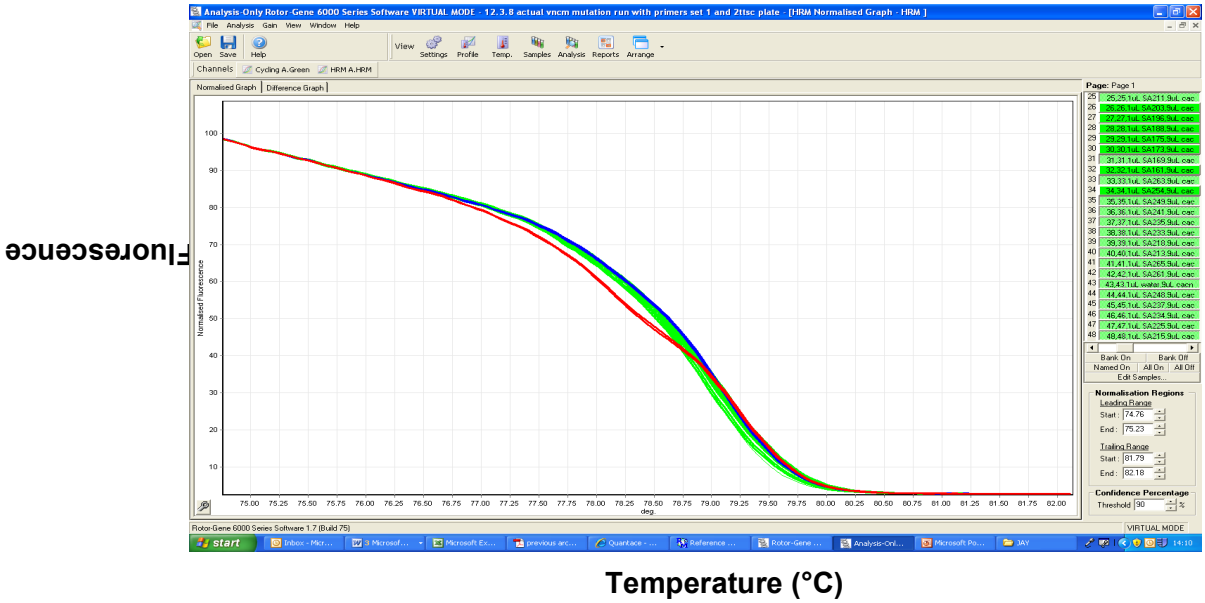

Figure 27 A High resolution melt (HRM) assay of a *CACNA1A* gene variation.

An HRM assay to identify the C.4110T>G p.Phe1370Leu (NM_000068.3) variation in 150 control chromasomes. The Rotorgene 6000 real-time thermocycler demonstrates that the melt profile for normal control subjects (GREEN) is identical to that of wildtype controls (VNCM-6 and VNCM-8, BLUE) and not sequence variation controls (VNCM-4 and VNCM-7, RED).

8.4 Discussion

The *CACNA1A* gene codes for the Cav2.1 subunit of P/Q type voltage gated Ca2+ channels expressed in the brain and particularly in cerebellar Purkinje and granule cells, as well as in neuromuscular junctions[202;203]. The protein is predicted to have four domains or repeats, each formed by six transmembrane hydrophobic segments. Segments S5 and S6 of each domain line the pore region. The S5–S6 linkers are highly conserved sequences folded to leave their extremes in the extracellular space, and place

within the pore a P sequence which exerts a critical role for ion selectivity and permeation of the Ca2+ channel[204].

Three allelic disorders are caused by mutations in this gene; spinocerebellar ataxia type 6 (SCA6, MIM 183086), familial hemiplegic migraine (FHM, MIM 141500) and episodic ataxia type 2 (EA2, MIM 108500). SCA6 is characterized by adult-onset, slowly progressive cerebellar ataxia, dysarthria, nystagmus, and impaired sensations of vibration and proprioception[205]. Symptoms of SCA6 can occur for the first time as late as 65 years of age, indeed patients with a genetically confirmed diagnosis may remain asymptomatic until old age[206;207]. FHM is characterised by migraine attacks preceded by symptoms such as unilateral limb paresis or paralysis, paraesthesias, dysphasia and interictal cerebellar signs which are reported in about 50% of patients[208]. EA2 is characterised by a complex and highly variable phenotype, widely overlapping that of SCA6[209;210]. Its main features are episodes of vertigo or ataxia of variable frequency and duration, a permanent cerebellar deficit of variable severity, sometimes progressive, and a cerebellar atrophy typically starting from the anterior portion of the vermis[205]. About 50% of individuals with EA2 have migraine headaches (suggesting overlap with FHM) and onset is typically in childhood or early adolescence although the age range is variable. Interestingly, it is commonly associated with interictal nystagmus and patients with EA2 mutations have been reported in whom the only interictal sign or symptom is nystagmus[195]. Other features occurring with EA2 include: dyskynesia, muscular weakness and epilepsy[205]. An interesting feature of EA2 and FHM is that oral acetazolamide treatment can prevent or abort the episodic symptoms[199;200]. Indeed, response to Acetazolamide is sometimes used diagnostically when EA2 is called by one of its alternative names; Acetazolamide-responsive hereditary paroxysmal cerebellar ataxia (APCA). Acetazolamide is also known to be effective in suppressing episodic or fluctuating symptoms of SCA6, although chronic progressive ataxia does not respond[211].

Typically, the nystagmus phenotype in these disorders may include vertical jerk nystagmus (downbeat, upbeat), gaze evoked nystagmus, acquired pendular nystagmus, periodic alternating nystagmus and rebound nystagmus[212;213]. However, many different

nystagmus phenotypes have been described including periodic alternating nystagmus[214] and vertical or horizontal nystagmus[215-217]. Smooth pursuit and fast OKN are mediated via the cerebellar flocculus/paraflocculus and vermis and so pursuit is typically saccadic and OKN is absent or of low gain. The vermis is involved in controlling the accuracy and timing of saccades and so they may be dysmetric in these disorders[212;213].

Point mutations in the *CACNA1A* gene are responsible for EA2 and FHM (see Figure 28), whereas small expansions of a CAG repeat characterise SCA6. However, an EA2 phenotype was also found in association with an expanded CAG allele of the *CACNA1A* gene[195] and with a point mutation of the auxiliary b4 subunit of the same P/Q Ca2+ channel, coded by gene *CACNB4*[218]. FHM patients carry exclusively missense mutations[219;220]. In the case of EA2 however, many truncating[205;215;221-224] and non truncating [205;225-232] mutations have been identified. Some point mutations in *CACNA1A* have been evaluated electrophysiologically and of 3 mutations causing EA2, all were found to decrease the current through these Ca channels[228;233]. Alternatively, some *CACNA1A* mutations, such as those seen in FHM, result in increased Ca^{2+} entry and, thereby, aberrant transmitter release and possibly excitotoxictly[196;219].

In a review of the previously published EA2 mutations by Mantuano *et al* in 2004 it was suggested that non-truncating mutations which have been associated with EA2 were preferentially located in the S5–S6 linkers (9/12), and particularly those of domain I and III (8/12), where they tended to cluster at the extremities and their borders[205]. Other groups have subsequently found mutations in many different parts and domains of this gene in subjects with EA2 and have suggested that the type of mutation, missense versus nonsense, or the location of altered or truncated amino acid residues does not predict the clinical phenotype[234].

Using a computer-annotated protein sequence and structure database (http://beta.uniprot.org/uniprot/O00555) the c.4110T>G p.Phe1370Leu (NM_000068.3) variation identified in this work is predicted to be located within a small 19bp topological domain of the Cav2.1 subunit of P/Q type voltage gated Ca2+ channel. This domain is located within the cytoplasm between segment 4 and segment 5 of the repeat

domain 3 (see Figure 28). It is interesting to note that the Phe-to-Leu result of the c.4110T>G p.Phe1370Leu (NM_000068.3) variation is a conservative change as phenylalanine and leucine are similarly non-polar amino acids with only a small physiochemical differences. This is unusual for mutations causing EA2 which tend to cause non-conservative amino acid changes[205].

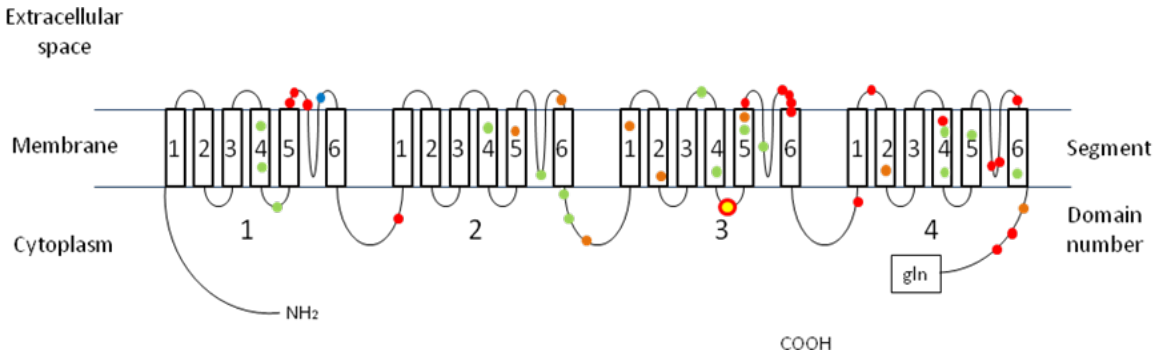

Figure 28 An illustration of the locations of pathogenic mutations in the *CACNA1A* gene.

Mutations are illustrated within the protein product of this gene (the Cav2.1 subunit of P/Q type voltage gated Ca2+ channel). Non-truncating mutations in subjects with EA2 are illustrated with red dots, truncating mutations in EA2 are illustrated with orange dots, those with FHM are illustrated with green dots. The blue dot shows a mutation in a family with severe progressive ataxia from age 44 years (diagnosed as SCA6 clinically). The red circle with yellow centre illustrates the c.4110T>G p.Phe1370Leu (NM_000068.3) mutation found in the VNCM family.

It can be seen that mutations and CAG repeat expansions in the *CACNA1A* gene are associated with a high degree of clinical heterogeneity. Furthermore, the clinical features of SCA6, EA2 and FHM are also associated with significant locus and allelic heterogeneity. In one study, up to 33% of individuals with 21 or more CAG repeats in *CACNA1A* had episodic features prominent enough to warrant the diagnosis of EA2[235]. In one family with a CAG repeat expansion, some members were reported to have had episodic ataxia and others had progressive ataxia[195]. In one family with a *CACNA1A* missense mutation, phenotypes of both SCA6 and FHM were observed[236]. In another family with a *CACNA1A* mutation, both SCA6 and EA2 phenotypes were reported[195]. Therefore, many different clinical phenotypes are known to exist due to various

mutations in the *CACNA1A* gene. However, the VNCM family presented with a number of features which are unusual for the spectrum of diagnoses spanning EA2, SCA6 and FHM. They presented to the clinic because of isolated nystagmus in a 3 month year old baby (VNCM-5) which has not been previously reported. Only when the rest of the family were examined in clinic was it found that many others also had undiagnosed (and asymptomatic) nystagmus. In EA2, interictal nystagmus tends to occur only after a series of attacks of episodic ataxia and other cerebellar symptoms. Interictal nystagmus in this disorder is also usually only evident after the development of cerebellar vermis atrophy which the index child in the VNCM family did not have. Only one (VNCM-3) of the 8 subjects in this pedigree describe migrainous headaches and none describe episodes of hemiplegia. Indeed, all but the 3 month year old proband with nystagmus and VNCM-3 with onset of subtle ataxia age 56, were completely asymptomatic and had no other signs of cerebellar dysfunction except for subtle nystagmus at the time of examination. Again, this has not been previously reported.

The nystagmus phenotype in this pedigree was largely typical of cerebellar disease with disturbed OKN and dysmetric saccades. It is interesting to note that of the 3 subjects in whom nystagmus had never been previously noted, one had no nystagmus in the primary position (VNCM-7) and the other 2 had fine nystagmus of low intensity (VNCM-1 and VNCM-4). Furthermore, rebound nystagmus was only noted in one subject. Also, subsequent to our examination of this family subject VNCM-4 (now age 31) has developed a mildly unsteady gait and minimal finger-nose ataxia with no other symptoms or signs. She still describes no episodic nature or migrainous symptoms. Therefore, this family represents an unusual clinical manifestation of a *CACNA1A* mutation which may be due to the mutations location in a novel part of the Cav2.1 subunit of P/Q type voltage gated Ca2+ channel.

Proving pathogenic causality of a given sequence variation for a given disease can be complex[11].There is however, some strong evidence that the c.4110T>G p.Phe1370Leu (NM_000068.3) variation identified in this pedigree is the pathogenic cause of the nystagmus phenotype. Firstly, this variation was not seen in 300 control

chromosomes suggesting that it is not a simple polymorphism. Secondly, as has been detailed above, the gene has a relevant and appropriate function and it is known that other mutations in this gene cause similar phenotypes. Thirdly, the variation was seen to segregate with the disease in this pedigree which has shown that the chance of the variation and the disease phenotype being unlinked is extremely low. Finally, this variation occurs in a highly conserved domain and the phenylalanine to leucine amino acid change occurs at a position which is also highly conserved throughout evolution (see Figure 29).

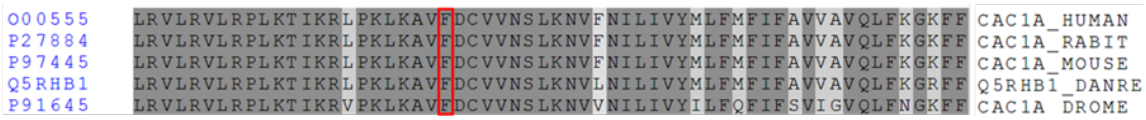

Figure 29 Evolutionary conservation of the *CACNA1A* gene.

An illustration of the conservation of a phenylalanine base which is altered to a leucine base by the c.4110T>G p.Phe1370Leu (NM_000068.3) variation identified in the VNCM family. The phenylalanine amino acid (F, surrounded by red box) is conserved throughout evolution, and resides within a highly conserved domain. Sequences are from the UNIPROT database (http://beta.uniprot.org/); Human *CACNA1A*, O00555; Rabbit CACNA1A, P27884; Mouse CACNA1A, P97445; Danio Rerio (zebrafish), novel protein similar to vertebrate voltage-dependent calcium channel, P/Q type, alpha 1A subunit, Q5RHB1; Drosophila Melanogaster (Fruit fly), Voltage-dependent calcium channel type A subunit alpha-, P91645.

This family was initially found after subject VNCM-5 presented to the ophthalmic unit aged 3 months with apparent isolated atypical CIN. After full ophthalmic, neurological and general physical examination and following a VEP, ERG and MR brain scan this child's diagnosis was one of isolated atypical CIN. Only after examination of the relatives was it found that many of them also had nystagmus and the clinical details of subtle cerebellar symptoms/signs was elicited in an older relative (VNCM 5). This emphasises the necessity for ophthalmic examination of relatives in cases of apparent sporadic CIN, particularly if the waveform is atypical. It also lends weight to the suggestion that idiopathic nystagmus, as is the case for any diagnosis of exclusion, is

likely to represent a range of underlying pathologies with similar functional results. Furthermore, it has suggested that perhaps *CACNA1A* mutations can cause subclinical nystagmus before the onset of other cerebellar symptoms and signs. In this pedigree the subtle cerebellar signs seem to occur at age 30-35. However, the nystagmus is likely to have been present in the affected members since very young age as in all patients there is an absence of oscillopsia which is usually a feature of early onset congenital nystagmus [76;77].

The distinction between CIN and NN has been blurred by the description of a number of families with predominant nystagmus and more subtle neurological symptoms or signs such as the VNCM family[237]. Perhaps, in searching for genes for idiopathic nystagmus we should prioritise the genes which are known to cause some of these other complex diseases.

9 CHAPTER NINE – Spatial and temporal *FRMD7* expression profiling during murine development

9.1 Introduction

The expression profile of the *FRMD7* gene is poorly understood. There is some evidence that the mRNA is present in most tissues at low levels and is possibly greatest in kidney and testis (http//symatlas.gnf.org/symatlas/). Using RT-PCR, *Tarpey et al* detected mRNA expression in human adult kidney, liver, pancreas and, at lower levels, in heart and brain[159]. In human foetal tissue they found the transcript only in kidney. Using *in situ* hybridisation this group found that in human embryonic brain at day 56 post ovulation, there was expression in the ventricular layer of the forebrain, midbrain, cerebellar primordium, spinal cord and developing neural retina. In day 37 post ovulation embryos, expression was restricted to the mid- and hindbrain, regions known to be involved in motor control of eye movement[159]. No further expression work has been published in any species.

It has been postulated that the *FRMD7* gene is likely to be involved in neuronal development[159;238;239]. It is also known that gaining an understanding of the spatial and temporal expression of genes can provide insights into complex self-organizing processes such as mammalian central nervous system development[240]. It is also thought that comparing gene expression patterns of neurodevelopment in the embryonic brain in relation to the adult can provide valuable information. Often clues to adult gene expression and gene function can be determined by examining embryonic development[241].

This chapter describes a detailed temporal expression study of *FRMD7* in the developing brain, lung and heart in mice.

9.2 Methods

9.2.1 Preparation of cDNA samples

Murine cDNA samples were kindly donated as a gift following their preparation by Dr Hans Michael Haitchi, Clinical Research Fellow, Roger Brooke Laboratory, University of Southampton. Specific pathogen free 6 weeks old out bred MF-1 mice (obtained from Harlan UK Limited, Bicester, UK), had been kept in the animal facility, and were time mated by detection of a vaginal plug. This day was taken as embryonic day (ED) 0. Pregnant mice between ED 10-20, newborn and juvenile mice had been killed using a Schedule 1 method (cervical dislocation). Gravid uteri had been removed under sterile conditions and embryos killed according to schedule 1 method (neural tube dissection, cervical dislocation). Maternal adult, embryonic and postpartum lungs, hearts and brains had been dissected in a laminar flow hood. Embryos had been dissected under a dissecting microscope (LEICA WILD M3Z, Wetzlar, Germany). The dissected lungs, hearts, and brains had then been placed in RNA*later*® (Catalog# AM7020; Ambion®, Applied Biosystems, Warrington, UK) or directly homogenised in TRIzol® (Invitrogen, Paisley, UK) and stored for later RNA extraction. Approximately, 10-18 embryos had been obtained from each pregnant mouse. Each time point was represented by 2 animals from 2 separate mothers. Therefore, 2 independent samples were obtained for heart, brain and lung for ED11-19, adult female mice and day 1 and day 8 post delivery pups. The RNA extraction and reverse transcription methods were performed by Dr Haitchi in the Roger Broke laboratory by near identical methods to those described in section 2.3.

9.2.2 Quantitative real time PCR protocol

Quantitative real-time PCR was performed to assess the relative abundance of murine *FRMD7* compared with 2 housekeeping genes; Glyceraldehyde-3-phosphate dehydrogenase (*GAPDH*) and Actin, beta (*ACTB*). Two housekeeping genes were used

due to the well known increase in accuracy of relative qPCR when using greater than one normalising control gene[242]. The choice of these 2 housekeeping genes was based on their previous use in heart, lung and brain tissues[243] and demonstration that their abundance is high and relatively similar in these tissues[242]. Furthermore, these 2 genes have been utilized previously for murine brain studies by RT-PCR and GAPDH has been shown to have an almost constant expression value from ED10-P0[244].

The quantitative real-time-PCR was carried out using a one-step PCR kit (Custom real-time PCR assay for use with SYBRgreen chemistry) (PrimerDesign Ltd, Southampton) in a real-time thermocycler (Rotor-Gene 6000, Corbett Robotics. Ltd). PCR reactions were performed according to the kit instructions for 45 cycles. Using this chemistry, the SYBRgreen dye intercalates between complimentary DNA strands. This DNA-dye-complex absorbs blue light (λmax = 488 nm) and emits green light (λmax = 522 nm). Therefore, fluorescence increases with the amount of PCR product.

Primers were designed by PrimerDesign Ltd (Southampton) for the *FRMD7* gene and 2 housekeeping genes (GAPDH and ACTB). The *FRMD7* gene had a sense primer: ATGCAAGGCTTTCTGGAAGAC and an antisense primer: CGGAAACTGGAACCTTTGCTA with an amplimer size of 111. The control gene sequences are the intellectual property of PrimerDesign Ltd and are not available.

PCR reactions were performed in 100 well Gene-Discs (6001-012, Corbett Life Science, Brisbane, Australia) on the Rotor-Gene™ 6000 real time thermo-analyser (Corbett Life Science, Brisbane, Australia). Each 20 µl comprised: 5 µl of cDNA (at approximately 50ng/ul), 1 µl of the reconstituted primer mix, 10 µl of PrimerDesign 2X Precision™ MasterMix with SYBRgreen and 4 µl PCR-Grade water. PrimerDesign 2X Precision™ MasterMix is a pre-prepared/optimized mastermix containing 2X reaction buffer, 0.025 U/ µl of a chemical Hotstart Taq, 5 mM $MgCl_2$ and DNTP mix (200 µM each dNTP).

The Rotor Gene run settings were according to the standard protocol suggested for custom qPCR assays by PrimerDesign. Briefly, the two-step amplification conditions

were: enzyme activation for 10min at 95°C, followed by 45 cycles of: 15 seconds denaturation at 95°C, 60 seconds annealing and extension at 60°C and fluorescence data collection at the end of the denaturation step. A high resolution melt was also performed for each run to assess product purity with ramping from 60-95°C with fluorescence data collection at 0.5°C increments. Each developmental time point was represented by 2 samples and all samples were run in duplicate with duplicate water controls (cDNA replaced by water) for each gene in each run.

9.2.3 Data analysis methods

By monitoring the fluorescence values of each sample it was possible to determine the quantity of PCR product on a cycle-by-cycle basis. To account for differences in background fluorescence, the Rotorgene software automatically normalised the data. Once normalization was complete, a threshold was set at which fluorescence data was analysed. This threshold was set at a level where the rate of amplification was greatest during the exponential phase. In this experiment the same threshold fluorescence value was used in all runs and was set at a normalised fluorescence value of 0.12. The number of cycles taken for each sample to reach the threshold level was defined as the Ct-value (threshold cycle) and was taken as a measure of the abundance of cDNA target present.

Results were analysed using the 'Comparative Ct method' which is also known as the 'delta delta CT' method[245]. This method involves comparing the values of the sample with those of a calibrator or control. For the purpose of these experiments, heart, brain and lung samples were analysed separately and calibrated to the earliest time point sample. Each tissue was represented by 2 samples per time point and each sample was run in duplicate for all genes. Therefore, for each time point the average Ct value (avr-Ct) for each gene was calculated from 4 recordings. Then the ΔCt-value was calculated according to the following equation:

ΔCt-value = avr-Ct(gene of interest) – avr-Ct(2 housekeeping genes)

Having calculated the ΔCt-values, the delta-delta Ct value (ΔΔCt) was calculated as follows:

ΔΔCt = ΔCt (ED11 control) – ΔCt (sample of interest)

In the last step of quantification the ΔΔCt values were transformed into absolute values of the level of comparative expression according to the formula below:

Comparative Expression Level = 2 ^ΔΔCt.

For this method of analysis to be successful, a validation experiment is required. This validation experiment is considered successful when the dynamic change of both the target and reference gene are similar[246]. Therefore, by serially diluting a sample and detecting corresponding serially lower CT values for housekeeping and target genes, the efficiency of the PCR is validated over a range of concentrations. However, for low copy number genes this method is not always applicable as serial dilution of a cDNA sample over a wide range of concentrations is not possible. As this is the case for the *FRMD7* gene, we performed a number of validation experiments which are detailed in the results section. However, validation of the delta-delta CT methodology is also provided by other evidence in this case, as each gene assay was designed and manufactured by the Primerdesign Ltd. company. Each of these assays has been tested for PCR efficiency during production using a linear regression analysis method at the point of exponential fluorescence change such that all assays are guaranteed to have a PCR efficiency close to 100%. This means that for analysis of relative mRNA expression, 1 CT value is equivalent to a one fold difference in copy number and the delta-delta CT method of analysis is appropriate and valid[246].

In summary, for each tissue, 12 developmental time points were taken and for each time point 2 animals were sacrificed to allow relative cDNA expression measurements. *FRMD7* expression was compared with expression of the *GAPDH* and *ACTB* control genes in each sample and samples were all compared to the ED11 samples for that given tissue.

9.3 Results

9.3.1 Assessment of assay validity

Initially, some preliminary qPCR runs were performed to confirm that the planned comparative experiments would be valid.

Three murine heart cDNA samples from 2 time points (ED14b, ED13a and ED13b) were run with all three test genes, appropriate water controls and in duplicate using the protocol and analysis method designed for the relative expression experiments (see Figure 30 and Table 11).

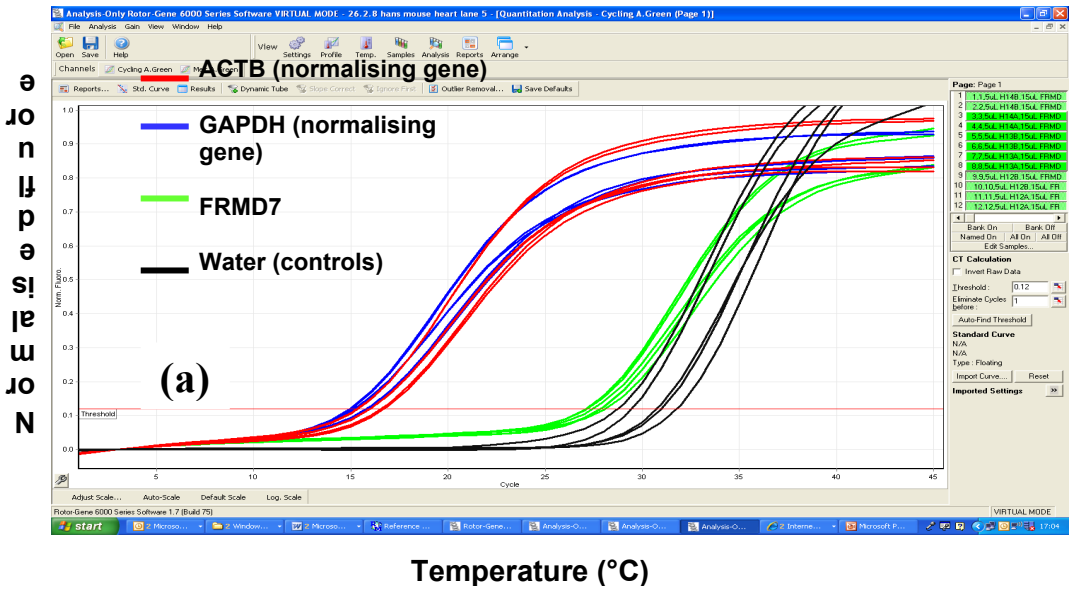

Figure 30 An amplification plot from a real-time quantitative PCR run.

This plot shows the amplification of 3 murine heart cDNA samples (ED14b, ED13a and ED13b), and water controls for 3 gene assays (*GAPDH*, *ACTB* and *FRMD7*), run in duplicate.

Sample	CT	Average replicate Ct
FRMD7 MIX,H14A	27.12	27.15

FRMD7 MIX,H14A	27.19	
FRMD7 MIX,H13B	27.85	27.86
FRMD7 MIX,H13B	27.88	
FRMD7 MIX,H13A	28.09	27.79
FRMD7 MIX,H13A	27.49	
GAPDH MIX,H14A	14.96	15
GAPDH MIX,H14A	15.05	
GAPDH MIX,H13B	15.81	15.87
GAPDH MIX,H13B	15.93	
GAPDH MIX,H13A	15.24	15.21
GAPDH MIX,H13A	15.17	
ACTB MIX,H14A	15.36	15.37
ACTB MIX,H14A	15.39	
ACTB MIX,H13B	16.73	16.65
ACTB MIX,H13B	16.57	
ACTB MIX,H13A	16.02	16.01
ACTB MIX,H13A	15.99	
FRMD7 MIX. 5 µl Water	28.76	29.12
FRMD7 MIX. 5 µl Water	29.48	
GAPDH MIX. 5 µl Water	30.78	30.78
GAPDH MIX. 5 µl Water	30.78	
ACTB MIX. 5 µl Water	31.8	31.41
ACTB MIX. 5 µl Water	31.02	

Table 11 Results of a real-time quantitative PCR run.

Threshold cycle (CT value) results are shown for 3 murine heart samples (ED14b, ED13a and ED13b), and water controls for 3 gene assays (*GAPDH*, *ACTB* and *FRMD7*), run in duplicate. CT values were calculated according to a normalised threshold CT value of 0.12 fluorescence units.

It can be seen that for each gene, the two separate samples from a single time point, and the 2 replicates of each sample had similar CT values. Similarly, by displaying the 2 replicates for a single sample (ED14a), it can be seen that the amplification plot is near identical for replicates (see Figure 31).

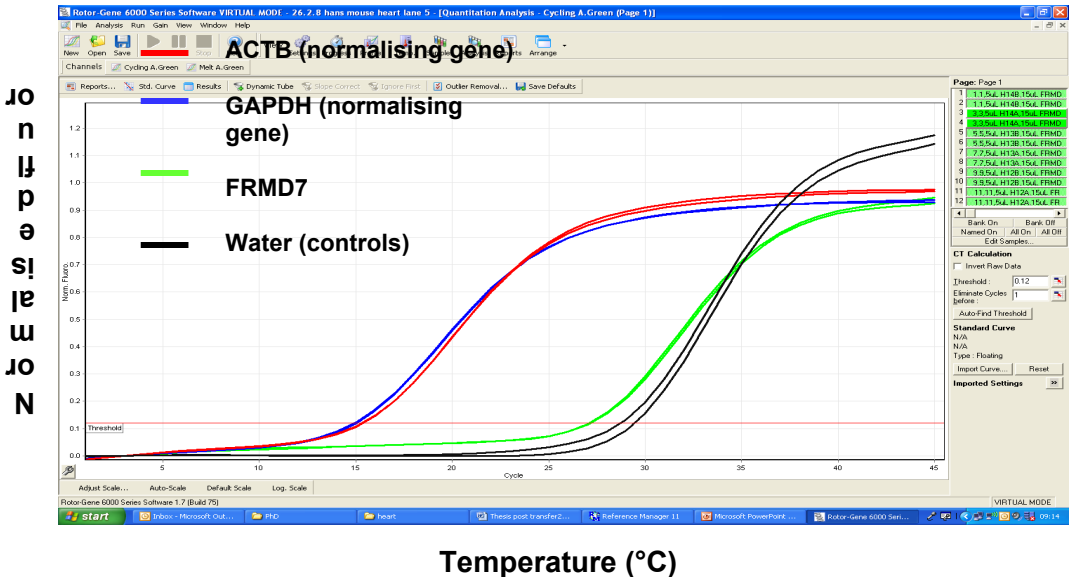

Figure 31 A calibrating amplification plot from a real-time quantitative PCR run.

This plot shows the amplification of a single murine cDNA sample (ED14b) run in duplicate for 3 gene assays (GAPDH, ACTB and *FRMD7*).

These results gave a preliminary indication that CT value variance was low between cDNA samples from the same tissue and time point, and duplicated runs using the same cDNA sample. For both *GAPDH* and *ACTB* control genes, the water control (no cDNA template) amplified significantly later than all cDNA samples (approximately 6 cycles later). This is an indication of the specificity of the PCR assays and excludes the possibility of sample contamination contributing significantly to PCR amplification. However, for the *FRMD7* gene assay, amplification in the water control is only 1.5 to 2 CT values behind the cDNA samples. Therefore, it is necessary to study the melt curve characteristics of these samples to check for the specificity of the PCR assay. By plotting the negative derivative of fluorescence (−dF/dT) with respect to temperature, the Rotorgene software can display a melting peak for each sample. Different PCR products have melting peaks at specific temperatures. Therefore, if a sample has a clear, narrow based, single peak, this indicates that the amplimer is a single product. Similarly, a broad, diffuse, low peak indicates mis-priming and multiple products. Furthermore, when different samples are compared using the same assay, a melting peak centred around the same temperature is expected. When primer-dimers are formed, these can

be seen as peaks occurring typically at a lower temperature that that of the desired amplimer. In this preliminary experiment it can be seen that the control gene assays have tall, thin specific melting peaks and that the melting peaks for the corresponding water controls were typical of nonspecific priming (see Figure 32):

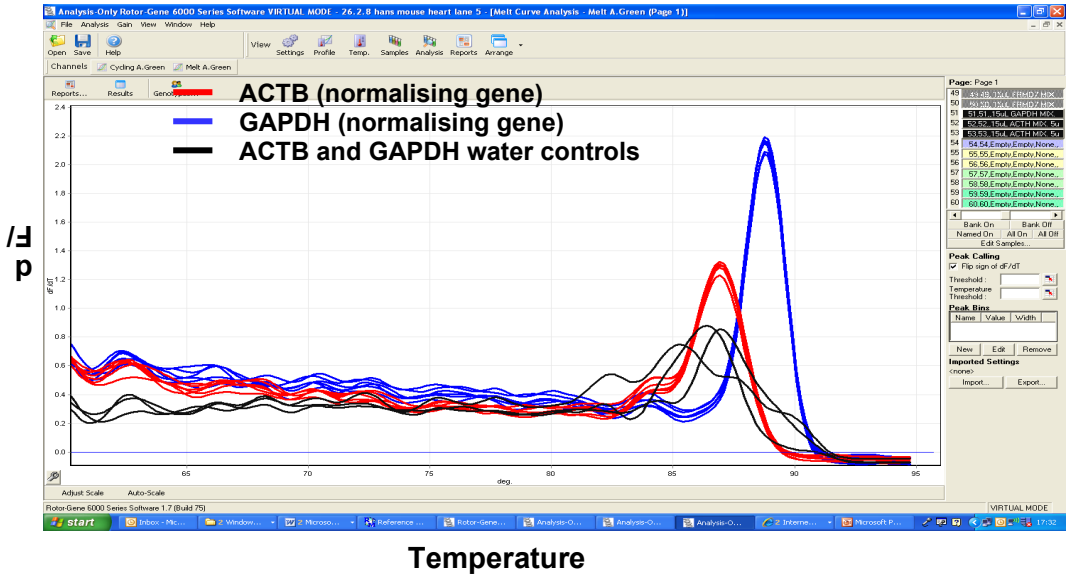

Figure 32 A melt curve analysis showing specific PCR product amplification.

This plot shows the negative derivative of fluorescence (−dF/dT) with respect to temperature during melting. *GAPDH* and *ACTB* gene assays are shown for each of 3 murine heart samples (ED14b, ED13a and ED13b) and water controls.

For the *FRMD7* gene assay, the cDNA samples also had tall thin melting peaks indicative of a specific product but that the corresponding water controls had a peak centring on a lower temperature (see Figure 33):

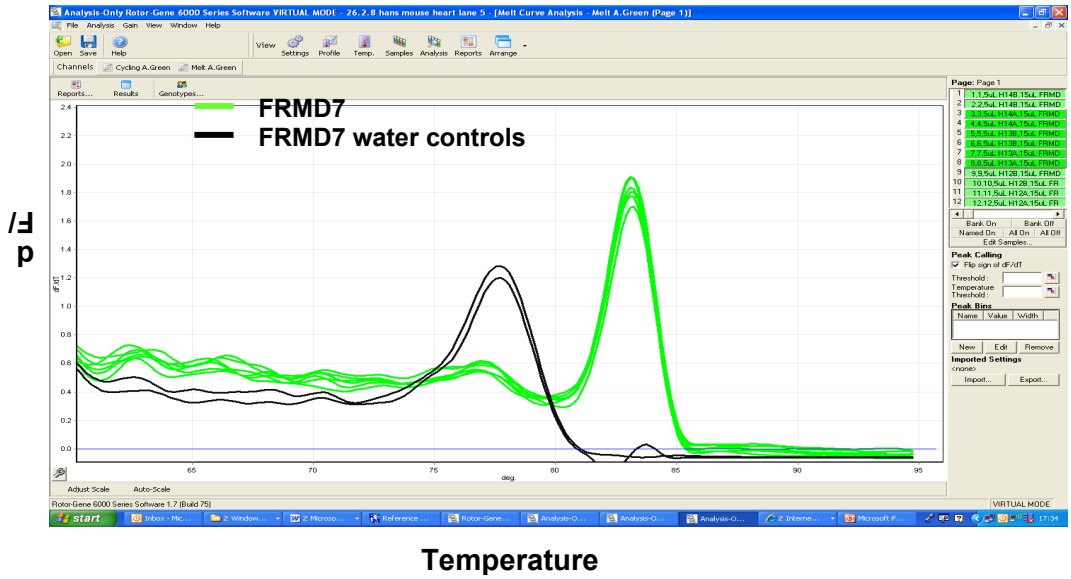

Figure 33 A melt curve analysis from a real-time quantitative PCR run.

This plot shows the negative derivative of fluorescence (−dF/dT) with respect to temperature during melting. The *FRMD7* gene assay is shown for each of 3 murine heart samples (ED14b, ED13a and ED13b) and water controls.

This result is typical of primer-dimer formation (or possibly a single misprimed product from contaminating DNA) for the water controls and shows that the cDNA samples had a valid amplification curve as they have a true product which is not due to DNA contamination or primer-dimer formation. It also showed that this assay would have a tendency to primer-dimer formation when the target cDNA was low or absent. It was therefore necessary to perform melt-curves analyses on all subsequent runs and exclude samples for which amplification was the result of primer-dimer formation.

The *FRMD7* PCR products for 2 samples subsequently underwent direct sequencing to confirm the identity of the single product. This confirmed that the amplimer was the intended murine *FRMD7* sequence. Similarly, the presumed primer-dimer products of the *FRMD7* water controls were also size banded on an agarose gel and directly sequenced showing absence of any PCR amplification product besides primer-dimer complexes.

In order to confirm the claimed 'near 100% PCR efficiency' guaranteed by the Primerdesign company, a serial dilution experiment was performed for all 3 gene assays.

For each assay a series of 6 serial 1/10 dilutions was performed in duplicate and run as a standard curve experiment with the original neat sample on the Rotorgene 6000 machine. For each standard curve, the Rotorgene 6000 software was used to perform a series of statistical calculations as follows:

M = the slope of a standard curve, i.e. the number of CT values corresponding to each 1:10 dilution in template cDNA. For a 100% efficient curve this value is -3.322.

R^2 (correlation coefficient) = the percentage of the data which is consistent with the hypothesis that the standards form a standard curve. If the R2 value is low, then the given standards cannot be easily fit onto a line of best fit. An excellent R2-value is around 0.99.

R-value (square root of correlation coefficient) = the square root of the R^2 value. This value is rarely used for standard curve analysis.

B = the CT value of the neat cDNA sample or that sample given as a concentration of 1. It is rarely used in standard curve analysis.

Efficiency = the calculated reaction efficiency for all standards represented by the formula efficiency = $[10^{(-1/M)}] – 1$. The optimal value for a 100% efficient amplification is 1.

It can be seen in Figure 34 that for both the GAPDH and ACTB assays, the PCR efficiency is close to 1 and that the R^2 is greater than 0.99. This confirms that the assays are very close to 100% efficient over a broad range in target gene copy number.

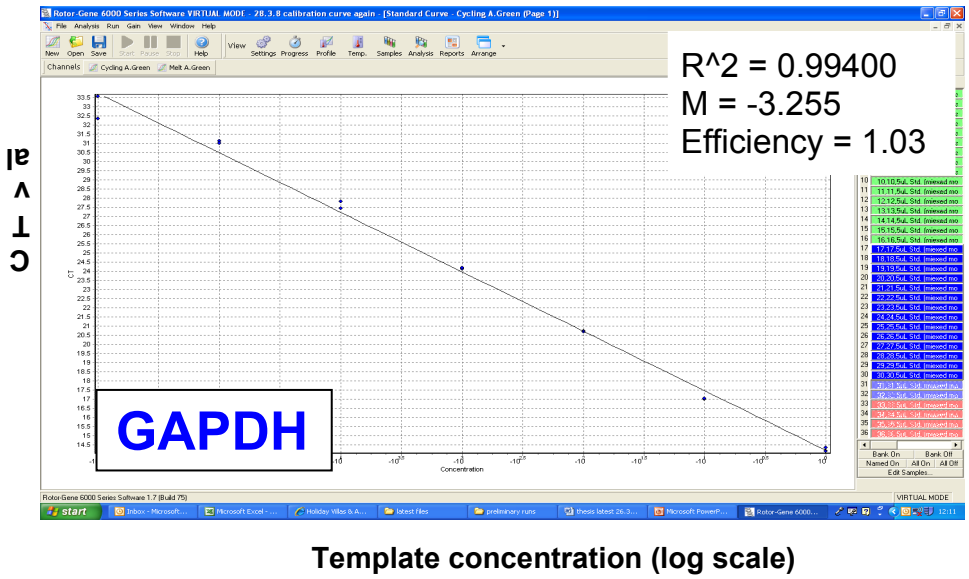

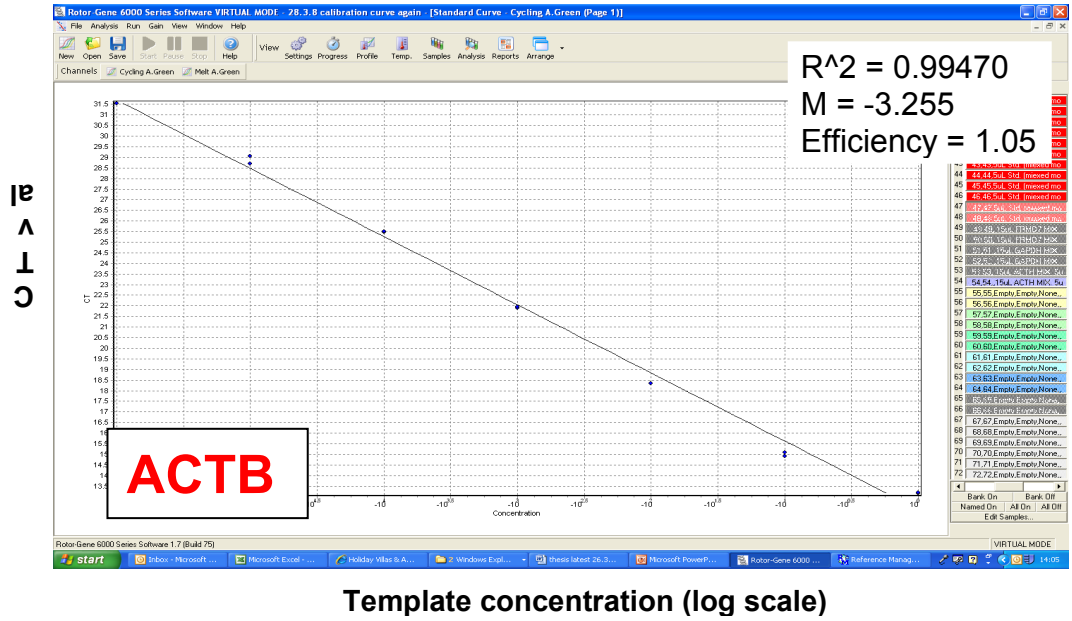

Figure 34 Standard curves for the qPCR assays for 2 housekeeping genes.

Standard curves are presented for *GAPDH* and *ACTB* by plotting CT values against template concentration on a log scale. The correlation coefficient (R^2), slope of the curve (M) and PCR -efficiency (efficiency) are also presented.

When the identical experiment was performed for the *FRMD7* assay, serial dilution beyond a 1:10 dilution resulted in significant shift towards primer-dimer formation and minimal *FRMD7* product amplification. It can be seen in Figure 35 that at high cDNA concentration (dark green lines) *FRMD7* product was present with no primer-dimer formation. However, as the cDNA concentration is reduced (progressively lighter

green lines) the *FRMD7* product reduces and the primer-dimer peak increases such that at a dilution of 1:100000 (lightest green line) only primer-dimer complexes are present. Therefore, as expected, a standard curve could not be completed over a wide range of copy number for this assay.

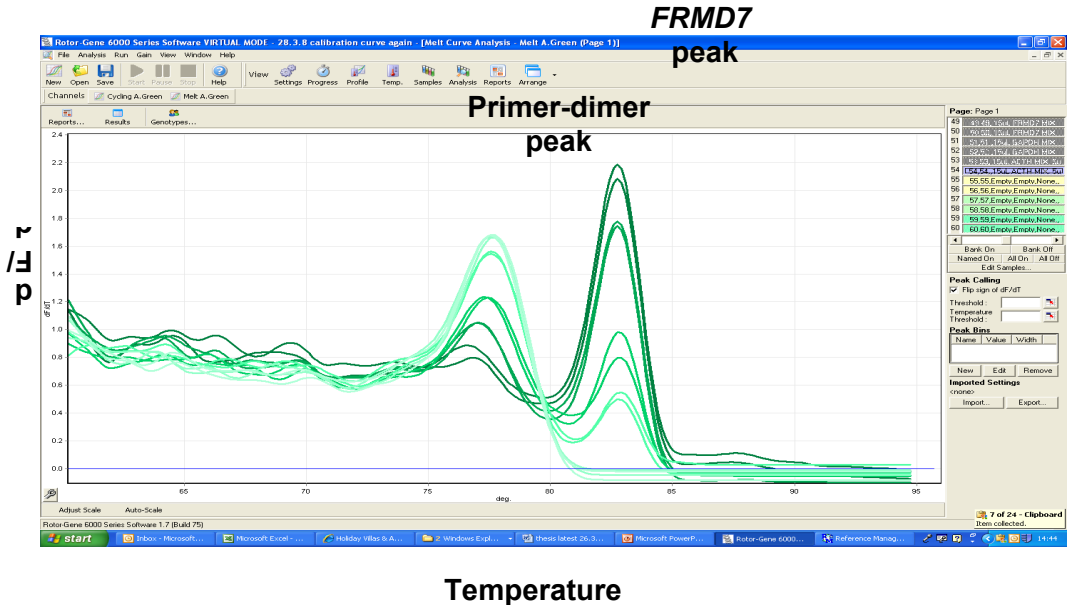

Figure 35 A melt curve analysis for the FRMD7 qPCR assay.

This plot shows the negative derivative of fluorescence (−dF/dT) with respect to temperature during melting. Two peaks are labelled which correspond to the qPCR target and a primer-dimer peak. A single cDNA sample (darkest green) was serially diluted (lighter green hues) 6 times in a 1:10 dilution.

Due to the low copy number of the *FRMD7* gene target sequence, it was now clear that the planned experiments would be performing close to the threshold resolution for qPCR by this technique. Therefore, to test the limits of accuracy for these assays, an experiment was performed in which one sample (brain PD8) was serially diluted again but with only a 1 fold dilution per step. All 3 assays were performed for these samples which were run in duplicate. Both *GAPDH* (R^2 = 0.974, efficiency = 0.99) and ACTB (R^2 = 0.996, efficiency = 1.07) standard curves were again indicative of near

100% PCR efficiency. For the *FRMD7* assay, dilution beyond 1/8 of cDNA template resulted in significant primer-dimer formation (see Figure 36).

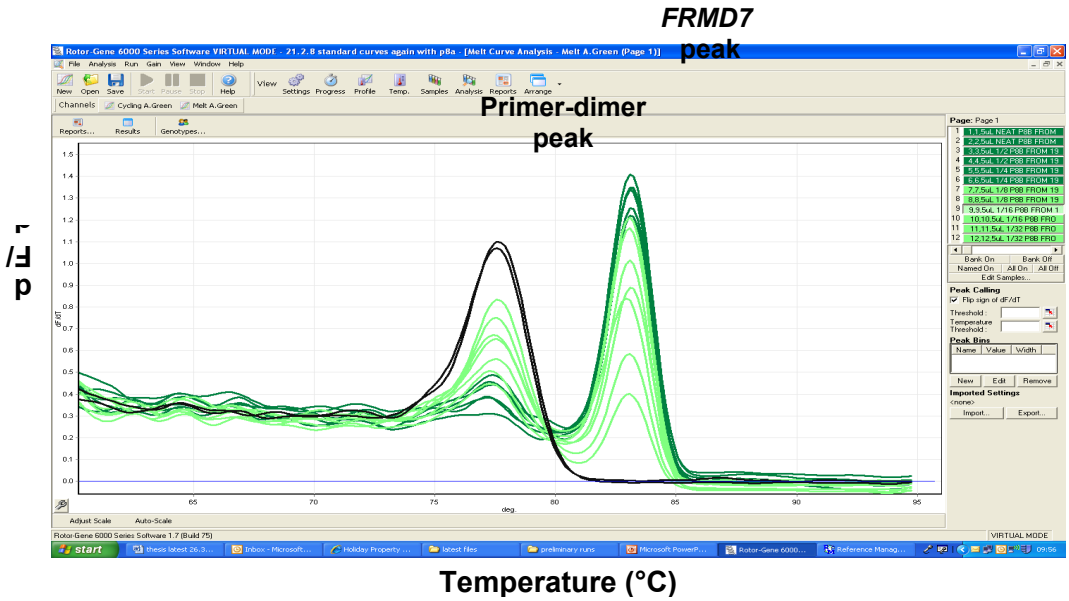

Figure 36 A melt curve analysis for the *FRMD7* calibration curve qPCR assay.

This plot shows the negative derivative of fluorescence (−dF/dT) with respect to temperature during melting. Two peaks are labelled which correspond to the qPCR target and a primer-dimer peak. A single cDNA sample was serially diluted (green lines) 6 times in a 1:2 dilution. Beyond a 1:8 dilution (light green lines) primer dimmer formation was significant. The black line is a no-template water control sample run in duplicate.

By performing a standard curve analysis on the 6 samples above this threshold, a standard curve with R^2 = 0.99628 and Efficiency = 0.92 was achieved (see Figure 37). This suggested that when samples with significant primer-dimer were excluded, PCR efficiency over this relatively narrow range in copy number, was similar to that of the control genes. Subsequently, any sample with a greater proportion of primer-dimer peak than that used in the above calculation (dark green curves in Figure 36) was excluded.

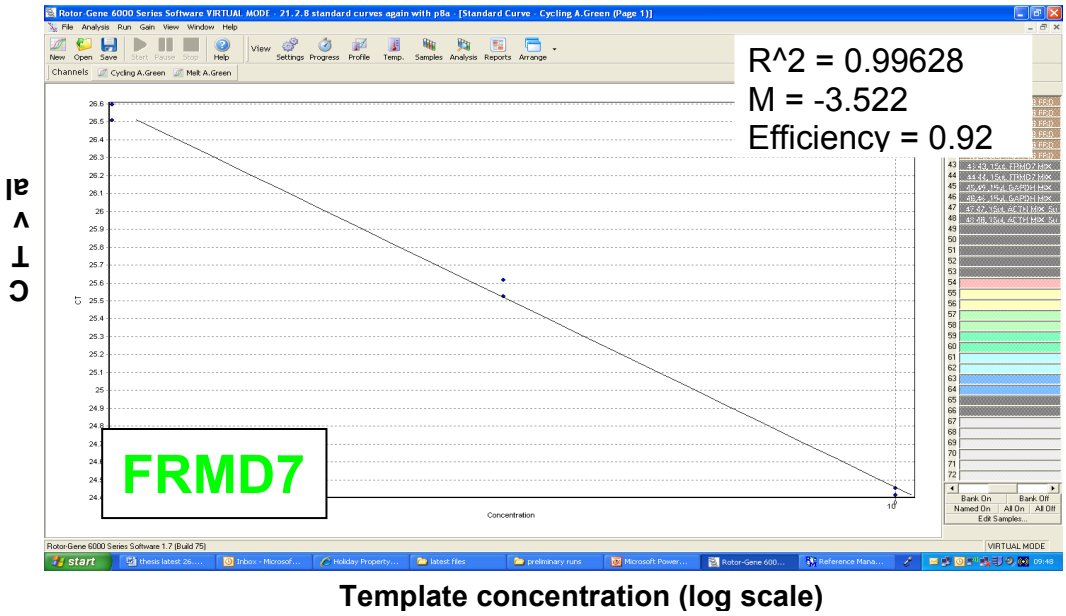

Figure 37 A standard curve for a qPCR assay for the *FRMD7* gene.

The standard curve is presented by plotting CT values against template concentration on a log scale. The correlation coefficient (R^2), slope of the curve (M) and PCR efficiency (efficiency) are also presented.

The final optimisation experiment was performed to confirm that the relative expression methodology and data analysis was reproducible. For this purpose, two time points were selected from murine brain (ED17 and ED18). These time points were selected as more cDNA was available for these samples (the original use of these cDNA samples was for lung research). Each time point had 2 separate samples and each sample was run in duplicate for the *GAPDH*, *ACTB* and *FRMD7* gene assays. This experiment (24 samples and 6 water controls) was run twice by the same protocol on two separate days and one after a freeze/thaw cycle for all reagents and samples. Results were analysed and are presented as the relative expression of *FRMD7* on ED18 compared with ED17 (see Table 12).

	Assay	Sample	CT values	Avr-CT	ΔCt-value	ΔΔCt	Comparative Expression Level
Experiment 1	FRMD7	Brain 18b	24.11	25.0575	8.8575	1.9375	**3.83**
	FRMD7	Brain 18b	24.45				
	FRMD7	Brain 18a	25.97				
	FRMD7	Brain 18a	25.7				
	FRMD7	Brain 17b	26.53	27.08	10.795		
	FRMD7	Brain 17b	26.68				
	FRMD7	Brain 17a	27.67				
	FRMD7	Brain 17a	27.44				
	GAPDH	Brain 18b	18.3	18.275			
	GAPDH	Brain 18b	18.72				
	GAPDH	Brain 18a	18.25				
	GAPDH	Brain 18a	17.83				
	GAPDH	Brain 17b	18.69	17.8625			
	GAPDH	Brain 17b	18.05				
	GAPDH	Brain 17a	17.55				
	GAPDH	Brain 17a	17.16				
	ACTB	Brain 18b	13.81	14.125			
	ACTB	Brain 18b	13.7				
	ACTB	Brain 18a	14.52				
	ACTB	Brain 18a	14.47				
	ACTB	Brain 17b	14.85	14.7075			
	ACTB	Brain 17b	15.01				
	ACTB	Brain 17a	14.57				
	ACTB	Brain 17a	14.4				
Experiment 2	FRMD7	Brain 18b	24.16	24.755	9.48625	1.5875	**3.01**
	FRMD7	Brain 18b	23.74				
	FRMD7	Brain 18a	25.72				
	FRMD7	Brain 18a	25.4				
	FRMD7	Brain 17b	26.33	26.7575	11.07375		
	FRMD7	Brain 17b	26.26				
	FRMD7	Brain 17a	27.34				
	FRMD7	Brain 17a	27.1				
	GAPDH	Brain 18b	16.28	16.4875			
	GAPDH	Brain 18b	16.36				
	GAPDH	Brain 18a	16.78				
	GAPDH	Brain 18a	16.53				
	GAPDH	Brain 17b	17.04	16.7975			
	GAPDH	Brain 17b	16.95				
	GAPDH	Brain 17a	16.57				
	GAPDH	Brain 17a	16.63				
	ACTB	Brain 18b	13.71	14.05			
	ACTB	Brain 18b	13.67				
	ACTB	Brain 18a	14.36				
	ACTB	Brain 18a	14.46				
	ACTB	Brain 17b	14.78	14.57			
	ACTB	Brain 17b	14.83				
	ACTB	Brain 17a	14.35				
	ACTB	Brain 17a	14.32				

Table 12 Results of a real-time quantitative PCR analysis.

An experiment was run on two separate occasions using the same samples, experimental protocol and analysis methods. Reagents in Experiment 2 had also undergone an additional freeze-thaw cycle.

The results showed that the relative expression of *FRMD7* on ED18, compared with ED17, was calculated as 3.8 and 3.0. Therefore, the expression of *FRMD7* was increased by approximately one third from the expression on ED17 and crucially, the values for the 2 experiments were similar.

Together, the results of these preliminary experiments showed that the methods, reagents and protocols to be used in the subsequent relative gene expression experiments were valid, appropriate and reproducible.

9.3.2 Changes in FRMD7 gene expression during murine development

All samples were run in duplicate according to the protocols above with the *GAPDH*, *ACTB* and *FRMD7* gene assays and water controls. Due to the number of samples and the necessity to include controls in each run, a total of 486 samples were analysed in 9 qPCR runs. In all runs, *GAPDH* and *ACTB* water controls showed no amplification until later than 8 CT values behind cDNA samples and had low broad melts indicative of mis-priming at very late CT values. Similarly, in all runs, the *FRMD7* water controls amplified later than 2 CT values after the cDNA samples and had melting peaks indicative of primer-dimer formation after many cycles.

Some samples were excluded due to a supra-threshold proportion of primer-dimer formation as discussed previously. This tended to occur in sequential time points when the copy number was low, indicating that this phenomenon was due to such low abundance of the target gene. In some cases this occurred for only one sample per time point (7 samples). In these cases this sample was excluded and analysis made based on the other sample only. These samples have no error bar in Figure 38. In samples where both samples from a given time point were excluded for this reason (Lung ED11 and ED12), these time points were excluded from analysis and relative abundance was

recorded as 0. The comparative expression levels in the lung samples were therefore normalised to the next earliest time point, ED13.

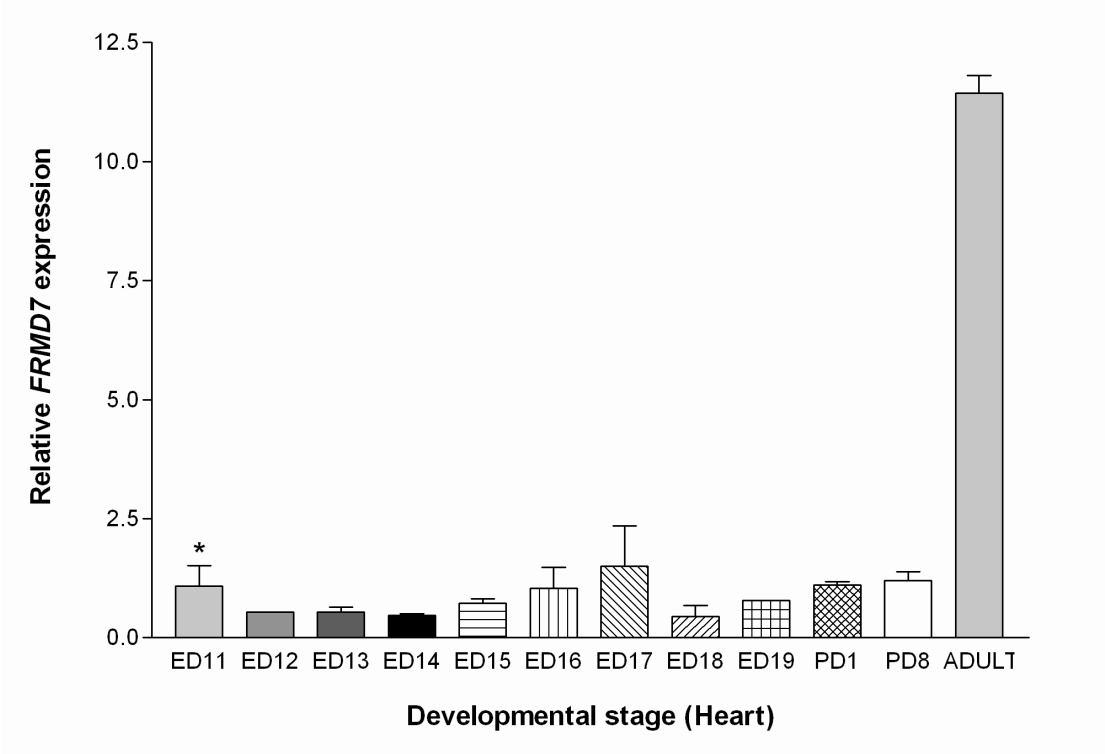
12.5
10.0
7.5
5.0
2.5
0.0
Relative FRMD7 expression
*
ED11 ED12 ED13 ED14 ED15 ED16 ED17 ED18 ED19 PD1 PD8 ADULT
Developmental stage (Heart)

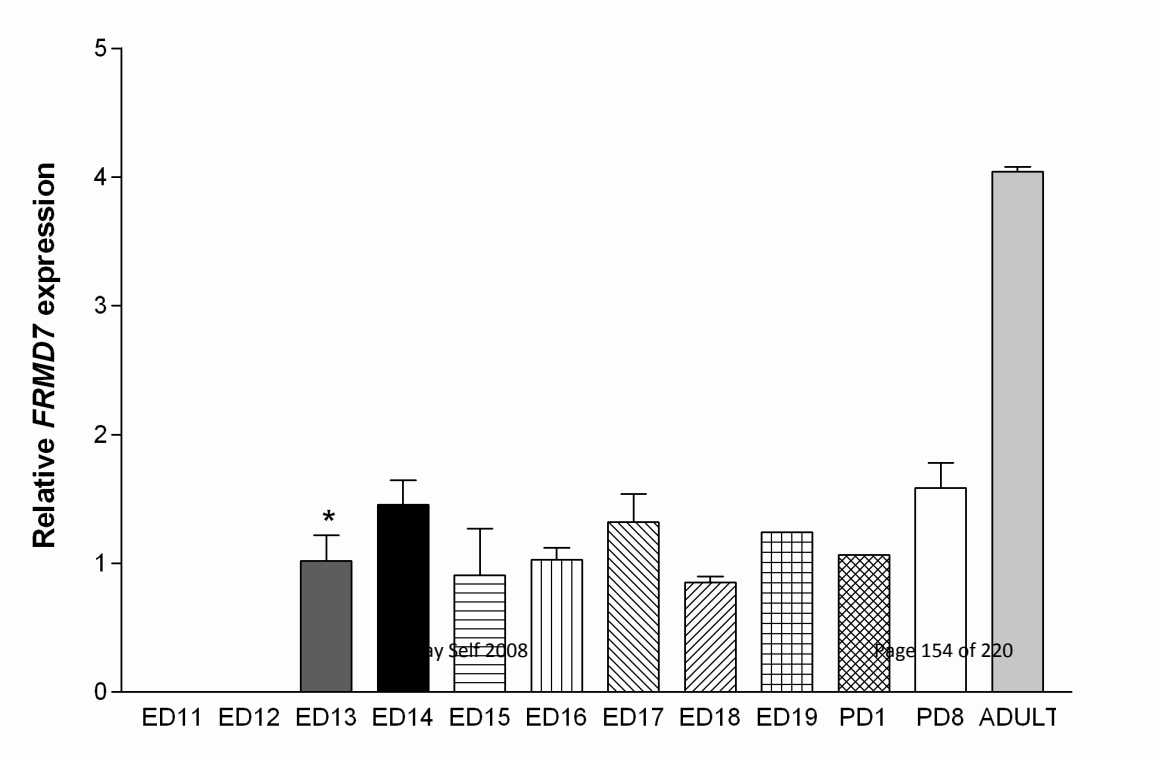
5
4
3
2
1
0
Relative FRMD7 expression
*
ED11 ED12 ED13 ED14 ED15 ED16 ED17 ED18 ED19 PD1 PD8 ADULT

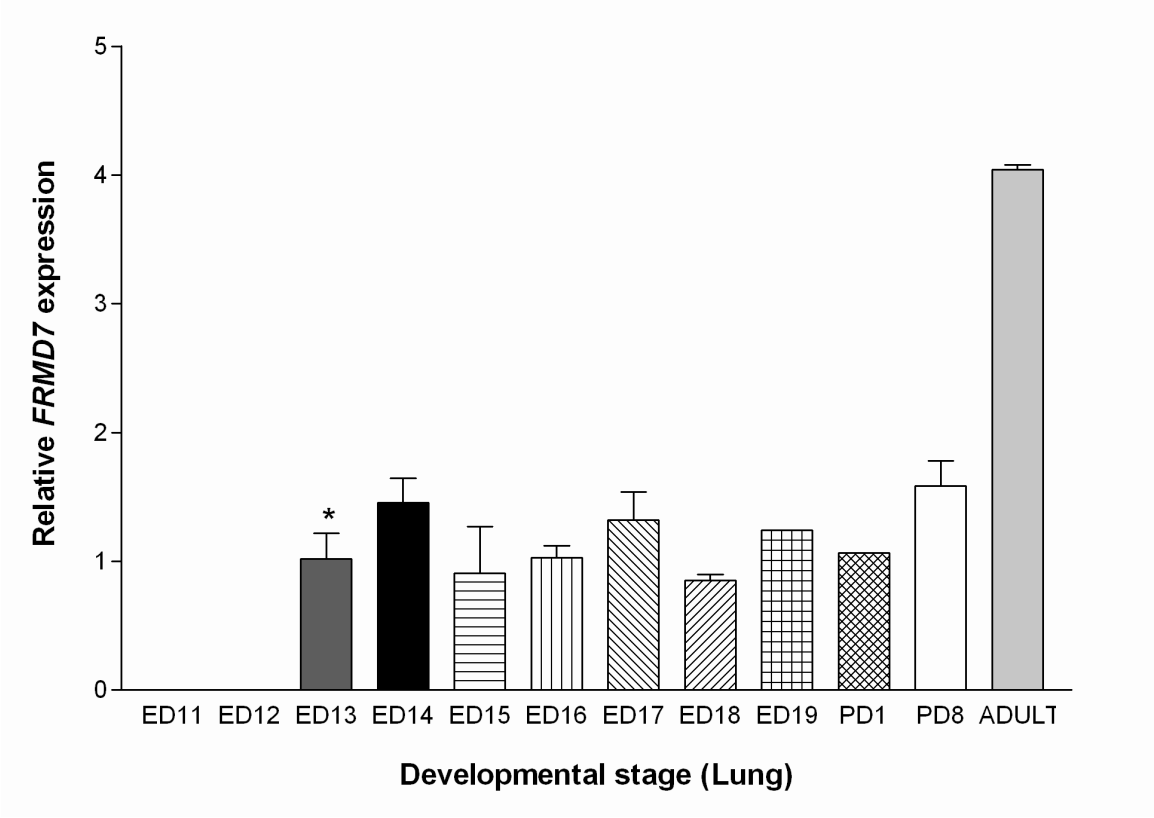
Relative FRMD7 expression
5
4
3
2
1
0
*
ED11
ED12
ED13
ED14
ED15
ED16
ED17
ED18
ED19
PD1
PD8
ADULT
Developmental stage (Lung)

.

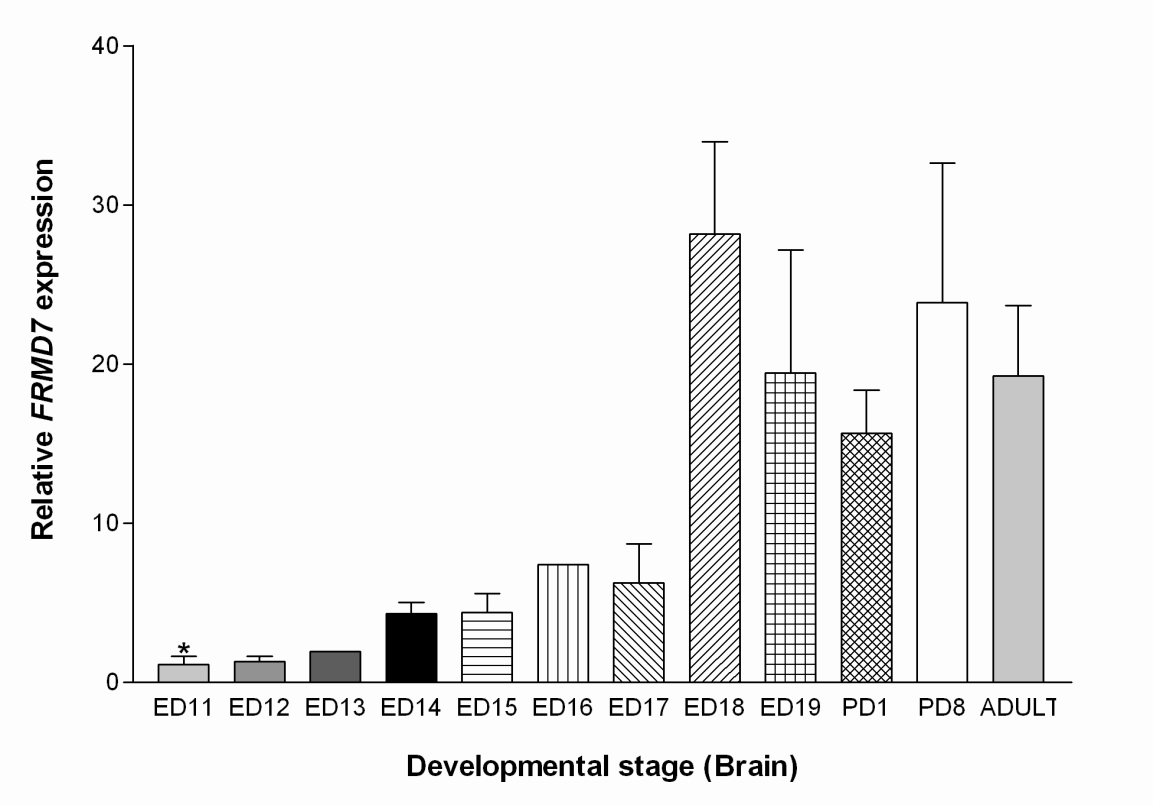

Figure 38 Relative expression profiles for the *FRMD7* gene.

cDNA samples were taken from 3 murine tissues during development and relative expression measurements for the *FRMD7* gene relative to *GAPDH* and *ACTB* housekeeping genes are presented. * = All samples were normalised to this sample. Error bars represent the Standard Error of the Mean (SEM).

9.4 Discussion

The results presented above show that in murine heart and lung, *FRMD7* expression varied very little between ED11 and PD8. Interestingly, for both tissues, expression increased significantly in the adult samples following a similar pattern. In these tissues, overall expression of *FRMD7* was very low and in most samples expression was at the limit of resolution for this technique. However, it is apparent that no significant increases in expression level occur during this critical period in murine development and that overall expression in these tissues during development is very low and consistent with the previously reported 'low levels of expression in most tissues'[159].

Overall expression levels in the murine brain samples were higher as seen by the low levels of primer dimer formation and earlier *FRMD7* amplification in these samples. However, as detailed previously, quantitative comparison between tissues can be difficult due to differences in control gene expression and so are not presented here.

Interestingly, the overall pattern of expression in the brain tissue is noticeably different to that seen in the lung and heart tissues. Expression is seen to increase slowly between ED11 and ED18. It seems that expression levels remain higher after ED18 although no more can be said about these subsequent samples as they have significantly greater error ranges representing greater differences between the 2 samples, per time point. However, it can be said with some certainty that *FRMD7* expression is greatly increased at ED18 compared with earlier time points during murine brain development.

It has been shown that genes expressed during murine develop exhibit functional clustering in terms of temporal and spatial expression profiles during development[244;247]. In 2005 Matsuki *et al* used an oligonucleotide-based microarray system to study the expression of 12,422 genes in the mouse brain between on ED11, ED15, ED18 and P0[244]. They found significant differential expression in 1413 of these genes when normalised to the ACTB gene. These genes were then grouped into 15 clusters based on cellular events involved in brain development and known/predicted gene function. Interestingly, only 4 of these clusters showed an overall temporal expression pattern similar to our *FRMD7* findings with characterised by low levels of expression until a significant increase at ED18. These 4 clusters were; 'carbohydrate, lipid and amino acid metabolism (CLAM)', 'cell adhesion and recognition', 'Neurotrophin hormone, growth factor and cytokine (NHGC)' and 'neurotransmitter and ion channel genes (NT)'. This is an interesting finding as the CLAM genes supply molecular components required for active neurogenesis and hisogenesis, NT genes supply molecular components for the formation of neurnal connectivity and circuits and NHGC genes have a role in signalling for neural differentiation and survival[244]. All these processes are known to be occurring at this developmental stage, showing the efficacy of this clustering methodology and a possible role for *FRMD7* in these processes in

murine brain. This group subsequently selected 397 of these differentially expressed genes for which strong functional data was available. These genes were characterised into eight new clusters based on their developmental function. Interestingly, the expression pattern of up regulation at ED18/P0 was most strongly seen in 2 clusters. These clusters pertained to genes involved in: synapse formation and function (e.g. genes coding GABA receptors and intracellular calcium channels) and axon growth and guidance-related genes (e.g. Sema4f and Cdh8). Again, these results suggest a role for *FRMD7* in these processes in murine brain development. However, samples were taken from whole brain and so there is no indication of which brain regions are expressing the gene at this time. Furthermore, earlier brain tissues used in this work (ED11 to approximately ED14) will have included the developing optic vesicle (developing eye) and all samples the developing primary visual cortex and connections. Therefore, no inference can be made from this work about which brain/eye structures are responsible for the peak in *FRMD7* expression at ED18 or the pathophysiology of CIN.

It is important to note that in this work, detection of *FRMD7* expression was occurring at the limit of resolution for quantitative real-time PCR. In many samples the CT difference between housekeeping genes and the *FRMD7* gene amplification curves was approximately 15 cycles. This corresponds to a difference in expression of 1:65536. At this very low level of expression primer-dimer formation occurred for poor samples which were then necessarily excluded. Possibilities for improving RT PCR results for such a low copy number gene include; increasing the number of animals/samples per time point to increase the power of identified expression differences, different *FRMD7* primers with a lower tendency for primer-dimer formation, gene specific RT PCR and the use of fluorescent labelled probes for specific detection of the target transcript.

The final caveat to this work is that expression analysis was performed on murine samples with the possibility of differences to expression profiles in human tissues. For example, mice do not have fovea and their eyes do not open until approximately P10/11. Therefore, the visual systems of humans and mice are structurally different and development occurs over differing timescales. However, the

role of *FRMD7* in mice is likely to direct further study of this gene in humans especially when a human *FRMD7* antibody is available.

10 CHAPTER TEN – A survey of *FRMD7* expression

10.1 Introduction

As detailed previously, the *FARP2* gene on chromosome 13 shares significant homology with a large portion of *FRMD7*. It is also known that *FARP2* alters neurite length and degree of sprouting in rat embryonic cortical neurones[184;185]. These observations have lead to the hypothesis that mutations in *FRMD7* may cause nystagmus by altering the neurite length and degree of branching of neurons as they develop in the midbrain, cerebellum or retina[159]. Furthermore, the results in chapter 9 have suggested that in mouse brain, the *FRMD7* expression profile is consistent with a gene which has a role in these processes. However, detailed functional work will require a greater understanding of the cells which express *FRMD7*. A monoclonal primary antibody to human *FRMD7* mRNA has been designed and purchased for this purpose and is currently in production with an expected availability date in December 2008 (EZBiolab, Westfield, USA). Furthermore, in early 2007 I nominated the murine *FRMD7*, *FARP1* and *FARP2* genes for knockout via the NIH backed Knockout Mouse Project (KOMP) which aims to 'generate a public resource of mouse embryonic stem (ES) cells containing a null mutation in every gene in the mouse genome' (http://www.nih.gov/science/models/mouse/knockout/). Subsequently, the *FRMD7* and *FARP2* genes were both been selected out of 17,350 genes for priority targeting and the development of knockout ES cells is currently underway. The ES cells will be available to the authors on completion which is anticipated to be in 2008/2009. Until these two resources are available, any information about which cell types express the *FRMD7* gene, and under what circumstances, will be valuable for directing future work.

This chapter describes an expression study of the *FRMD7* mRNA in cells from various human sources in order to identify differences in *FRMD7* expression between tissues, cell types, and stages of differentiation.

10.2 Tissues used in this experiment

The tissues and cells used in this experiment are listed below:

- Human neuroblastoma derived cell line SHSY5Y (LGC Promochem-ATCC Middlesex, UK)
- Human retinoblastoma derived cell line Y-79 (LGC Promochem-ATCC Middlesex, UK)
- Human adult kidney tissue

SH-SY5Y cells are a good model system for studying neuronal properties in culture, as many of their receptor systems have been well characterized and they display developmental phenotype plasticity[248;249]. These cells are widely used as a model system for investigations into neuritegenesis[250-253] which can be stimulated via a variety of pathways. Nerve growth factor (NGF) has been reported to induce neuritegenesis[252] and cell flattening in SH-SY5Y cells, predominantly via TrkA receptor activation[254]. Treatment with retinoic acid (RA) has been reported to induce differentiation of SH-SY5Y cells with resultant neuritegenesis[248], without altering TrkA expression[255]. Cyclic AMP (CAMP) has been shown to cause SHSY-5Y cells to form neurite-like extensions[256] via a pathway involving cAMP-dependent protein kinase (PKA) activation[256]. These methods were chosen as models of neuritegenesis in which *FRMD7* expression could be evaluated.

Y-79 cells are derived from retinoblastoma and thus originate from retinal cells. They can be differentiated into cells with a neuronal phenotype[257-259]. They were selected as an additional neuritegenesis model because of the hypothesis that *FRMD7* may have a role in neuronal development in the retina[159].

It has been reported that kidney is one of the adult human tissues with the greatest *FRMD7* expression[159]. Therefore, comparison of expression between different parts of this organ and between adult and embryonic kidney may yield insights into which tissues/cells express this gene.

10.3 Methods

10.3.1 Differentiation and RNA extraction from SHSY5Y cells

SHSY5Y cells were purchased from LGC Promochem-ATCC (Middlesex, UK) and cultured as described in section 2.4. Differentiation was attempted by 3 different methodologies having placed cells in a 6 well cell culture plate (Nunclon, Cat no.140685) at densities ranging from 10 to 100 thousand per well. Cells at passage 24-28 were grown in 2 mls of either standard SHSY5Y culture media or NB-B27 media (see section 2.4) which was changed 3 times per week. For all differentiation protocols, cells were viewed by direct microscopy on an inverted stage microscope at 24hours, 3 days, 7 days and 10 days.

Initially, recombinant nerve growth factor β-NGF (R and D systems, Cat no. 256-GF) was used in standard growth media at a concentration of 100ng/ml according to previously published protocols[252;253]. Subsequently, the concentration of NGF was varied from 10-200ng/ml both with, and without the addition of 10nM FK506 monohydrate (Sigma, Cta no. F4679) which may potentiate the neurite outgrowth effects of NGF[252].

A second protocol was followed in which cells were transferred to NB-B27 media (see section 2.4) containing di-butyryl-cyclic AMP (cAMP, Sigma, Cat no.D0260) at 1mM concentration as previously decribed[256]. Subsequently, the cAMP concentration was varied between 100uM and 10mM concentrations.

The third protocol used for differentiation of the SHSY5Y cell line was according to a previously published protocol[248] using 75uM all-trans retinoic acid (RA, Sigma, Cat no.R2625) in standard SHSY5Y media.

Following optimisation of all differentiation protocols, each method was employed using 2 wells of a 6 well culture plate. 2 wells from each protocol were used for mRNA extraction after 1 week of differentiation protocol. For the all-trans retinoic acid protocol, mRNA was extracted at 24hours, 48 hours, 3 days, 7 days and 10 days.

10.3.2 Differentiation and RNA extraction from Y-79 cells

Y-79 cells were purchased from LGC Promochem-ATCC (Middlesex, UK) and cultured in standard Y-79 media as described in section 2.4. Differentiation was attempted by a number of different methodologies having placed cells at passage P6 in a 6 well cell culture plate 6 well cell culture plates (Nunclon, Cat no.140685) at densities ranging from 10 to 100 thousand per well. For all differentiation protocols, cells were viewed by direct microscopy on an inverted stage microscope at 24hours, 3 days, 7 days and 10 days.

Initially, a differentiation protocol was followed as previously described[257;259;260]. Cells were grown in full Y-79 media and moved into identical media but without FBS and grown on for 1 week. Cells were then plated at a density of 1-10,000 cells per well in a 6 well cell culture plate which had been pre-coated with poly-l-lysine (poly-D-lysine in the original protocol description). These cells were grown on in Y-79 media without FBS but with 20ug/ml of Laminin (Invitrogen, Cat no.23017-015) in the media. Both Laminin and media were replaced 3 times/week. This protocol was varied by culturing Y-79 cells for 1 week prior to plating in y-79 media without FBS (as per protocol) or one of 2 brands of minimal essential medium (ATCC MEM eagle, Cat no. 30-2003 or Gibco MEM, Cat no. 320-11). Additionally, a gradual reduction in FBS content of the media (by 25% per day) was tested over 1 week prior to removal of FBS from the media.

Due to lack of viable cells after following these protocols, RNA extraction and cDNA synthesis were completed (see section 2.3.2), for Y-79 cells cultured in full medium only.

10.3.3 RNA extraction from human adult kidney tissues

Human kidney tissues used in this experiment were anonymised generous gifts from Dr Jane Collins (Senior Lecturer, IIR Division, Southampton University). Human adult kidney tissues included samples that had been retrieved at nephrectomy in 2 patients with transitional cell carcinoma (TCC). Small biopsies of healthy renal medulla and cortex had been taken immediately by the investigating pathologist and stored in RNA*later*® (Catalog# AM7020; Ambion®, Applied Biosystems, Warrington, UK). RNA extraction and cDNA synthesis were completed as detailed in section 2.3.2.

10.3.4 Imaging of cell lines during differentiation protocols

Imaging was performed on an inverted DM IRB microscope (Leica Microsystems UK Ltd, Milton Keynes, UK). The morphology of SHSY5Y and Y-79 cells is changed significantly by differentiation and so cells were viewed and photographed by direct microscopy at 10X and 20X magnification. Cell counting and measurement of cell death was performed using the haemocytometer method as described in section 2.4.4.

Immunohistochemistry was performed as detailed in section 2.4.8. Monoclonal anti-neuronal Class III ß-Tubulin (TUJ1) had been created commercially by raising against microtubules derived from rat brain. It is well characterized and highly reactive to neuron specific Class III ß-tubulin (ßIII) but does not identify ß-tubulin found in glial cells. Conversely, monoclonal anti-Glial Fibrillary Acidic Protein (GFAP) had been commercially derived from the hybridoma produced by the fusion of mouse myeloma cells and splenocytes from an immunized mouse. Purified GFAP from pig spinal cord was used as the immunogen. Anti-GFAP is a specific marker of glial cells. 4',6-diamidino-2-

phenylindole (DAPI) is a fluorescent stain which binds to DNA in live and fixed cells. It can be used to identify the nucleus of any cell type.

Therefore, DAPI was used to identify all cells, staining with anti-TUJ1 was used to indicate cells which have undergone some degree of neuronal differentiation and staining with anti-GFAP would suggest that cells have retained some glial cell characteristics.

10.3.5 Quantitative real time PCR protocol

Quantitative real-time PCR was performed to assess the relative abundance of human *FRMD7* compared with 2 housekeeping genes; Glyceraldehyde-3-phosphate dehydrogenase (*GAPDH*) and Actin, beta (*ACTB*). The choice of these 2 housekeeping genes was based on their previous use in human tissues[243] and demonstration that their abundance is high and relatively similar in these tissues[242]. The quantitative real-time-PCR was carried out using one custom designed (*FRMD7*) and 2 off-the-shelf (housekeeping genes) PerfectProbe™ assays (PrimerDesign Ltd, Southampton). These assays include predesigned primer pairs with a probe comprising a fluorogenic dye and quencher. The design of these probes is such that background noise is reduced but a strong target signal is received for the desired amplification product.

The control gene sequences are the intellectual property of PrimerDesign Ltd and are not available. The *FRMD7* gene assay had a sense primer: agggttccagtttccgctat and an antisense primer: agatgggtaatgtttcctttcaaat with an amplimer size of 96bp. PCR reactions were performed in 100 well Gene-Discs (6001-012, Corbett Life Science, Brisbane, Australia) on the Rotor-Gene™ 6000 real time thermo-analyser (Corbett Life Science, Brisbane, Australia). Each 20 µl reaction comprised: 5 µl of cDNA (at approximately 50ng/ul), 1 µl of Perfectprobe/primer mix, 10 µl of PrimerDesign 2X Precision™ MasterMix and 4 µl PCR-Grade water. PrimerDesign 2X Precision™ MasterMix is a pre-prepared/optimized mastermix containing 2X reaction buffer, 0.025 U/ µl of a chemical Hotstart Taq, 5 mM MgCl2 and DNTP mix (200 µM each dNTP).

The Rotor Gene run settings were according to the standard protocol suggested for Perfectprobe qPCR assays by PrimerDesign. Briefly, the two-step amplification conditions were: enzyme activation for 10min at 95°C, followed by 45 cycles of: 15 seconds denaturation at 95°C, 30 seconds annealing at 50°C and extension at 72°C for 15 seconds with fluorescence data collection at the end of the annealing step. Each different tissue/time-point was represented by 2 separate samples and all samples were run in duplicate with duplicate water controls (cDNA replaced by water).

10.3.6 Data analysis methods

Results were analysed using the delta-delta CT method[245] as described in Chapter 10. The Validation of the delta-delta CT methodology for use with the Perfectprobe assays is provided during their manufacture by Primerdesign Ltd. Each of these assays has been tested for PCR efficiency during production and validation using a linear regression analysis method at the point of exponential fluorescence change and all assays are guaranteed to have PCR efficiency close to 100%. However, to test this claim, a standard curve analysis was performed for all 3 probe assays as described in Chapter 910.

10.4 Results

10.4.1 Differentiation of SHSY5Y cells

Neither the β-NGF or the cAMP protocols resulted in differentiation of SHSY5Y cells into a morphologically distinct phenotype. Despite altering all parameters including exposure time, exposure concentration and addition of FK506, no change in cell morphology was observed when viewed on an inverted stage microscope at 24 hours, 3 days, 7 days and 10 days. Conversely, differentiation with all-trans retinoic acid was readily achieved and significant morphological changes were seen after just 24 hours of exposure.

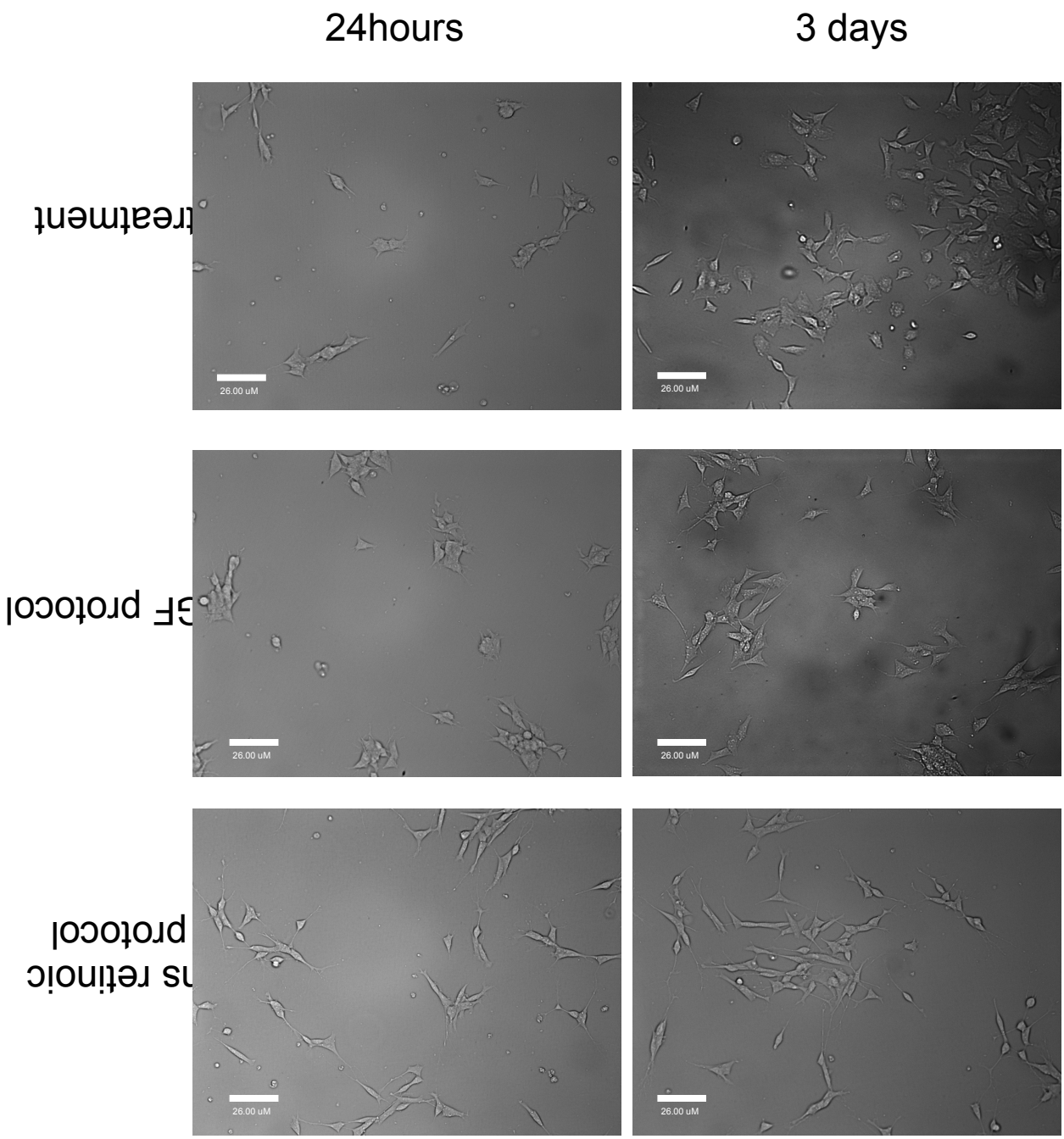
24hours
3 days
treatment
GF protocol
ns retinoic
protocol
26.00 uM
26.00 uM
26.00 uM
26.00 uM
26.00 uM
26.00 uM

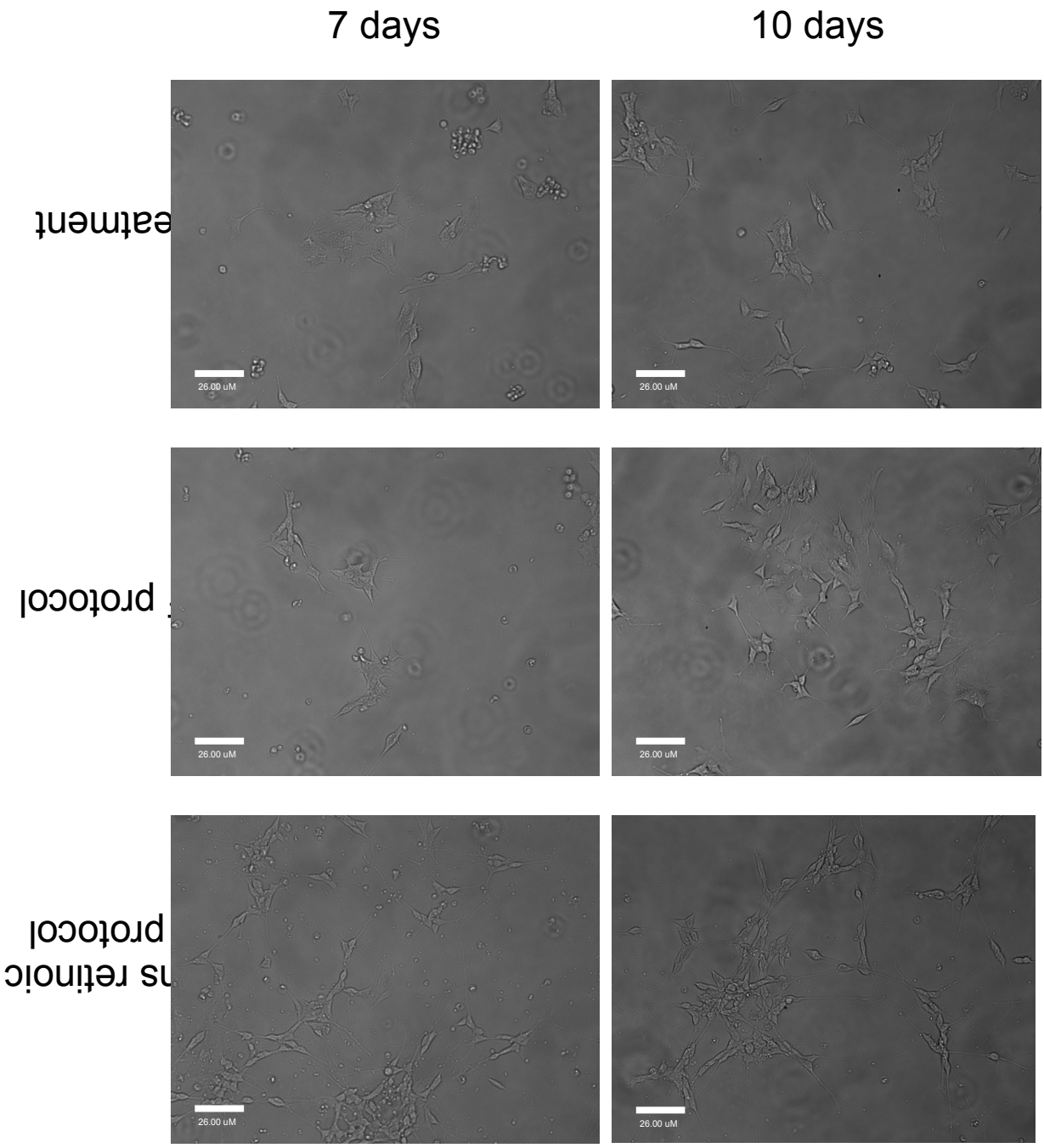

Figure 39 Differentiation of SHSY5Y cells.

Cells imaged with an inverted stage microscope (20x magnification) at 24 hours, 3 days, 7 days an 10 days. A scale bar is presented in each image.

It can be seen that SHSY5Y cells 24 hours after plating have a rounded appearance with short neurite extensions. With no treatment, the NGF protocol, or indeed with any of the differentiation protocols besides all-trans retinoic acid, cells tended to extend neuritis over the 10 day period at a constant rate. After 10 days these cells have adopted a flatter, longer morphology with numerous neurite extensions. With all-trans retinoic acid, cells adopt this appearance as early as 24 hours after initial exposure and by day 10 have significantly flatter, longer morphology than controls with longer and more numerous neurite extensions. In addition they tended to form fewer cell clusters than untreated cells. For comparison, Figure 40 shows the typical morphology of SHSY5Y cells following either no treatment or the all-trans retinoic acid protocol after 24 hours and Figure 41 shows these cells after 10 days. To highlight the neurite extensions, in Figure 41 the images were captured whilst focussing the camera at a lower level in each well. Cell bodies and extensions appear darker for this reason.

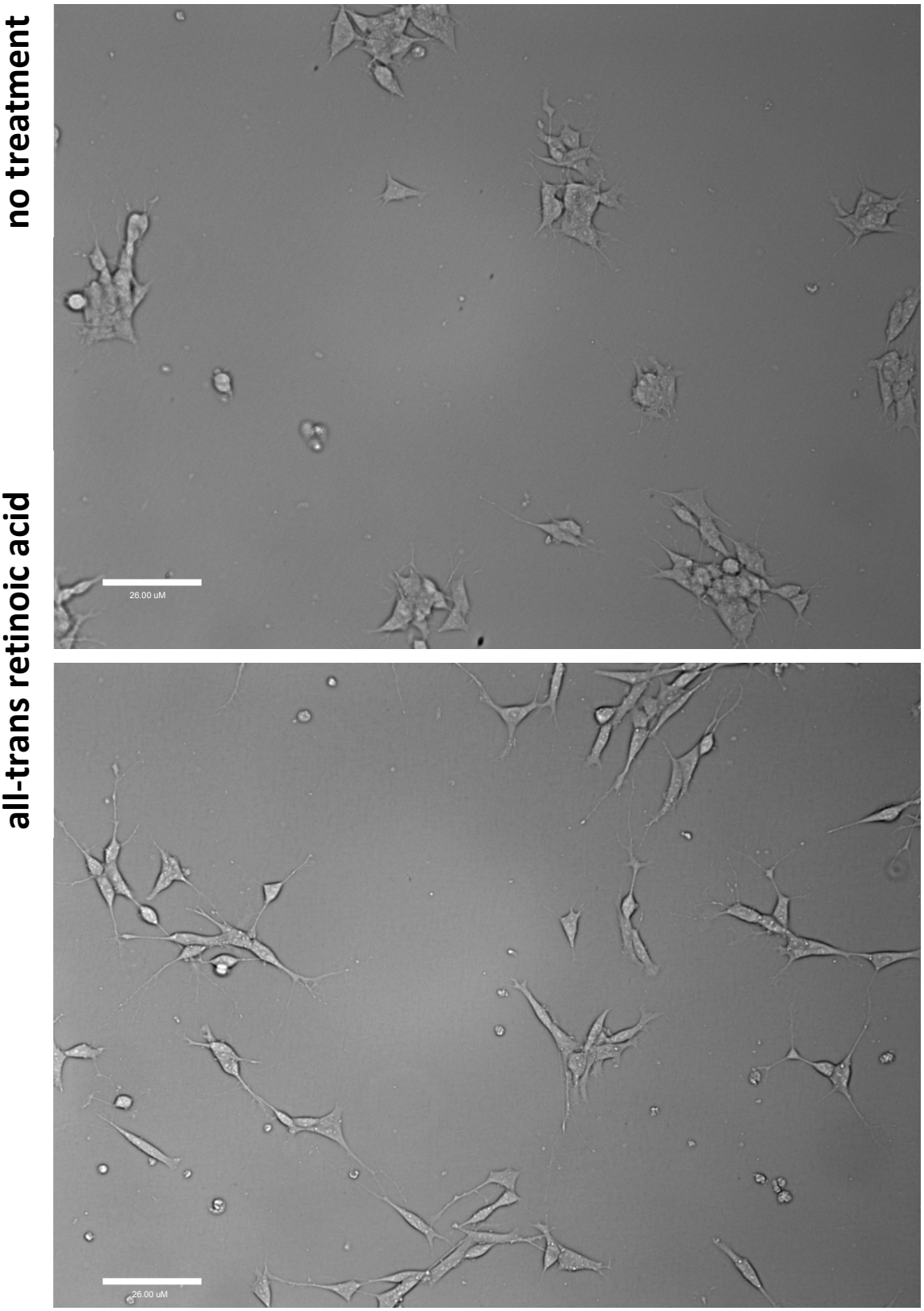
no treatment
26.00 uM
all-trans retinoic acid
26.00 uM

Figure 40 Morphology of SHSY5Y cells after 24 hours of differentiation

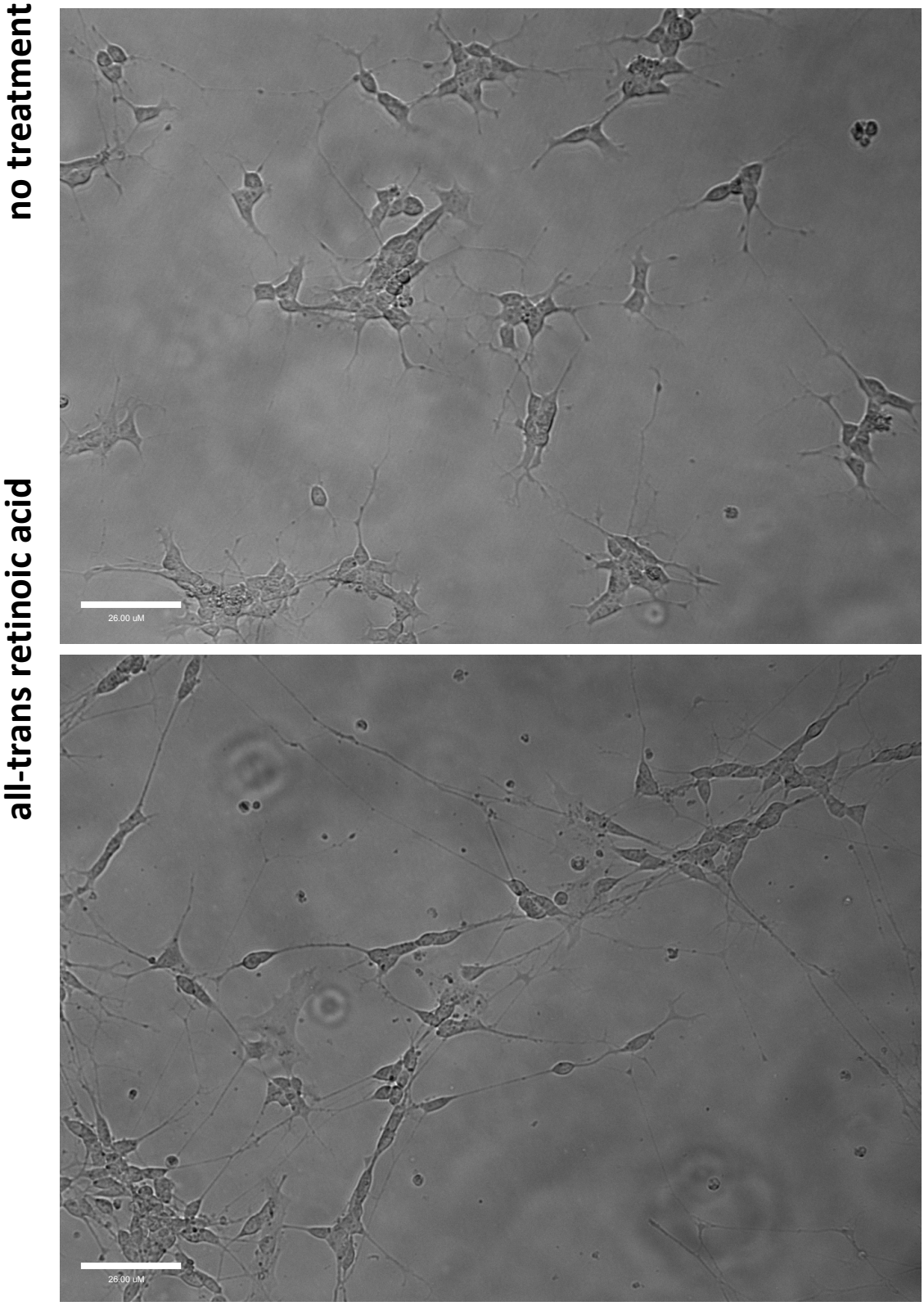

Figure 41 Morphology of SHSY5Y cells after 10 days of differentiation

10.4.2 Immunohistochemistry results

As details previously, anti-TUJ1 (Green fluorescence) was used to indicate cells which have undergone some degree of neuronal differentiation and staining with anti-GFAP (Red fluorescence) would suggest that cells have retained some glial cell characteristics. DAPI (Blue fluorescence) was employed to identify all cell nuclei. Immunohistochensitry was performed after 10 days of all-trans retinoic acid differentiation. Controls included cells cultured without all-trans retinoic acid and immunofluorescence control wells which had undergone the standard immunohistochemical protocol but without a primary antibody (to exclude non-specific secondary antibody binding).

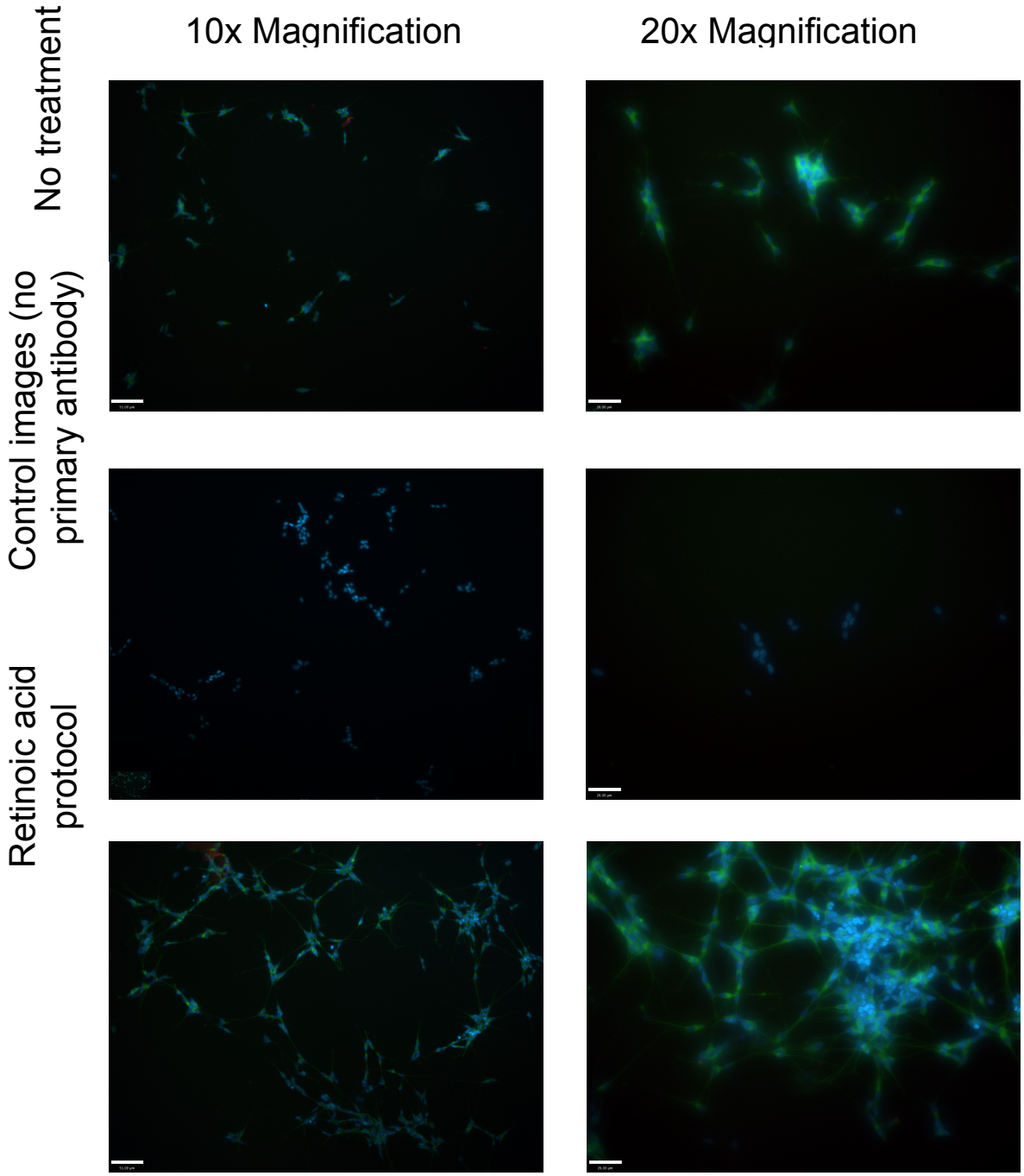

Figure 42 Immunostaining of differentiated and undifferentiated SHSY5Y cells.

SHSY5Y cells are shown having undergone differentiation for 10 days with all-trans retinoic acid. Cells were viewed on a fluorescent inverted stage microscope. Immunohistochemistry was performed using anti-TUJ1 (Green fluorescence), anti-GFAP (Red fluorescence) and DAPI (Blue fluorescence).

Anti-GFAP staining was non-specific in all assays. Both undifferentiated and differentiated cells exhibited significant anti-TUJ1 staining. DAPI successfully stained cell nuclei. The 'no primary control' wells showed no fluorescence with either antibody but good nuclear staining with DAPI suggesting that fluorescence in other wells was specific. These results suggested that the SHSY5Y cells already had a strongly neuronal phenotype prior to any differentiation protocols.

10.4.3 Differentiation of Y-79 cells

Differentiation of Y-79 cells was not achieved. Despite varying the serum free growth media and slowly reducing the serum content of the media, it was not possible to culture cells without serum for greater than 3 days. Cell death occurred quickly such that after 1 week, less than 0.001% cells remained. Applying the differentiation protocol to cells grown in medium containing serum resulted in no changes in cell morphology.

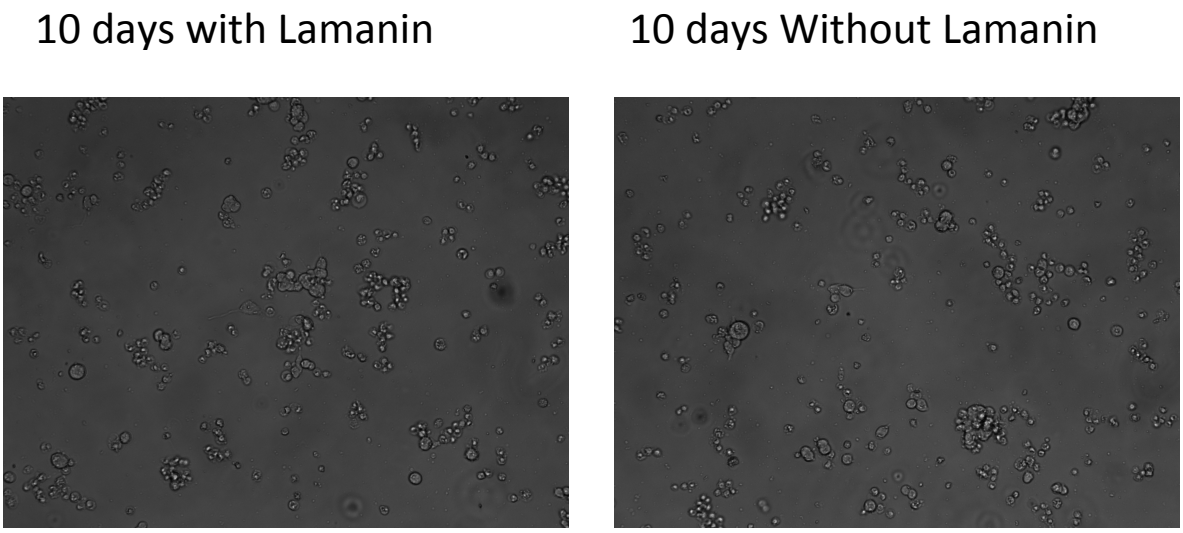

Figure 43 Differentiation of Y79 cells.

Cells imaged with an inverted stage microscope (10x magnification) after 10 days of culture in medium with full serum, in 6 well plates pre-coated with poly-l-lysine, either with or without lamanin (20 µg/ml).

It can be seen that cells cultured in medium containing serum for 10 days had similar morphology regardless of lamanin inclusion in the medium. A very small minority of cells produce neurite like extensions regardless of alterations in the protocol as detailed previously. Interestingly, after 2 vigorous washes of any of these plates the cells with neurite like extensions tended to remain in the wells to a great extent than the other cells, perhaps due to better adhesion. However, these cells were extremely sparse and only 15-20 cells were seen in each well.

In summary, differentiation or a change in morphology was not achieved for this cell line.

10.4.4 Relative expression in SHSY5Y and Y-79 cells

To confirm the viability of the delta-delta CT method of analysis for expression data, calibration curves were completed for each of the three gene assays (*GAPDH* and *ACTB* control genes and the *FRMD7* gene of interest). Due to low expression of the *FRMD7* gene, an oligonucleotide template was purchased and serially diluted as for the cDNA template used for the other 2 assays.

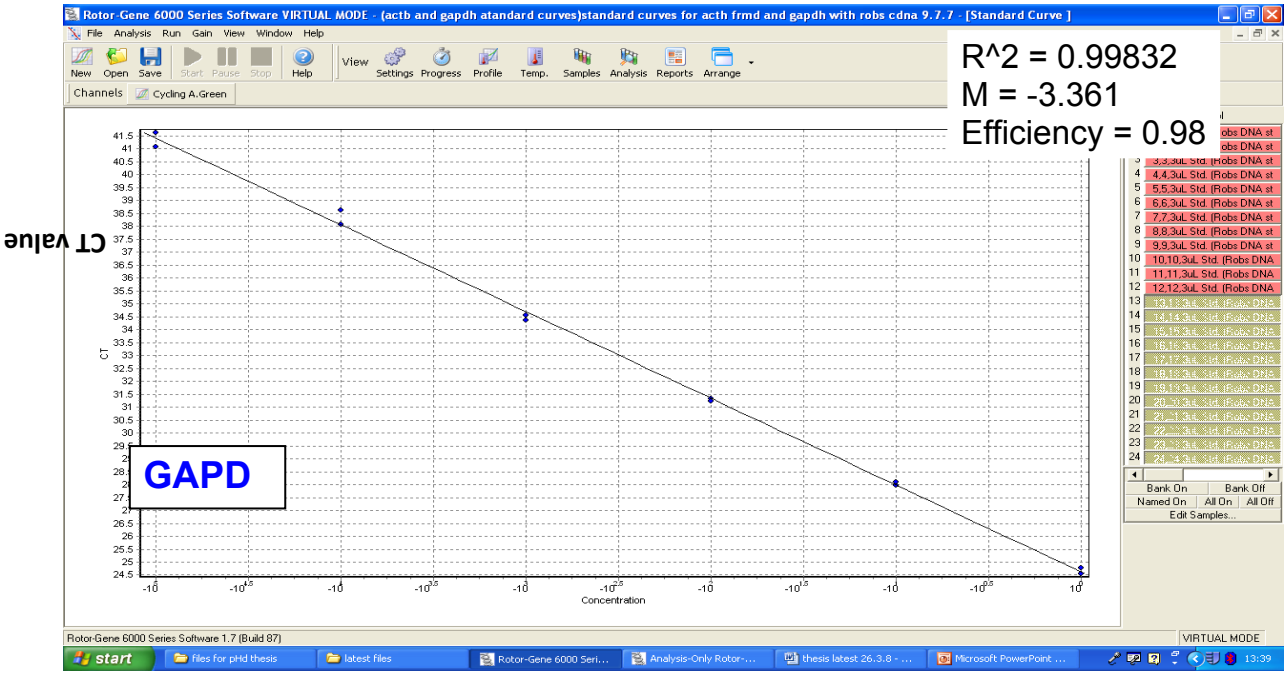
Rotor-Gene 6000 Series Software VIRTUAL MODE - (actb and gapdh atandard curves)standard curves for acth frmd and gapdh with robs cdna 9.7.7 - [Standard Curve]
R^2 = 0.99832
M = -3.361
Efficiency = 0.98
GAPD
CT value
Concentration
Template concentration (log scale)

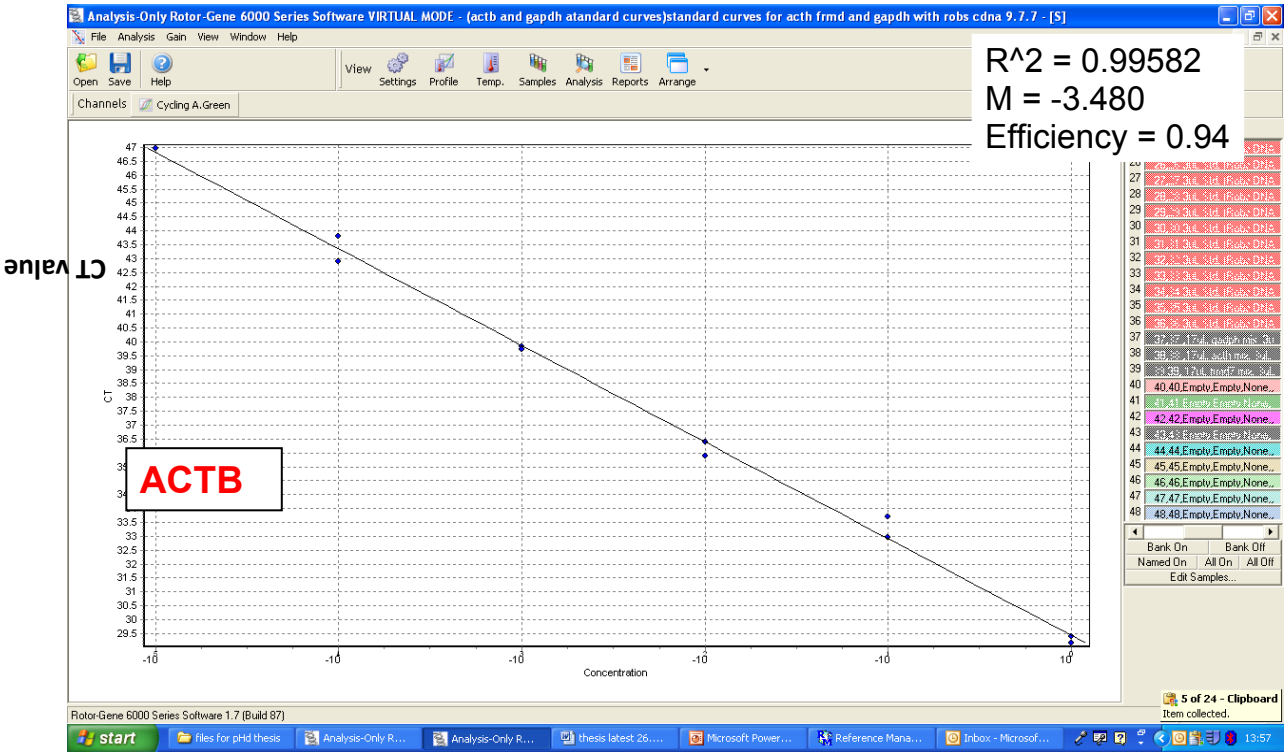

Template concentration (log scale)

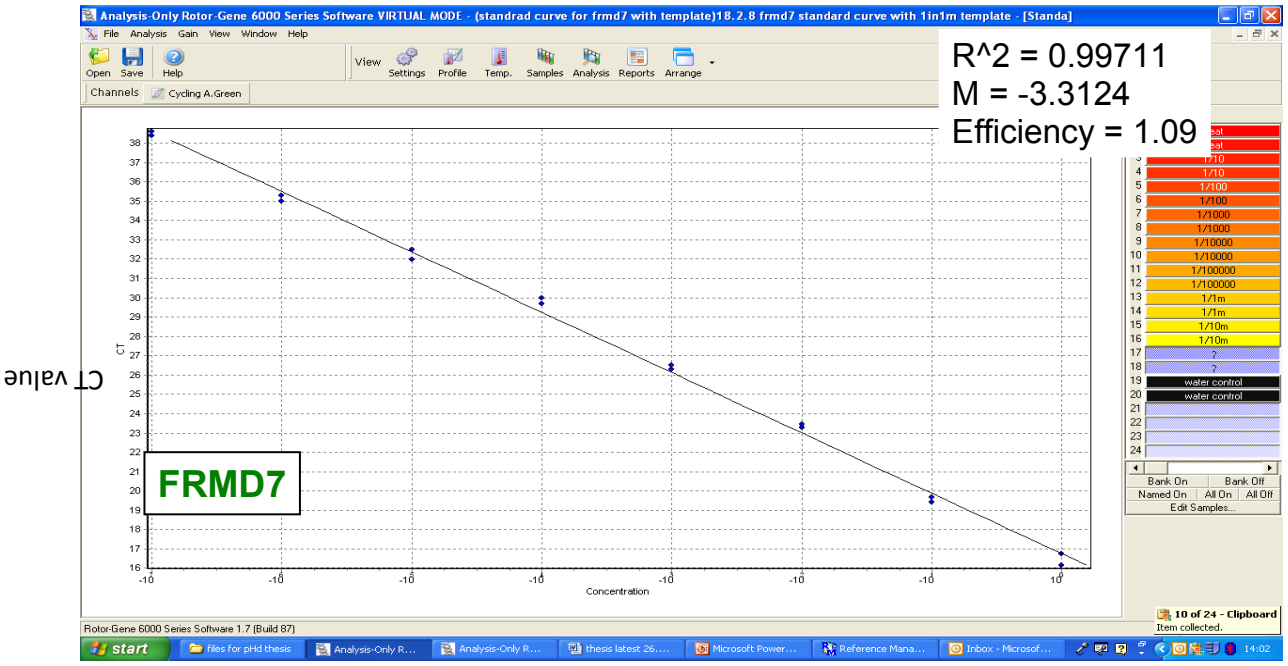

Template concentration (log scale)

Figure 44 Standard curves for the human probe based qPCR assays.

Standard curves are presented for *GAPDH*, *ACTB* and *FRMD7* by plotting CT values against template concentration on a log scale. The correlation coefficient (R^2), slope of the curve (M) and PCR -efficiency (efficiency) are also presented.

It can be seen in that for all three assays, the PCR efficiency is close to 1 and that the R^2 value is greater than 0.99. This confirmed that the assays were very close to 100% efficient over a broad range in target gene copy number and that the delta-delta CT method of analysis was appropriate.

All samples were run by the quantitative PCR methodology detailed previously on a series of 4 runs. Water controls and rt- controls were run for all experiments to confirm the specificity of the PCR assays. In all runs these controls either showed no amplification or amplification at greater than 4 cycles below the lowest cDNA sample. Each tissue/time-point was represented by 2 separately prepared cDNA samples which were in turn run in duplicate such that each tissue/time-point was represented by four wells. Calculation of the relative expression of *FRMD7* was performed by the delta-delta CT method described in section 9.2.3. An example of the calculation method is shown in Table 13.

Source of cDNA	Description	Assay	CT values	ΔCt-value	ΔΔCt	Comparative Expression Level per tissue/timepoint
SHSY5Y sample 1	Full media for 1 week	*FRMD 7*	35.67	15.61	0	**1.00**
SHSY5Y sample 1	Full media for 1 week	GAPDH	18.7			
SHSY5Y sample 1	Full media for 1 week	ACTB	21.42			
SHSY5Y sample 2	Full media for 1 week	*FRMD 7*	38.91	15.51	0.1	**1.07**
SHSY5Y sample 2	Full media for 1 week	GAPDH	21.42			
SHSY5Y sample 2	Full media for 1 week	ACTB	25.38			
SHSY5Y sample 1	Full media +	*FRMD*	38.45	17.275	-1.665	**0.32**

	NGF for 1 week	*7*				
SHSY5Y sample 1	Full media + NGF for 1 week	GAPDH	19.75			
SHSY5Y sample 1	Full media + NGF for 1 week	ACTB	22.6			
SHSY5Y sample 2	Full media + NGF for 1 week	*FRMD 7*	37.6	16.98	-1.37	**0.39**
SHSY5Y sample 2	Full media + NGF for 1 week	GAPDH	20.01			
SHSY5Y sample 2	Full media + NGF for 1 week	ACTB	21.23			

Table 13 An example of the method for analysis of comparative expression levels.

A sample of the spreadsheet calculation of the relative expression of *FRMD7* mRNA in the SHSY5Y cell line after 1 week of *in vitro* culture in medium with/without Nerve Growth Factor (βNGF) at 100ng/ml.

Using this method a comparative expression level was calculated for all samples relative to that of the SHSY5Y cells following culture in full serum alone media for 1 week. Results are shown in Figure 45.

(a)

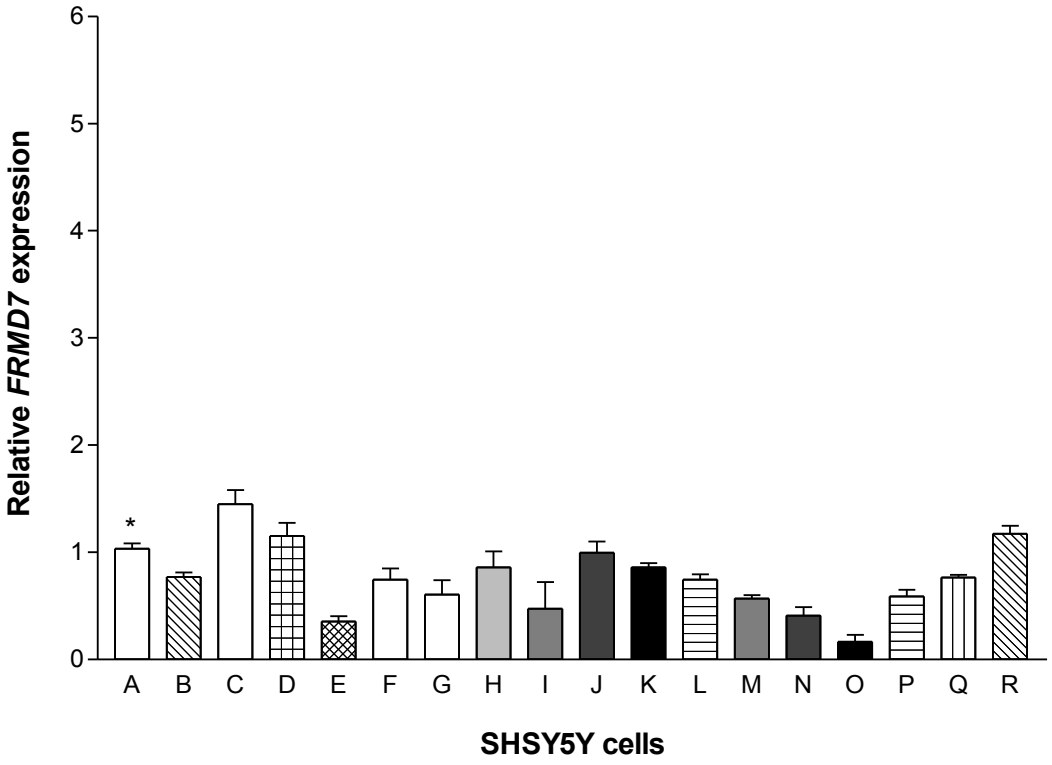
Relative FRMD7 expression
0
1
2
3
4
5
6
*
A B C D E F G H I J K L M N O P Q R
SHSY5Y cells

(b)

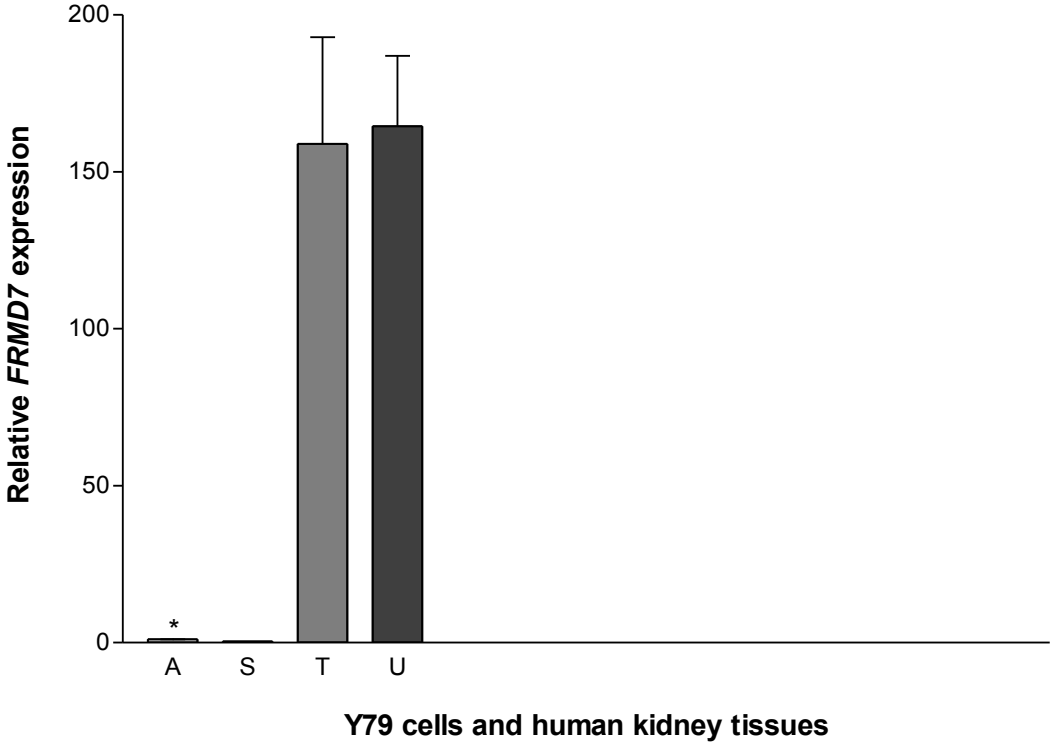
Relative FRMD7 expression
0
50
100
150
200
*
A S T U
Y79 cells and human kidney tissues

(c)

Label	Cells	Description
A	SHSY5Y	Full FBS media for 1 week
B	SHSY5Y	1/2 FBS media for 1 week
C	SHSY5Y	Neurobasal media for 1 week
D	SHSY5Y	no FBS media for 3/7
E	SHSY5Y	Full FBS media + NGF for 1 week
F	SHSY5Y	Full FBS media +NGF+ FK801 for 1 week
G	SHSY5Y	Full FBS media +CAMP for 1 week
H	SHSY5Y	1/2 FBS media + NGF for 1 week
I	SHSY5Y	1/2 FBS media +NGF+FK801 for 1 week
J	SHSY5Y	1/2 FBS media + cAMP for 1 week
K	SHSY5Y	no FBS media + NGF for 3/7
L	SHSY5Y	no FBS media +NGF+FK801 for 3/7
M	SHSY5Y	no FBS media cAMP for 3/7
N	SHSY5Y	with full FBS media + Retinoic acid for 24 hours
O	SHSY5Y	with full FBS media + Retinoic acid for 48 hours
P	SHSY5Y	with full FBS media + Retinoic acid for 3/7
Q	SHSY5Y	with full FBS media + Retinoic acid for 1 week
R	SHSY5Y	with full FBS media + Retinoic acid for 10/7
S	Y79	with full FBS media for 1 week
T	HK1 medulla	human adult kidney medulla
U	HK1 cortex	human adult kidney cortex

Figure 45 Relative expression of FRMD7 in 3 tissues.

Relative expression values for *FRMD7* mRNA are shown for the SHSY5Y cell line relative to the two housekeeping genes *GAPDH* and *ACTB*. Results are shown as comparative expression levels to cells grown in full standard media for 1 week (a). Relative expression values for *FRMD7* mRNA are shown for the Y-79 cell lines and human adult kidney tissues relative to the SHSY5Y cell line grown in full standard media for 1 week (b). A key legend is provided for all samples (c). Error bars represent the standard deviation (SD).

The results above demonstrate that the variation in expression levels for *FRMD7* mRNA for the SHSY5Y cell line were very small. Despite a variety of differentiation protocols, very little change in the low levels of expression were found. The expression pattern for SHSY5Y cells during the all-trans retinoic acid differentiation protocol (samples N-R in Figure 45) shows a slow increase until day 10. Expression levels in the Y-79 cell line were also low. Interestingly, human adult kidney samples show a significantly higher expression level in both medulla and cortex samples which can be seen in comparison to the SHSY5Y cell line sample in Figure 45b.

10.5 Discussion

The results presented above show that in all tissues studies thus far, *FRMD7* mRNA expression is low. This is consistent with previous expression work[159]. All relative expression calculations were therefore based on the comparison of a very low level of *FRMD7* expression with the significantly higher expression of housekeeping genes.

Differentiation assays were tested and altered using various parameters but the only clear change in cell morphology was achieved using all-trans retinoic acid with the SHSY5Y cell line. However, a rigorous morphology assessment was not employed and it is conceivable that subtle morphological changes reflecting differentiation of the cells may have been overlooked. For example, some groups have employed rigorous counting and measuring of neurite number, branching and interconnection[249;255]. Others have advocated fully automated image capture and analysis using multichannel fluorescent immunohistochemical techniques[248]. Therefore, it is possible that these protocols did induce some differentiation. This is why cells from each differentiation assay, regardless of morphological changes, were studied for changes in *FRMD7* expression levels.

It is apparent that no significant change in *FRMD7* expression occurred in either cell line during attempted differentiation. All changes in expression level were very small and likely within the margin of error for this methodology on a low copy number mRNA. Disappointingly, this shows that neither cell line, using the methods described, provides a good model for understanding the molecular biology of the *FRMD7* gene product due to the consistently low copy number of the mRNA.

Interestingly, as illustrated in Figure 45b, the relative expression of *FRMD7* is significantly higher in the human adult kidney samples. Expression appears to be over 150 times greater than in either the SHSY5Y or Y-79 cell lines which is in keeping with the previous observation that the human adult kidney expresses this gene in higher abundance than most other tissues tested[159]. However, expression in this tissue was calculated relative to the GAPDH and ACTB housekeeping genes and in comparison to

expression in the SHSY5Y neuroblastoma cell line. It is important to note that although the chosen housekeeping genes have been used extensively in multiple tissues, expression can vary between tissue types[261]. Therefore, direct comparison of differing tissues should be interpreted with caution although averaging 2 housekeeping genes reduces this confounding effect.

The work detailed in this chapter has demonstrated that *FRMD7* expression is low in 2 cell lines which are commonly used for models of neurite growth / extension and ocular development. Therefore, neither of these cell lines represents a good opportunity for the study of *FRMD7* gene function using the current differentiation protocols. This work has also confirmed that expression of this gene is significantly greater in human adult kidney samples, suggesting a potential role for cells derived from these tissues in the study of *FRMD7*. Assays and protocols for the rapid assessment and analysis of expression levels for the *FRMD7* mRNA have been optimised and refined during this study.

11 CHAPTER ELEVEN – Final Discussion

11.1 Thesis summary

The work presented in this thesis has contributed to the recent advances in understanding Congenital Idiopathic Nystagmus (CIN). My early work in this project showed the variability in phenotype and necessity for detailed investigation of CIN pedigrees[38;132]. Subsequently, I refined the genetic locus for this disease significantly on the X chromosome by linkage analysis[38]. After collection of a large cohort of CIN cases I quantified the contribution of a newly identified nystagmus gene (*FRMD7*) to CIN, identified a novel mutation in this gene and provided the first detailed phenotype genotype correlation for a mutation in this gene[239]. This work illustrated the small contribution of *FRMD7* mutations to sporadic cases of CIN and illustrated the likely presence of other significant nystagmus genes or parts/regulatory elements of the *FRMD7* gene. I also investigated skewed X-inactivation and variable penetrance in female carriers of *FRMD7* mutations and identified a possible role for skewed X-inactivation in these families[239]. Additionally, I identified a novel mutation in the *CACNA1A* gene which causes apparent isolated congenital nystagmus until the onset of subtle cerebellar ataxia after the age of 30[262]. This has shown that mutations in this gene can cause variable phenotypes and that apparent congenital nystagmus may be a prelude to cerebellar disease in some patients. Furthermore, I have performed the first detailed study of *FRMD7* mRNA expression by RT-PCR in murine brain heart and lung during development[263]. This work has shown low levels of expression of this gene in all tissues tested with a peak at ED18 in brain suggesting a possible role for this gene in synapse formation/function and axon growth and guidance. A final preliminary study of *FRMD7* expression in human tissues has showed the low levels of expression of this gene in human neuronal cell lines and no significant changes in expression during neurite extension and growth of the SHSY5Y cell line. Furthermore, this study showed that human adult kidney samples show the highest levels of *FRMD7* expression of any

tissue tested so far. This has suggested that kidney derived cells may represent a promising opportunity for initial investigations into *FRMD7* gene expression and function.

This work has been timely and has incorporated many different avenues of nystagmus research. It has been completed at a time of renewed interest in understanding the underlying pathophysiology of anomalous eye movements. Much of my work has been hypothesis-generating and has provided preliminary information which is allowing us, and other groups to pursue further work with the common goals of understanding the underlying mechanisms of eye movement control and their malfunction. Also, to understand the role and pathophysiology of the *FRMD7* gene with the potential to identify novel treatment and diagnostic modalities in the future.

11.2 Future work

Due to recent advances in the field of nystagmus research, including the discovery of the *FRMD7* gene in 2006, many new avenues of study have opened up during the tenure of this PhD project. The following sections describe some of these avenues and illustrate the work which is continuing in our group.

11.2.1 Clinical and genetics studies

My resent work and that by others has illustrated the necessity of accurate and detailed phenotyping of nystagmus patients to allow the study of homogeneous subgroups of patients who have the greatest likelihood of similar underlying pathophysiologys. In a recent investigation of the phenotype of CIN patients with and without *FRMD7* mutations, the *FRMD7* mutant subgroup had a significantly lower number of subjects with pronounced head turn and, correspondingly, had relatively smaller nystagmus amplitudes in the primary position of gaze[264]. I have also noted previously that patients with different classes of *FRMD7* mutations seem to exhibit greater or lesser penetrance rates in female carriers[265]. It is therefore clear that further work is needed to investigate the phenotype/genotype correlation between mutations

in *FRMD7* (and other genes under current investigation) and phenotype to include; penetrance in female carriers, X-inactivation, age of onset of the disease and detailed clinical characteristics such as head turns and null points. It is likely that this work will shed light on possible molecular mechanisms occurring in this disease and also the efficacy of diagnostic techniques and genetic counselling.

The work presented in chapter 6, and that of others has suggested the existence of other nystagmus genes and the strong possibility of mutations in other, as yet unidentified parts of the *FRMD7* gene[159;239;239;265]. This is supported by the pedigrees for which we (unpublished work) and Tarpey *et al* have found linkage to the *FRMD7* locus but no mutations in the currently known exons of that gene. Therefore, if these sites were identified and characterised, they would provide strong candidates for the identification of additional nystagmus causing mutations. Furthermore, the full extent of the contribution of mutations affecting the *FRMD7* gene product could be assessed. Identification of regulatory sites and potential promoters is complex. Many indicators can be used to identify such sequences, for example; CpG islands[266] and evolutionary conservation[267]. Several papers have associated these conserved regions with regulatory sites[268] and generally the assumption seems valid that evolutionary conservation of non-coding DNA sequence is due to conservation of regulatory DNA including transcription factor binding sites[267]. Furthermore, many algorithms have been developed to combine multiple factors and motifs to identify sequence which have a high statistical chance of containing regulatory sites. Using these tools I have performed a detailed *in silico* bioinformatic mining study of the genetic sequence surrounding the *FRMD7* gene to highlight any potential regions which contain additional exons, promoters and other regulatory elements (unpublished work). This was achieved by annotating the genomic sequence of *FRMD7* and 5kb of flanking region at the 3 and 5-prime ends. The sequence was annotated with information derived from 46 separate algorithms designed to locate any one, or combination of features/motifs including; exapted conserved non-exonic elements, homology with known regulatory elements in 7 species, transcription factor binding sites in 3 species, RNA secondary structure prediction, predicted alternative

conserved exons, evolutionary conservation across 28 species, homology with known promoter sequences, CpG islands and Predicted Start and stop codon sequences. Known *FRMD7* exons were identified by multiple algorithms illustrating the power of this method of combined data mining (see Figure 46). This work has yielded some very exciting preliminary data. I have identified a strong candidate promoter region close to the transcription start site of *FRMD7* which was identified as putative promoter sequence by 18 separate algorithms but could also represent an additional alternatively spliced/untranslated exon:

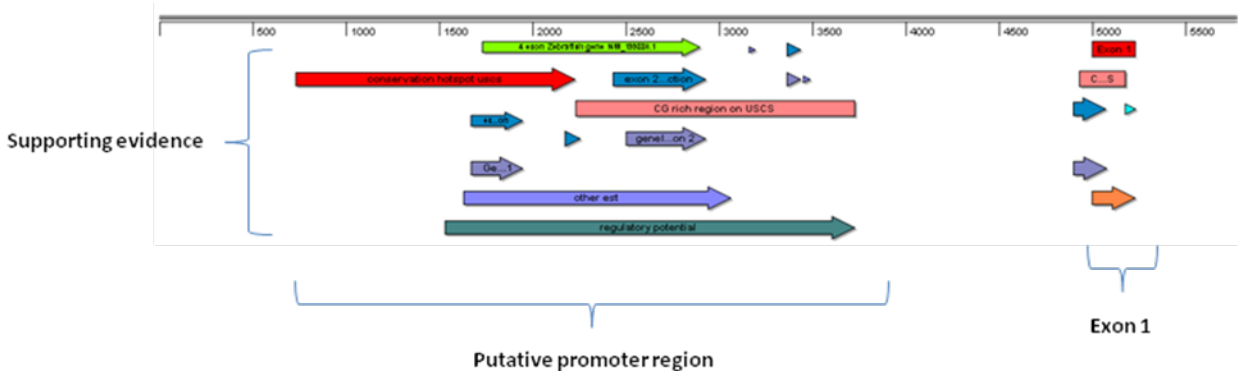

Figure 46 Annotation of the *FRMD7* gene sequence.

A screen shot from SeqBuilder module of the Lasergene 6 DNA & Protein Sequence Analysis suite (DNASTAR, Inc., Madison, USA)). An illustration of evidence for exon 1 and for the putative promoter region (which includes; conservation, 5 exon prediction algorithms, cross-species identification exons , multiple transcription factor binding sites, a predicted conserved transcription factor binding site, and a region identified as highly likely of having regulatory potential by the ESPERR Regulatory Potential algorithm and cross reference with 7 other species).

Similarly, a number of intra-intronic regions were identified which have some evidence to suggest that they may contain additional, alternatively spliced/untranslated exons. It is hoped that investigation of these regions of the *FRMD7* gene will identify new sites in which nystagmus causing mutations may occur (thus increasing the yield of *FRMD7* gene screening in CIN) and provide information about the regulation, transcription and alternative splicing of this gene. This work has been planned and it is

hoped that it will begin within the next year. We will investigate these regions using dual-reporter Luciferase assays and the pGL-3 vector series (Promega) using methods which have been previously described[269;270]. In brief, we will design PCR primers to amplify putative regulatory sequence from genomic DNA in amplimers up to 1kb in length. These fragments will be cloned into vectors from the pGL-3 series as follows: the pGL3-enhanser vector that lacks an internal promoter and will be used to test for promoter activity, the pGL3-promoter vector which lacks an internal enhancer and will be used to test sequences for enhancer or silencer activity, the pGL3-control vector that contains both internal promoter and enhancer elements which will be used as a positive control and an additional test for repressor activity and the pGL3-basic vector with neither internal promoter nor internal enhancer element which will be used as a negative control and to examine sequence for core promoter activity (when indicated). All the vectors will be sequenced to exclude additional point mutations acquired during the PCR and cloning process. These vectors will subsequently be co-transfected into a number of cell lines available in our laboratory (initially *SHSY5Y*, *PC12* and *Y-79* cells) with the Renilla luciferase-containing pRL-TK control plasmid (Promega) using the FuGENE6 Lipofectamine Reagent (Roche). After 24 hours, cell lysates will be prepared from each transfected culture and transferred to 96-well microtiter plates. The firefly and Renilla luciferase activities will be analyzed in our 96-well plate luminometer with Doc-It^{R}LS software (UVP) according to the manufacturer's protocol. The activity of each promoter sequence will be assessed by normalising the firefly luciferase fluorescence to that of the renilla luciferase fluorescence for each sample (to control for transfection efficiencies) and comparing with control samples. Sequences with evident promoter, or other regulatory activity will then be prioritised for further study using the same methodologies to identify the functional regulatory elements by serial deletions of the initial transfected sequence. Any sequence of a suitable size, with regulatory activity will be prioritised for mutation scanning by direct sequencing.

During the course of this study I have collected and expanded my nystagmus cohort significantly. Currently the cohort includes 31 probands which are either sporadic

cases or part of an X-linked pedigree, which have not been screened for *FRMD7* mutations. Following the initial studies detailed above we hope to screen all these probands for mutations in the *FRMD7* gene and the additional promoter/regulatory sequences by direct sequencing.

Skewed X-inactivation, (significant deviation away from the expected 50:50 contribution of each X chromosome in females) has been described in various ocular diseases [186;188] and may explain why X-linked nystagmus pedigrees with *FRMD7* mutations have shown such varied inheritance patterns[38;104;159;178]. Many X-linked disorders do not fit classical dominant or recessive modes of inheritance and it is known that X-linked genes can cause partial cell selection and incompletely skewed X-inactivation[192]. The vast majority of genes on the long arm of the X chromosome are subject to X-inactivation, including those immediately flanking *FRMD7*: *MST4*, *MBNL3* and *RAP2C* [27] and since genes which are subject to, or escape from, X-inactivation tend to be clustered into domains, it is very likely that *FRMD7* is inactivated. We have tested the hypothesis that Skewed X-inactivation is responsible for the variable penetrance in X-linked CIN pedigrees by performing 2 X-inactivation assays in a large X-linked CIN pedigree (see chapter 7). Results showed a significant overall excess of skewing in this pedigree (10 of 16 females including 3 with >95% skewing)[239]. Recently, Kaplan et al replicated our findings by describing a significantly increased susceptibility to skewed X-inactivation in affected females in a large CIN pedigree with a missense *FRMD7* mutation[190]. This preliminary work has provided the first exciting evidence to suggest that X-inactivation contributes to variable phenotype in CIN pedigrees and that more detailed studies are warranted. It is hoped that such studies will provide clinically useful information and also provide insights into the pathogenic mechanisms of *FRMD7* mutations including gain or loss of function effects. To build on this exciting work we would like to contrast X-inactivation patterns in hair and lymphocyte derived DNA, run 3 different assays to ensure maximum information in 7 pedigrees and design a novel assay to look directly at inactivation of the *FRMD7* gene. In brief: we would like to extract DNA from scalp hair root samples for one pedigree (in the first instance) because it has been

postulated that the X-inactivation pattern in the brain and retina (where *FRMD7* is most likely expressed) is possibly replicated in hair root follicles due to their common ectodermal origin during embryonic development[271;272]. We would then use 3 X-inactivation assays, 2 of which we have used before (*HUMAR*[24] and *ZNF261*[187]) and one which utilizes a region closer to the *FRMD7* gene than the previous assays (*FMR1* assay[273]). These assays will be used to asses the difference in X-inactivation pattern between hair follicle and lymphocyte derived DNA in one large family. If differences exist, hair follicle samples will be collected from 6 additional families and used for further analysis. We hope to identify and characterise the promoter of *FRMD7* (as detailed above) which will provide the exciting possibility of designing a novel X-inactivation assay(s) to directly study inactivation of the *FRMD7* gene. This novel assay(s) will be designed following identification of the *FRMD7* promoter and run initially to definitively answer the question of whether *FRMD7* is inactivated and then to assess the precise X-inactivation pattern in affected females and female carriers from all 7 CIN pedigrees. The resulting data will allow us to: determine whether *FRMD7* undergoes X-inactivation, look for a correlation between X-inactivation and penetrance in *FRMD7* mutant CIN pedigrees and elucidate the potential role of X-inactivation in the pathology of CIN and whether this is dependant on the class of *FRMD7* mutation or not.

Mutations in the Ocular Albinism Type 1 gene (OA1, or GPR143, OMIM 300500) causes a form of X-linked ocular albinism[274]. In many cases the most prominent feature of the phenotype is nystagmus. Additional features such as iris transillumination, foveal hypoplasia and retinal hypopigmentation are only identified when specifically saught[275]. Abnormal optic nerve fibre decussation at the optic chiasm is also found in these patients but can only be identified by electrophysiological testing with Visual Evoked Potentials (VEPs). Many families with OA1 mutations have been described in whom nystagmus is the only clinical finding even when extensively examined by slitlamp bio-microscopy. These families have been described and published as 'congenital nystagmus' pedigrees with novel OA1 mutations[276;277]. However, electrodiagnostic testing was not always presented for these cases and it seems likely that crossed

asymmetry may have been demonstrated if VEPs had been performed. This illustrates two interesting points. Firstly, without any electrodiagnostic testing it is difficult to exclude OA1 in male patients with nystagmus. Secondly, description of these pedigrees as 'Congenital Nystagmus' is misleading especially when a mutation in the OA1 gene has been identified, therefore these families arguably represent a phenotypic variation of ocular albinism type 1. Using MRI, Schmitz et al. (2003) found that the abnormal decussation at the optic chiasm in OA1 was identical to that found in tyrosinase gene-related OCA1 (203100) and P gene(611409)-related OCA2 (203200). He later showed that the misrouting was due to changes in cell cycle regulation in the developing retina which is in part controlled by melanin[278]. Therefore, lack of pigment in the developing eye and visual pathways is responsible for the crossed asymmetry in albinism irrespective of the causative gene mutation. As has been detailed above, mutations in the OA1 gene can cause extremely variable pigmentation levels in the eye. It is possible that nystagmus develops independently of the chasmal routing process and therefore conceivable that some patients may exist in whom nystagmus has occurred due to an OA1 mutation but in whom abnormal chiasmal decussation has not occurred. These patients would be likely to be those with the greatest amount of visible ocular pigmentation and would therefore be diagnosed as CIN due to a normal clinical and electrodiagnostic examination. The OA1 gene is a relatively small, 8 exon gene which is therefore quite amenable to direct sequencing on individual patients. Perhaps this gene represents a reasonable candidate for an 'apparent congenital nystagmus' gene. Therefore, it may be fruitful to screen my cohort of clinically and electrophysiological examined, *FRMD7* negative patients for mutations in this gene.

Other potential nystagmus genes have been identified by recent work. The *FRMD7* gene is a member of the protein 4,1 superfamily and contains 2 domains (B41 and FERM-C) around which all the identified mutations in CIN have clustered[159] (see). Two other members of the protein 4.1 superfamily show significant homology, particularly to these domains of the *FRMD7* gene. These are *FARP1* (FERM, RhoGEF (ARHGEF) and pleckstrin domain protein 1 (chondrocyte-derived)) and *FARP2* (FERM,

RhoGEF and pleckstrin domain protein 2). The *FARP1* gene on chromosome 13 is also located within the interval identified for a family with an unknown familial vestibulo-cerebellar disorder[279] with predominant nystagmus phenotype. The *FARP2* gene on chromosome 2 is also known to alter neurite length and degree of sprouting in rat embryonic cortical neurones when over-expressed[184;185] and thus has a function relevant to the nystagmus phenotype. Additionally, other potential nystagmus genes are likely to be identified by functional studies of *FRMD7* including protein-protein interactions and co-expression studies. All these genes may be used by future studies to identify novel mutations which may cause CIN.

11.2.2 Understanding the function of *FRMD7*

In chapters 9 and 10 I have detailed some interesting preliminary studies of *FRMD7* expression. I now have 3 custom designed *FRMD7* monoclonal antibodies which have been delivered with the corresponding hybridoma cell lines to allow continued antibody production. This exciting resource will allow a more detailed study of spatial tissue expression patterns for the *FRMD7* transcript and also characterisation of sub-cellular expression. These antibodies have not been used and will require various preliminary test to evaluate their specificity and optimal experimental protocols. Initially, we plan to study protein extract from human adult kidney samples by both direct Immunostaining at various antibody concentrations and also using a western blot. Furthermore, the initial antigen was chosen for its homology between human, rat and mouse *FRMD7* protein. Therefore, it will be necessary to identify which of these species it will be possible to use for these studies. The results of these preliminary experiments will largely dictate the subsequent work but it is hoped that we will be able to utilize our resource of wax embedded murine embryo samples, human foetal tissue, fresh adult rat brain and ocular tissue and human donor eye tissue. We hope to characterise the expression of the *FRMD7* protein and identify potential binding partners and sites of function. These studies will help to; identify where and when the *FRMD7* protein is

functioning, identify good models for further siRNA knockdown experiments, identify novel putative nystagmus genes, unravel some of the details of eye movement control, and even identify potential sites of therapeutic intervention.

An additional resource which is likely to become available within 2 years is an *FRMD7* knockout mouse. In early 2007 I nominated the murine *FRMD7*, *FARP1* and *FARP2* genes for knockout via the NIH backed Knockout Mouse Project (KOMP) which aims to 'generate a public resource of mouse embryonic stem (ES) cells containing a null mutation in every gene in the mouse genome' (http://www.nih.gov/science/models/mouse/knockout/). Subsequently, the *FRMD7* and *FARP2* genes were selected out of 17,350 genes for priority targeting and the development of knockout ES cells is currently underway. The ES cells will be available to the authors on completion which is anticipated to be in early 2009. Subsequently, the KOMP repository will create mice from the ES cells for individual researchers on request. Supply of pups following recovery from cryo-preserved ES cell lines has an anticipated cost of approximately £3500 with an estimated 6-9 months production time depending on ES implantation and pup generation (information from direct correspondence with Dr. Colin Fletcher, Program Director, Knock Out Mouse Program (KOMP)). All Experiments will be carried out in accordance with the European Communities Council Directive of 24 November 1986 (86/609/EEC) and under a personal animal license (No.PIL504b) held by Dr Thompson.

When the KOMP generated *FRMD7* mouse knockout is received will use our local expertise and experience with organotypic murine brain slice cultures and in vitro analysis of brain sections to investigate the anatomical and physiological anomalies in these animals. The knockout of any gene is potentially embryologically lethal. It seems unlikely that this is the case with *FRMD7* as it is not lethal in humans who are hemizygous for truncating mutations resulting in no detectable *FRMD7* protein expression in peripheral blood[159]. However, should this be this case, aborted foetuses could be studies by similar techniques. Ocular and neuroanatomical comparisons will be performed by light microscopy of simple wax embedded whole brain, visual pathway

and eye sections from the knockout and control wildtype mice. Similarly, investigation of cell type and distribution (as directed by the aforementioned immunohistochemical protein expression profiles) will we performed by identification of cell markers by simple staining and fluorescent labelled antibody assays used routinely in our laboratory. These initial anatomical/histological studies will direct further work. For example, to study neuroanatomical changes in more detail, neuronal cell distribution could be determined by thionin-staining (a Nissl stain) followed by a more specific investigation of changes in synaptic connectivity using antibodies against pre- and post-synaptic proteins, markers of axonal and dendrite morphology and specific markers of glutamatergic and GABAergic pathways (including vesicular transporter proteins and receptor subunits).

Organotypic murine brain slice cultures preserve intact neuronal circuitry. This feature can be exploited to look for neural pathway anomalies in these animals by performing in vitro electrophysiological assessment of the optic pathways and the cerebellum. Again, these investigations will be directed by initial neuro-anatomical studies and may include direct techniques such as stimulus evoked inhibition of spontaneous purkinje cell firing in the cerebellum.

11.2.3 Summary of future work

This project and the resent work of other groups has provided a broad platform for further study in the field of nystagmus research. Many avenues of clinical, genetic and molecular biological study have been created and are becoming ever more possible with the arrival of specific antibodies and even a mouse knockout model. It is likely that within the next 5 years, significant advances in the understanding of the development of the oculo-motor control pathways will take place. Along with genotype/phenotype correlations, clinical studies and a greater understanding of the contribution of genetics to nystagmus it is hoped that novel diagnostic and therapeutic opportunities will be found for nystagmus patients. Furthermore, as nystagmus forms a part of many different disorders, it is likely that a by-product of this work will be a greater

understanding of some of these disorders at the molecular level possibly even the development of novel treatments.

Reference List

1. Coffey AJ, Brooksbank RA, Brandau O, Oohashi T, Howell GR, Bye JM *et al*. Host response to EBV infection in X-linked lymphoproliferative disease results from mutations in an SH2-domain encoding gene. *Nat.Genet.* 1998;**20**:129-35.

2. Ross MT, Grafham DV, Coffey AJ, Scherer S, McLay K, Muzny D *et al*. The DNA sequence of the human X chromosome. *Nature* 2005;**434**:325-37.

3. LYON MF. Gene action in the X-chromosome of the mouse (Mus musculus L.). *Nature* 1961;**190**:372-3.

4. Oni SB, Osunkoya BO, Luzzatto L. Paroxysmal nocturnal hemoglobinuria: evidence for monoclonal origin of abnormal red cells. *Blood* 1970;**36**:145-52.

5. Vogelstein B, Fearon ER, Hamilton SR, Feinberg AP. Use of restriction fragment length polymorphisms to determine the clonal origin of human tumors. *Science* 1985;**227**:642-5.

6. Allen RC, Zoghbi HY, Moseley AB, Rosenblatt HM, Belmont JW. Methylation of HpaII and HhaI sites near the polymorphic CAG repeat in the human androgen-receptor gene correlates with X chromosome inactivation. *Am.J.Hum.Genet.* 1992;**51**:1229-39.

7. Fialkow PJ. Clonal origin of human tumors. *Biochim.Biophys.Acta* 1976;**458**:283-321.

8. Dow LW, Martin P, Moohr J, Greenberg M, Macdougall LG, Najfeld V *et al*. Evidence for clonal development of childhood acute lymphoblastic leukemia. *Blood* 1985;**66**:902-7.

9. Gale RE, Bunch C, Moir DJ, Patterson KG, Goldstone AH, Linch DC. Demonstration of developing myelodysplasia/acute myeloid leukaemia in haematologically normal patients after high-dose chemotherapy and autologous bone marrow transplantation using X-chromosome inactivation patterns. *Br.J.Haematol.* 1996;**93**:53-8.

10. Anger B, Janssen JW, Schrezenmeier H, Hehlmann R, Heimpel H, Bartram CR. Clonal analysis of chronic myeloproliferative disorders using X-linked DNA polymorphisms. *Leukemia* 1990;**4**:258-61.

11. Strachan and Read. *Human Molecular Genetics 3*. 3 ed. Garland Science, 2003.

12. Brown CJ, Ballabio A, Rupert JL, Lafreniere RG, Grompe M, Tonlorenzi R *et al*. A gene from the region of the human X inactivation centre is expressed exclusively from the inactive X chromosome. *Nature* 1991;**349**:38-44.

13. Brockdorff N, Ashworth A, Kay GF, Cooper P, Smith S, McCabe VM *et al*. Conservation of position and exclusive expression of mouse Xist from the inactive X chromosome. *Nature* 1991;**351**:329-31.

14. Heard E, Lovell-Badge R, Avner P. Anti-Xistentialism. *Nat.Genet.* 1999;**21**:343-4.

15. Marahrens Y. X-inactivation by chromosomal pairing events. *Genes Dev.* 1999;**13**:2624-32.

16. Migeon BR. Non-random X chromosome inactivation in mammalian cells. *Cytogenet.Cell Genet.* 1998;**80**:142-8.

17. Luzzatto L, Usanga EA, Bienzle U, Esan GF, Fusuan FA. Imbalance in X-chromosome expression: evidence for a human X-linked gene affecting growth of hemopoietic cells. *Science* 1979;**205**:1418-20.

18. Abkowitz JL, Taboada M, Shelton GH, Catlin SN, Guttorp P, Kiklevich JV. An X chromosome gene regulates hematopoietic stem cell kinetics. *Proc.Natl.Acad.Sci.U.S.A* 1998;**95**:3862-6.

19. Abkowitz JL, Catlin SN, Guttorp P. Evidence that hematopoiesis may be a stochastic process in vivo. *Nat.Med.* 1996;**2**:190-7.

20. Gale RE, Fielding AK, Harrison CN, Linch DC. Acquired skewing of X-chromosome inactivation patterns in myeloid cells of the elderly suggests stochastic clonal loss with age. *Br.J.Haematol.* 1997;**98**:512-9.

21. Christensen K, Kristiansen M, Hagen-Larsen H, Skytthe A, Bathum L, Jeune B *et al*. X-linked genetic factors regulate hematopoietic stem-cell kinetics in females. *Blood* 2000;**95**:2449-51.

22. Vickers MA, McLeod E, Spector TD, Wilson IJ. Assessment of mechanism of acquired skewed X inactivation by analysis of twins. *Blood* 2001;**97**:1274-81.

23. Naumova AK, Plenge RM, Bird LM, Leppert M, Morgan K, Willard HF *et al*. Heritability of X chromosome--inactivation phenotype in a large family. *Am.J.Hum.Genet.* 1996;**58**:1111-9.

24. Sharp A, Robinson D, Jacobs P. Age- and tissue-specific variation of X chromosome inactivation ratios in normal women. *Hum.Genet.* 2000;**107**:343-9.

25. Belmont JW. Insights into lymphocyte development from X-linked immune deficiencies. *Trends Genet.* 1995;**11**:112-6.

26. Carrel L, Cottle AA, Goglin KC, Willard HF. A first-generation X-inactivation profile of the human X chromosome. *Proc.Natl.Acad.Sci.U.S.A* 1999;**96**:14440-4.

27. Carrel L, Willard HF. X-inactivation profile reveals extensive variability in X-linked gene expression in females. *Nature* 2005;**434**:400-4.

28. Walls GL. *The evolutionary history of eye movements*. 2 ed. 1962: 69-80.

29. Daroff RB. A personal introduction to eye movements. *Ann.N.Y.Acad.Sci.* 2002;**956**:1-6.

30. Leigh RJ, Zee DS. *The Neurology of Eye Movements*. 3rd ed. New York: Oxford University Press, 1999.

31. WARTENBER G R. *Diagnostic Tests in Neurology. Year Book.* Year Book. Chicago., 1953: 42.

32. Oxford University Press. AskOxford.com, Online Dictionary. 2006.
Ref Type: Internet Communication

33. Abel LA. In: Daroff RB NA, ed. *Neurological Organisation of Ocular Movements*. Kluger & Ghedini, 1990: 163-89.

34. Dell'Osso LF. In: Daroff RB NA, ed. *Neurological Organisation of Ocular Movements*. Kluger & Ghedini, 1990: 19-33.

35. Ebers Papyri, 1550 BC.Leipzig museum.Case 99. Picture 855. 1550.
Ref Type: Serial (Book,Monograph)

36. Stedman. *Stedmans medical dictionary. 27th edition. 2000*. 2000.

37. Casteels I, Harris CM, Shawkat F, Taylor D. Nystagmus in infancy. *Br.J.Ophthalmol.* 1992;**76**:434-7.

38. Self JE, Ennis S, Collins A, Shawkat F, Harris CM, Mackey DA *et al*. Fine mapping of the X-linked recessive congenital idiopathic nystagmus locus at Xq24-q26.3. *Mol.Vis.* 2006;**12**:1211-6.

39. Abel LA. Infantile nystagmus: current concepts in diagnosis and management. *Clin.Exp.Optom.* 2006;**89**:57-65.

40. Dell'Osso LF, Daroff RB. Congenital nystagmus waveforms and foveation strategy. *Doc.Ophthalmol.* 1975;**39**:155-82.

41. Yee RD, Wong EK, Baloh RW, Honrubia V. A study of congenital nystagmus: waveforms. *Neurology* 1976;**26**:326-33.

42. Abadi RV, Dickinson CM, Lomas MS, Ackerley R. Congenital idiopathic nystagmus in identical twins. *Br.J.Ophthalmol.* 1983;**67**:693-5.

43. Spooner SN, Bateman JB, Yee RD. Congenital nystagmus in identical twins: discordant features 321. *J.Pediatr.Ophthalmol.Strabismus* 1986;**23**:115-9.

44. Zee DS, Leigh RJ, Mathieu-Millaire F. Cerebellar control of ocular gaze stability. *Ann.Neurol.* 1980;**7**:37-40.

45. Dell'Osso LF, Flynn JT, Daroff RB. Hereditary congenital nystagmus. An intrafamilial study 433. *Arch.Ophthalmol.* 1974;**92**:366-74.

46. Halperin E, Yolton RL. Is the driver drunk? Oculomotor sobriety testing. *J.Am.Optom.Assoc.* 1986;**57**:654-7.

47. Goding GS, Dobie RA. Gaze nystagmus and blood alcohol. *Laryngoscope* 1986;**96**:713-7.

48. Casteels I, Harris CM, Shawkat F, Taylor D. Nystagmus in infancy 42. *Br.J.Ophthalmol.* 1992;**76**:434-7.

49. Pierrot-Deseilligny C, Milea D, Sirmai J, Papeix C, Rivaud-Pechoux S. Upbeat nystagmus due to a small pontine lesion: evidence for the existence of a crossing ventral tegmental tract. *Eur.Neurol.* 2005;**54**:186-90.

50. Zingler VC, Strupp M, Jahn K, Glaser M, Herberger S, Kretzschmar HA *et al*. Upbeat nystagmus as the initial clinical sign of Creutzfeldt-Jakob disease. *Ann.Neurol.* 2005;**57**:607-8.

51. Taylor D. Ophthalmological features of some human hereditary disorders with demyelination. *Bull.Soc.Belge Ophtalmol.* 1983;**208 Pt 1**:405-13.

52. Marmor MF. Hereditary vertical nystagmus 1. *Arch.Ophthalmol.* 1973;**90**:107-11.

53. Ragge NK, Hartley C, Dearlove AM, Walker J, Russell-Eggitt I, Harris CM. Familial vestibulocerebellar disorder maps to chromosome 13q31-q33: a new nystagmus locus 59. *J.Med.Genet.* 2003;**40**:37-41.

54. Halmagyi GM, Aw ST, Dehaene I, Curthoys IS, Todd MJ. Jerk-waveform see-saw nystagmus due to unilateral meso-diencephalic lesion. *Brain* 1994;**117 (Pt 4)**:789-803.

55. Daroff RB. SEE-SAW NYSTAGMUS. *Neurology* 1965;**15**:874-7.

56. Drachman DA. See-saw nystagmus. *J.Neurol.Neurosurg.Psychiatry* 1966;**29**:356-61.

57. Druckman R, Ellis P, Kleinfeld J, Waldman M. Seesaw nystagmus. *Arch.Ophthalmol.* 1966;**76**:668-75.

58. Harding AE, Thomas PK. The clinical features of hereditary motor and sensory neuropathy types I and II. *Brain* 1980;**103**:259-80.

59. Manto MU. Episodic see-saw nystagmus in spino-cerebellar ataxia type 2 (SCA-2). *Cerebellum.* 2002;**1**:91-2.

60. Zelt RP, Biglan AW. Congenital seesaw nystagmus. *J.Pediatr.Ophthalmol.Strabismus* 1985;**22**:13-6.

61. Schmidt D, Kommerell G. [Congenital seewaw nystagmus (author's transl)]. *Albrecht.Von.Graefes Arch.Klin.Exp.Ophthalmol.* 1974;**191**:265-72.

62. Leitch RJ, Thompson D, Harris CM, Chong K, Russell-Eggitt I, Kriss A. Achiasmia in a case of midline craniofacial cleft with seesaw nystagmus. *Br.J.Ophthalmol.* 1996;**80**:1023-4.

63. May EF, Truxal AR. Loss of vision alone may result in seesaw nystagmus. *J.Neuroophthalmol.* 1997;**17**:84-5.

64. Bergin DJ, Halpern J. Congenital see-saw nystagmus associated with retinitis pigmentosa. *Ann.Ophthalmol.* 1986;**18**:346-9.

65. Dell'Osso LF, Jacobs JB, Serra A. The sub-clinical see-saw nystagmus embedded in infantile nystagmus. *Vision Res.* 2006.

66. Furman JM, Wall C, III, Pang DL. Vestibular function in periodic alternating nystagmus. *Brain* 1990;**113 (Pt 5)**:1425-39.

67. Keane JR. Periodic alternating nystagmus with downward beating nystagmus. A clinicoanatomical case study of multiple sclerosis. *Arch.Neurol.* 1974;**30**:399-402.

68. Gradstein L, Reinecke RD, Wizov SS, Goldstein HP. Congenital periodic alternating nystagmus. Diagnosis and Management. *Ophthalmology* 1997;**104**:918-28.

69. Abadi RV, Pascal E. Periodic alternating nystagmus in humans with albinism. *Invest Ophthalmol.Vis.Sci.* 1994;**35**:4080-6.

70. Abadi RV, Bjerre A. Motor and sensory characteristics of infantile nystagmus. *Br.J.Ophthalmol.* 2002;**86**:1152-60.

71. Yee RD, Baloh RW, Honrubia V. Eye movement abnormalities in rod monochromacy. *Ophthalmology* 1981;**88**:1010-8.

72. Sharma P, Tandon R, Kumar S, Anand S. Reduction of congenital nystagmus amplitude with auditory biofeedback. *J.AAPOS.* 2000;**4**:287-90.

73. Tkalcevic LA, Abel LA. The effects of increased visual task demand on foveation in congenital nystagmus
14. *Vision Res.* 2005;**45**:1139-46.

74. Bedell HE, Currie DC. Extraretinal signals for congenital nystagmus. *Invest Ophthalmol.Vis.Sci.* 1993;**34**:2325-32.

75. McKee SP, Welch L. Sequential recruitment in the discrimination of velocity. *J.Opt.Soc.Am.A* 1985;**2**:243-51.

76. Leigh RJ, Dell'Osso LF, Yaniglos SS, Thurston SE. Oscillopsia, retinal image stabilization and congenital nystagmus. *Invest Ophthalmol.Vis.Sci.* 1988;**29**:279-82.

77. Grunfeld EA, Morland AB, Bronstein AM, Gresty MA. Adaptation to oscillopsia: a psychophysical and questionnaire investigation. *Brain* 2000;**123 (Pt 2)**:277-90.

78. Tkalcevic LA, Abel LA. Effects of stimulus size and luminance on oscillopsia in congenital nystagmus. *Vision Res.* 2003;**43**:2697-705.

79. Dell'Osso LF. Eye movements, visual acuity and spatial constancy. *Acta Neurol.Belg.* 1991;**91**:105-13.

80. Dell'Osso LF. Congenital, latent and manifest latent nystagmus--similarities, differences and relation to strabismus. *Jpn.J.Ophthalmol.* 1985;**29**:351-68.

81. Dell'Osso LF, Schmidt D, Daroff RB. Latent, manifest latent, and congenital nystagmus. *Arch.Ophthalmol.* 1979;**97**:1877-85.

82. Abadi RV, Scallan CJ. Waveform characteristics of manifest latent nystagmus. *Invest Ophthalmol.Vis.Sci.* 2000;**41**:3805-17.

83. Kestenbaum A. *Clinical Methods of Neuroophthalmologic Examination*. 2nd ed. New York, 1961.

84. Lueck CJ. A simple guide to nystagmus. *Hosp.Med.* 2000;**61**:544-9.

85. CEMAS Workshop. Classification of Eye Movement Abnormalities and Strabismus (CEMAS) Workshop report. 2001. National Eye Institute Sponsored Workshop. Ref Type: Report

86. Kalla R, Deutschlander A, Hufner K, Stephan T, Jahn K, Glasauer S *et al*. Detection of floccular hypometabolism in downbeat nystagmus by fMRI. *Neurology* 2006;**66**:281-3.

87. Nakamagoe K, Ishii K, Tamaoka A, Shoji S. Upward gaze-evoked nystagmus with organoarsenic poisoning. *Neurology* 2006;**66**:131-2.

88. Bogousslavsky J, Meienberg O. Eye-movement disorders in brain-stem and cerebellar stroke. *Arch.Neurol.* 1987;**44**:141-8.

89. Beversdorf DQ, Jenkyn LR, Petrowski JT, III, Cromwell LD, Nordgren RE. Vertical gaze paralysis and intermittent unresponsiveness in a patient with a thalamomesencephalic stroke. *J.Neuroophthalmol.* 1995;**15**:230-5.

90. Deleu D. Selective vertical saccadic palsy from unilateral medial thalamic infarction: clinical, neurophysiologic and MRI correlates. *Acta Neurol.Scand.* 1997;**96**:332-6.

91. Schmahmann JD. Vascular syndromes of the thalamus. *Stroke* 2003;**34**:2264-78.

92. Blitshteyn S, Hentschel K, Czervionke LF, Eidelman BH. Transient vertical diplopia and nystagmus associated with acute thalamic infarction. *Clin.Imaging* 2006;**30**:54-6.

93. Dell'Osso LF, Weissman BM, Leigh RJ, Abel LA, Sheth NV. Hereditary congenital nystagmus and gaze-holding failure: the role of the neural integrator. *Neurology* 1993;**43**:1741-9.

94. Fielder AR, Evans NM. Is the geniculostriate system a prerequisite for nystagmus? *Eye* 1988;**2 (Pt 6)**:628-35.

95. Apkarian P, Shallo-Hoffmann J. VEP projections in congenital nystagmus; VEP asymmetry in albinism: a comparison study
256. *Invest Ophthalmol.Vis.Sci.* 1991;**32**:2653-61.

96. Harris, C. A Developmental Model of Congenital Nystagmus. 2-9-2005. 2-9-2005.
Ref Type: Conference Proceeding

97. Cheng H, Yang JC, Xia H. Ultrastructural study of proprioceptors in extraocular muscles of congenital nystagmus subjects
50. *Zhonghua Yan.Ke.Za Zhi.* 2003;**39**:24-7.

98. Hertle RW, Chan CC, Galita DA, Maybodi M, Crawford MA. Neuroanatomy of the extraocular muscle tendon enthesis in macaque, normal human, and patients with congenital nystagmus. *J.AAPOS.* 2002;**6**:319-27.

99. Chaum E, Hatton MP. Congenital nystagmus associated with multiple congenital anomalies of the extraocular muscles
153. *J.Pediatr.Ophthalmol.Strabismus* 1999;**36**:155-7.

100. Peng GH, Zhang C, Yang JC. Ultrastructural study of extraocular muscle in congenital nystagmus
177. *Ophthalmologica* 1998;**212**:1-4.

101. Kerrison JB, Giorda R, Lenart TD, Drack AV, Maumenee IH. Clinical and genetic analysis of a family with X-linked congenital nystagmus (NYS1). *Ophthalmic Genet.* 2001;**22**:241-8.

102. Stayte M, Reeves B, Wortham C. Ocular and vision defects in preschool children. *Br.J Ophthalmol* 1993;**77**:228-32.

103. Forssman B, Ringner B. Prevalence and inheritance of congenital nystagmus in a Swedish population. *Ann.Hum.Genet.* 1971;**35**:139-47.

104. Kerrison JB, Vagefi MR, Barmada MM, Maumenee IH. Congenital motor nystagmus linked to Xq26-q27. *Am.J.Hum.Genet.* 1999;**64**:600-7.

105. Kerrison JB, Koenekoop RK, Arnould VJ, Zee D, Maumenee IH. Clinical features of autosomal dominant congenital nystagmus linked to chromosome 6p12
29. *Am.J.Ophthalmol.* 1998;**125**:64-70.

106. Klein C, Vieregge P, Heide W, Kemper B, Hagedorn-Greiwe M, Hagenah J *et al*. Exclusion of chromosome regions 6p12 and 15q11, but not chromosome region 7p11, in a German family with autosomal dominant congenital nystagmus. *Genomics* 1998;**54**:176-7.

107. Patton MA, Jeffery S, Lee N, Hogg C. Congenital nystagmus cosegregating with a balanced 7;15 translocation
226. *J.Med.Genet.* 1993;**30**:526-8.

108. Linnankivi T, Tienari P, Somer M, Kahkonen M, Lonnqvist T, Valanne L *et al*. 18q deletions: Clinical, molecular, and brain MRI findings of 14 individuals. *Am.J.Med.Genet.A* 2006;**140**:331-9.

109. Oetting WS, Armstrong CM, Holleschau AM, DeWan AT, Summers GC. Evidence for genetic heterogeneity in families with congenital motor nystagmus (CN)
114. *Ophthalmic Genet.* 2000;**21**:227-33.

110. Hoffmann S, Becker A, Hoerle S, Metz A, Oertel WH, Sommer N *et al*. Autosomal dominant congenital nystagmus is not linked to 6p12, 7p11, and 15q11 in a German family. *Am.J.Ophthalmol.* 2004;**138**:439-43.

111. Dryja TP, McGee TL, Reichel E, Hahn LB, Cowley GS, Yandell DW *et al*. A point mutation of the rhodopsin gene in one form of retinitis pigmentosa. *Nature* 1990;**343**:364-6.

112. Jiao X, Ventruto V, Trese MT, Shastry BS, Hejtmancik JF. Autosomal recessive familial exudative vitreoretinopathy is associated with mutations in LRP5. *Am.J.Hum.Genet.* 2004;**75**:878-84.

113. Kerrison JB, Vagefi MR, Barmada MM, Maumenee IH. Congenital motor nystagmus linked to Xq26-q27
28. *Am.J.Hum.Genet.* 1999;**64**:600-7.

114. Cabot A, Rozet JM, Gerber S, Perrault I, Ducroq D, Smahi A *et al*. A gene for X-linked idiopathic congenital nystagmus (NYS1) maps to chromosome Xp11.4-p11.3
157. *Am.J.Hum.Genet.* 1999;**64**:1141-6.

115. Oetting WS, Armstrong CM, Holleschau AM, DeWan AT, Summers GC. Evidence for genetic heterogeneity in families with congenital motor nystagmus (CN)
114. *Ophthalmic Genet.* 2000;**21**:227-33.

116. Pearce WG, Johnson GJ, Gillan JG. Nystagmus in a female carrier of ocular albinism. *J.Med.Genet.* 1972;**9**:126-8.

117. Ruttum MS, Lewandowski MF, Bateman JB. Affected females in X-linked congenital stationary night blindness. *Ophthalmology* 1992;**99**:747-52.

118. Lambert SR, Taylor D, Kriss A. The infant with nystagmus, normal appearing fundi, but an abnormal ERG. *Surv.Ophthalmol.* 1989;**34**:173-86.

119. Apkarian P, Bour LJ, Barth PG, Wenniger-Prick L, Verbeeten B, Jr. Non-decussating retinal-fugal fibre syndrome. An inborn achiasmatic malformation associated with visuotopic misrouting, visual evoked potential ipsilateral asymmetry and nystagmus. *Brain* 1995;**118 (Pt 5)**:1195-216.

120. Brecelj J, Stirn-Kranjc B, Pecaric-Meglic N, Skrbec M. VEP asymmetry with ophthalmological and MRI findings in two achiasmatic children. *Doc.Ophthalmol.* 2007.

121. Guo X, Li S, Jia X, Xiao X, Wang P, Zhang Q. Linkage analysis of two families with X-linked recessive congenital motor nystagmus. *J.Hum.Genet.* 2006;**51**:76-80.

122. Kerrison JB, Koenekoop RK, Arnould VJ, Zee D, Maumenee IH. Clinical features of autosomal dominant congenital nystagmus linked to chromosome 6p12. *Am.J.Ophthalmol.* 1998;**125**:64-70.

123. Mellott ML, Brown J, Jr., Fingert JH, Taylor CM, Keech RV, Sheffield VC *et al*. Clinical characterization and linkage analysis of a family with congenital X-linked nystagmus and deuteranomaly. *Arch.Ophthalmol.* 1999;**117**:1630-3.

124. Oetting WS, Armstrong CM, Holleschau AM, DeWan AT, Summers GC. Evidence for genetic heterogeneity in families with congenital motor nystagmus (CN). *Ophthalmic Genet.* 2000;**21**:227-33.

125. Zhang B, Xia K, Ding M, Liang D, Liu Z, Pan Q *et al*. Confirmation and refinement of a genetic locus of congenital motor nystagmus in Xq26.3-q27.1 in a Chinese family. *Hum.Genet.* 2005;**116**:128-31.

126. Dell'Osso LF, Weissman BM, Leigh RJ, Abel LA, Sheth NV. Hereditary congenital nystagmus and gaze-holding failure: the role of the neural integrator
222. *Neurology* 1993;**43**:1741-9.

127. Shallo-Hoffmann J, Watermeier D, Petersen J, Muhlendyck H. Fast-phase instabilities in normally sighted relatives of congenital nystagmus patients--autosomal dominant and x-chromosome recessive modes of inheritance
306. *Neurosurg.Rev.* 1988;**11**:151-8.

128. Spooner SN, Bateman JB, Yee RD. Congenital nystagmus in identical twins: discordant features
321. *J.Pediatr.Ophthalmol.Strabismus* 1986;**23**:115-9.

129. MORTON NE. Sequential tests for the detection of linkage. *Am.J.Hum.Genet.* 1955;**7**:277-318.

130. Terwilliger JD, Ott J. *Handbook of human genetic linkage*. John Hopkins University Press, Baltimore, 1994.

131. Kerrison JB, Vagefi MR, Barmada MM, Maumenee IH. Congenital motor nystagmus linked to Xq26-q27
28. *Am.J.Hum.Genet.* 1999;**64**:600-7.

132. Self J, Lotery A. The molecular genetics of congenital idiopathic nystagmus. *Semin.Ophthalmol.* 2006;**21**:87-90.

133. Yang D, Hertle RW, Hill VM, Stevens DJ. Gaze-dependent and time-restricted visual acuity measures in patients with Infantile Nystagmus Syndrome (INS). *Am.J.Ophthalmol.* 2005;**139**:716-8.

134. Zubcov AA, Reinecke RD, Gottlob I, Manley DR, Calhoun JH. Treatment of manifest latent nystagmus. *Am.J.Ophthalmol.* 1990;**110**:160-7.

135. Bietti GB BB. Traitement medicochirurgical du nystagmus. *Ther Clin Ophtalmol* 1960;268-93.

136. Abadi RV, Carden D, Simpson J. A new treatment for congenital nystagmus 397. *Br.J.Ophthalmol.* 1980;**64**:2-6.

137. Flynn JT, Scott WE, Kushner BJ, Parks MM, Hoyt CS, Metz HS *et al*. Large rectus muscle recessions for the treatment of congenital nystagmus. *Arch.Ophthalmol.* 1991;**109**:1636-8.

138. Casteels I, Harris CM, Shawkat F, Taylor D. Nystagmus in infancy 42. *Br.J.Ophthalmol.* 1992;**76**:434-7.

139. Halmagyi GM, Rudge P, Gresty MA, Leigh RJ, Zee DS. Treatment of periodic alternating nystagmus. *Ann.Neurol.* 1980;**8**:609-11.

140. Larmande P, Pautrizel B. Treatment of congenital nystagmus with 5-hydroxytryptophan. *Nouv.Presse Med.* 1981;**10**:3166.

141. Sarvananthan N, Proudlock FA, Choudhuri I, Dua H, Gottlob I. Pharmacologic treatment of congenital nystagmus. *Arch.Ophthalmol.* 2006;**124**:916-8.

142. Sprenger A, Rambold H, Sander T, Marti S, Weber K, Straumann D *et al*. Treatment of the gravity dependence of downbeat nystagmus with 3,4-diaminopyridine. *Neurology* 2006;**67**:905-7.

143. verbuch-Heller L, Tusa RJ, Fuhry L, Rottach KG, Ganser GL, Heide W *et al*. A double-blind controlled study of gabapentin and baclofen as treatment for acquired nystagmus. *Ann.Neurol.* 1997;**41**:818-25.

144. Stahl JS, verbuch-Heller L, Leigh RJ. Acquired nystagmus. *Arch.Ophthalmol.* 2000;**118**:544-9.

145. McLean R, Proudlock F, Thomas S, Degg C, Gottlob I. Congenital nystagmus: randomized, controlled, double-masked trial of memantine/gabapentin. *Ann.Neurol.* 2007;**61**:130-8.

146. Kalla R, Glasauer S, Buttner U, Brandt T, Strupp M. 4-Aminopyridine restores vertical and horizontal neural integrator function in downbeat nystagmus. *Brain* 2007.

147. Abadi RV. Visual performance with contact lenses and congenital idiopathic nystagmus. *Br.J.Physiol Opt.* 1979;**33**:32-7.

148. Allen ED, Davies PD. Role of contact lenses in the management of congenital nystagmus 363. *Br.J.Ophthalmol.* 1983;**67**:834-6.

149. Biousse V, Tusa RJ, Russell B, Azran MS, Das V, Schubert MS *et al*. The use of contact lenses to treat visually symptomatic congenital nystagmus. *J.Neurol.Neurosurg.Psychiatry* 2004;**75**:314-6.

150. Golubovic S, Marjanovic S, Cvetkovic D, Manic S. The application of hard contact lenses in patients with congenital nystagmus
299. *Fortschr.Ophthalmol.* 1989;**86**:535-9.

151. HALE JR. Contact-lens application in four cases of congenital nystagmus. *Optom.Wkly.* 1962;**53**:1865-8.

152. Safran AB, Gambazzi Y. Congenital nystagmus: rebound phenomenon following removal of contact lenses
238. *Br.J.Ophthalmol.* 1992;**76**:497-8.

153. Mezawa M, Ishikawa S, Ukai K. Changes in waveform of congenital nystagmus associated with biofeedback treatment
272. *Br.J.Ophthalmol.* 1990;**74**:472-6.

154. Ciuffreda KJ, Goldrich SG, Neary C. Use of eye movement auditory biofeedback in the control of nystagmus. *Am.J.Optom.Physiol Opt.* 1982;**59**:396-409.

155. Blekher T, Yamada T, Yee RD, Abel LA. Effects of acupuncture on foveation characteristics in congenital nystagmus
171. *Br.J.Ophthalmol.* 1998;**82**:115-20.

156. Glasner L, Benezra D. Injection of botulinum toxin into the oculomotor muscles in disorders of ocular motility. *Klin.Oczna* 1991;**93**:264-5.

157. Oleszczynska-Prost E. Botulinum toxin A in the treatment of congenital nystagmus in children. *Klin.Oczna* 2004;**106**:625-8.

158. Pradeep A, Thomas S, Roberts EO, Proudlock FA, Gottlob I. Reduction of congenital nystagmus in a patient after smoking cannabis. *Strabismus* 2008;**16**:29-32.

159. Tarpey P, Thomas S, Sarvananthan N, Mallya U, Lisgo S, Talbot CJ *et al*. Mutations in FRMD7, a newly identified member of the FERM family, cause X-linked idiopathic congenital nystagmus. *Nat.Genet.* 2006;**38**:1242-4.

160. Saiki RK, Scharf S, Faloona F, Mullis KB, Horn GT, Erlich HA *et al*. Enzymatic amplification of beta-globin genomic sequences and restriction site analysis for diagnosis of sickle-cell anemia. *Science* 1985;**230**:1350-4.

161. Barnes WM. PCR amplification of up to 35-kb DNA with high fidelity and high yield from lambda bacteriophage templates. *Proc.Natl.Acad.Sci.U.S.A* 1994;**91**:2216-20.

162. Richie KL, Goldsborough MD, Darfler MM, Benzinger EA, Lovekamp ML, Reeder DJ *et al*. Long PCR for VNTR analysis. *J.Forensic Sci.* 1999;**44**:1176-85.

163. Abdollahi MR, Gaunt TR, Syddall HE, Cooper C, Phillips DI, Ye S *et al*. Angiotensin II type I receptor gene polymorphism: anthropometric and metabolic syndrome traits. *J.Med.Genet.* 2005;**42**:396-401.

164. Cheng S, Fockler C, Barnes WM, Higuchi R. Effective amplification of long targets from cloned inserts and human genomic DNA. *Proc.Natl.Acad.Sci.U.S.A* 1994;**91**:5695-9.

165. Dabrowski S, Kiaer AB. Cloning, expression, and purification of the His6-tagged hyper-thermostable dUTPase from Pyrococcus woesei in Escherichia coli: application in PCR. *Protein Expr.Purif.* 2003;**31**:72-8.

166. Self J, Abeysiri P, Lotery A J. A review of Age related Macular Degeneration. *Geriatric Medicine* 2006.

167. Levy S, Sutton G, Ng PC, Feuk L, Halpern AL, Walenz BP *et al*. The Diploid Genome Sequence of an Individual Human. *PLoS.Biol.* 2007;**5**:e254.

168. Cooper DN, Smith BA, Cooke HJ, Niemann S, Schmidtke J. An estimate of unique dna-sequence heterozygosity in the human genome. *Human Genetics* 1985;**69**:201-5.

169. Forrest S, Cotton R, Landegren U, Southern EM. How to find all those mutations. *Nature Genetics* 1995;**10**:375-6.

170. Orita M, Iwahana H, Kanazawa H, Hayashi K, Sekiya T. Detection of polymorphisms of human DNA by gel electrophoresis as single-strand conformation polymorphisms. *Proc Natl Acad Sci U S A* 1989;**86**:2766-70.

171. Orita M, Iwahana H, Kanazawa H, Hayashi K, Sekiya T. Detection of polymorphisms of human DNA by gel electrophoresis as single-strand conformation polymorphisms. *Proc.Natl.Acad.Sci.U.S.A* 1989;**86**:2766-70.

172. Sheffield VC, Beck JS, Kwitek AE, Sandstrom DW, Stone EM. The sensitivity of single-strand conformation polymorphism analysis for the detection of single base substitutions. *Genomics* 1993;**16**:325-32.

173. Meldrum D. Automation for genomics, part one: preparation for sequencing. *Genome Res.* 2000;**10**:1081-92.

174. Higuchi R, Fockler C, Dollinger G, Watson R. Kinetic PCR analysis: real-time monitoring of DNA amplification reactions. *Biotechnology (N.Y.)* 1993;**11**:1026-30.

175. Heid CA, Stevens J, Livak KJ, Williams PM. Real time quantitative PCR. *Genome Res.* 1996;**6**:986-94.

176. Wells D. Use of real-time polymerase chain reaction to measure gene expression in single cells. *Methods Mol.Med.* 2007;**132**:125-33.

177. Kerrison JB, Arnould VJ, Barmada MM, Koenekoop RK, Schmeckpeper BJ, Maumenee IH. A gene for autosomal dominant congenital nystagmus localizes to 6p12. *Genomics* 1996;**33**:523-6.

178. Cabot A, Rozet JM, Gerber S, Perrault I, Ducroq D, Smahi A *et al*. A gene for X-linked idiopathic congenital nystagmus (NYS1) maps to chromosome Xp11.4-p11.3. *Am.J.Hum.Genet.* 1999;**64**:1141-6.

179. O'Connell JR, Weeks DE. The VITESSE algorithm for rapid exact multilocus linkage analysis via genotype set-recoding and fuzzy inheritance. *Nat.Genet.* 1995;**11**:402-8.

180. O'Connell JR, Weeks DE. PedCheck: a program for identification of genotype incompatibilities in linkage analysis. *Am.J.Hum.Genet.* 1998;**63**:259-66.

181. Kong X, Murphy K, Raj T, He C, White PS, Matise TC. A combined linkage-physical map of the human genome. *Am.J.Hum.Genet.* 2004;**75**:1143-8.

182. D.F.Schorderet et al. A Family With Congenital X-Linked Inherited Nystagmus and Mutation in CDR1. 3-5-2005. 3-5-2005.
Ref Type: Conference Proceeding

183. Webster AR, Heon E, Lotery AJ, Vandenburgh K, Casavant TL, Oh KT *et al*. An analysis of allelic variation in the ABCA4 gene. *Invest Ophthalmol.Vis.Sci.* 2001;**42**:1179-89.

184. Kubo T, Yamashita T, Yamaguchi A, Sumimoto H, Hosokawa K, Tohyama M. A novel FERM domain including guanine nucleotide exchange factor is involved in Rac signaling and regulates neurite remodeling. *J.Neurosci.* 2002;**22**:8504-13.

185. Toyofuku T, Yoshida J, Sugimoto T, Zhang H, Kumanogoh A, Hori M *et al*. FARP2 triggers signals for Sema3A-mediated axonal repulsion. *Nat.Neurosci.* 2005;**8**:1712-9.

186. McMullan TF, Collins AR, Tyers AG, Robinson DO. A novel X-linked dominant condition: X-linked congenital isolated ptosis. *Am.J.Hum.Genet.* 2000;**66**:1455-60.

187. Beever C, Lai BP, Baldry SE, Penaherrera MS, Jiang R, Robinson WP *et al*. Methylation of ZNF261 as an assay for determining X chromosome inactivation patterns. *Am.J.Med.Genet.A* 2003;**120**:439-41.

188. LYON MF. X-chromosome inactivation. Pinpointing the centre. *Nature* 1996;**379**:116-7.

189. mos-Landgraf JM, Cottle A, Plenge RM, Friez M, Schwartz CE, Longshore J *et al*. X chromosome-inactivation patterns of 1,005 phenotypically unaffected females. *Am.J.Hum.Genet.* 2006;**79**:493-9.

190. Kaplan Y, Vargel I, Kansu T, Akin B, Rohmann E, Kamaci S *et al*. Skewed X-inactivation in an X-linked Nystagmus Family Resulted From a Novel, p.R229G, Missense Mutation in the FRMD7 Gene. *Br.J.Ophthalmol.* 2007.

191. Dobyns WB, Filauro A, Tomson BN, Chan AS, Ho AW, Ting NT *et al*. Inheritance of most X-linked traits is not dominant or recessive, just X-linked. *Am.J.Med.Genet.A* 2004;**129**:136-43.

192. Plenge RM, Tranebjaerg L, Jensen PK, Schwartz C, Willard HF. Evidence that mutations in the X-linked DDP gene cause incompletely penetrant and variable skewed X inactivation. *Am.J.Hum.Genet.* 1999;**64**:759-67.

193. Schmucker B, Meindl A, Achatz H, Mittermuller J, Kruger G, Hergersberg M *et al*. A PCR based X-chromosome inactivation assay for carrier detection in X-linked immunodeficiencies using differential methylation of the androgen receptor gene. *Immunodeficiency* 1995;**5**:187-92.

194. Greer WL, Kwong PC, Peacocke M, Ip P, Rubin LA, Siminovitch KA. X-chromosome inactivation in the Wiskott-Aldrich syndrome: a marker for detection of the carrier state and identification of cell lineages expressing the gene defect. *Genomics* 1989;**4**:60-7.

195. Jodice C, Mantuano E, Veneziano L, Trettel F, Sabbadini G, Calandriello L *et al*. Episodic ataxia type 2 (EA2) and spinocerebellar ataxia type 6 (SCA6) due to CAG repeat expansion in the CACNA1A gene on chromosome 19p. *Hum.Mol.Genet.* 1997;**6**:1973-8.

196. Ophoff RA, Terwindt GM, Vergouwe MN, van ER, Oefner PJ, Hoffman SM *et al*. Familial hemiplegic migraine and episodic ataxia type-2 are caused by mutations in the Ca2+ channel gene CACNL1A4. *Cell* 1996;**87**:543-52.

197. Ishikawa K, Fujigasaki H, Saegusa H, Ohwada K, Fujita T, Iwamoto H *et al*. Abundant expression and cytoplasmic aggregations of [alpha]1A voltage-dependent calcium channel protein associated with neurodegeneration in spinocerebellar ataxia type 6. *Hum.Mol.Genet.* 1999;**8**:1185-93.

198. Zhuchenko O, Bailey J, Bonnen P, Ashizawa T, Stockton DW, Amos C *et al*. Autosomal dominant cerebellar ataxia (SCA6) associated with small polyglutamine expansions in the alpha 1A-voltage-dependent calcium channel. *Nat.Genet.* 1997;**15**:62-9.

199. Griggs RC, Moxley RT, III, Lafrance RA, McQuillen J. Hereditary paroxysmal ataxia: response to acetazolamide. *Neurology* 1978;**28**:1259-64.

200. Bouchard JP, Roberge C, van Gelder NM, Barbeau A. Familial periodic ataxia responsive to acetazolamide. *Can.J.Neurol.Sci.* 1984;**11**:550-3.

201. Ott J. *Analysis of Human Genetics Linkage 3E*. The Johns Hopkins University Press, Baltimore & London., 1999.

202. Volsen SG, Day NC, McCormack AL, Smith W, Craig PJ, Beattie R *et al*. The expression of neuronal voltage-dependent calcium channels in human cerebellum. *Brain Res.Mol.Brain Res.* 1995;**34**:271-82.

203. Westenbroek RE, Sakurai T, Elliott EM, Hell JW, Starr TV, Snutch TP *et al*. Immunochemical identification and subcellular distribution of the alpha 1A subunits of brain calcium channels. *J.Neurosci.* 1995;**15**:6403-18.

204. Armstrong CM, Hille B. Voltage-gated ion channels and electrical excitability. *Neuron* 1998;**20**:371-80.

205. Mantuano E, Veneziano L, Spadaro M, Giunti P, Guida S, Leggio MG *et al*. Clusters of non-truncating mutations of P/Q type Ca2+ channel subunit Ca(v)2.1 causing episodic ataxia 2. *J.Med.Genet.* 2004;**41**:e82.

206. Mariotti C, Gellera C, Grisoli M, Mineri R, Castucci A, Di DS. Pathogenic effect of an intermediate-size SCA-6 allele (CAG)(19) in a homozygous patient. *Neurology* 2001;**57**:1502-4.

207. Ishikawa K, Tanaka H, Saito M, Ohkoshi N, Fujita T, Yoshizawa K *et al*. Japanese families with autosomal dominant pure cerebellar ataxia map to chromosome 19p13.1-p13.2 and are strongly associated with mild CAG expansions in the spinocerebellar ataxia type 6 gene in chromosome 19p13.1. *Am.J.Hum.Genet.* 1997;**61**:336-46.

208. The International Classification of Headache Disorders. *cephalalgia* 2004;**24**:28-9.

209. Frontali M. Spinocerebellar ataxia type 6: channelopathy or glutamine repeat disorder? *Brain Res.Bull.* 2001;**56**:227-31.

210. Mantuano E, Veneziano L, Jodice C, Frontali M. Spinocerebellar ataxia type 6 and episodic ataxia type 2: differences and similarities between two allelic disorders. *Cytogenet.Genome Res.* 2003;**100**:147-53.

211. Jen JC, Yue Q, Karrim J, Nelson SF, Baloh RW. Spinocerebellar ataxia type 6 with positional vertigo and acetazolamide responsive episodic ataxia. *J.Neurol.Neurosurg.Psychiatry* 1998;**65**:565-8.

212. Rett D. Gaze-evoked nystagmus: a case report and literature review. *Optometry.* 2007;**78**:460-4.

213. Durig JS, Jen JC, Demer JL. Ocular motility in genetically defined autosomal dominant cerebellar ataxia. *Am.J.Ophthalmol.* 2002;**133**:718-21.

214. Hashimoto T, Sasaki O, Yoshida K, Takei Y, Ikeda S. Periodic alternating nystagmus and rebound nystagmus in spinocerebellar ataxia type 6. *Mov Disord.* 2003;**18**:1201-4.

215. Spacey SD, Materek LA, Szczygielski BI, Bird TD. Two novel CACNA1A gene mutations associated with episodic ataxia type 2 and interictal dystonia. *Arch.Neurol.* 2005;**62**:314-6.

216. Terwindt G, Kors E, Haan J, Vermeulen F, Van den MA, Frants R *et al*. Mutation analysis of the CACNA1A calcium channel subunit gene in 27 patients with sporadic hemiplegic migraine. *Arch.Neurol.* 2002;**59**:1016-8.

217. Takahashi T, Igarashi S, Kimura T, Hozumi I, Kawachi I, Onodera O *et al*. Japanese cases of familial hemiplegic migraine with cerebellar ataxia carrying a T666M mutation in the CACNA1A gene. *J.Neurol.Neurosurg.Psychiatry* 2002;**72**:676-7.

218. Escayg A, De WM, Lee DD, Bichet D, Wolf P, Mayer T *et al*. Coding and noncoding variation of the human calcium-channel beta4-subunit gene CACNB4 in patients with idiopathic generalized epilepsy and episodic ataxia. *Am.J.Hum.Genet.* 2000;**66**:1531-9.

219. Ducros A, Denier C, Joutel A, Cecillon M, Lescoat C, Vahedi K *et al*. The clinical spectrum of familial hemiplegic migraine associated with mutations in a neuronal calcium channel. *N.Engl.J.Med.* 2001;**345**:17-24.

220. Lopes LR, Peres MF, Vanmolkot KR, Tobo PR, Zukerman E, Frants RR *et al*. Mutation analysis of CACNA1A and ATP1A2 genes in Brazilian FHM families. *Arq Neuropsiquiatr.* 2006;**64**:549-52.

221. Scoggan KA, Chandra T, Nelson R, Hahn AF, Bulman DE. Identification of two novel mutations in the CACNA1A gene responsible for episodic ataxia type 2. *J.Med.Genet.* 2001;**38**:249-53.

222. Matsuyama Z, Murase M, Shimizu H, Aoki Y, Hayashi M, Hozumi I *et al*. A novel insertion mutation of acetazolamide-responsive episodic ataxia in a Japanese family. *J.Neurol.Sci.* 2003;**210**:91-3.

223. Jouvenceau A, Eunson LH, Spauschus A, Ramesh V, Zuberi SM, Kullmann DM *et al*. Human epilepsy associated with dysfunction of the brain P/Q-type calcium channel. *Lancet* 2001;**358**:801-7.

224. Yue Q, Jen JC, Thwe MM, Nelson SF, Baloh RW. De novo mutation in CACNA1A caused acetazolamide-responsive episodic ataxia. *Am.J.Med.Genet.* 1998;**77**:298-301.

225. Cricchi F, Di LC, Grieco GS, Rengo C, Cardinale A, Racaniello M *et al*. Early-onset progressive ataxia associated with the first CACNA1A mutation identified within the I-II loop. *J.Neurol.Sci.* 2007;**254**:69-71.

226. Jen J, Wan J, Graves M, Yu H, Mock AF, Coulin CJ *et al*. Loss-of-function EA2 mutations are associated with impaired neuromuscular transmission. *Neurology* 2001;**57**:1843-8.

227. van den Maagdenberg AM, Kors EE, Brunt ER, van PW, Pascual J, Ravine D *et al*. Episodic ataxia type 2. Three novel truncating mutations and one novel missense mutation in the CACNA1A gene. *J.Neurol.* 2002;**249**:1515-9.

228. Yue Q, Jen JC, Nelson SF, Baloh RW. Progressive ataxia due to a missense mutation in a calcium-channel gene. *Am.J.Hum.Genet.* 1997;**61**:1078-87.

229. Guida S, Trettel F, Pagnutti S, Mantuano E, Tottene A, Veneziano L *et al*. Complete loss of P/Q calcium channel activity caused by a CACNA1A missense mutation carried by patients with episodic ataxia type 2. *Am.J.Hum.Genet.* 2001;**68**:759-64.

230. Denier C, Ducros A, Vahedi K, Joutel A, Thierry P, Ritz A *et al*. High prevalence of CACNA1A truncations and broader clinical spectrum in episodic ataxia type 2. *Neurology* 1999;**52**:1816-21.

231. Friend KL, Crimmins D, Phan TG, Sue CM, Colley A, Fung VS *et al*. Detection of a novel missense mutation and second recurrent mutation in the CACNA1A gene in individuals with EA-2 and FHM. *Hum.Genet.* 1999;**105**:261-5.

232. Jen J, Yue Q, Nelson SF, Yu H, Litt M, Nutt J *et al*. A novel nonsense mutation in CACNA1A causes episodic ataxia and hemiplegia. *Neurology* 1999;**53**:34-7.

233. Wan J, Khanna R, Sandusky M, Papazian DM, Jen JC, Baloh RW. CACNA1A mutations causing episodic and progressive ataxia alter channel trafficking and kinetics. *Neurology* 2005;**64**:2090-7.

234. Jen J, Kim GW, Baloh RW. Clinical spectrum of episodic ataxia type 2. *Neurology* 2004;**62**:17-22.

235. Geschwind DH, Perlman S, Figueroa KP, Karrim J, Baloh RW, Pulst SM. Spinocerebellar ataxia type 6. Frequency of the mutation and genotype-phenotype correlations. *Neurology* 1997;**49**:1247-51.

236. Alonso I, Barros J, Tuna A, Coelho J, Sequeiros J, Silveira I *et al*. Phenotypes of spinocerebellar ataxia type 6 and familial hemiplegic migraine caused by a unique CACNA1A missense mutation in patients from a large family. *Arch.Neurol.* 2003;**60**:610-4.

237. Ragge NK, Hartley C, Dearlove AM, Walker J, Russell-Eggitt I, Harris CM. Familial vestibulocerebellar disorder maps to chromosome 13q31-q33: a new nystagmus locus 59. *J.Med.Genet.* 2003;**40**:37-41.

238. Schorderet DF, Tiab L, Gaillard MC, Lorenz B, Klainguti G, Kerrison JB *et al*. Novel mutations in FRMD7 in X-linked congenital nystagmus. Mutation in brief #963. Online. *Hum.Mutat.* 2007;**28**:525.

239. Self JE, Shawkat F, Malpas CT, Thomas NS, Harris CM, Hodgkins PR *et al*. Allelic Variation of the FRMD7 Gene in Congenital Idiopathic Nystagmus. *Arch.Ophthalmol.* 2007;**125**:1255-63.

240. Wen X, Fuhrman S, Michaels GS, Carr DB, Smith S, Barker JL *et al*. Large-scale temporal gene expression mapping of central nervous system development. *Proc.Natl.Acad.Sci.U.S.A* 1998;**95**:334-9.

241. Brumwell CL, Curran T. Developmental mouse brain gene expression maps. *J.Physiol* 2006;**575**:343-6.

242. Vandesompele J, De PK, Pattyn F, Poppe B, Van RN, De PA *et al*. Accurate normalization of real-time quantitative RT-PCR data by geometric averaging of multiple internal control genes. *Genome Biol.* 2002;**3**:RESEARCH0034.

243. Candenas L, Seda M, Noheda P, Buschmann H, Cintado CG, Martin JD *et al*. Molecular diversity of voltage-gated sodium channel alpha and beta subunit mRNAs in human tissues. *Eur.J.Pharmacol.* 2006;**541**:9-16.

244. Matsuki T, Hori G, Furuichi T. Gene expression profiling during the embryonic development of mouse brain using an oligonucleotide-based microarray system. *Brain Res.Mol.Brain Res.* 2005;**136**:231-54.

245. Schmittgen TD. Real-time quantitative PCR. *Methods* 2001;**25**:383-5.

246. Bustin SA. Absolute quantification of mRNA using real-time reverse transcription polymerase chain reaction assays. *J.Mol.Endocrinol.* 2000;**25**:169-93.

247. Carotenuto P, Marino N, Bello AM, D'Angelo A, Di PU, Lombardi D *et al*. PRUNE and NM23-M1 expression in embryonic and adult mouse brain. *J.Bioenerg.Biomembr.* 2006;**38**:233-46.

248. Simpson PB, Bacha JI, Palfreyman EL, Woollacott AJ, McKernan RM, Kerby J. Retinoic acid evoked-differentiation of neuroblastoma cells predominates over growth factor stimulation: an automated image capture and quantitation approach to neuritogenesis. *Anal.Biochem.* 2001;**298**:163-9.

249. Feng Z, Porter AG. NF-kappaB/Rel proteins are required for neuronal differentiation of SH-SY5Y neuroblastoma cells. *J.Biol.Chem.* 1999;**274**:30341-4.

250. LoPresti P, Poluha W, Poluha DK, Drinkwater E, Ross AH. Neuronal differentiation triggered by blocking cell proliferation. *Cell Growth Differ.* 1992;**3**:627-35.

251. Hynds DL, Burry RW, Yates AJ. Gangliosides inhibit growth factor-stimulated neurite outgrowth in SH-SY5Y human neuroblastoma cells. *J.Neurosci.Res.* 1997;**47**:617-25.

252. Price RD, Yamaji T, Matsuoka N. FK506 potentiates NGF-induced neurite outgrowth via the Ras/ Raf/MAP kinase pathway. *Br.J.Pharmacol.* 2003;**140**:825-9.

253. Price RD, Oe T, Yamaji T, Matsuoka N. A simple, flexible, nonfluorescent system for the automated screening of neurite outgrowth. *J.Biomol.Screen.* 2006;**11**:155-64.

254. Kim CJ, Matsuo T, Lee KH, Thiele CJ. Up-regulation of insulin-like growth factor-II expression is a feature of TrkA but not TrkB activation in SH-SY5Y neuroblastoma cells. *Am.J.Pathol.* 1999;**155**:1661-70.

255. Encinas M, Iglesias M, Llecha N, Comella JX. Extracellular-regulated kinases and phosphatidylinositol 3-kinase are involved in brain-derived neurotrophic factor-mediated survival and neuritogenesis of the neuroblastoma cell line SH-SY5Y. *J.Neurochem.* 1999;**73**:1409-21.

256. Sanchez S, Jimenez C, Carrera AC, az-Nido J, Avila J, Wandosell F. A cAMP-activated pathway, including PKA and PI3K, regulates neuronal differentiation. *Neurochem.Int.* 2004;**44**:231-42.

257. Campbell MA, Chader GJ. Effects of laminin on attachment, growth and differentiation of cultured Y-79 retinoblastoma cells. *Invest Ophthalmol.Vis.Sci.* 1988;**29**:1517-22.

258. Vento R, Giuliano M, Lauricella M, Carabillo M, Main H, Gerbino E *et al*. Differentiation of Y79 cells induced by prolonged exposure to insulin. *Mol.Cell Biochem.* 1997;**170**:163-70.

259. Wagner N, Wagner KD, Schley G, Coupland SE, Heimann H, Grantyn R *et al*. The Wilms' tumor suppressor Wt1 is associated with the differentiation of retinoblastoma cells. *Cell Growth Differ.* 2002;**13**:297-305.

260. Wagner N, Wagner KD, Sefton M, Rodriguez-Tebar A, Grantyn R. An abnormal response of retinoblastoma cells (Y-79) to neurotrophins. *Invest Ophthalmol.Vis.Sci.* 2000;**41**:1932-9.

261. Barber RD, Harmer DW, Coleman RA, Clark BJ. GAPDH as a housekeeping gene: analysis of GAPDH mRNA expression in a panel of 72 human tissues. *Physiol Genomics* 2005;**21**:389-95.

262. Self J, Mercer C, Boon E, Murugavel M, Shawkat F, Hammans S, Hodgkins P, Griffiths H, and Lotery AJ. Infantile nystagmus and late onset ataxia associated with a CACNA1A mutation in the intracellular loop between s4 and s5 of domain 3. Eye . 2008.
Ref Type: In Press

263. Self JE, Haitchi H, Chen X, Holgate S, Davies D, and Lotery AJ. FRMD7 expression in developing mouse brain. Eye . 9-9-2008.
Ref Type: In Press

264. Thomas S, Proudlock FA, Sarvananthan N, Roberts EO, Awan M, McLean R *et al*. Phenotypical characteristics of idiopathic infantile nystagmus with and without mutations in FRMD7. *Brain* 2008.

265. Self J, Lotery A. A Review of the Molecular Genetics of Congenital Idiopathic Nystagmus (CIN). *Ophthalmic Genet.* 2007;**28**:187-91.

266. Pedersen AG, Baldi P, Chauvin Y, Brunak S. The biology of eukaryotic promoter prediction--a review. *Comput.Chem.* 1999;**23**:191-207.

267. Dieterich C, Cusack B, Wang H, Rateitschak K, Krause A, Vingron M. Annotating regulatory DNA based on man-mouse genomic comparison. *Bioinformatics.* 2002;**18 Suppl 2**:S84-S90.

268. Hardison RC. Conserved noncoding sequences are reliable guides to regulatory elements. *Trends Genet.* 2000;**16**:369-72.

269. Trinklein ND, Aldred SJ, Saldanha AJ, Myers RM. Identification and functional analysis of human transcriptional promoters. *Genome Res.* 2003;**13**:308-12.

270. Liu J, Francke U. Identification of cis-regulatory elements for MECP2 expression. *Hum.Mol.Genet.* 2006;**15**:1769-82.

271. Willemsen R, Anar B, De Diego OY, de Vries BB, Hilhorst-Hofstee Y, Smits A *et al*. Noninvasive test for fragile X syndrome, using hair root analysis. *Am.J.Hum.Genet.* 1999;**65**:98-103.

272. Willemsen R, Olmer R, De Diego OY, Oostra BA. Twin sisters, monozygotic with the fragile X mutation, but with a different phenotype. *J.Med.Genet.* 2000;**37**:603-4.

273. Lee ST, McGlennen RC, Litz CE. Clonal determination by the fragile X (FMR1) and phosphoglycerate kinase (PGK) genes in hematological malignancies. *Cancer Res.* 1994;**54**:5212-6.

274. Bassi MT, Schiaffino MV, Renieri A, De NF, Galli L, Bruttini M *et al*. Cloning of the gene for ocular albinism type 1 from the distal short arm of the X chromosome. *Nat.Genet.* 1995;**10**:13-9.

275. Iannaccone A, Gallaher KT, Buchholz J, Jennings BJ, Neitz M, Sidjanin DJ. Identification of two novel mutations in families with X-linked ocular albinism. *Mol.Vis.* 2007;**13**:1856-61.

276. Zhou P, Wang Z, Zhang J, Hu L, Kong X. Identification of a novel GPR143 deletion in a Chinese family with X-linked congenital nystagmus. *Mol.Vis.* 2008;**14**:1015-9.

277. Liu JY, Ren X, Yang X, Guo T, Yao Q, Li L *et al*. Identification of a novel GPR143 mutation in a large Chinese family with congenital nystagmus as the most prominent and consistent manifestation. *J.Hum.Genet.* 2007;**52**:565-70.

278. Schmitz B, Krick C, Kasmann-Kellner B. [Morphology of the optic chiasm in albinism]. *Ophthalmologe* 2007;**104**:662-5.

279. Ragge NK, Hartley C, Dearlove AM, Walker J, Russell-Eggitt I, Harris CM. Familial vestibulocerebellar disorder maps to chromosome 13q31-q33: a new nystagmus locus 59. *J.Med.Genet.* 2003;**40**:37-41.

Publications arising from this work